SEISMIC PERFORMANCE OF CIRCULAR REINFORCED CONCRETE BRIDGE COLUMNS CONSTRUCTED WITH GRADE 80 REINFORCEMENT

Final Report

SRS 500-610

SEISMIC PERFORMANCE OF CIRCULAR REINFORCED CONCRETE BRIDGE COLUMNS CONSTRUCTED WITH GRADE 80 REINFORCEMENT

SRS 500-610

A report in partial completion of the PacTrans project

NEW STRATEGIES FOR MAINTAINING POST-SEISMIC OPERATIONS OF LIFELINE CORRIDORS

by

David Trejo, Ph.D., André R. Barbosa, Ph.D., and Tim Link
Oregon State University

Sponsorship
PacTrans and Oregon Department of Transportation

for

Oregon Department of Transportation
Research Section
555 13th Street NE
Salem, OR 97301

And

Pacific Northwest Transportation Consortium (PacTrans)
USDOT University Transportation Center for Federal Region 10
University of Washington
More Hall 112, Box 352700
Seattle, WA 98195-2700

In cooperation with US Department of Transportation-Research and Innovative Technology Administration (RITA)

August 2014

Technical Report Documentation Page

1. Report No.	2. Government Accession No.	3. Recipient's Catalog No.
FHWA-OR-RD-15-02		

4. Title and Subtitle	5. Report Date
SEISMIC PERFORMANCE OF CIRCULAR REINFORCED CONCRETE BRIDGE COLUMNS CONSTRUCTED WITH GRADE 80 REINFORCEMENT	August 2014
	6. Performing Organization Code

7. Author(s)	8. Performing Organization Report No.
David Trejo, Andre R. Barbosa, and Tim Link	

9. Performing Organization Name and Address	10. Work Unit No. (TRAIS)
Oregon State University 101 Kearney Hall Corvallis, OR 97331	11. Contract or Grant No. SRS 500-610

12. Sponsoring Agency Name and Address		13. Type of Report and Period Covered
Oregon Dep't of Transp. 555 13th Street NE Salem, OR 97301	Pacific NW Transportation Consortium University of Washington More Hall 112, Box 352700 Seattle, WA 98195-2700	Final Report for SRS 500-610
		14. Sponsoring Agency Code

15. Supplementary Notes

16. Abstract

This project assessed the use of ASTM A706 Grade 80 reinforcing bars in reinforced concrete columns. Grade 80 is not currently allowed in reinforced concrete columns due to lack of information on the material characteristics and column performance. Six half-scale, circular columns were tested: three constructed with Grade 60 reinforcement and three constructed with Grade 80 reinforcement. Designs followed standard design methodologies used by State Highway Agencies (including AASHTO). Results indicate that columns constructed with Grade 80 reinforcement performed similar to columns constructed with conventional ASTM A706 Grade 60 reinforcement. Computational modeling was performed using OpenSees for all six columns. Results indicate that the columns constructed with Grade 80 reinforcement achieved similar resistance and displacement and curvature ductility values when compared with the reference columns constructed with Grade 60 reinforcement. The columns constructed with Grade 60 reinforcement showed larger hysteretic energy dissipation than the columns constructed with Grade 80 reinforcement.

17. Key Words	18. Distribution Statement
Earthquake performance; high-strength steel; reinforced concrete, columns	Copies available from NTIS, and online at http://www.oregon.gov/ODOT/TD/TP_RES/

19. Security Classification (of this report)	20. Security Classification (of this page)	21. No. of Pages	22. Price
Unclassified	Unclassified	258	

SI* (MODERN METRIC) CONVERSION FACTORS

APPROXIMATE CONVERSIONS TO SI UNITS

Symbol	When You Know	Multiply By	To Find	Symbol
		LENGTH		
in	inches	25.4	millimeters	mm
ft	feet	0.305	meters	M
yd	yards	0.914	meters	M
mi	miles	1.61	kilometers	Km
		AREA		
in^2	square inches	645.2	millimeters squared	mm^2
ft^2	square feet	0.093	meters squared	m^2
yd^2	square yards	0.836	meters squared	m^2
ac	acres	0.405	hectares	Ha
mi^2	square miles	2.59	kilometers squared	km^2
		VOLUME		
fl oz	fluid ounces	29.57	milliliters	Ml
gal	gallons	3.785	liters	L
ft^3	cubic feet	0.028	meters cubed	m^3
yd^3	cubic yards	0.765	meters cubed	m^3
NOTE: Volumes greater than 1000 L shall be shown in m^3.				
		MASS		
oz	ounces	28.35	grams	G
lb	pounds	0.454	kilograms	Kg
T	short tons (2000 lb)	0.907	megagrams	Mg
		TEMPERATURE (exact)		
°F	Fahrenheit	(F-32)/1.8	Celsius	°C

APPROXIMATE CONVERSIONS FROM SI UNITS

Symbol	When You Know	Multiply By	To Find	Symbol
		LENGTH		
mm	millimeters	0.039	inches	in
m	meters	3.28	feet	ft
m	meters	1.09	yards	yd
km	kilometers	0.621	miles	mi
		AREA		
mm^2	millimeters squared	0.0016	square inches	in^2
m^2	meters squared	10.764	square feet	ft^2
m^2	meters squared	1.196	square yards	yd^2
ha	hectares	2.47	acres	ac
km^2	kilometers squared	0.386	square miles	mi^2
		VOLUME		
ml	milliliters	0.034	fluid ounces	fl oz
L	liters	0.264	gallons	gal
m^3	meters cubed	35.315	cubic feet	ft^3
m^3	meters cubed	1.308	cubic yards	yd^3
		MASS		
g	grams	0.035	ounces	oz
kg	kilograms	2.205	pounds	lb
Mg	megagrams	1.102	short tons (2000 lb)	T
		TEMPERATURE (exact)		
°C	Celsius	1.8C+32	Fahrenheit	°F

*SI is the symbol for the International System of Measurement

ACKNOWLEDGEMENTS

The contents of this report reflect the views of the authors, who are responsible for the facts and accuracy of the data herein. The contents do not necessarily reflect the official view or policies of the Federal Highway Administration (FHWA) or the Oregon Department of Transportation (ODOT). This report does not constitute a standard, specification, or regulation. The researcher in charge was David Trejo, Ph.D.

The United States Government and the State of Oregon do not endorse products or manufacturers. Trade or manufacturers' names appear herein solely because they are considered essential to the objective of this report.

DISCLAIMER

TABLE OF CONTENTS

LIST OF TABLES

LIST OF FIGURES

1.0 INTRODUCTION

1.1 PROJECT OBJECTIVE

Although high strength steel (HSS) reinforcement is commercially available, its use is limited. Current codes do not allow HSS reinforcement in plastic hinge regions (i.e., bridge columns). In general, higher strength steel exhibits lower ductility. However, Grade 80 (80 ksi [550 MPa]) reinforcing steel (considered herein as Grade 80) meeting ASTM A706 has been reported to have adequate ductility. Even with these reports, there is an overall lack of data on the performance of reinforced concrete (RC) members fabricated with Grade 80 reinforcement. Therefore, the objective of this study is to assess the behavior of circular reinforced-concrete (RC) bridge columns constructed with Grade 80 reinforcing steel meeting ASTM A706 specifications subjected to reversed cyclic lateral loading.

1.2 REPORT OUTLINE

This report includes 9 chapters. A brief description of the chapters follows.

1.2.1 Chapter 1

This chapter provides a general introduction to the project and provides a brief overview of each chapter in the report.

1.2.2 Chapter 2

This chapter provides a brief literature review for the project. The literature review covers the history of Grade 80 reinforcement, a summary of Grade 80 reinforcement reported in code documents, and an overview of the performance of systems containing HSS.

1.2.3 Chapter 3

Chapter 3 provides details on the experimental program and specimen design. This chapter includes details on the design for bending moment capacity, transverse reinforcement design, RC header design, and RC footing design. In addition, this chapter contains details of the instrumentation of the specimens. This chapter also includes specifics of the test set-up and testing procedure. Lastly, it provides details on the construction of the test specimens.

1.2.4 Chapter 4

This chapter provides details on the materials used in the construction of the test specimens. The chapter is separated into two main sections: steel and concrete. The steel section provides mill sheet data for the reinforcement as well as material testing results from the materials testing program in this research. The section on concrete materials provides details on the concrete mix proportions and material testing results from the materials testing program in this research.

1.2.5 Chapter 5

This chapter presents the experimental results of columns C1, C2, C3 and C4. Although limited preliminary analyses were performed on the raw data, no comparisons between the performances of the columns were made in this chapter. Analyses and comparison are provided in Chapter 7. Items presented in this chapter include visual observations of cracking, concrete spalling, reinforcing bar buckling, and reinforcing bar fracture. Measured observations include column tilt, axial load, footing and strong wall displacements, column lateral displacements, steel reinforcing strains, column curvature, and applied horizontal load.

1.2.6 Chapter 6

This chapter presents the experimental results of columns C5 and C6. Although limited preliminary analyses were performed on the raw data, no comparisons between the performance of columns C5 and C6 were made in this chapter. Analyses and comparison are provided in Chapter 7. Items presented in this chapter include visual observations of cracking, concrete spalling, reinforcing bar buckling, and reinforcing bar fracture. Measured observations include column tilt, axial load, footing and strong wall displacements, column lateral displacements, steel reinforcing strains, column curvature, and applied horizontal load.

1.2.7 Chapter 7

This chapter presents the analysis of the experimental data presented in Chapters 5 and 6. The objective of this chapter is to examine the effect of reinforcement grade, longitudinal reinforcement ratio, and shear span ratio. The items presented in Chapters 5 and 6 are further discussed in this chapter along with energy dissipation, displacement ductility, and curvature ductility.

1.2.8 Chapter 8

This chapter presents an overview of the computational modeling of the columns using OpenSees. The models were created to predict the performance of RC columns reinforced with either Grade 60 or Grade 80 reinforcement.

1.2.9 Chapter 9

This chapter provides a summary of the research program and states the main conclusions obtained from the research program.

2.0 LITERATURE REVIEW

This chapter presents the literature review for the project. The history of Grade 80 reinforcement is presented first followed by a review of high strength steel materials. Following this, information relating to Grade 80 reinforcement in relevant code documents is discussed. This is followed by a review of the performance of structural systems containing HSS. Lastly, a summary of the literature review is presented.

2.1 HISTORY OF GRADE 80 REINFORCEMENT

The first specifications for reinforcing bars were developed by the American Association of Steel Manufacturers in 1910 (Concrete Reinforcing Steel Institute [CRSI] 2001). The following year the American Society for Testing and Materials *(ASTM 2012)* adopted the standard specification A15 for billet steel reinforcement, which, for structural grade reinforcement, required a yield strength of 33,000 psi (228 MPa) (CRSI 2001). In 1959, the American Society for Testing and Materials (ASTM) developed specifications for reinforcement with yield strengths of 60 ksi (414 MPa) and 75 ksi (520 MPa) *(Gustafson 2010)*. In 1967, Hognested presented at the CRSI Fall Business Meeting and emphasized that Grade 80 reinforcement needed to be produced and that it would soon be in demand *(Gustafson 2010)*. However, it took several decades for the Grade 80 reinforcement to make its way into the standards. Gustafson *(Gustafson 2010)* reported that the allowable compressive stress in vertical reinforcement was limited to $0.40f_y$, and could not exceed 30 ksi (207 MPa). This translated to a maximum allowable yield strength of 75 ksi (520 MPa) which is the current limit for HSS reinforcement in plastic hinge regions.

In 1976, Rice and Gustafson *(Rice and Gustafson 1976*) assessed the effects of Grade 80 reinforcement in structural elements for buildings using code provisions at that time. However, at that time an ASTM specification for Grade 80 steel reinforcement did not exist and Grade 80 reinforcement was not produced *(Rice and Gustafson 1976)*. The study found that many code requirements restricted or prohibited the use of Grade 80 reinforcement. Using moment interaction diagrams Rice and Gustafson *(Rice and Gustafson 1976)* showed that columns reinforced with Grade 80 reinforcing bars had a significant increase in moment capacity compared to columns reinforced with Grade 60 reinforcing bars when loaded predominantly in flexure. The authors also conducted an economic analysis and reported that the use of Grade 80 reinforcement could have a significant reduction in cost if large quantities were manufactured.

Due to the encouragement from structural engineers, contractors, bar producers, and fabricators, ASTM developed a specification for reinforcement with a minimum yield strength of 80 ksi (550 MPa) in ASTM A706/706M–13 Standard Specification for Low-Alloy Steel Deformed and Plain Bars for Concrete Reinforcement in December 2009 *(Gustafson 2010*). The encouragement was due to the fact that higher strength reinforcement could improve constructability by reducing the congestion of reinforcement in earthquake-resistant structures *(Gustafson 2010)*.

2.2 HIGH STRENGTH STEEL MATERIAL

ASTM A706/A706M provides standard specifications for reinforcement with a minimum yield strength of 80 ksi (550 MPa) (ASTM 2012). The chemical composition requirements are the same requirements specified for A706 Grade 60 reinforcement. Besides strength requirements, Grade 80 reinforcement requires a 2 percent lower minimum elongation for bar sizes 3, 4, 5, and 6 and requires a slightly larger pin diameter for the bend test requirements.

Yield strength and ductility are critical parameters for design. Measuring the yield strength can be achieved with several methods. Paulson *(Paulson 2013)* reported three main methods for measuring yield strength. These include:

1. Observed Yield Point (YP), which defines the yield stress as the perfect-plastic horizontal portion of the stress-strain curve. This method is only acceptable for reinforcement that exhibits sharp yielding, where the stress-strain curve is elastic, perfectly-plastic. ASTM A-15 Grade 40 (40 ksi [280 MPa]) reinforcement exhibited this behavior.

2. Offset Method (OM), which specifies an offset of the elastic region of the stress-strain curve. The offset was initially specified as 0.1 percent but was later increased to 0.2 percent. In general, this method was developed for more rounded stress-strain curves for which the YP method did not apply.

3. Extension Under Load (EUL), which has a specified strain value under load. In this method, the stress corresponding to a specified strain value is defined as the yield stress. This method was initially recommended in 1967 by an ad-hoc group to replace the 0.1 percent offset method with a series of EUL strains. This method was implemented due to the lack of specialty instrumentation to make offset strain measurements of the reinforcement at the rolling mills.

ASTM A706 requires the use of the OM with a 0.2 percent strain offset and this is defined in ASTM A370-12a *Standard Test Methods and Definitions for Mechanical Testing of Steel Products.* This method applied to reinforcement not exhibiting a “sharp-kneed or well defined type of yield point.” ASTM A706 also requires a minimum yield strength determined by the EUL method. The standard states “the stress corresponding to a tensile strain of 0.0035 shall be a minimum of 60 000 psi [420 MPa] for Grade 60 and a minimum of 80 000 psi [550 MPa] for Grade 80.”

The general process of making reinforcement starts by processing scrap steel. This scrap steel along with added alloys is melted in a large vat and formed into billets. Billets are typically cooled and stored. Later, these billets are reheated and then pulled through dies, forming the desired reinforcing bar size.

Two properties of reinforcing bars, strength and ductility, are directly related, by definition. An increase in the steel strength reduces the ductility and softens the strain hardening region of the stress-strain curve. Thus, most steel grades are a compromise between the desired strength and ductility *(Selzer 2013).*

Micro-alloying, the addition of specific alloys in small percentages, can be used to induce grain refinement and to increase the strength of reinforcement. Alloy types can include niobium, vanadium, titanium, molybdenum, and other rare earth metals. During processing, steel develops grains that grow as the steel solidifies and cools. Micro-alloys that result in a larger number of smaller grains will increase the strength of the steel *(Selzer 2013)*. However, micro-alloying decreases ductility of the steel, but not nearly as much as conventional alloys *(Selzer 2013)*. Vanadium is a commonly used micro-alloy *(Selzer 2013)*. Vanadium carbide particles form and "pin" the grain boundaries, resulting in smaller grains *(Nissen 2013)*. This "chemical grain refinement" tends to make the stress-strain curve rounder compared to conventional alloys. Selzer *(Selzer 2013)* reported that the ductility trade-off for increased strength is reduced. Grain refinement can also be accomplished with the rolling/forming process. This process breaks down grains and allows them to regrow as smaller grains as the steel cools *(Selzer 2013)*. Grain refinement is also affected by thermal conditions—high reheating temperatures induce grain growth, resulting in larger grains *(Selzer 2013)*.

Micro-alloying requires a controlled cooling after rolling. Selzer *(Selzer 2013*) reported an ideal cooling rate of approximately 300 ^{o}F/min (149 ^{o}C/min) for maximizing strength gains. If the cooling rate is too slow, newly formed grains grow after forming, coarsening the grain structure, which results in lower strengths. If the cooling rate is too fast precipitates remain in solution, reducing the effectiveness of the micro-alloy *(Selzer 2013)*. In the mill production of reinforcing bars, smaller bar sizes are rolled more times than larger bar sizes, producing additional grain refinement. Increased rolling results in more rounded stress-strain curves in smaller bars sizes compared to larger bar sizes *(Selzer 2013)*. Heat-treating bars generally tends to increase the yield strength at higher ratios than the tensile strength, resulting in a lower tension to yield ratio (T/Y) values *(Selzer 2013)*. ASTM A706 reinforcement requires a T/Y ratio of 1.25. Grade 80 reinforcement strengths are typically achieved by using existing processes for producing Grade 60 reinforcement plus the addition of micro-alloys *(Nissen 2013)*.

Producers of reinforcement have to consider requirements for both minimum and maximum yield strengths, ultimate tensile strengths, and elongations. Therefore, the reinforcement producers typically produce an average strength larger than three standard deviations to ensure that the bars produced meet minimum specified values. The goal is to produce reinforcement with higher strengths, while still having the desired ductility levels and low-cycle fatigue performance.

Mander et al. *(Mander et al. 1994b*) reported on a study on the low-cycle fatigue behavior of conventional ASTM A615 Grade 40 ([40 ksi] 280 MPa) reinforcing bars and ASTM A722 Grade 157 (157 ksi [1080 MPa]) high-strength prestressing threaded bars. All bars were tested as-received to better represent and simulate their seismic behavior in structural concrete members. The researchers concluded that a stress greater than yield can be sustained over the entire compression range if the lateral support spacing is less than or equal to six longitudinal bar diameters in confined structural concrete members *(Mander et al. 1994)*. If the spacing is larger than this then the reinforcement yield *(Mander et al. 1994)*. The six longitudinal bar diameter spacing may prove to be an ultimate limit controlling the spacing of HSS reinforcement used as transverse reinforcement, but further research is needed. Mander et al. *(Mander et al. 1994)* also reported that the peak cycle stress dropped quickly in the first few cycles (softening occurs) for the high-strength prestressing bars, while the Grade 40 exhibited hardening over the first few

cycles. This may provide insight on the use of HSS reinforcing bars. The test results indicated that the displacement ductility (ratio of the ultimate strain to the yield strain) of the HSS threaded bar was only 17 percent of the deformed mild-steel bar. This is likely a large contribution to the specification limits on the strength of reinforcement. However, the researchers noted that the prestressing threaded bar (i.e., HSS) are designed for ultimate tensile strengths and not yield properties. This indicates that HSS deformed bars designed for both ultimate and yield strengths has potential for use as reinforcement for concrete members if the desired displacement ductility can be achieved. The test results also indicated that HSS exhibited superior energy dissipation capacity when compared to the conventional strength steel *(Mander et al. 1994)*. Although promising, the energy dissipation is also a function of the number of reinforcing bars. One objective of using HSS reinforcement could be to reduce the amount of reinforcing bars needed—reducing reinforcing bars could result in reduced energy dissipation. Further research is needed.

Dodd and Restrepo-Posada (1995) reported that the tension and compression cyclic stress-strain behavior of reinforcement is symmetric up to necking (point of plastic instability). The modulus of elasticity of mill produced steel reinforcement is reduced after the steel has been strained beyond the elastic limit—this is known as the Bauschinger effect *(Bauschinger 1887)*. Dodd and Restrepo-Posada (1995) concluded that the shape of the Bauschinger effect is not dependent on the monotonic stress-strain curve. However the researchers did conclude that the shape of the Bauschinger effect is dependent on carbon content—an increase in carbon content softens (less bilinear) the Bauschinger curve. This is an important finding when assessing the effect of HSS. Historically, a common approach to increase the strength of the steel was to add more carbon.

Rodriguez et al. *(Rodriguez et al. 1999*) conducted a study expanding on the work of Dodd and Restrepo-Posada. The researchers further investigated the effects of buckling in the reverse cyclic loading of steel reinforcement. Longitudinal reinforcement in RC structural elements may undergo large tension and compression strain reversals during strong earthquakes *(Rodriguez et al. 1999)*. If insufficient tie spacing exists and is combined with large tension and compression strain reversals progressing into the inelastic range, buckling of longitudinal reinforcement can occur *(Rodriguez et al. 1999)*. The researchers concluded that the onset of buckling of a reinforcing bar subjected to cyclic loading may occur after a reversal from tension and is dependent of the maximum value of the tensile strain prior to the reversal. When this occurs, buckling of the reinforcement is believed to occur on the tension side of the hysteresis cycle *(Rodriguez et al. 1999)*. An important finding of the research was that the maximum available curvature could be overestimated when buckling is not included in the compression stress-strain steel model for a reinforced concrete element *(Rodriguez at al. 1999)*. This indicates that the increased tensile capacity of the reinforcing bar may not be fully utilized due to effect of buckling, which controls the fracture strain under reversed cyclic loading. Further research is needed.

2.3 ASTM A706 GRADE 80 REINFORCEMENT IN CODE DOCUMENTS

Provisions for Grade 80 were added to the ASTM A706/A706M in December 2009. Since then, state and federal codes have been adjusting their provisions to account for the new ASTM A706 Grade 80 reinforcement. The use of Grade 80 reinforcement has not yet been approved for use in

columns, or more specifically members designed to form a plastic hinge. The following sections provide an overview of existing codes on the use of Grade 80 steel reinforcement.

2.3.1 2004 ODOT Bridge Design and Drafting Manual

The Oregon Department of Transportation's (ODOT's) Bridge Design and Drafting Manual (BDDM) allows the use of A706 Grade 80 in bridge decks, drilled shafts, crossbeams and end beams, but specifically states "do not use A706 Grade 80 reinforcement in members designed for plastic seismic performance (such as bridge columns)" *(ODOT 2012)*. In this document, however, ODOT acknowledges that A706 Grade 80 reinforcement has similar ductility properties compared to Grade 60 reinforcement. It is reported that ODOT does not allow the use of A706 Grade 80 in members designed for plastic seismic performance due to a lack of testing of reinforcing bars and of full-scale structural elements *(ODOT 2012)*.

ODOT also limits the maximum yield strength of spirals to 60 ksi (420 MPa) for determining the spiral pitch *(ODOT 2012)*. Allowing a yield strength of spirals equal to 80 ksi (550 MPa) could potentially increase the spiral pitch resulting in a longer unbraced length of reinforcing bar after the column concrete cover spalls. Because reinforcing bar buckling may govern, the increase in strength may not compensate for the increase in the braced length. Design modifications may be necessary.

2.3.2 AASHTO Load and Resistance Factor Design (LRFD) Bridge Design Specifications

The American Association of State Highway and Transportation Officials LRFD Bridge Design Specifications (AASHTO LRFD BDS) (*ASSHTO 2012*) limits the yield strength used for design purposes to 75.0 ksi (520 MPa). AASHTO limits the design strength of transverse reinforcement to the stress corresponding to a strain of 0.0035 and not to exceed 75 ksi *(AASHTO 2012)*. Although not reported, these are likely a result of insufficient data on performance. Further research is needed.

2.3.3 AASHTO Guide Specifications for LRFD Seismic Bridge Design

Section 8.4.1 of the AASHTO Guide Specifications for LRFD Seismic Bridge Design (AASHTO LRFD SBD) states that reinforcing steel used for Seismic Design Categories (SDC) B, C, and D can have an ultimate tensile strength of up to 250 ksi (1,720 MPa) as long as it can be demonstrated through testing that the low-cycle fatigue properties are equal to or better than conventional grade reinforcement allowed by the code (AASHTO 2011). AASHTO (*ASSHTO 2012*) also requires A706 reinforcement to be used in any member where plastic hinging is expected for SDC D. This would prevent the use of all high strength steels except for ASTM A706 Grade 80 in elements such as bridge columns where plastic hinges are expected to form. However, Grade 80 reinforcement exceeds the maximum yield stress for members designed to form a plastic hinge.

2.3.4 Other State Highway Agencies

The Washington Department of Transportation (WSDOT) has nearly identical restrictions as ODOT on the use of A706 Grade 80 reinforcing bars *(WSDOT 2012)*. The WSDOT Bridge Design Manual states "ASTM A706 Grade 80 reinforcing steel shall not be used for elements and connections that are proportioned and detailed to ensure the development of significant inelastic deformations for which moment curvature analysis is required to determine the plastic moment capacity of ductile concrete members and expected nominal moment capacity of capacity protected members." This statement describes members designed for inelastic seismic performance. WSDOT does not allow the use of Grade 80 reinforcement in these members due to a lack of research establishing the shape, model, and characteristic values of the stress-strain curve. Furthermore, there is also a lack of data on the expected reinforcing bar strengths and strain limits for concrete components constructed with ASTM A706 Grade 80 reinforcing steel *(WSDOT 2012)*.

The California Department of Transportation (Caltrans) Seismic Design Criteria (SDC) Version 1.6 limits the range of the yield stress of ASTM A706 to between 60 ksi (420 MPa) and 78 ksi (540 MPa) in the *Materials Properties for Concrete Components (Caltrans 2012)*. This statement prohibits the use of ASTM A706 Grade 80 reinforcing steel (which is required to have a minimum yield stress of 80 ksi (550 MPa)).

2.4 PERFORMANCE OF SYSTEMS WITH HSS

2.4.1 Columns with Low Longitudinal Reinforcement Ratios

Priestley and Benzoni (*Priestley and Benzoni 1996*) conducted a study to investigate the seismic performance of circular columns with low longitudinal reinforcement ratios. The researchers tested two 0.4:1 scale, 24-inch (610 mm) diameter, 72-inch (1.8 m) tall circular columns. One column had the minimum longitudinal reinforcement ratio of 1.0 percent and one column had a longitudinal reinforcement ratio of 0.5 percent (this is one-half of the minimum reinforcement ratio required by AASHTO BDS). The researchers applied an axial load of 5.7 percent of the axial capacity of the column. The test results showed the elastic cracked-section stiffness average was 0.23 EI_{gross} for the two columns *(Priestley and Benzoni 1996)*. This value is less than half of the commonly used value of 0.5 EI_{gross} value. If this reduction is due to the low longitudinal reinforcement ratio it may be a key design factor for designing a column with HSS, which could have lower reinforcement ratios when compared to a column containing conventional Grade 60 reinforcement. Test results indicated that the column with a longitudinal steel ratio of 0.5 percent exhibited a ductile response, adequate distribution of flexural cracking, and failed at a displacement ductility, $\mu_{\Delta,}$ of 10 due to shear failure. The maximum drift angle was reported to be 2.6 percent *(Priestley and Benzoni 1996)*. Test results for the column with a longitudinal steel ratio of 1.0 percent indicated that failure was due to shear *(Priestley and Benzoni 1996)*. The researchers did not report on the anticipated reduction in the capacity due to the low longitudinal reinforcement ratio. However, the authors did recommend that the strength of the concrete component should be considered independently from the reinforcement ratio. The authors concluded that results confirmed analytical predictions that 0.5 percent can safely be used as the lower longitudinal reinforcement ratio for circular bridge columns subjected to low axial loads.

This conclusion may prove critical to the full implementation of the use of Grade 80 reinforcement because current codes limit the ratio to 1.0 percent.

Ziehl et al. (*Ziehl et al. 2004*) conducted a study investigating the minimum longitudinal reinforcement requirements for concrete columns. However, this study evaluated 24 small-scale specimens and focused on the effects of the low longitudinal reinforcement ratio on the long-term performance of axially loaded columns. The columns tested had longitudinal reinforcement ratios ranging from zero to 0.72 percent. The researchers concluded that none of the reinforcement ratios prevented passive yielding of the longitudinal reinforcement for the concrete strengths and axial loads used in the study. This conclusion assumed compatibility of deformations for concrete and the longitudinal reinforcement and the authors used a rather liberal estimate of sustained service-level axial load ($0.4f'_cA_g$). The authors reported that under smaller sustained loads with a low probability of exceedance (i.e., bridge columns), smaller, long-term deformations would be expected and it may be possible to safely use a lower longitudinal reinforcement ratio. This conclusion, combined with the conclusions from Priestley and Benzoni *(Priestley and Benzoni 1996)*, indicate that the use of Grade 80 reinforcement in columns may hold promise.

2.4.2 Columns with HSS Longitudinal Reinforcement

The use of HSS reinforcement in concrete columns was evaluated by Rautenberg et al. *(Rautenberg et al. 2010*). The researchers reported that HSS reinforcing bars reduced bar congestion without significantly reducing the performance for RC columns with low axial loads. Test results indicated that columns reinforced with conventional A615 Grade 60 and HSS (ASTM A1035 Grade 120) exhibited drift ratios exceeding 4 percent and both had similar moment capacities *(Rautenberg et al. 2010)*. Their results indicated that as long as the fracture strain of the longitudinal reinforcement exceeded 7 percent for a reference gage length (8 inches [203 mm]) and the amount and detailing of the transverse reinforcement is adequate to prevent shear failure, bond failure, and bar buckling, then the amount of reinforcement can be reduced proportionally with the increased yield strength. The authors reported a noticeable difference in hysteretic energy dissipation between columns and noted that the difference was a result of the difference in stiffness. The column constructed with the HSS reinforcement had about half the amount of longitudinal reinforcement as the columns constructed with the conventional strength steel reinforcement. This resulted in the columns reinforced with HSS having about half the stiffness compared to the columns containing conventional steel. The decrease in stiffness results in a smaller area contained in the hysteretic loop and therefore, the energy dissipated is smaller.

A reduction in energy dissipation will likely be observed with columns constructed with Grade 80 reinforcing steel because the amount of steel will be about a third less than a column reinforced with conventional ASTM A706 Grade 60 reinforcement. However, the reduction in energy dissipation may be lower when using ASTM A706 Grade 80 reinforcement compared to ASTM A1035 Grade 120 reinforcement because of the difference in stress-strain performance. ASTM A706 Grade 80 reinforcement exhibits more ductile behavior when compared with ASTM A1035 Grade 120 reinforcement. Columns constructed with Grade 80 reinforcement will likely have a decrease in energy dissipation, however, the extent of the reduction is unknown and further testing is needed.

2.4.3 Columns with HSS Transverse Reinforcement

Saatcioglu and Baingo *(1999)* reported on the effects of HSS transverse reinforcement on the performance of circular high-strength concrete columns subjected to simulated seismic loadings. The columns contained concrete ranging in strength from 9 ksi (60 MPa) to 19 ksi (130 MPa). The transverse steel yield strength ranged from 60 ksi (420 MPa) to 145 ksi (1,000 MPa) and both hoops and spirals were used for the transverse reinforcement. The results from nine column tests indicated that the columns with higher strength transverse reinforcement developed significantly higher deformability compared to the columns reinforced with conventional Grade 60 transverse reinforcement. Test results showed a good relationship between the volumetric ratio and transverse yield strength, and thus the authors suggested the product of these two parameters could be an important factor in design using HSS reinforcement. With respect to the use of hoops versus spirals the hoops were observed to straighten in the plastic hinge region during testing while the spirals did not. The authors reported that instability of the longitudinal bars occurred due to the relaxation of the restraining action of the hoops. In general, the authors concluded that spirals were more effective in controlling stability on the inelastic behavior of the longitudinal reinforcement. This observation supports Oregon DOT's requirement for spiral type reinforcement in columns designed for seismic loading.

Paultre et al. *(2001)* investigated the influence of concrete strength and transverse reinforcement yield strength on behavior of high strength concrete (HSC) columns. Concrete strengths investigated ranged from 12 ksi (80 MPa) to 17 ksi (120 MPa) and the transverse steel yield stress ranged from 58 ksi (400 MPa) to 116 ksi (800 MPa). The results from eight columns indicated that the ductility of HSC columns is dependent on the concrete strength. The results showed good agreement with the results by Saatcioglu and Baingo *(1999)* in that the spacing of the transverse reinforcement can be decreased when the yield strength of the transverse steel is increased. The authors also reported that the required amount of transverse reinforcement should be a function of volumetric ratio and the yield strength of the transverse reinforcement. It is important to note that the authors also concluded that a high yield strength is not totally effective when columns are poorly confined. This indicates that the spacing of transverse reinforcement cannot be directly proportionally increased if the yield strength of the transverse reinforcement is increased.

2.5 SUMMARY

Although Grade 80 reinforcing steel has the potential to make RC members more efficient, further research is needed. Early results indicate that Grade 80 reinforcement can reduce the required amount of longitudinal steel reinforcement and transverse reinforcement. However, these reductions may not be a function of the percent increase in yield strengths. Further research is needed on characterizing Grade 80 reinforcement and on assessing the performance of columns (and other members) containing Grade 80 reinforcement.

3.0 EXPERIMENTAL PROGRAM AND SPECIMEN DESIGN

An experimental program was developed to assess the performance of RC columns containing Grade 80 reinforcement meeting ASTM A706 requirements subjected to cyclic loadings. This experimental program consisted of testing six half-scale circular RC bridge columns. Three of the experimental columns were reinforced with ASTM A706 Grade 80 reinforcement and the remaining three columns were reinforced with ASTM A706 Grade 60 reinforcement. In addition to the reinforcement grade, two additional parameters were investigated:

1. Longitudinal reinforcement ratio, and;

2. Column moment-shear span ratio.

The experimental plan is shown in Table 3.1. Note that all six columns have the same spiral pitch of 2.50 inches (63.5 mm). The spiral reinforcement bar size is #3 (#10M) for all six columns. This corresponded to a transverse reinforcement ratio of 0.82 percent. The longitudinal and transverse reinforcement ratios, ρ_l and ρ_t, provided in Table 3.1 are computed using the following equations:

$$\rho_l = \frac{A_{sl}}{A_g - A_{sl}} \quad \textbf{(3.1)}$$

$$\rho_t = \frac{4A_{st}}{sD_{cc}} \quad \textbf{(3.2)}$$

where A_{sl} is the total cross-sectional area of the longitudinal reinforcing bars, A_g is the gross cross-sectional area of the column, A_{st} is the cross-sectional area of a single transverse reinforcing bar, s is the spiral pitch, and D_{cc} is the diameter of the column core, measured out-to-out of the spiral.

Table 3.1: Experimental test matrix

Tests	Moment-shear span ratio *M / VD*	Design concrete strength, f_c'	Longitudinal reinforcement	Transverse reinforcement
C1	6	4 ksi (30 MPa)	ASTM A706 Grade 60 ksi (420 MPa) 16 #5 (#16M) ρ_l = 1.11%	ASTM A706 Grade 60 ksi (420 MPa)
C2	6	4 ksi (30 MPa)	ASTM A706 Grade 80 ksi (550 MPa) 12 #5 (#16M) ρ_l = 0.83%*	ASTM A706 Grade 80 ksi (550 MPa)
C3	6	4 ksi (30 MPa)	ASTM A706 Grade 60 ksi (420 MPa) 22 #6 (#19M) ρ_l = 2.19 %	ASTM A706 Grade 60 ksi (420 MPa)
C4	6	4 ksi (30 MPa)	ASTM A706 Grade 80 ksi (550 MPa) 16 #6 (#19M) ρ_l = 1.58%	ASTM A706 Grade 80 ksi (550 MPa)
C5	3	4 ksi (30 MPa)	ASTM A706 Grade 60 ksi (420 MPa) 22 #6 (#19M) ρ_l = 2.19 %	ASTM A706 Grade 60 ksi (420 MPa)
C6	3	4 ksi (30 MPa)	ASTM A706 Grade 80 ksi (550 MPa) 16 #6 (#19M) ρ_l = 1.58%	ASTM A706 Grade 80 ksi (550 MPa)

*The longitudinal reinforcement ratio for column C2 is lower than the 1 percent minimum reinforcement ratio defined in Sec. 5.10.11.4.1.a for seismic zones 3 and 4 (*AASHTO 2012*). This value was chosen to assess through testing if a value lower than 1 percent may be used. The value chosen does, however, meet the general minimum reinforcement ratio for compression members defined in Sec. 5.7.4.2, which does take into account the strengths of reinforcement and concrete materials (*AASHTO 2012*).

Figure 3.1 shows the test elevations for the six test columns. Figure 3.1(a) represents columns C1, C2, C3, and C4 and Figure 3.1(b) represents columns C5 and C6. The axial load is applied through the center of the header (and column).

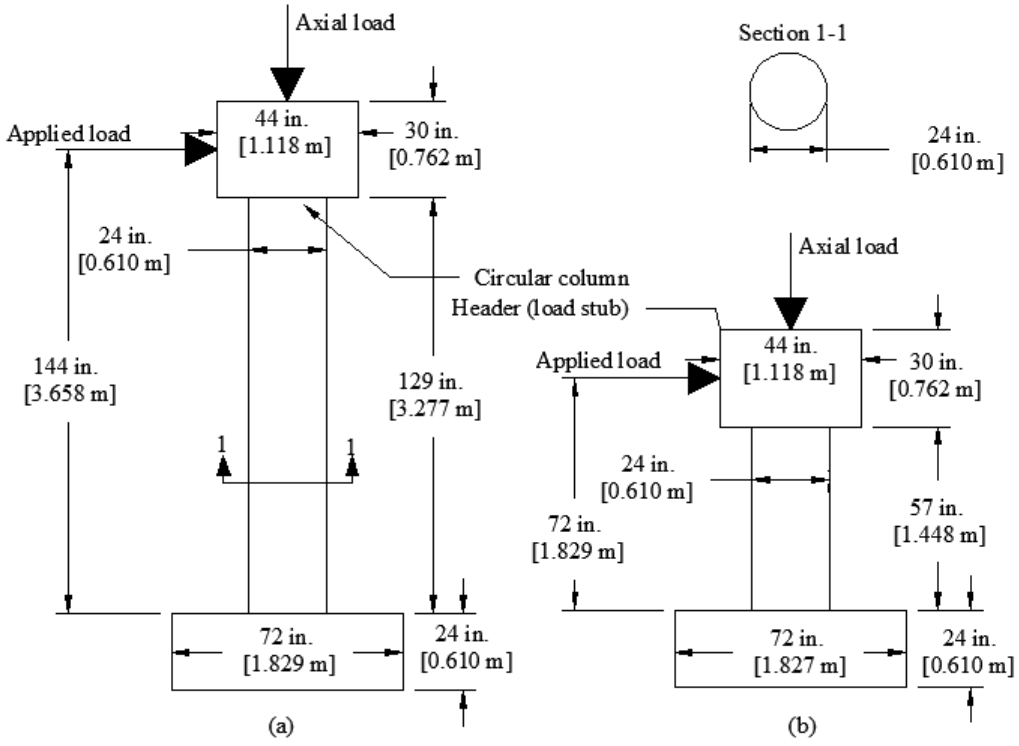

Figure 3.1: Test elevations for: (a) columns C1 through C4 and (b) columns C5 and C6

3.1 DESIGN OF TEST COLUMNS

This section presents the design procedure used for the test columns in this study. This procedure does not directly follow the practices of ODOT and should not be used verbatim for design of actual columns. The columns were tested as cantilever columns and correspond to a moment-shear span ratio of M/VD = 6 for columns C1, C2, C3 and C4 and M/VD=3 for columns C5 and C6 (M is the moment capacity, V is the moment-shear capacity, and D is the column diameter). The test columns are representative of a bridge containing a single pier and the two different shear heights tested correspond to the behavior in the transverse and longitudinal directions of the bridge. Column C1 was designed with a reinforcement ratio just above the minimum requirement ratio of 1 percent defined by AASHTO Sec. 5.10.11.4.1.a. Column C2 was designed to provide approximately the same capacity as column C1 but using Grade 80 reinforcement. Columns C3 and C4 were designed to have larger reinforcement ratios and columns C5 and C6 have the same reinforcement ratio as columns C3 and C4 but with half the moment-shear span ratio. For the design, the following assumptions were made:

1. Axial Load:

$$P = 0.05 f_c' A_g \tag{3.3}$$

where f'_c represents the nominal concrete strength and A_g is the gross cross-sectional area of the column, and;

2. An overstrength resistance factor of $\lambda = 1.4$ was applied to the nominal moment capacity to predict the expected moment capacity.

It should be noted that AASHTO Guide Specification for LRFD Seismic Bridge Design (GSD) Section 8.5 states the overstrength magnifier be equal to 1.2 for ASTM A706 reinforcement. However, an overstrength factor of 1.4 was chosen for this research to more accurately predict the plastic moment capacity of the experimental test columns. The applied axial load is 90 kips (400 kN), corresponding to 5 percent of the nominal axial capacity of the column. Expected material strengths were not used in the design; instead the over-strength resistance factor was applied to the calculated nominal moment capacity of the columns. Designs included nominal material strengths for steel and concrete. Actual material strengths were determined with laboratory testing and these are described in Chapter 4.

The general methodology for the design verification for each test specimen is presented in the following sections. Detailed computations are provided in Appendices A and B.

The procedures and assumptions used in the design of the test columns, footings, and header are presented next. The longitudinal reinforcement ratios were pre-defined as shown in Table 3.1. Checks performed correspond to the verification of the peak expected shear force and peak expected bending moments, which are then used to back-calculate design forces, which are then used in the verifications of the designs.

3.1.1 Bending Moment Capacity

The steps for the column cross-section design follow.

1. Assume an applied axial load determined by Eq. (3.3);

2. Determine column-cross section properties based on experimental plan and half-scale 1.25 inch (31.8 mm) clear cover. Note that full-scale clear cover was assumed to be 2.5 inch (63.5 mm), which is the minimum cover for a spiral as defined by BDDM Sec. 1.1.13.12 *(ODOT 2012)*. Figure 3.2 shows the column cross-sections. Note that columns C3 and C5 have identical cross-sections and columns C4 and C6 also have identical cross-sections;

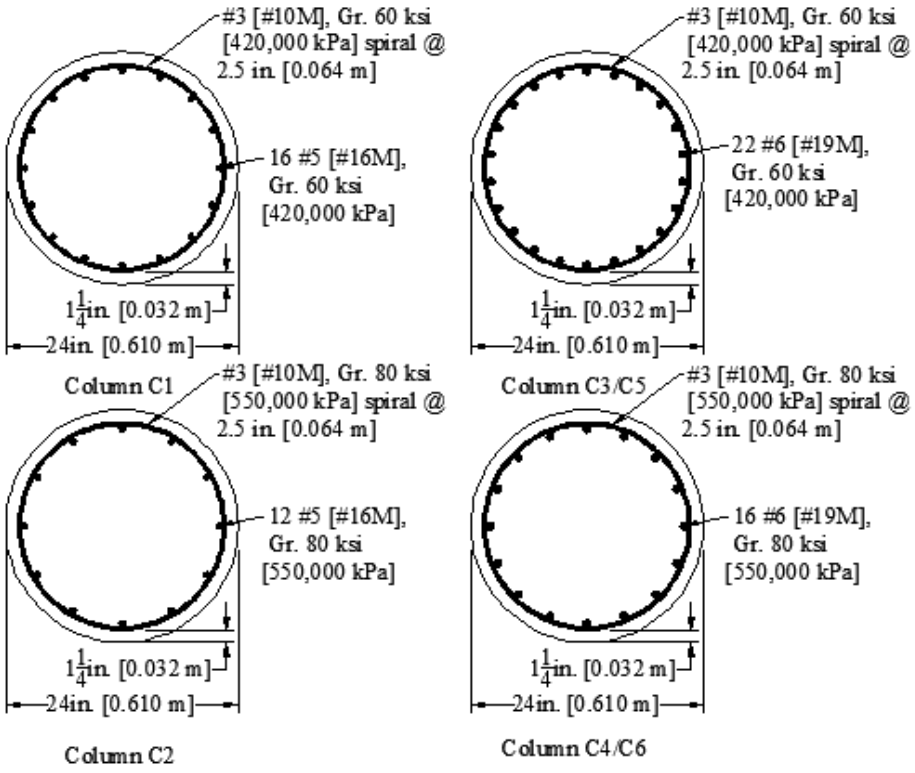

Figure 3.2: Tested column cross-sections

3. Determine the nominal moment capacity based on the nominal material strengths. Response 2000 structural analysis software was used to determine these values. The material stress strain models used are summarized in Table 3.2. Appendix A contains printouts of the Response 2000 inputs and the sectional response output;

Table 3.2: Response 2000 material stress strain properties

	Steel	**Concrete**		
		Base curve	**Compression softening**	**Tension stiffening**
Model	Elastic-Perfectly Plastic	Popovics/Thorenfeldt/Collins *(Collins and Mitchell 1991)*	Vecchio-Collins 1986 *(Vecchio and Collins 1986)*	Bentz 1999 *(Bentz 2000)*

4. Check solutions from step (3). DT Column *(Texler 2001)* and OpenSees *(The Regents of the University of California 1999)* were used to check this design;

5. Compute the expected bending moment capacity as the product of the nominal moment capacity and the over-strength factor which accounts for the increase in actual material strength. Results for all columns are shown in Table 3.3. Note that columns C3 and C5 have the same nominal moment capacity. Columns C4 and C6 also have the same nominal moment capacity. The slight difference in moment capacities between columns C3/C5 and

columns C4/C6 results from columns C3 and C5 using 22 reinforcing bars while only 16 reinforcing bars are used in columns C4 and C6. The reduction in longitudinal reinforcement cross-sectional area from 22 to 16 reinforcing bars is greater than the increase in yield strength of the bars from 60 ksi (420 MPa) to 80 ksi (550 MPa), thus leading to the small difference;

Table 3.3: Column nominal and expected moment capacities

Column	Nominal moment capacity from Response 2000 ft-kip (m-kN)	Overstrength plastic moment capacity ft-kip (m-kN)	Associated plastic shear kip (kN)
C1	287.8 (390.2)	402.9 (546.3)	33.6 (149)
C2	284.7 (386.0)	398.6 (540.4)	33.2 (148)
C3	463.2 (628.0)	648.5 (879.2)	54.0 (240)
C4	448.2 (607.7)	627.5 (850.8)	52.3 (233)
C5	463.2 (628.0)	648.5 (879.2)	108.1 (480.8)
C6	448.2 (607.7)	627.5 (850.8)	104.6 (465.3)

6. Using the expected bending moment capacity from step (5), determine the internal compression and tension resultant forces of the cross-section, and;

7. Check answer from step (6) by summing the internal forces and setting them equal to the applied axial load determined in step (1).

3.1.2 Transverse Reinforcement Design

Spiral reinforcement was used in the construction of all columns. Spirals were chosen over circular hoops because spirals are required by ODOT's BDDM and these are typically more economical than hoop reinforcement *(ODOT 2012)*.

All spirals were fabricated with ASTM A706 reinforcing bars following common practice and following requirements in the Caltrans SDC (*CALTRANS 2012*). The grade of the transverse reinforcement is the same grade used for the longitudinal reinforcement for each column (i.e., either Grade 60 or Grade 80).

Following the guidelines from AASHTO *(AASHTO 2012)* Sec. 5.10.6.2, each end of the spiral will be anchored with at least an additional 1.5 extra turns. Actual construction of spirals included 2.0 extra turns. To determine the required pitch of the transverse spiral, the column can be divided into two regions: the plastic hinge region and the non-plastic hinge region. In the plastic hinge region, the pitch was designed to ensure it met the demands for confinement. The required pitch for the plastic hinge region is less than the non-plastic hinge region. To simplify the construction of the columns, a uniform pitch was used for the entire height of the column. This met the requirements of a constant spaced continuous spiral in ODOT's BDDM *(ODOT 2012)* and AASHTO's LRFD BDS *(AASHTO 2012*). The length of the plastic hinge region, l_p, was calculated as the greater value of the maximum cross-section dimension (column height)

divided by 6 or 18 inches (457 mm) following ODOT's BDDM section 1.1.10.2-2 *(ODOT 2012*). The plastic hinge length is considered to be 24 inches (610 mm) long measured from the face of the footing. Note this height is larger than the required analytical plastic hinge length computed following Caltrans SDC of 19.35 inches (491 mm).

Columns C2, C4, and C6 are transversely reinforced with Grade 80. A yield strength of 80 ksi (550 MPa) was used for the spiral reinforcement in the design. This value exceeds the maximum spiral yield strength value allowed in Sec. 1.1.9.5 of ODOT's BDDM *(ODOT 2012*). The transverse reinforcement has the same pitch and termination details for all six columns. Detailed step-by-step calculations for the transverse reinforcement were performed using MATHCAD®. These calculations for each of the six columns are shown in Appendix B. The procedure for the spiral design is as follows:

1. Adjust input values according to column properties and loading conditions;

2. Determine the shear force demand according to Sec. 5.8.2.9 AASHTO LRFD BDS (*AASHTO 2012*);

3. Determine the maximum and minimum spiral pitch according to the current AASHTO code requirements:

   A. Sec. 5.10.6.2 AASHTO LRFD BDS (*AASHTO 2012*)

   B. Sec. 5.8.2.7 AASHTO LRFD BDS *(AASHTO 2012*)

   C. Sec. 5.7.4.6 AASHTO LRFD BDS (*AASHTO 2012*)

   D. Sec. 5.10.11.4.1d AASHTO LRFD BDS *(AASHTO 2012*)

   E. Sec. 5.8.2.5 AASHTO LRFD BDS *(AASHTO 2012)*

   F. Sec. 5.10.11.4.3 AASHTO LRFD BDS *(AASHTO 2012)*

   G. Sec. 8.6.5 AASHTO LRFD SBD *(AASHTO 2012)*

   H. Sec. 8.8.9 AASHTO LRFD SBD *(AASHTO 2012)*

   I. Determine the controlling maximum and minimum spiral pitch;

4. Calculate the concrete contribution to the shear capacity, V_c, according to Sec. 8.6.2 of AASHTO LRFD SBD *(AASHTO 2012*);

5. Calculate the maximum allowed reinforcing steel contribution to the shear capacity, V_s, according to Sec. 8.6.4 of AASHTO LRFD SBD *(AASHTO 2012);*

6. Calculate V_s according to Sec. 8.6.1 of AASHTO LRFD SBD *(AASHTO 2012*) and check against the maximum shear reinforcement calculated in step (5);

7. Calculate the required pitch according to Sec. 8.6.3 of AASHTO LRFD SBD *(AASHTO 2012)*, and;

8. Determine the final pitch to be used over the entire height of the column and the corresponding transverse reinforcement ratio.

3.1.3 Reinforced Concrete Header Design

The column header is designed to allow for the transfer of lateral forces from the actuator to the test specimen. The header also is used to transfer the applied axial load to the columns. The header was designed using the strut-and-tie method. The reinforcement details are the same for all test specimens except for the spiral reinforcement within the header. Columns C1 and C2 have hoops instead of spirals in the header. In addition, the grade of the spiral within the header is the same grade as the longitudinal and transverse reinforcement within the column. The spacing for both types of transverse reinforcement was kept constant. The RC header has plan view dimensions of 44 inches (1118 mm) by 44 inches (1118 mm) and is 30 inches (762 mm) deep, as shown in Figure 3.3 and Figure 3.4. The spacing of reinforcement mats in the header is the same in both directions. A clear cover of 3 inches (76 mm) is used to accommodate the recesses used to attach the actuator to the header. Figure 3.4 shows an elevation view of the header reinforcement details for columns C1 and C2. Columns C3, C4, C5, and C6 have the same headers as shown in Figure 3.4 except a spiral was used for columns C3, C4, C5 and C6 instead of the 6 hoops used for columns C1 and C2.

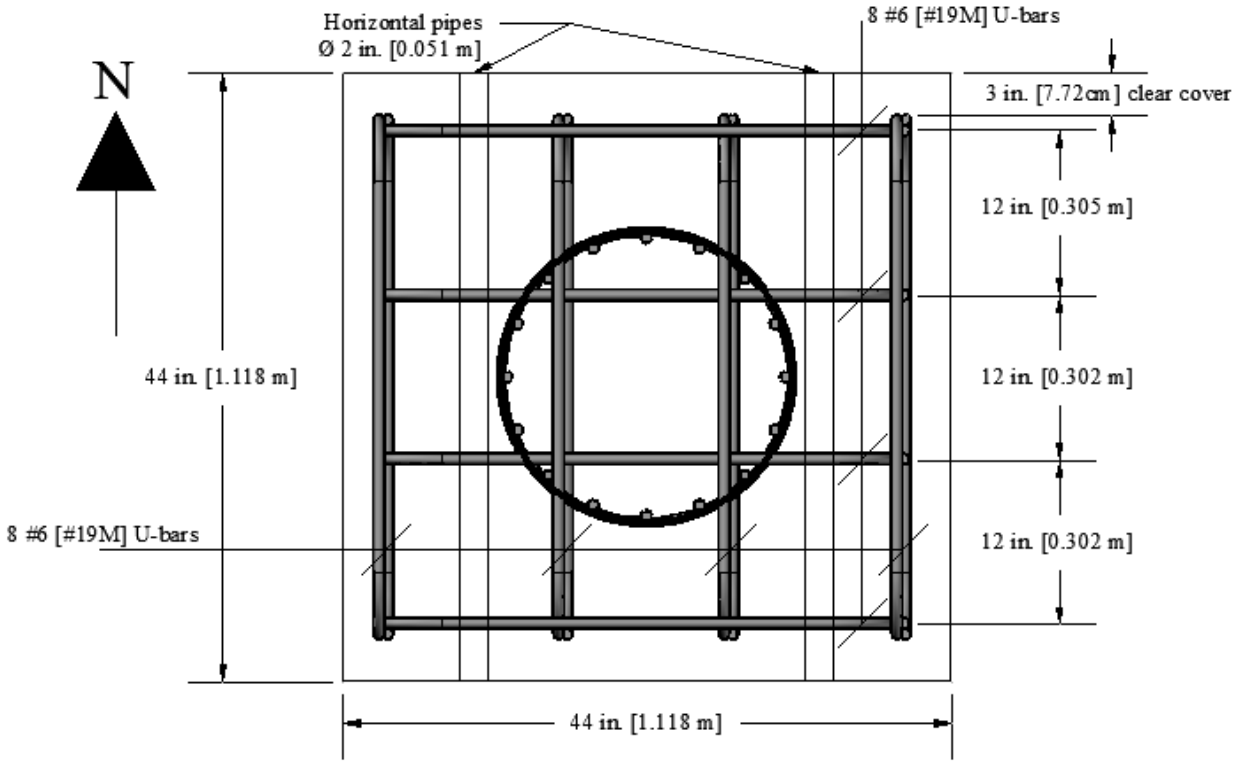

Figure 3.3: Plan view of header reinforcement

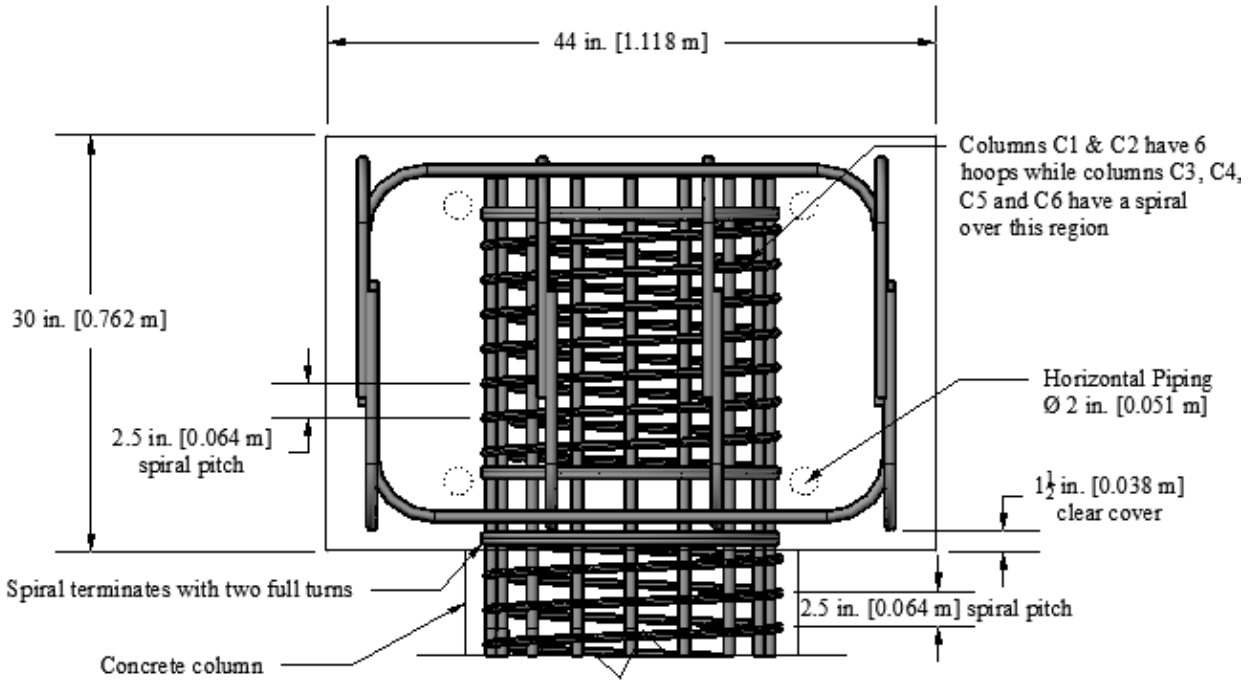

Figure 3.4: North-south elevation view of header reinforcement

3.1.4 Footing Design

The test column footing was designed using a strut-and-tie method following ODOT's BDDM *(ODOT 2012*) and AASHTO's LRFD *(AASHTO 2012*). The footing reinforcement consists of top and bottom reinforcement mats with additional horizontal and vertical bars. The additional reinforcing bars were added because the strut-and-tie model indicated that these were needed to transfer the footing tie down and axial load forces. All footing reinforcement is #6 (#19M) ASTM A706 Grade 60 reinforcing bars. The longitudinal bars in the column extend down into the footing and terminate with 90 degree hooks at the bottom reinforcement mat. The legs of the hooks are 12 inches (305 mm), as specified in Sec. 1.1.13.1.10 of ODOT's BDDM (*ODOT 2012)*. Figure 3.5 and Figure 3.6 show the plan view and elevation view of the footing, respectively.

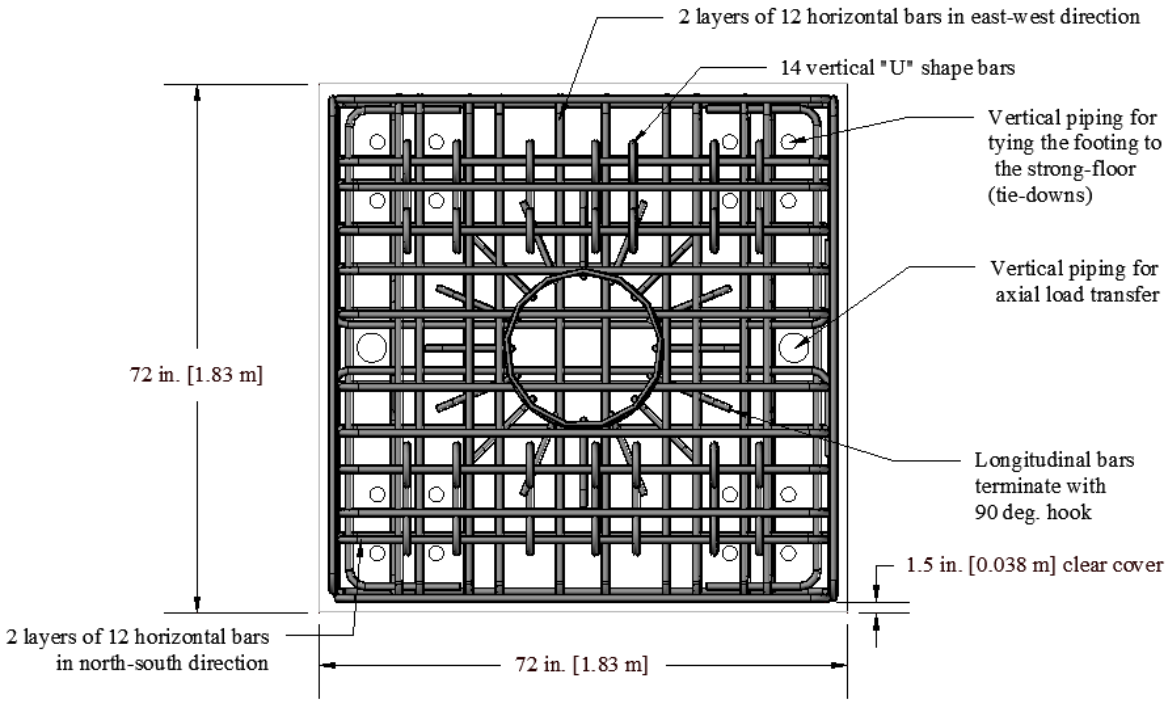

Figure 3.5: Plan view of footing reinforcement

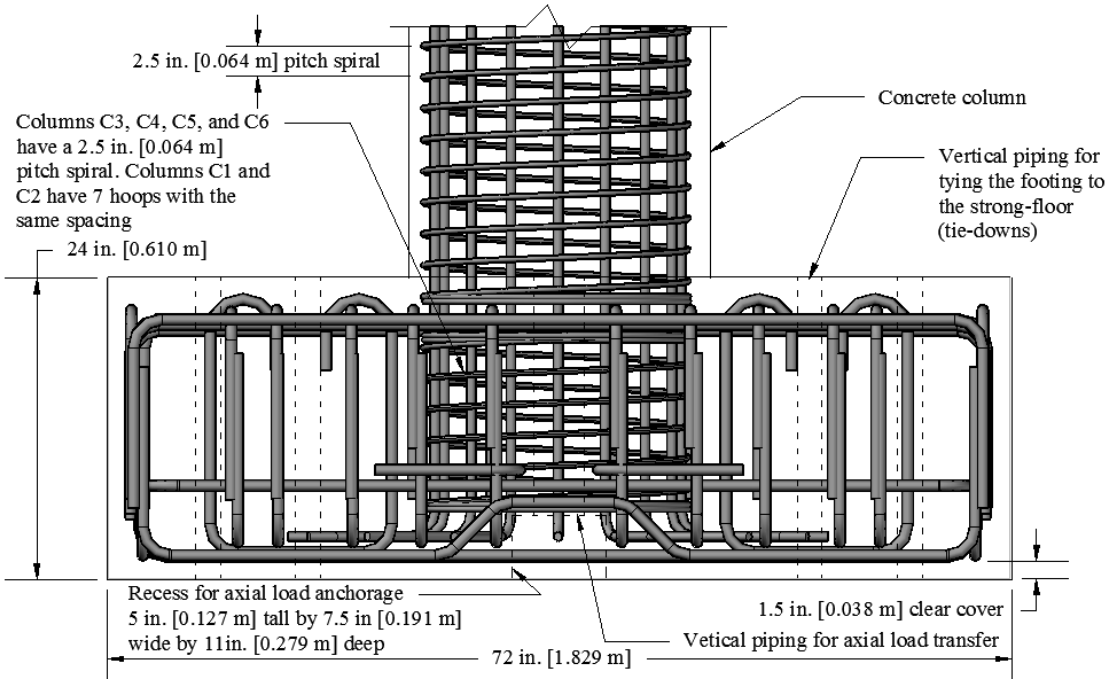

Figure 3.6: North-south elevation view of footing reinforcement

3.2 INSTRUMENTATION OF TEST SPECIMENS

Each test specimen was instrumented to determine the performance of each column. A summary of instrumentation used for each column test is shown in Table 3.4.

Table 3.4: Summary of measure observations and instrumentation

Measured observation	Instrumentation	Drawing label*
Column lateral deflection	6 string pots	(A)
Column curvature	20 string pots	(B)
Shear deformations	8 string pots	(C)
Longitudinal reinforcing steel strain	22 strain gages	(D)
Transverse reinforcing steel strain	7 strain gages	(E)
Column tilt	1 tilt sensor	(F)
Applied lateral load	1 load cell	(G)
Applied vertical load	1 load cell 2 pressure gages	(H) (I)
Footing movement	4 LVDTs (vertical) 2 LVDTs (horizontal) 2 string pots (horizontal)	(J) (K) (L)
Strong wall movement	2 string pots	(M)

*See Figure 3.7 through Figure 3.11

Locations for all instrumentation listed in Table 3.4 are shown in Figure 3.7 through Figure 3.11. All tests used a data sampling rate of five samples per second or greater. Two 3/8 inch (9.5 mm) diameter threaded rods were cast into the column at each instrumentation levels (5 layers of 2 rods; 10 total). The rods were spaced at either 4 inches (102 mm) or 5 inches (127 mm) and were horizontally centered in the column. The 4-inch (102 mm) spacing was the default spacing and the 5-inch (127 mm) spacing was used when the longitudinal reinforcement prevented the default spacing from being used. Aluminum angles were attached to the threaded rods and the string pots were attached to the aluminum angles.

Strain gages were placed on both longitudinal and transverse reinforcement. Strain gages on the longitudinal reinforcement were placed on the farthest northern and southern bars, i.e., in the direction of the applied horizontal load. Two strain gages were placed in the plastic hinge zone on both the east and west sides of the reinforcement bar. Duplicate gages were installed for redundancy. Single gages were placed outside of the plastic hinge zone on the east side of the bar. Transverse strain gages were placed on the outer most surface of the spiral reinforcement at approximately the same elevations as the strain gages on the longitudinal bars.

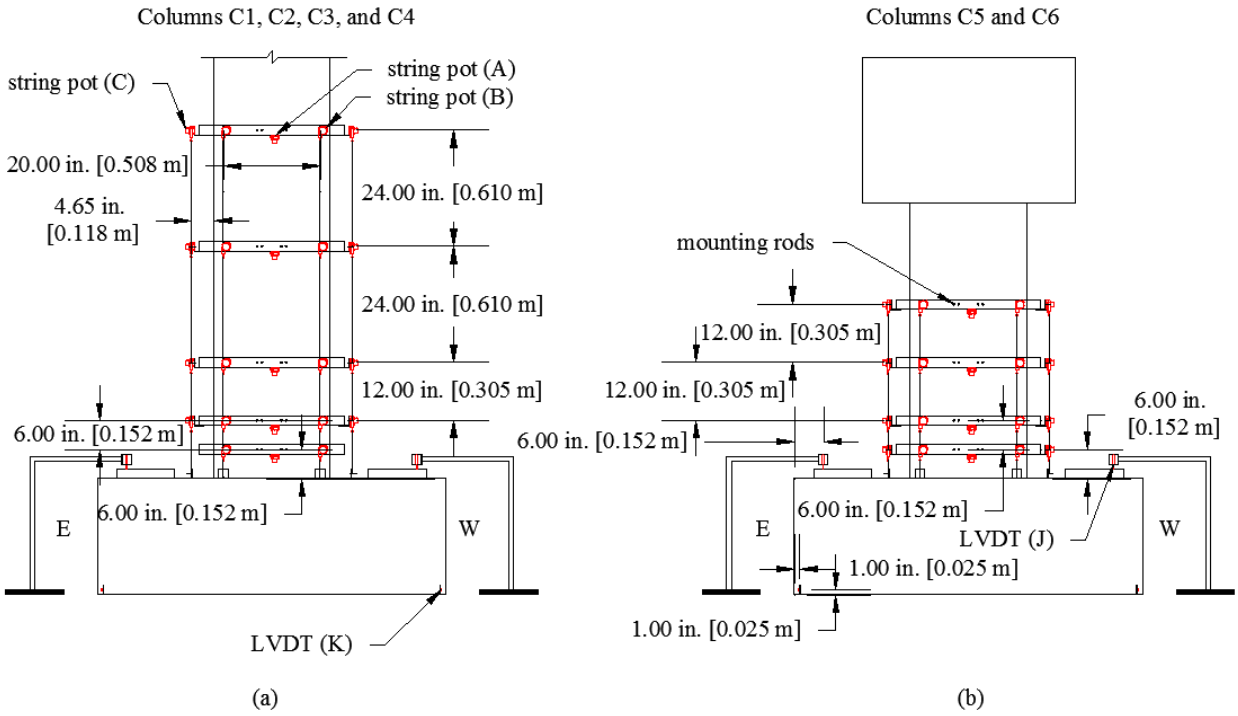

Figure 3.7: North elevation view of external instrumentation for (a) columns C1 through C4 and (b) columns C5 and C6

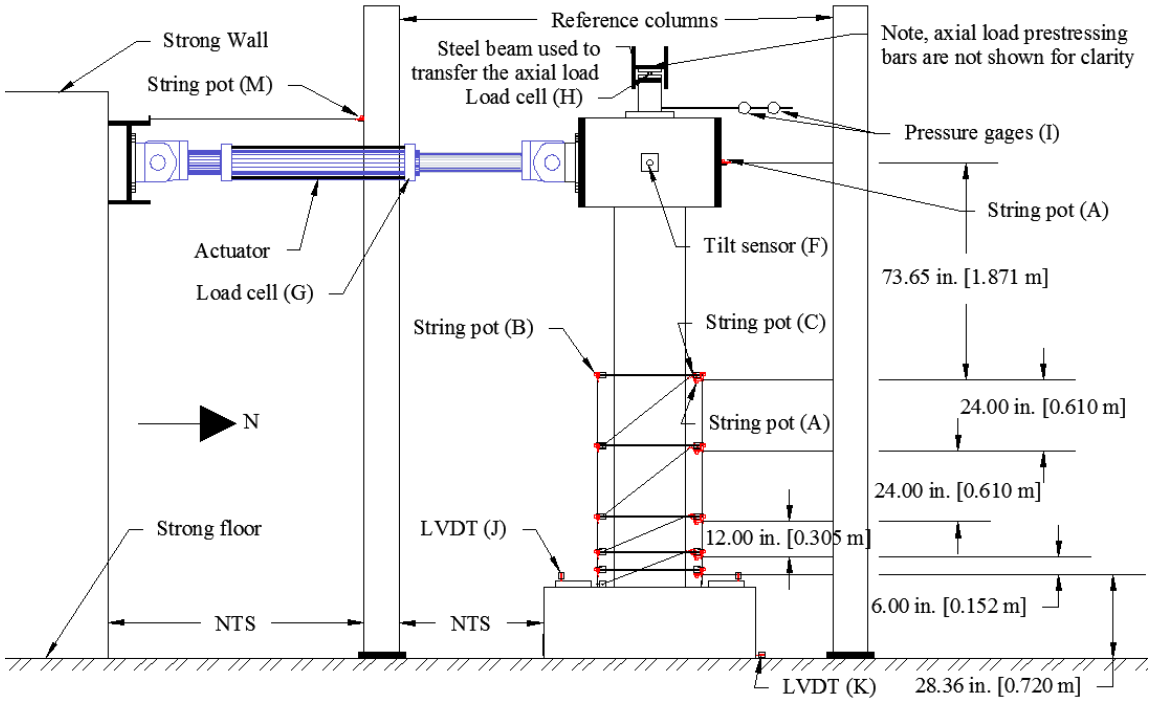

Figure 3.8: Elevation view of column C1, C2, C3 and C4 external instrumentation (NTS = not to scale)

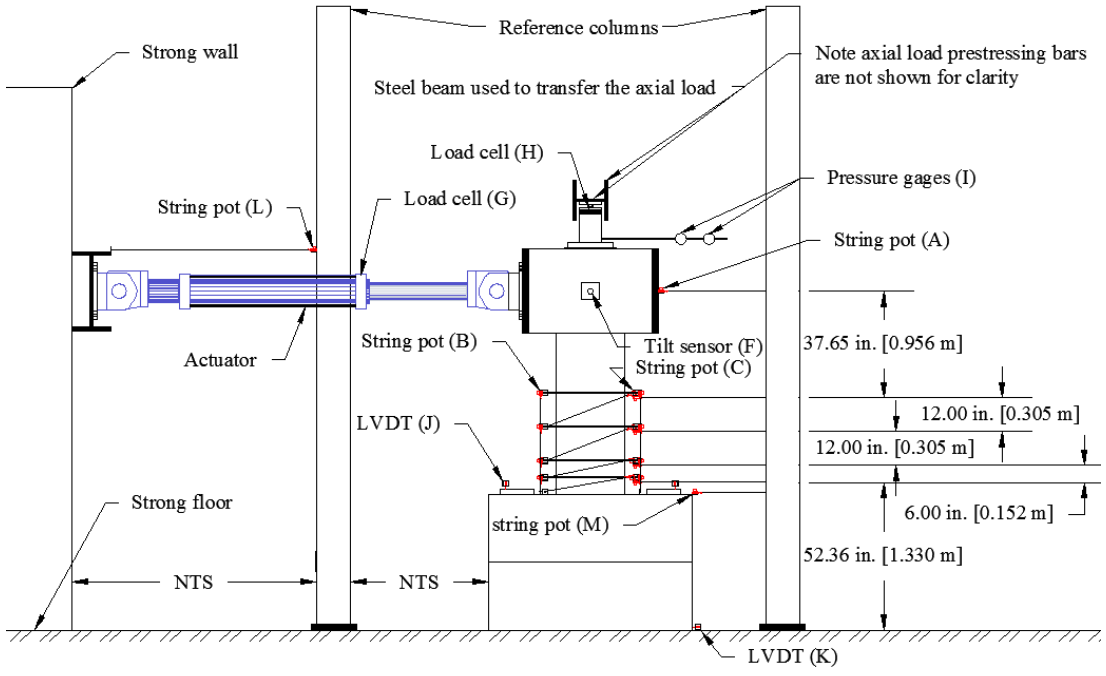

Figure 3.9: Elevation view of column C5 and C6 external instrumentation (NTS = not to scale)

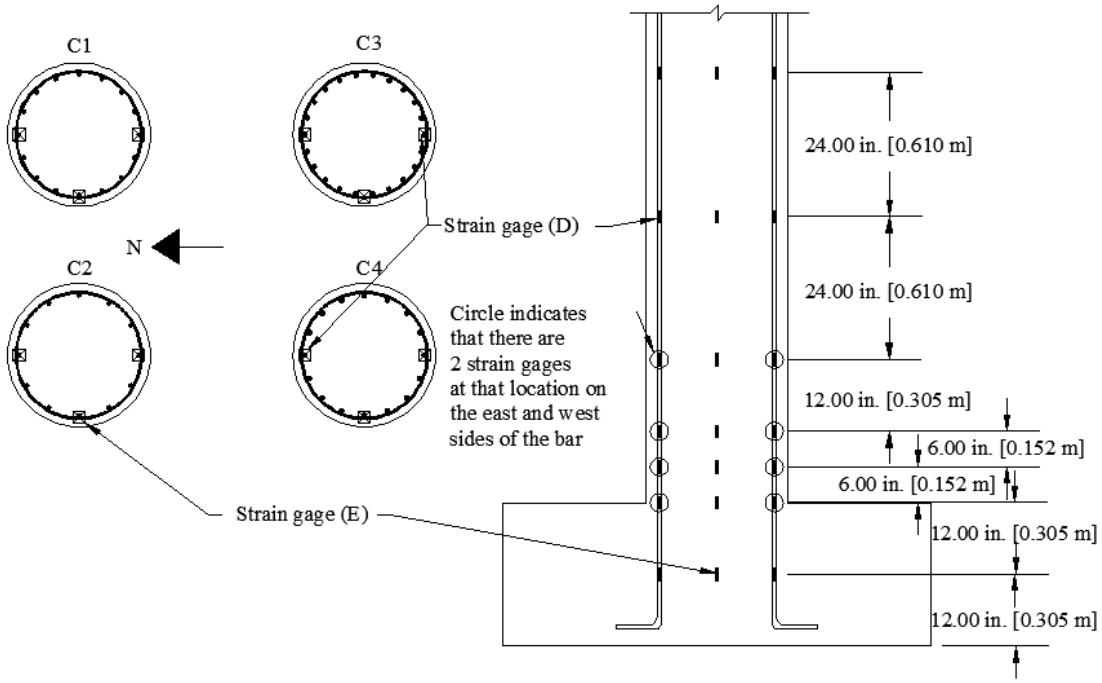

Figure 3.10: Column C1, C2, C3, and C4 internal instrumentation

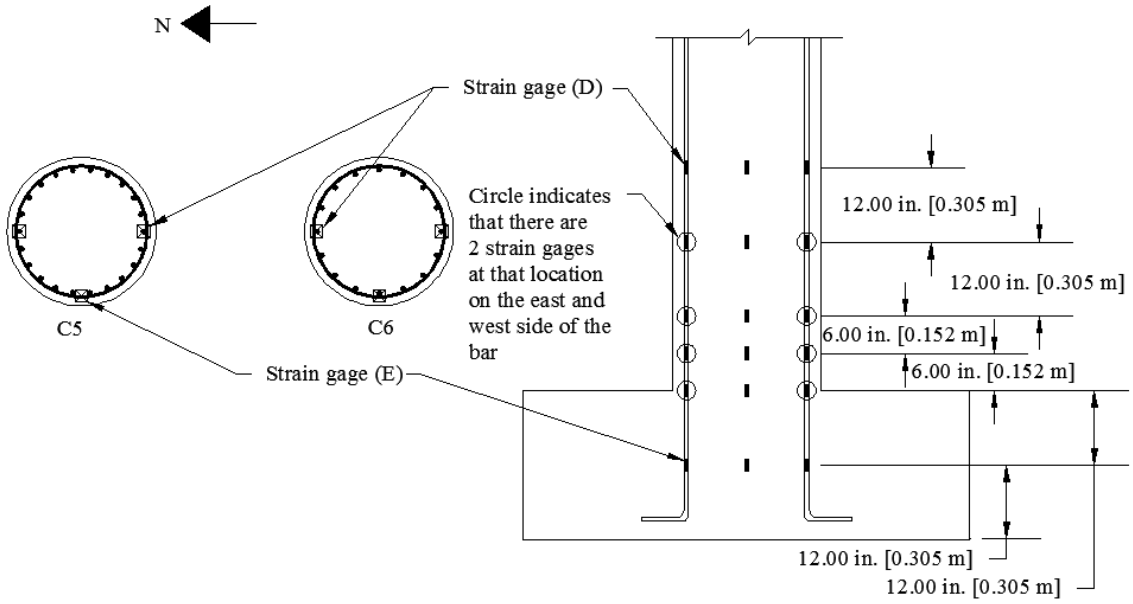

Figure 3.11: Column C5 and C6 internal instrumentation

3.3 TEST SET-UP AND TESTING PROCEDURE

A rendering of the test set-up is shown in Figure 3.12 and Figure 3.13 shows a photograph of column C1 during testing. Test set-up initiated with stressing the column footing to the strong floor. The specified stress is defined by the footing capacity. The hydraulic actuator was then bolted to the RC header. Lastly, the axial load system was assembled. Note that the researchers had concerns with changes in axial load when the specimen was laterally loaded. As a result, the test set-up included systems to minimize changes in axial loads. Figure 3.14 shows a photograph of the concave plate and convex nut used to allow rotation of the prestressing rod to minimize changes in axial load. The top beam is balanced on a steel cylinder to allow rotation. In addition a pneumatic nitrogen accumulator was placed in series with the hydraulic jack to help prevent the axial load from changing. Details of the axial load system can be seen in Figure 3.15 through Figure 3.18.

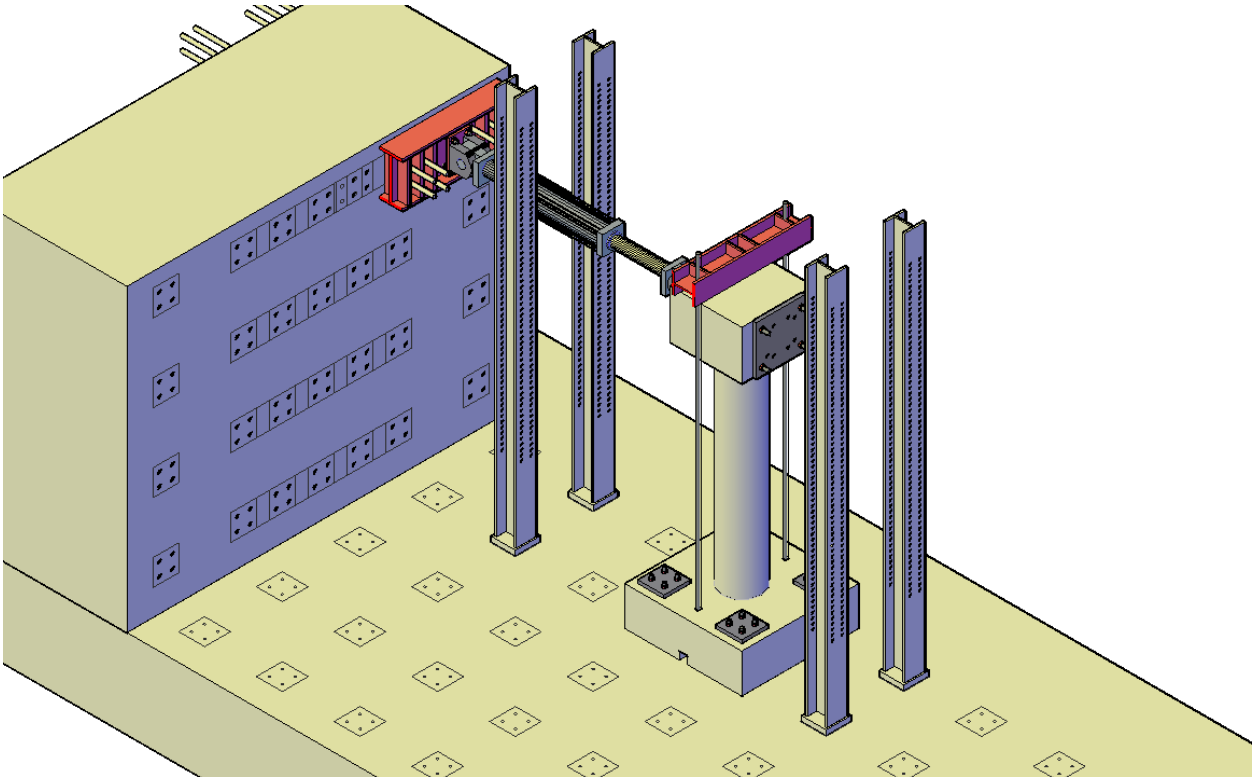

Figure 3.12: Three-dimensional rendering of test set-up for columns C1, C2, C3 and C4

Figure 3.13: Photograph of the column during testing

Figure 3.14: Photograph of the concave plate and convex nut

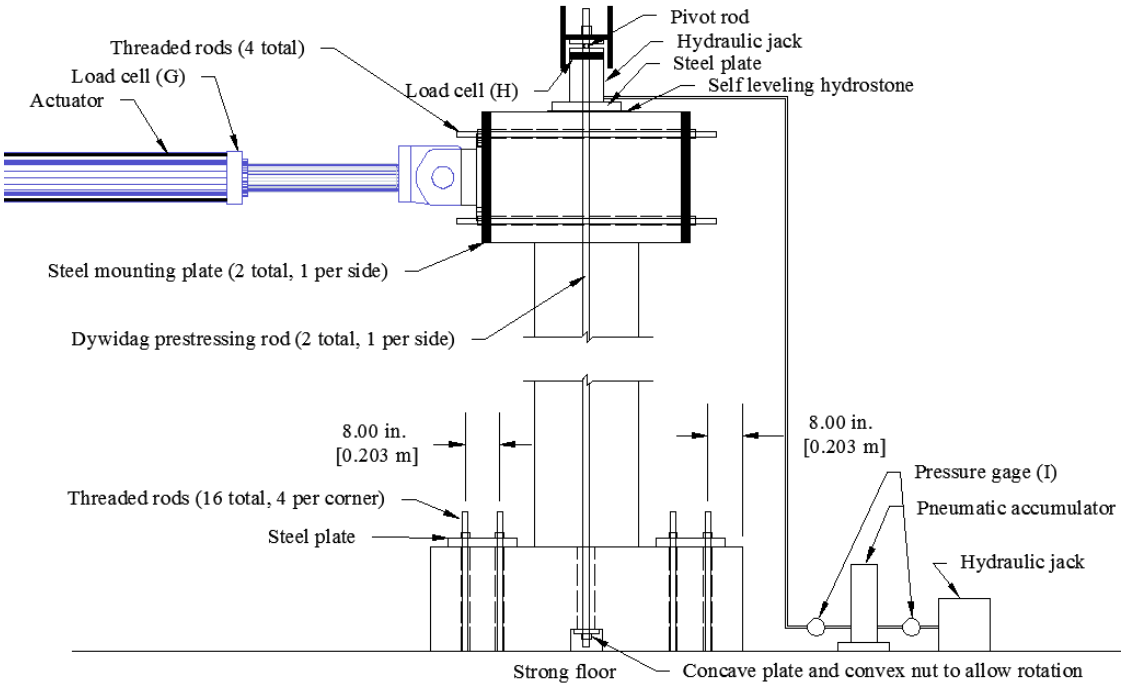

Figure 3.15: Column C1, C2, C3 and C4 east elevation view of test set-up

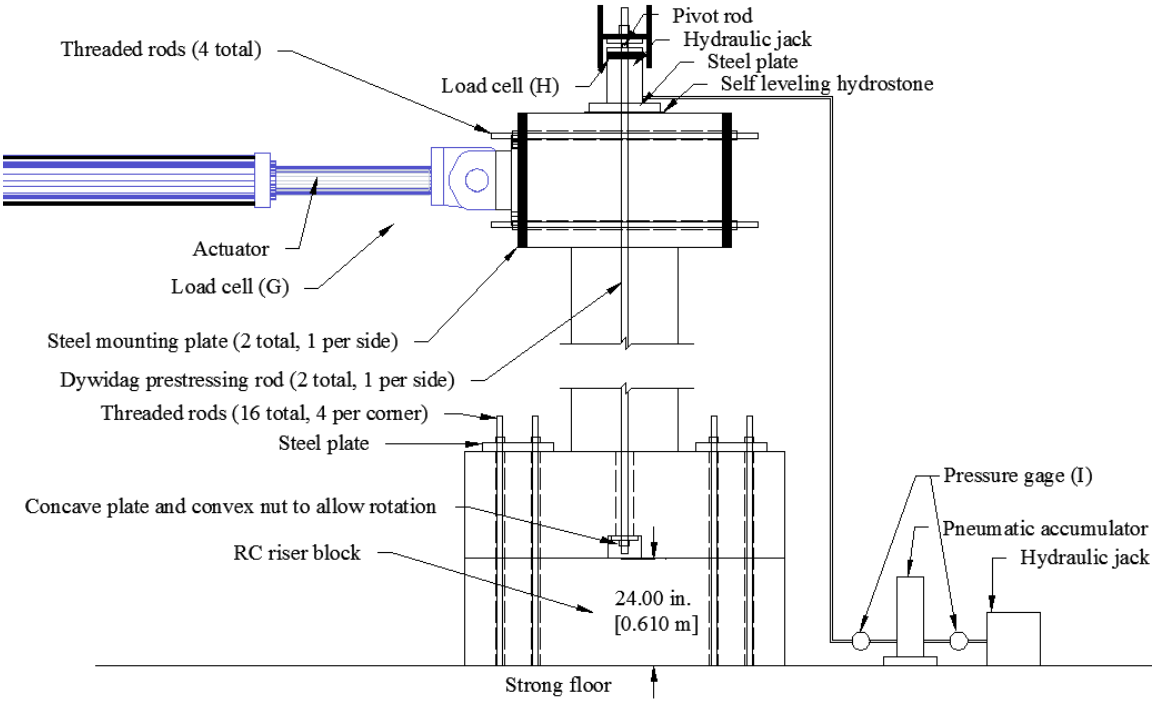

Figure 3.16: Column C5 and C6 east elevation view of test set-up

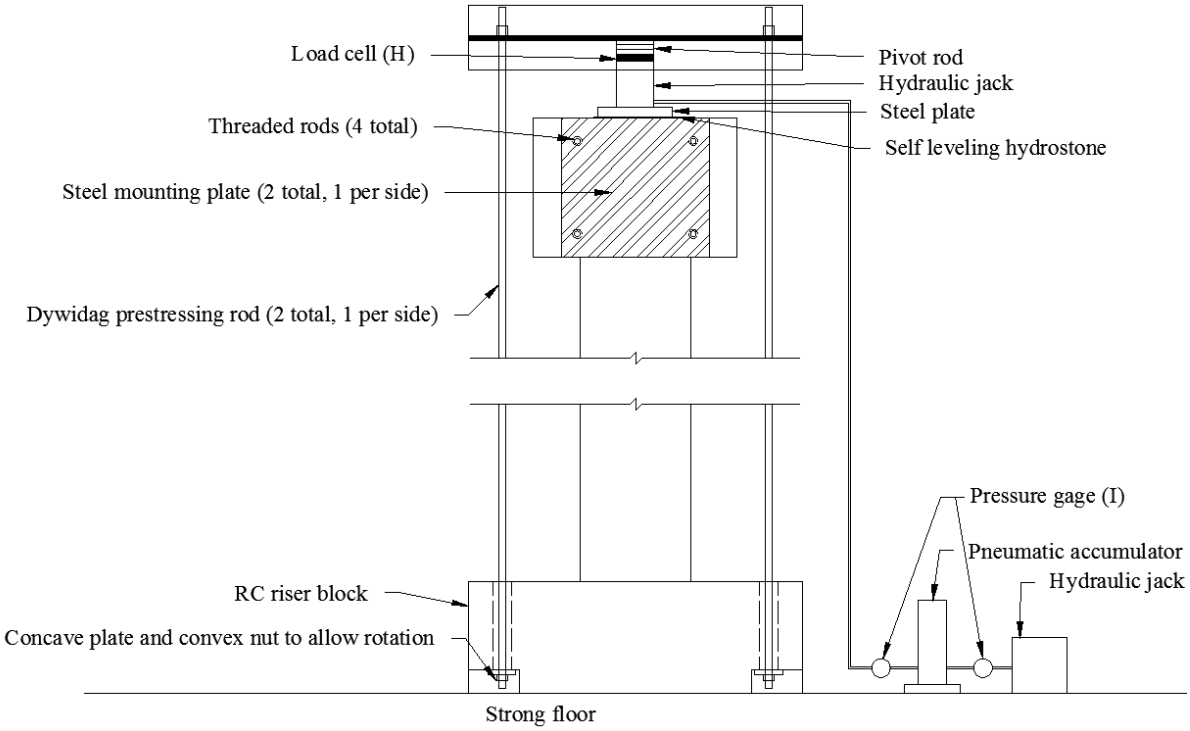

Figure 3.17: Column C1, C2, C3 and C4 south elevation of test set-up

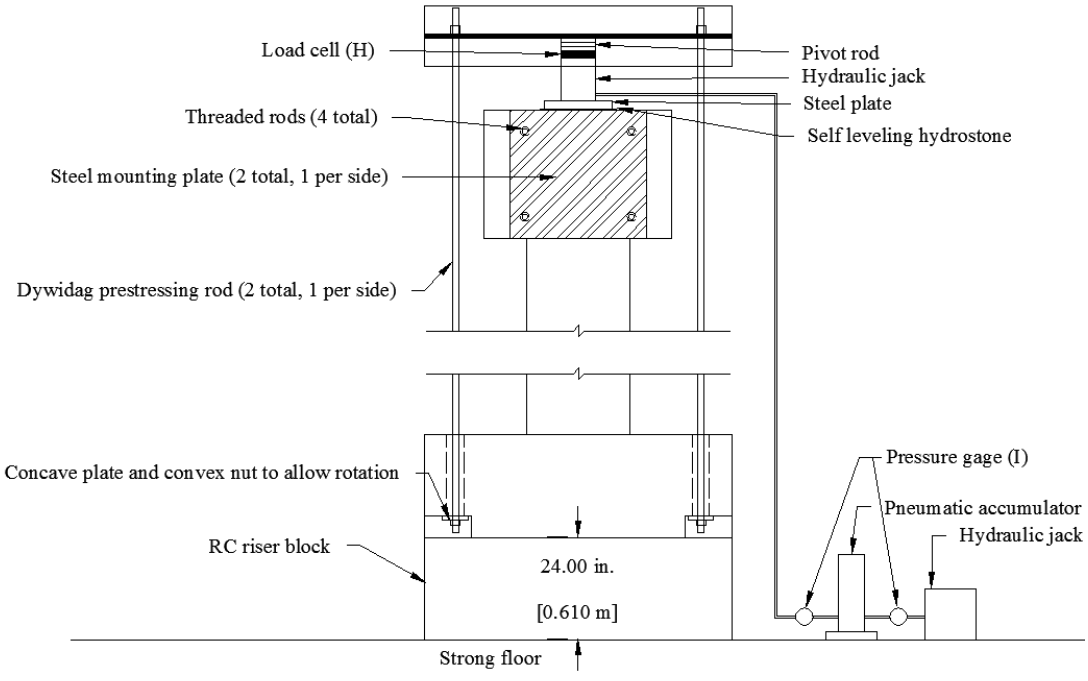

Figure 3.18: Column C5 and C6 south elevation of test set-up

Horizontal loading consisted of pushing and pulling the column to predetermined displacement levels. Each displacement level consisted of three cycles (six peaks): each cycle started at zero displacement, was then loaded in the positive maximum displacement (away from the strong wall), was then loaded in the negative maximum displacement (towards the strong wall), and was finally returned back to zero displacement. Table 3.5 shows the loading profiles for columns C1, C2, C3 and C4.

Table 3.6 shows the loading profiles for columns C5 and C6. Note the loading profile for columns C5 and C6 displacement and rate is reduced by half to represent a fixed-fixed column corresponding to the column being loaded in the longitudinal direction. After all the instrumentation is installed and calibrated, the testing procedure is as follows:

1. Null all instrumentation;

2. Apply axial load, and;

3. Begin horizontal loading according to the cyclic displacement loading profile listed in Table 3.5 and Table 3.6. The horizontal loading was paused at the last two peaks of each displacement cycle to visually inspect the column and perform crack mapping.

Table 3.5: Loading Profile for columns C1 through C4

Displacement cycle, in. (mm)	Number of cycles	Loading rate, in/s (mm/s)
0.10 (2.5)	3	0.01 (0.25)
0.25 (6.4)	3	0.01 (0.25)
0.50 (13)	3	0.01 (0.25)
0.75 (19)	3	0.01 (0.25)
1.00 (25.4)	3	0.01 (0.25)
1.25 (31.8)	3	0.02 (0.51)
2.50 (63.5)	3	0.04 (1.0)
3.75 (95.3)	3	0.08 (2.0)
5.00 (127)	3	0.08 (2.0)
6.25 (159)	3	0.08 (2.0)
7.50 (191)	3	0.08 (2.0)
8.75 (222)	3	0.08 (2.0)
10.00 (254)	3	0.16 (4.1)

Table 3.6: Loading profile for columns C5 and C6

Displacement cycle, in. (mm)	Number of cycles	Loading rate, in/s (mm/s)
0.05 (1.3)	3	0.005 (0.1)
0.13 (3.3)	3	0.005 (0.1)
0.25 (6.4)	3	0.005 (0.1)
0.38 (9.7)	3	0.005 (0.1)
0.50 (13)	3	0.005 (0.1)
0.63 (16)	3	0.01 (0.3)
1.25 (31.8)	3	0.02 (0.51)
1.88 (47.8)	3	0.04 (1.0)
2.50 (63.5)	3	0.04 (1.0)
3.13 (79.5)	3	0.04 (1.0)
3.75 (95.3)	3	0.04 (1.0)
4.38 (111)	3	0.04 (1.0)
5.00 (127)	3	0.08 (2.0)

3.4 CONSTRUCTION PROCEDURE

Each pair of columns (C1 and C2, C3 and C4, C5 and C6) was constructed at the same time. Thus, two sets of formwork were built and the concrete placements for both columns occurred on the same day, the concrete was from the same concrete truck to minimize variability in the concrete. The construction of the test columns can be summarized in the following steps:

1. Application of strain gages on longitudinal column reinforcement. Figure 3.19 shows a photograph of the strain gages applied to the longitudinal reinforcement;

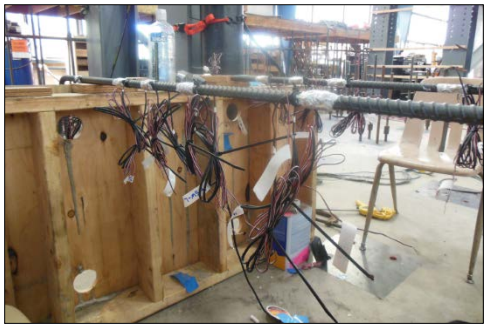

Figure 3.19: Photograph of strain gages on longitudinal column rebar

2. Tying the column reinforcing bar cage and applying strain gages to column transverse reinforcement. A cross-section jig was used at both ends of the column reinforcing bar cage to maintain the cross-sectional geometry of the cage section. Note that an additional cross-

section jig and temporary support were also placed at the mid span of the cage (not shown in photograph) to keep the cage straight. Figure 3.20 shows a photograph of column C2 rebar cage;

Figure 3.20: Photograph of Column C2 rebar cage

3. Tie bottom mat of the footing. Figure 3.21 shows a photograph of the bottom reinforcing mat of the footing;

Figure 3.21: Photograph of the bottom reinforcing mat of the footing

4. Tie column reinforcing bar cage to the bottom reinforcing bar mat of the footing and finish tying the remaining footing reinforcement. Figure 3.22a shows a photograph of the column reinforcing bar cage tied to the bottom reinforcing bar mat of the footing and Figure 3.22b shows a photograph of the finished footing reinforcement;

(a) **(b)**

Figure 3.22: Photograph of the placement of reinforcement for: (a) column, and (b) footing

5. Construct footing formwork and place concrete for the footings. Figure 3.23 shows a photograph of the concrete being placed within the footing formwork. Note that two footings were cast at the same time. The concrete was pumped into the footing formwork and consolidated using a concrete vibrator;

Figure 3.23: Photograph of the footing formwork and concrete pour

6. Construct the column header shoring and false decking. Sonotube was used for the column formwork. Holes were made on the East and West sides (direction perpendicular to loading) of the formwork to pass strain gage cables to the outside of the column. Figure 3.24 shows a photograph of the header shoring and false decking;

Figure 3.24: Photograph of the header shoring and false decking

7. Tie the header reinforcing bar cage. Figure 3.25 shows a photograph of the header reinforcement, and;

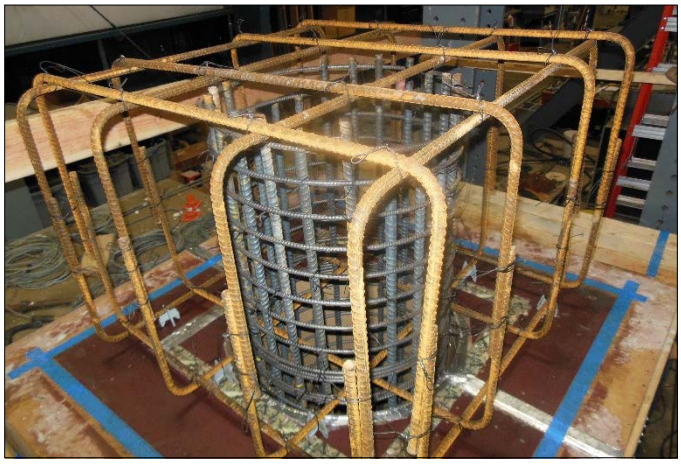

Figure 3.25: Photograph of the header reinforcing bar cage

8. Construct the header formwork and place pipes for actuator tie-rods. Figure 3.26 shows a photograph of the completed header formwork and shoring system. Then place the concrete in the columns and headers. Note that two columns and headers were cast on the same day and from the same concrete truck. The concrete was pumped into position using a tremie tube. This prevented aggregate segregation. Concrete was consolidated using a concrete vibrator.

Figure 3.26: Photograph of the header and column formwork and shoring

Two columns, one containing Grade 60 reinforcement and the other containing Grade 80 reinforcement, were fabricated to assess the influence of high strength reinforcing bars on column performance. Figure 3.27 shows a photograph of columns C1 and C2 fully constructed with all formwork and shoring removed.

Figure 3.27: Photograph of columns C1 and C2

4.0 MATERIALS USED IN CONSTRUCTION OF TEST SPECIMENS

4.1 REINFORCING STEEL

Two grades of reinforcing steel, Grade 60 and Grade 80, were used in the construction of the test specimens. Both reinforcing steels met the relevant requirements for *ASTM A706/A706M Standard Specification for Low-Alloy Steel Deformed and Plain Bars for Concrete Reinforcement*. Three bar sizes, #3 (#10M), #5 (#16M) and #6 (#19M) were used in the construction of the test specimens. The #3 (#10M) bar was produced into a coil while the #5 (#16M) and #6 (#19M) bars were produced in 20 ft (6.1 m) long straight bars. The ASTM A706 Grade 80 reinforcement was produced by Cascade Steel in McMinnville, OR for this research project. Farwest Steel in Eugene, OR fabricated all the reinforcement and provided the Grade 60 reinforcement material (also produced by Cascade Steel). Mechanical properties and chemical compositions of the reinforcement are shown in Table 4.1 and Table 4.2, respectively. Note that the heat numbers are the same for the different reinforcing steels in both tables. The heat numbers are shown in Table 4.1.

Table 4.1: Reinforcement mechanical and physical properties of reinforcement (mill data)

Bar size	ASTM A706 grade ksi (MPa)	Heat #	Yield ksi (MPa)	Tensile ksi (MPa)	Elong. % 8 in. (0.2 m)	Nom. wt %
#3 (#10M)	Gr. 60 (420)	087313	69.0 (476)	99.0 (683)	18	100
#5 (#16M)	Gr. 60 (420)	095113	65.5 (452)	97.5 (672)	16	100
#6 (19M)	Gr. 60 (420)	302213	66.5 (459)	97.0 (669)	17	95
#3 (#10M)	Gr. 80 (550)	083513	96.5 (665)	124.0 (855)	23	96
#5 (#16M)	Gr. 80 (550)	327612	87.5 (603)	114.0 (786)	13	96
#6 (#19M)	Gr. 80 (550)	327612	88.0 (607)	115.0 (793)	14	96

Table 4.2: Chemical composition of reinforcement (mill data)

Bar size	ASTM A706 grade, ksi (MPa)	C	Mn	P	S	Si	Cu	Ni	Cr	Mo	V	CE
#3 (#10M)	Gr. 60 (420)	0.280	1.280	0.007	0.024	0.190	0.180	0.070	0.060	0.020	0.020	0.500
#5 (#16M)	Gr. 60 (420)	0.290	1.250	0.009	0.022	0.170	0.220	0.080	0.080	0.021	-	0.510
#6 (19M)	Gr. 60 (420)	0.300	1.220	0.018	0.022	0.190	0.250	0.090	0.140	0.020	0.025	0.530
#3 (#10M)	Gr. 80 (550)	0.270	1.340	0.008	0.018	0.190	0.220	0.080	0.080	0.01	0.102	0.500
#5 (#16M)	Gr. 80 (550)	0.290	1.300	0.011	0.00	0.230	0.360	0.090	0.050	0.017	-	0.520
#6 (#19M)	Gr. 80 (550)	0.290	1.300	0.011	0.005	0.230	0.360	0.090	0.050	0.017	-	0.520

Testing was performed using a MTS Universal Testing Machine (UTM) connected to a Data Acquisition system (DAQ). The testing program was operated using a commercial software package. The UTM force and displacement were recorded. Tension testing was performed on each size and grade of reinforcement following ASTM E8/E8M-13a, *Standard Test Methods for Tension Testing of Metallic Materials* and ASTM A370-12a, *Standard Test Methods and Definitions for Mechanical Testing of Steel Products*. Three samples were tested for each size and grade. A two-inch (51 mm) gage length extensometer meeting ASTM E83-10a Standard Practice for Verification and Classification of Extensometer Systems was used to determine yield behavior. Figure 4.1 shows a photograph of the test set-up used. The extensometer was removed from the reinforcing bar sample at the onset of necking to prevent damaging the extensometer. When analyzing the Grade 60 reinforcement stress-strain data, the strain values up to 12 percent were obtained by the extensometer. For the Grade 80 reinforcement the extensometer was used for strain values up to 14 percent. This corresponds to the minimum elongation percent for an 8-inch (203 mm) gage length defined by ASTM A706 for Grade 60 and the Grade 80 reinforcement, respectively. After the extensometer was removed, the UTM displacement was used to compute the strain of the sample. Note that necking occurred prior to the 12 percent strain value for the #3 (#10M) Grade 80 bar so the extensometer was only used to log strain values up to 8 percent strain. The size of the raw data set was reduced by averaging every 20 data points to remove the noise or scatter of the data. The starting point was shifted to start at zero strain and zero stress. The yield stress and strain were determined using the 0.2 percent offset method (based off the modulus elasticity (slope) of the elastic region of the stress strain curve). As required by ASTM A706, the stress corresponding to a strain value of 0.0035 in./in. (mm/mm) is also reported. The stress and strain values at the onset of strain hardening is defined here as the point where the stress-strain curve begins to have a positive slope after the initial yield point. The tensile strength and corresponding strain are the values obtained at the maximum stress. The ultimate strain and corresponding stress are the values obtained at the maximum strain which occurred directly prior to the reinforcing bar fracturing. Data were

procured for all bar sizes and grades. Table 4.3 shows a summary of the tensile test results and Table 4.4 shows a summary of the tensile testing strain hardening results. Note the values in Table 4.3 and Table 4.4 are from the same tensile tests but were separated into two tables due to space constraints. Figures 4.2 through 4.7 show the stress-strain plots for each bar size and grade.

Figure 4.1: Photographs of reinforcement tensile testing

Table 4.3: Summary of tensile testing results for reinforcing bar

Bar size	Grade, ksi (MPa)	Yield point* (0.2% offset)		Yield point** (0.0035 EUL***)		Tensile strength		Ultimate strain		Elong. % in 8 inch (203 mm)
		Stress, ksi (MPa)	Strain, in./in. (mm/mm)	Stress, ksi (MPa)	Strain, in./in. (mm/mm)	Stress, ksi (MPa)	Strain, in./in. (mm/mm)	Stress, ksi (MPa)	Strain, in./in. (mm/mm)	
#3 (#10M)	Gr. 60 (420)	72.8 (502)	0.0045	69.9 (482)	0.0035	102.1 (704)	0.1185	73.2 (505)	0.1571	15
#5 (#16M)	Gr. 60 (420)	66.7 (460)	0.0046	66.6 (459)	0.0035	93.7 (646)	0.1310	71.8 (495)	0.1982	17
#6 (#19M)	Gr. 60 (420)	67.2 (463)	0.0043	66.7 (460)	0.0035	100.1 (690)	0.1402	81.5 (562)	0.2155	16
#3 (#10M)	Gr. 80 (550)	85.6 (590)	0.0055	73.3**** (590)	0.0035	120.5 (831)	0.0947	85.2 (588)	0.1378	13
#5 (#16M)	Gr. 80 (550)	86.2 (594)	0.0051	85.4 (589)	0.0035	114.3 (788)	0.1066	86.8 (598)	0.1555	14
#6 (#19M)	Gr. 80 (550)	86.1 (593)	0.0048	84.3 (581)	0.0035	114.0 (786)	0.1225	93.9 (647)	0.1893	15

* The yield point is defined as intersection of the 0.2 percent offset line and stress-strain curve

** The yield point is defined as the point on the stress-strain curve corresponding to a value 0.0035 strain

*** EUL: Extension Under Load

**** Did not meet specifications but other analysis methods indicate yield strength is greater than 80 ksi

Table 4.4: Summary of tensile rebar testing strain hardening results

Bar size	Grade, ksi (MPa)	Strain hardening point	
		Stress, ksi (MPa)	Strain, in./in. (mm/mm)
#3 (#10M)	Gr. 60 (420)	N.A.*	N.A.*
#5 (#16M)	Gr. 60 (420)	65.9 (454)	0.0123
#6 (#19M)	Gr. 60 (420)	67.0 (462)	0.0043
#3 (#10M)	Gr. 80 (550)	N.A.*	N.A.*
#5 (#16M)	Gr. 80 (550)	85.9 (592)	0.0084
#6 (#19M)	Gr. 80 (550)	85.5 (590)	0.0098

*N.A.: not available for the #3 reinforcing bar; this reinforcing bar exhibited a "round house" stress strain curve and did not exhibit yield plateau; as such, strain hardening data could not be determined.

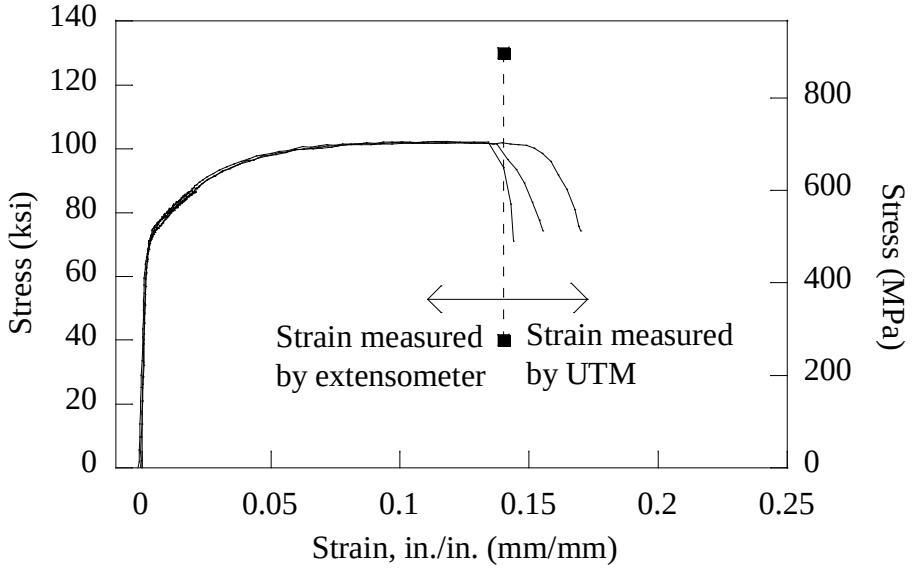

Figure 4.2: Stress strain plot of Grade 60 #3 (#10M) reinforcing bars

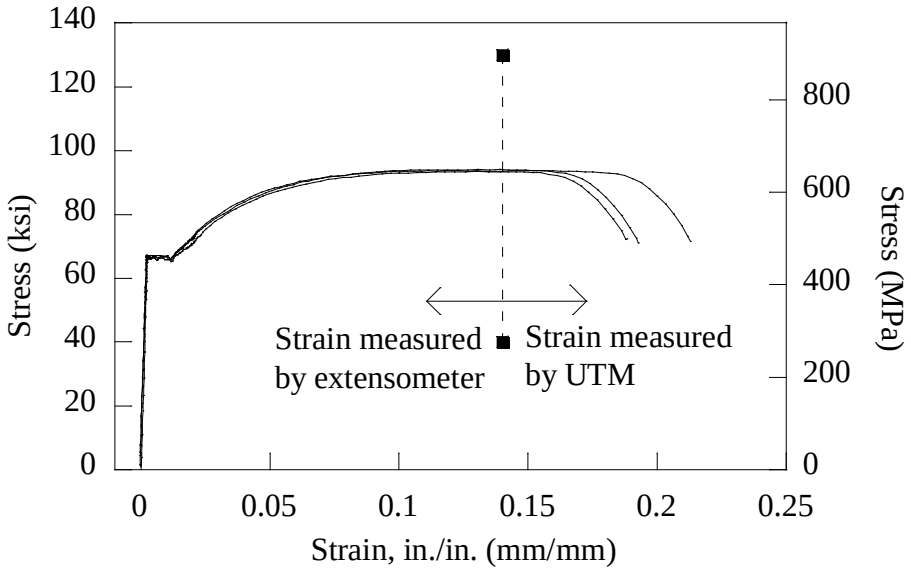

Figure 4.3: Stress-strain plot of Grade 60 #5 (#16M) reinforcing bars

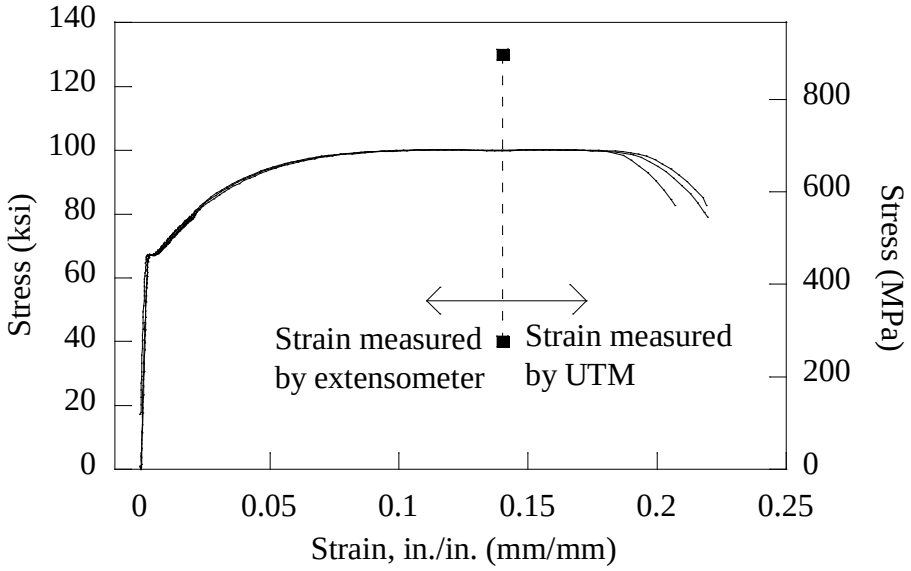

Figure 4.4: Stress-strain plot of Grade 60 #6 (#19M) reinforcing bars

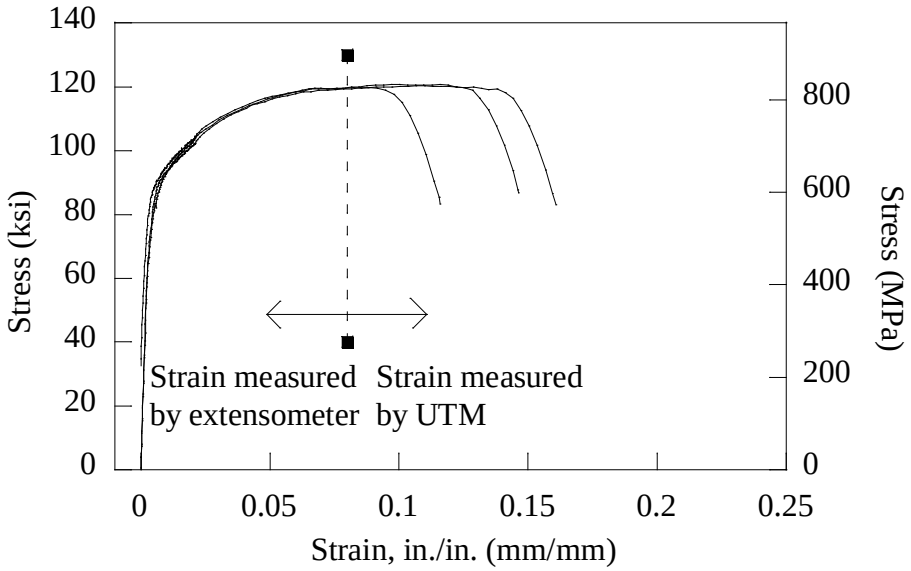

Figure 4.5: Stress-strain plot of Grade 80 #3 (#10M) reinforcing bars

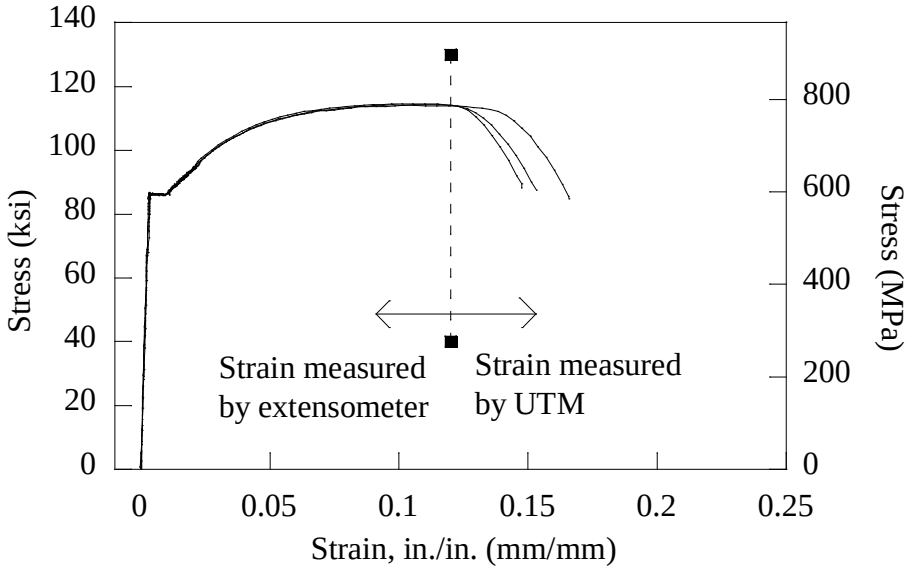

Figure 4.6: Stress-strain plot of Grade 80 #5 (#16M) reinforcing bars

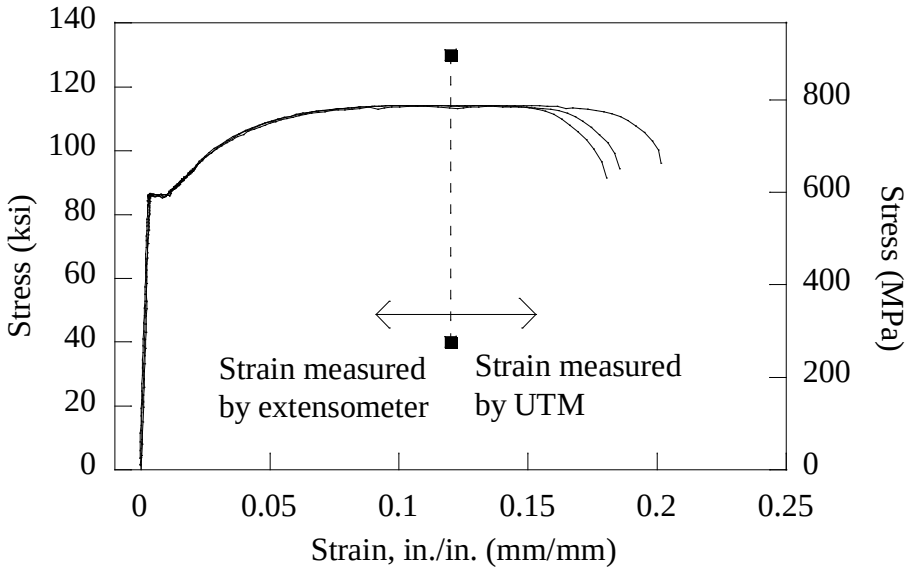

Figure 4.7: Stress-strain plot of Grade 80 #6 (#19M) reinforcing bars

4.2 CONCRETE

All concrete used in the construction of the test specimens was supplied by Knife River Corporation (Corvallis, OR). The concrete mixture contained a 3/8 inch (9.5 mm) maximum size aggregate (half scale of typical 3/4 inch (19.1 mm) and had a 28-day design compressive strength of 4 ksi (28 MPa). The mixture was also proportioned to be pumpable and had a minimum required slump of 5 inches (127 mm). The same mixture proportions were used for all specimens. A matrix of the tests conducted to characterize the concrete is shown in Table 4.5. The mixture proportions are shown in Table 4.6. A summary of the concrete properties are shown in Table 4.7. All concrete samples were made and cured following *ASTM C31/31M-12 Standard Practice for Making and Curing Concrete Test Specimens in the Field*, for making and curing specimens in the field. The standard cylinder size, 4-inch (102 mm) diameter by 8 inches (203 mm) tall, was used for compression strength testing according to *ASTM C39/39M-12a Standard Test Method for Compressive Strength of Cylindrical Concrete Specimens*, Modulus of elasticity (MOE) testing according to *ASTM C469/469M-10 Standard Test Method for Static Modulus of Elasticity and Poisson's Ratio of Concrete in Compression*, and splitting tensile testing according to *ASTM C496/496M-11 Standard Test Method for Splitting Tensile Strength of Cylindrical Concrete Specimens*. Beams (6-inch [152 mm] × 6-inch [152 mm] × 20-inch [508 mm]) were used for modulus of rupture (MOR) testing following *ASTM C78/78M-10 Standard Test Method for Flexural Strength of Concrete (Using Simple Beam with Third-Point Loading).* All concrete samples were stored next to the test columns to match cure conditions of the columns. Cylinders were demolded at the same time as the formwork of the columns was removed. Both ends of all concrete test cylinders were mechanically ground prior to compression testing to prevent eccentric loading. Three specimens were tested for each type of test.

Table 4.5: Concrete testing matrix

Sample	Compressive strength (ASTM C39)	Tensile strength (ASTM C496)	Modulus of elasticity (ASTM C469)	Modulus of rupture (ASTM C78)
Column and header	3-day, 7-day, 14-day, 28-day, days of testing	7-day, 28-day, days of testing	7-day, 28-day, days of testing	28-day, days of testing
Footing	7-day, 14-day, 28-day	Not tested*	Not tested*	Not tested*

*The footing concrete samples were only tested to confirm the 28-day strength and to determine when the footing formwork could be safely removed.

Table 4.6: Concrete mix proportions per cubic yard (meter)

Mix	W/(C+P) ratio	Coarse agg. (3/8 in) lbs (kg)	Fine agg. 1 (sand) lbs (kg)	Fine agg. 2 (mansand) lbs (kg)	Cement lbs (kg)	Fly ash lbs (kg)	Water gal (L)	Ad. mix. (WRDA_64) oz (g)
Average of all pours	0.47	1193 (541)	1597 (724)	278 (126)	506 (230)	91 (41)	20 (74)	24 (680)

Table 4.7: Summary of concrete properties for all columns*

Sample	Compressive Strength (ASTM C39), ksi (MPa)	Tensile Strength (ASTM C496), ksi (MPa)	Avg. Modulus of Elasticity (ASTM C469), ksi (MPa)	Modulus of Rupture (ASTM C78), ksi (MPa)
Column C1/C2 Footing 28-Day	4.247 (29.28)	Not tested*	Not tested*	Not tested*
Column C1/C2 day of C1 test (28-day)	4.770 (32.89)	0.682 (4.7)	3,011 (20,760)	0.507 (3.5)
Column C1/C2 day of C2 test (35-day)	4.837 (33.35)	0.677 (4.67)	2,585 (17,820)	0.539 (3.72)
Column C3/C4 Footing 28-Day	4.264 (29.40)	Not tested*	Not tested*	Not tested*
Column C3/C4 day of C3 test (19-day)	3.588 (24.74)	0.704 (4.85)	3,126 (21,560)	0.510 (3.51)
Column C3/C4 day of C4 test (27-day)	4.657 (32.11)**	0.619 (4.27)***	3,890 (26,821)****	0.619 (4.27)
Column C5/C6 Footing 28-Day	3.572 (24.63)	Not tested*	Not tested*	Not tested*
Column C5/C6 day of C5 test (94-day)	3.575 (24.65)*****	0.550 (3.79)	3,078 (21,220)	0.486 (3.35)
Column C5/C6 day of C6 test (103-day)	3.846 (26.51)*****	0.695 (4.79)	2,759 (19,020)	0.605 (4.17)

*The concrete for the footing samples were only tested to confirm the 28-day strength and to determine when the footing formwork could be safely removed

**Tested data are not available; Abram's Formula with experimental parameter equations determined by Yeh (*Yeh 2006*) was used to estimate the 27-day strength

***Tested data are not available. Value was estimated as the value of MOR.

****Tested data are not available. The value is estimated based on the estimated compressive strength following American Concrete Institute (ACI) 318-11 Section 8.5 (ACI Committee 318 2011)

*****A large number of variables effect the concrete strength. The same research assistants made and tested all of the samples for consistency. The exact cause of the lower concrete strength is unknown.

5.0 EXPERIMENTAL RESULTS: COLUMNS C1, C2, C3 AND C4

5.1 INTRODUCTION

This chapter provides test results from four of the six column test specimens; two columns were constructed with Grade 60 reinforcing bars (C1 and C3) and two columns were constructed with Grade 80 reinforcing bars (C2 and C4). Table 3.1 shows the testing matrix. The main objective of the testing is to assess the performance of the columns when subjected to cyclic loading when both columns are designed to have approximately the same moment capacity. Both columns were designed following the same design codes and standards.

The column testing procedure was described in Chapter 3. Visual and quantifiable measured observations are both reported in this chapter. Visual observations refer to cracking, concrete spalling, bar buckling, and bar fracture. Quantifiable measured observations include column lateral displacement, steel reinforcement strains, column tilt, applied axial load, footing and strong wall displacement, column curvature, and applied horizontal load. The column tilt, applied axial load, and footing and strong wall displacements serve as checks and results are not compared between columns. All data are analyzed until first bar fracture in this chapter.

5.2 COLUMN C1 EXPERIMENTAL RESULTS

This section provides the experimental test results for column C1. Column C1 was reinforced with A706 Grade 60 reinforcement corresponding to approximately the minimum longitudinal reinforcement ratio value (1.11 percent). The column has a moment-shear span ratio equal to six (6). This column will be used as a baseline to compare column C2 reinforced with A706 Grade 80 in Chapter 7.

5.2.1 Concrete Cracking

Crack mapping was performed after the final two peaks of each displacement cycle. Figure 5.1 shows two photographs of the crack mapping near the end of the testing. It can be seen that cracking was primarily dominated by flexure and cracking extended to approximately half the column height.

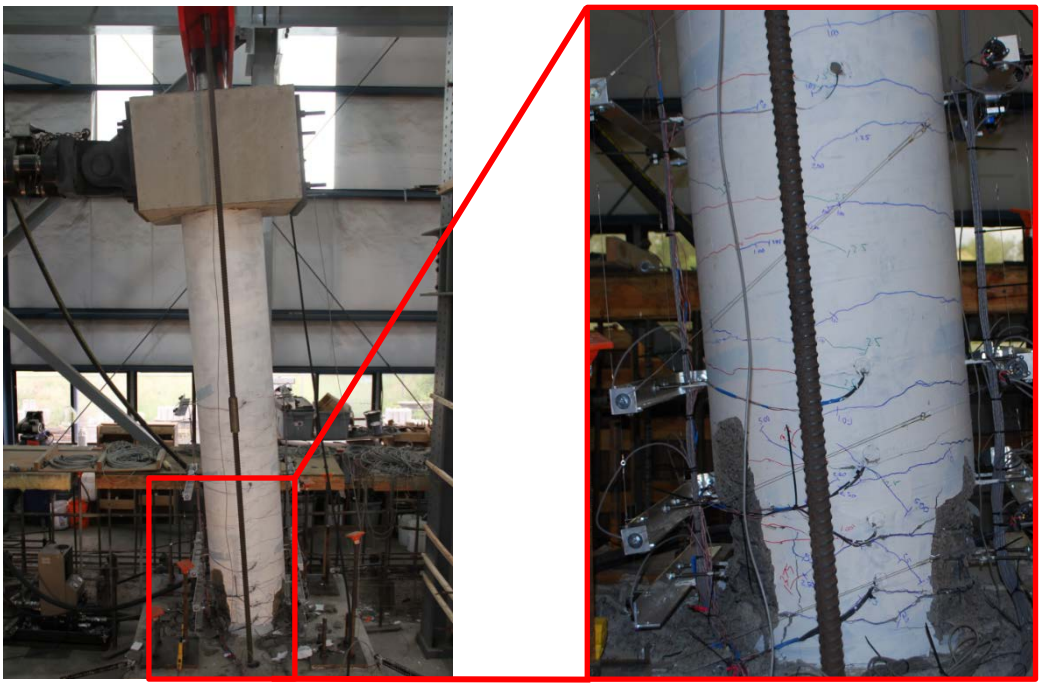

Figure 5.1: Photograph of column C1 crack mapping

5.2.2 Concrete Spalling

To assess time to spalling, the researchers recorded the displacement cycle at the onset of concrete spalling, at concrete spalling, and at deep concrete spalling. Onset of concrete spalling is defined here as the time (or in this case, cycle) when the concrete cover begins to exhibit vertical cracks. Figure 5.2 shows a photograph of the onset of concrete spalling as defined in this report. Concrete spalling is defined here as the cycle when the concrete cover begins to delaminate from the column core—note that this occurs on the faces in line with the loading direction. Also note that the column core is defined as the region contained by the spiral. Figure 5.3 shows a photograph of concrete spalling as defined in this report. Deep concrete spalling is defined as the cycle when the concrete core begins to crush. This was defined when the concrete contained within the spiral (core) spalled and the longitudinal bar was exposed. Figure 5.4 shows a photograph of deep concrete spalling as defined in this report. Table 5.1 provides a summary of the concrete spalling and values. All concrete spalling occurred after the longitudinal reinforcement yielded.

Figure 5.2: Photograph of the onset of concrete spalling

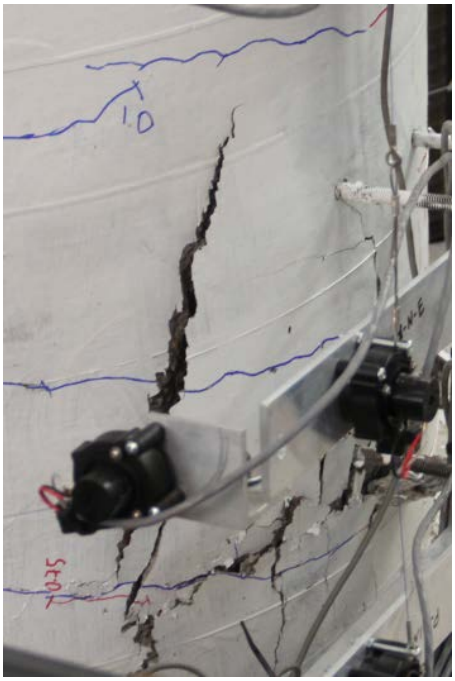

Figure 5.3: Photograph of concrete spalling

Figure 5.4: Photograph of deep concrete spalling

Table 5.1: Summary of column C1 concrete spalling

	Onset of concrete spalling	Concrete spalling	Deep concrete spalling
Displacement cycle in. (mm)	2.50 (63.5)	3.75 (95.3)	6.25 (159)
Drift ratio cycle	1.7%	2.6%	4.3%

5.2.3 Steel Reinforcing Bar Buckling

When the researchers were mapping cracks, a visual assessment of the reinforcement was also performed to assess if the longitudinal reinforcing bars exhibited buckling. The first longitudinal reinforcing bar buckled on the second to last peak of the 7.50-inch (191 mm) displacement cycle. Figure 5.5 shows a photograph of the first reinforcing bar that buckled. This reinforcing bar was the longitudinal reinforcing bar that was furthest south. The apex (away from verticality) of the buckled bar was located approximately 6 inches (150 mm) from the base of the column. Figure 5.5 shows the reinforcing bar buckled in very close proximity to the location of the strain gage. The silver tape in the photograph is part of the protection for the strain gages and is believed to have negligibly influenced the buckling of the reinforcing bar. However, the very slight reduction in area of the reinforcing bar cross-sectional area where the strain gage was installed may have had a minor influence on the location where the bar buckled, but negligible effects on the strength provided by the bar at onset of buckling.

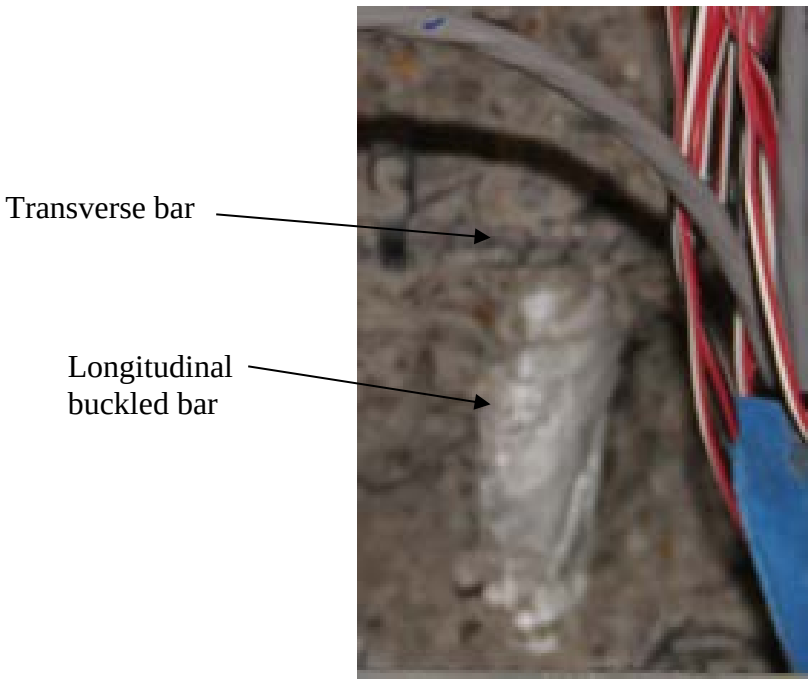

Figure 5.5: Photograph of column C1 bar at onset of buckling

5.2.4 Steel Reinforcing Bar Fracture

The first longitudinal bar to fracture occurred during loading to final peak of the 7.50-inch (191 mm) displacement cycle with an applied load of 27.22 kips (121.1 kN). The tip displacement was 7.51 inches (191 mm)—the tip displacement is defined here as the displacement of the north face of the header at the level of the longitudinal axis of the actuator. Post-failure observations indicate that the reinforcing bar fractured after a microcrack formed due to the bar buckling. The southernmost longitudinal bar fractured at an elevation approximately 6 inches (152 mm) from the base of the column. Figure 5.6 shows the fractured reinforcing bar—note that it is in very close proximity to the location of the strain gage. As mentioned above, the silver tape in the photo is part of protection for the strain gages and is believed to have had negligible influence on the buckling or the fracture of the reinforcing bar. This is the same bar shown in Figure 5.5.

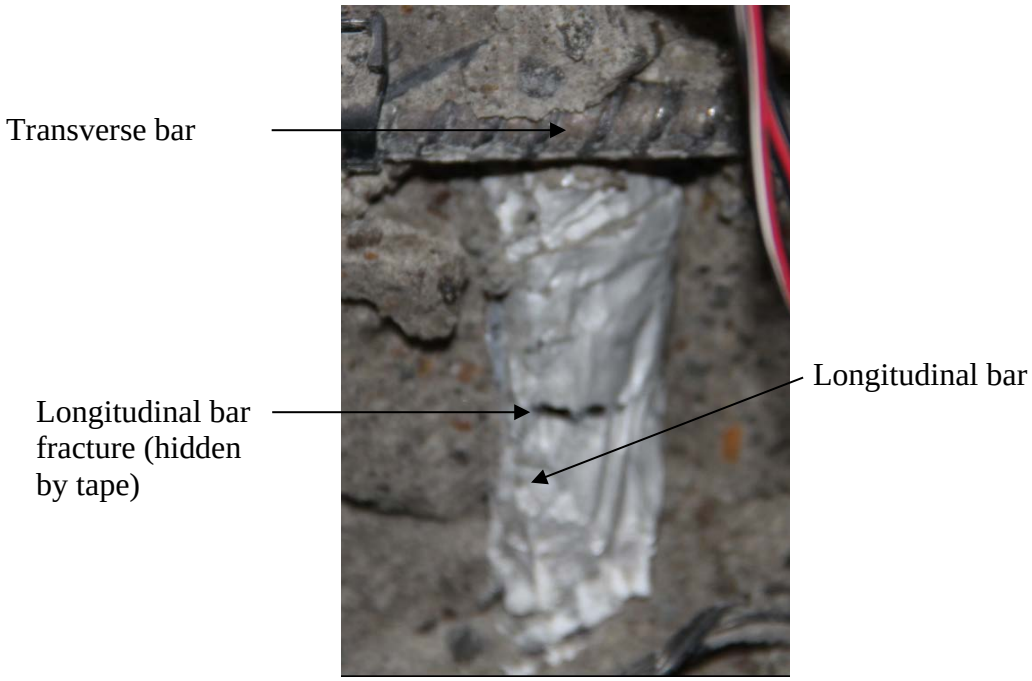

Figure 5.6: Photograph of column C1 first bar fracture

5.2.5 Column Tilt

The column tilt is measured using a tilt sensor mounted at the center of east face of the header and using a string potentiometer attached to the center of the north face of the header. Figure 5.7 shows a plot of the measured tilt (from tilt sensor) and the calculated tilt (from the string potentiometer) versus the applied force. Note that the tilt sensor was used only to validate the string potentiometer measurements. The calculated tilt is the tip displacement divided by the column height converted into degrees. As shown in the plot there is an increasing difference between the measured tilt and the calculated tilt as the applied force reaches its maximum and minimum values. This is likely due to the positioning of the string pot that measures the tip displacement. As the column is being pushed horizontally the column also bends creating an additional vertical component measured by the string pot.

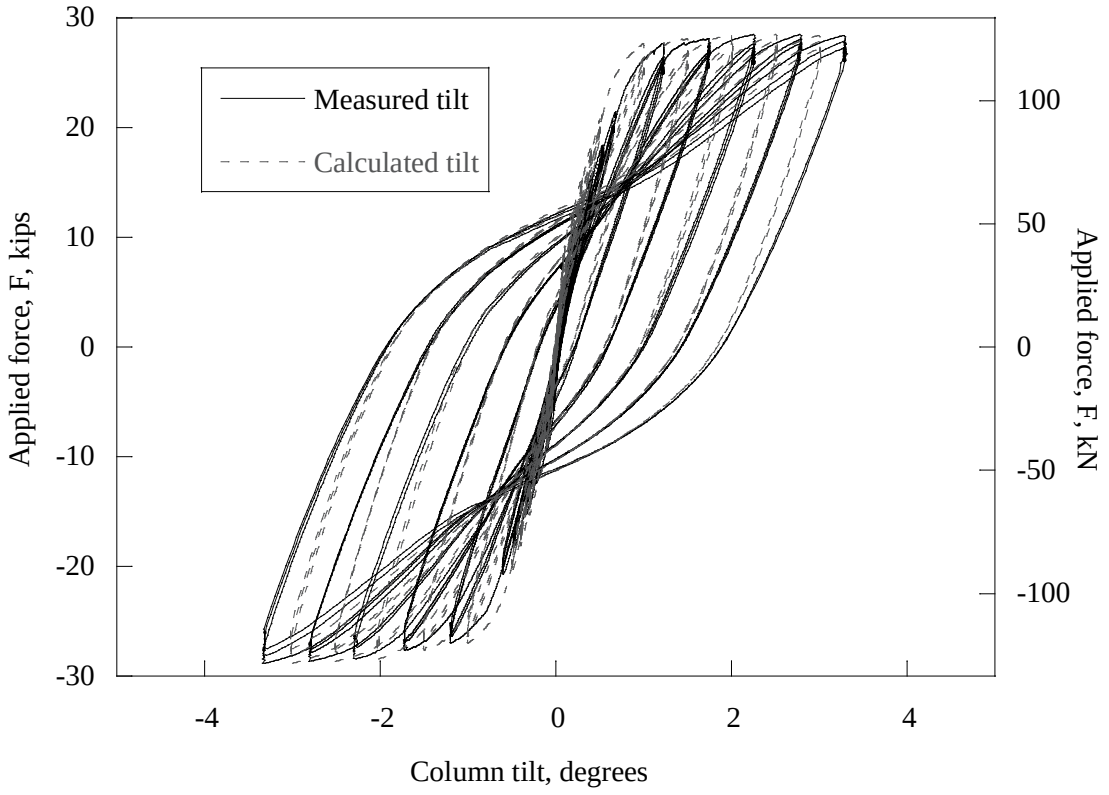

Figure 5.7: Tilt versus applied force of column C1

5.2.6 Vertical Load

The applied axial (vertical) load was measured using a load cell placed between the hydraulic jack and the column header. The initial target axial load was set to 90 kips (400 kN). A pneumatic nitrogen charged accumulator was used to attempt to keep the target axial load constant throughout testing. As shown in Figure 5.8, the axial load increased as the applied horizontal load increased. This is due to the prestressing bars being stressed as a result of the lateral displacement of the column. The axial load also dropped below 90 kips (400 kN) during the larger displacement cycles. This is likely due to the reduction in axial stiffness of the column as a result of concrete cracking and spalling.

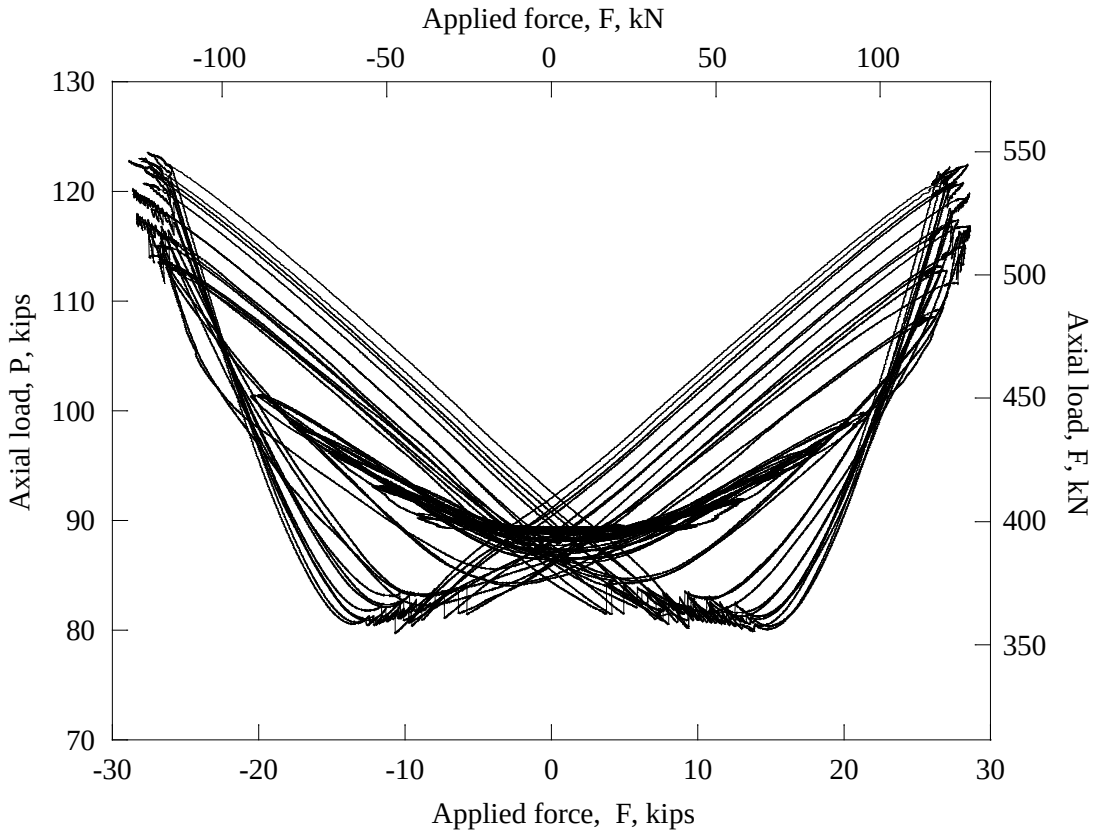

Figure 5.8: Applied force versus axial load of column C1

5.2.7 Footing Displacement and Strong Wall Displacement

The footing was instrumented with four vertical LVDTs at each corner of the footing top face and two LVDTs on the north face of the footing. These LVDTs were used to determine if the footing rotated or was displaced laterally during the testing. The data from the six LVDTs showed that there was neither significant rotation nor horizontal displacement of the footing. LVDT recordings never exceeded 0.03 inches (0.76 mm). The strong wall was instrumented with two string pots. The data from the string pots showed there was no significant displacement of the strong wall. The string pot recordings never exceeded 0.02 inches (0.51 mm).

5.2.8 Column Lateral Displacement

The lateral displacement of the column was measured at six (6) points along the height of the column. Locations of each point were provided in Chapter 3. Figure 5.9 shows the maximum and minimum lateral deflection at the 6 instrumentation levels for peak displacements of the 11 displacement cycles. In this figure, the elevation is normalized with respect to the column diameter, D, and the lateral displacement, Δ, is normalized by the column test height, H.

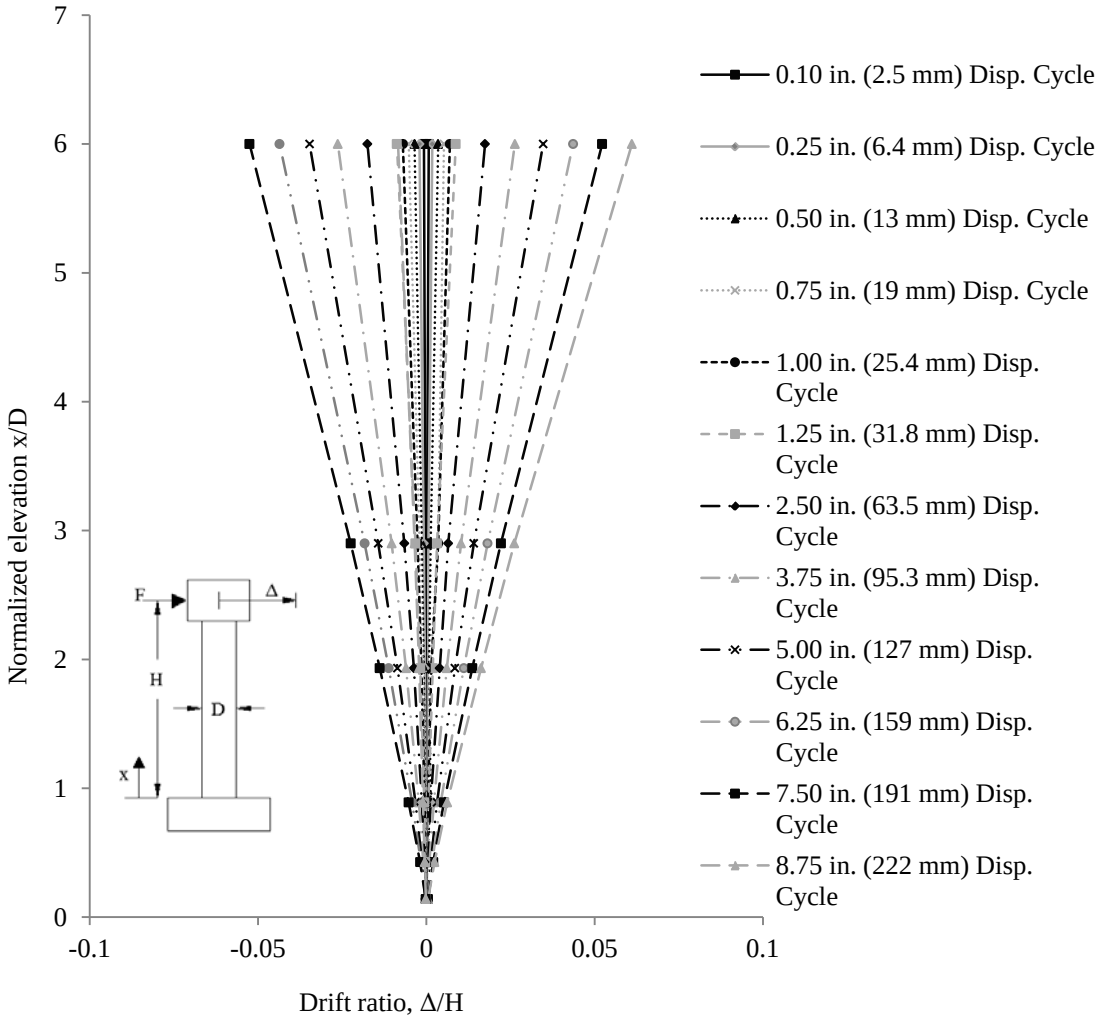

Figure 5.9: Drift ratio versus normalized elevation of column C1

5.2.9 Steel Reinforcement Strains

Reinforcing bar strains were recorded on both the longitudinal and transverse reinforcement. Locations of strain gages are provided in Chapter 3. The yield strain is defined as the strain determined using the 0.2 percent offset (point A) method minus 0.2 percent strain. A physical representation of this calculation is shown in Figure 5.10, where point A is the point determined by the 0.2 percent strain offset method and point B is the point used as the yield strain in the analysis. Point B was used in the analysis because it better represents when the steel first yields. For the longitudinal reinforcement where the stress-strain curve exhibited a yield plateau, point B represents the start of the yield plateau. For the spiral reinforcement where the stress-strain curve is represented with a round house curve, point B approximates the point where the curve is no longer linear. Figure 5.11 shows the maximum transverse reinforcement steel strains in column

C1, normalized by the yield strain value of the transverse reinforcement, for each displacement cycle along the height of the column. It is worth noting that only the maximum strains are shown in Figure 5.11 because the transverse reinforcement (spiral) never went into compression during testing. Table 5.2 shows the experimental yield strain values used to determine the yield strain used in the analysis. Note that normalized strain values in Figure 5.11 and Figure 5.12 represent the 11 cycles with normalized strains for the smallest cycles on the bottom of the stacks, and the largest cycles on the top.

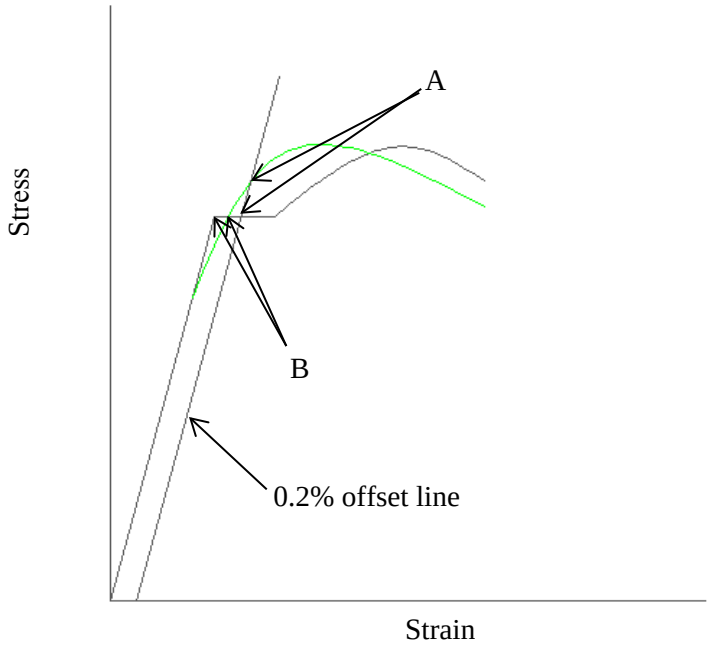

Figure 5.10: Diagram of yield strain determination

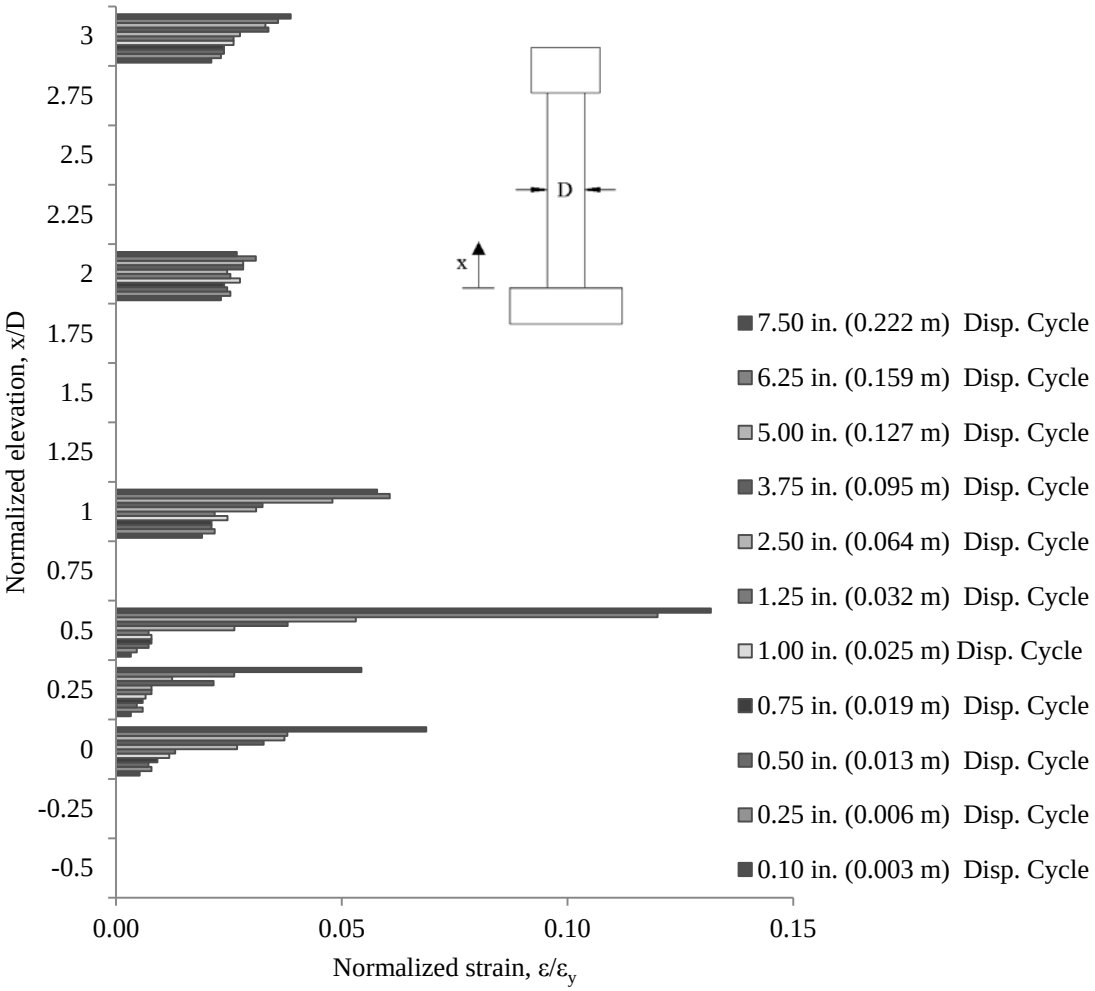

Figure 5.11: Strains of transverse reinforcement of column C1

Table 5.2: Column C1 yield strains used in the strain analysis

Reinforcement	Calculated yield strain	Measured yield strain (0.2% OM)
#3 (#10M) Grade 60 ksi (420 MPa)	0.0025	0.0045
#5 (#16M) Grade 60 ksi (420 MPa)	0.0026	0.0046

Occasionally a strain gage would electronically clip (reach maximum strain capacity) or get damaged and the data from the strain gage was no longer used. If this occurred at a location where there were two strain gages, the data from the damaged gage were no longer used, but data from the strain gage still functioning were used. The strain gage instrumentation level and displacement cycle where this occurred are:

1. level 4 during the 3.75-inch (95.3 mm) displacement cycle, and;

2. level 3 during the 5.00-inch (127 mm) displacement cycle.

Once the longitudinal strains exceed the 3 percent strain capacity of the strain gages, the value was reported as 3 percent for the tensile strains and the compression strain data were not used. The strain gage instrumentation level and the displacement cycle when the 3 percent limit was hit are:

1. level 2 during the 5.00-inch (127 mm) displacement cycle, and;

2. levels 3 and 4 during the 6.25-inch (159 mm) displacement cycle.

Figure 5.12 shows the maximum longitudinal reinforcement steel strains for column C1. Note that the longitudinal strains are dependent on both the positive and negative displacement cycles. The maximum positive displacement cycle corresponds to the maximum tension strain. The maximum negative displacement cycle corresponds to the maximum compressive strain. The ordinates in the figure are normalized by the column diameter, *D*, and the steel strain is normalized by the yield strain of the longitudinal reinforcement. The yield strain was computed in the same manner as the transverse yield strain. For the locations where two strain gages existed the average reading of the two gages was used for calculations. If one of the two strain gages electronically clipped or was damaged, the data for that strain gage were not used for the corresponding and future displacement cycles. The strain range of the strain gages was 3 percent. Once the strain gage data exceeded 3 percent, maximum compression strains were no longer reported and maximum tension strains were set at 3 percent. The normalized strain values are stacked in the same order as the transverse reinforcement strain plot.

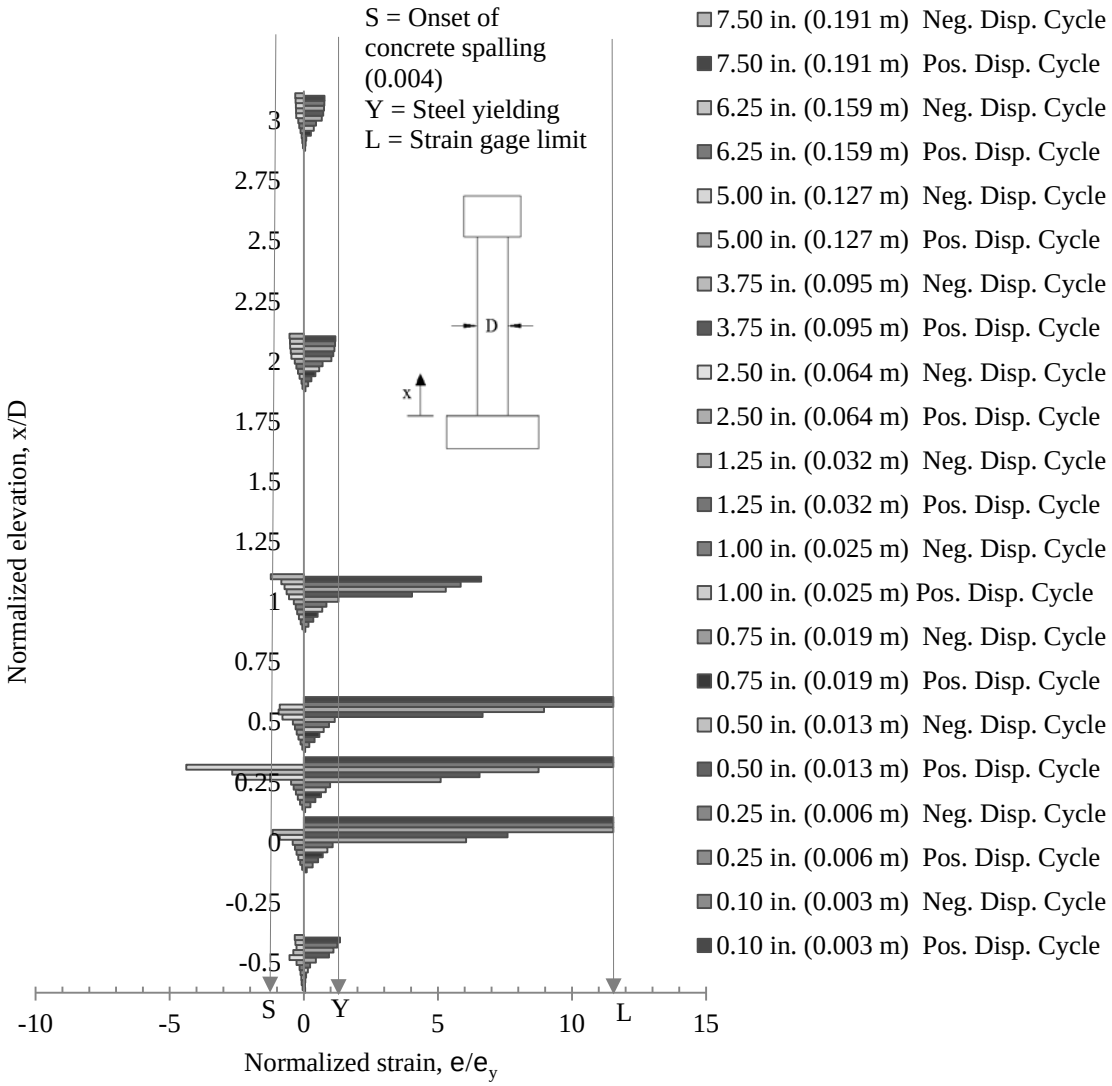

Figure 5.12: Strains of longitudinal reinforcement of column C1

5.2.10 Column Curvature

Flexural deformations of the columns can be determined using the rotation of the columns segments, measured using a pair of left and right linear potentiometers located at the left and right chords. This assessment and analysis assumes that the Bernoulli hypothesis, that plane sections remain plane after deformation, is valid. Figure 5.13 shows the physical representation of the variables used in the curvature analysis. The change of slope between two sections (e.g., sections *a* and *b*) is given by:

$$\theta_{ba} = \frac{\Delta S_2 - \Delta N_2}{h_p} \tag{5.1}$$

where ΔS_2 and ΔN_2 are the extensions and shortening of the left (south) and right (north) column chords measured using a pair of string potentiometers at section *b* relative to section *a* and h_p is the horizontal distance between the north and south string potentiometers (e.g., ΔS_2 and ΔN_2). Thus, the column end deflection obtained from the change of slope between *a* and *b* can be determined as follows:

$$b\Delta c,\, fl = \frac{\Delta S_2 - \Delta N_2}{h_p}\left(H - x_b\right) \tag{5.2}$$

where *H* is the column test height and x_b is the vertical distance to the centroid of section *b* measured from the top of the footing face. Using the same procedure the flexural deformation of another segment of the column can be determined using the change in slope between sections *b* and *c* as follows:

$$c\Delta c,\, fl = \frac{\Delta S_3 - \Delta N_3}{h_p}\left(H - x_c\right) \tag{5.3}$$

where ΔS_3 and ΔN_3 are the extensions and shortening of the left (south) and right (north) column chords measured using a pair of string potentiometers at section *c* relative to section *b*.

This same procedure can be used to determine the slope between sections *c* and *d* and to determine the slope between sections *d* and *e*. The sum of the discrete column flexural deformation gives the total column flexural deformations, $\Delta c,fl$:

$$\Delta c,\, fl = b\Delta c,\, fl + c\Delta c,\, fl + d\Delta c,\, fl + e\Delta c,\, fl \tag{5.4}$$

The fixed-end rotation of the column can be estimated using data from a pair of linear string potentiometers placed a short distance (approximately 6 inches [152 mm]) from the top of the footing face. As shown in Figure 5.13, the column and lateral movement due to the fixed-end rotation can be estimated as:

$$\Delta c,\, fe = \theta_{fe}(H - x_a) = \frac{\Delta S_1 - \Delta N_1}{h_p}\left(H - x_a\right) \tag{5.5}$$

where ΔS_1 and ΔN_1 are the extensions and shortening measured from the string potentiometers to the south and north of the column.

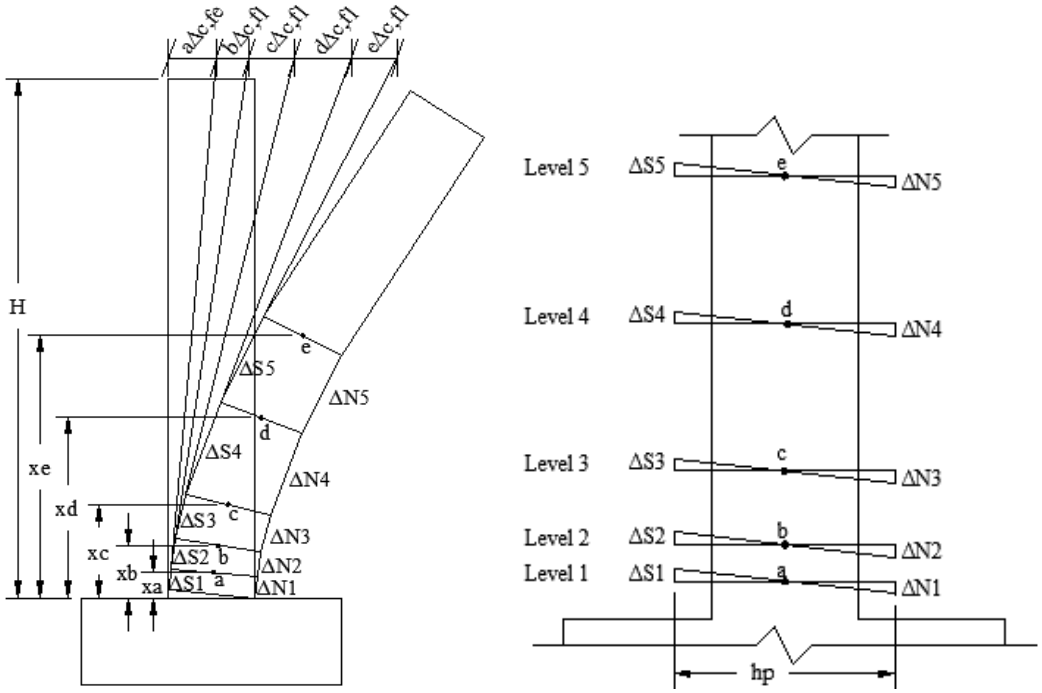

Figure 5.13: Physical representation of variables used in the curvature analysis

There are three main sources contributing to the fixed-end rotation. One contribution is from the deformations of the reinforcing bars passing through the joint core. Another contributing factor is from the global slippage of the reinforcing bars. The last source is the actual flexural deformation of the first 6 inches (153 mm) of the column.

The method adopted here to compute the deformations is approximate because the contributions of reinforcing bar elongation (strain penetration) and bond slip cannot be separated with this experimental set-up.

The curvature is computed at each of the five instrumentation levels described in Chapter 3 for each displacement level. Note that with the instrumentation set-up the computed curvatures are actually an average of the curvature over a section of the columns height in between each instrumentation level. The curvature is reported for the elevation corresponding to the midpoint between each instrumentation level. The elevation and curvature are both normalized by the column diameter, *D*. The elevation is divided by the column diameter, *D*, and the curvature is multiplied by the column diameter, *D*. The calculation procedure used to determine the curvature at each level, *i*, is as follows:

1. Compute ΔN_i and ΔS_i:

$$\Delta N_i = \frac{\Delta N_{Ei} + \Delta N_{Wi}}{2} \tag{5.6}$$

$$\Delta S_i = \frac{\Delta S_{Ei} + \Delta S_{Wi}}{2} \tag{5.7}$$

where ΔN_{Ei} and ΔN_{Wi} are the measured changes in lengths of the curvature string potentiometers on the north side of the column at level, *i*, and ΔS_{Ei} and ΔS_{Wi} are the measured change in length of the curvature string pots on the south side of the column at level, *i*, respectively. The values of ΔN_i and ΔS_i are the average change in lengths of the curvature string potentiometers at each level, *i*, on the north and south sides respectively;

2. Compute the maximum Δ at each level for each displacement cycle as follows:

$$\Delta_i = \Delta S_i - \Delta N_i \tag{5.8}$$

where Δ_i is the total change in length of the curvature string potentiometers at each level, *i*. This value is used as the vertical component of a right triangle to compute the rotation, θ, at each level, *i*;

3. Compute the rotation, θ, at each level, *i*, as follows:

$$\Delta\theta_i = \frac{\Delta_i}{h_p} \tag{5.9}$$

where $\Delta\theta_i$ is the rotation at each level, *i*;

4. Compute the curvature, Ψ, at each level, *i*, as follows:

$$\Psi_i = \frac{\Delta\theta_i}{\Delta_i} \tag{5.10}$$

where Ψ_i is the curvature at each level, *i*.

Figure 5.14 shows the curvature for each displacement cycle along the height of the column.

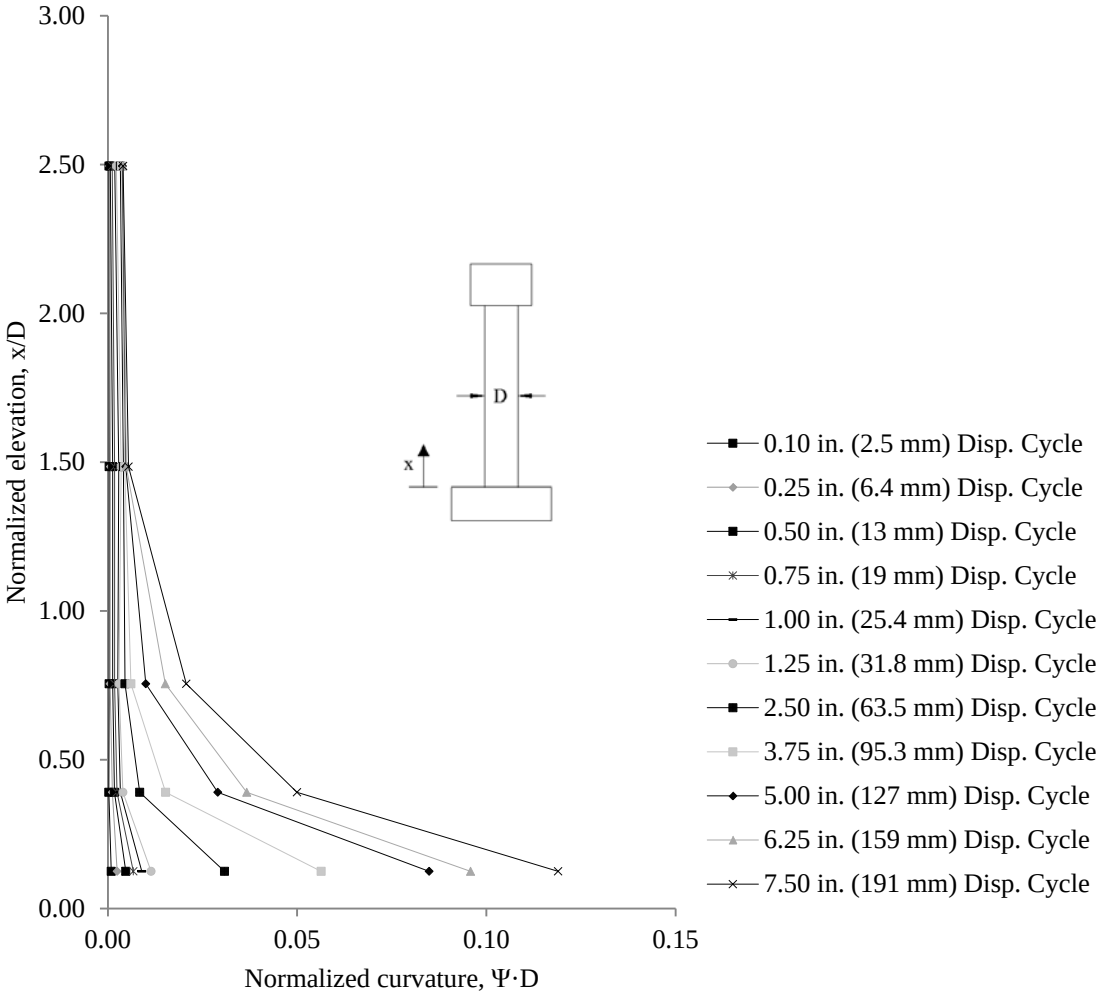

Figure 5.14: Normalized curvature versus normalized elevation of column C1

5.2.11 Applied Horizontal Load

The applied horizontal load was measured using a group of parallel load cells within the actuator. Figure 5.15 shows the applied load versus the drift ratio. The maximum applied force was 28.86 kips (128.4 kN) and the maximum drift ratio was 5.3 percent.

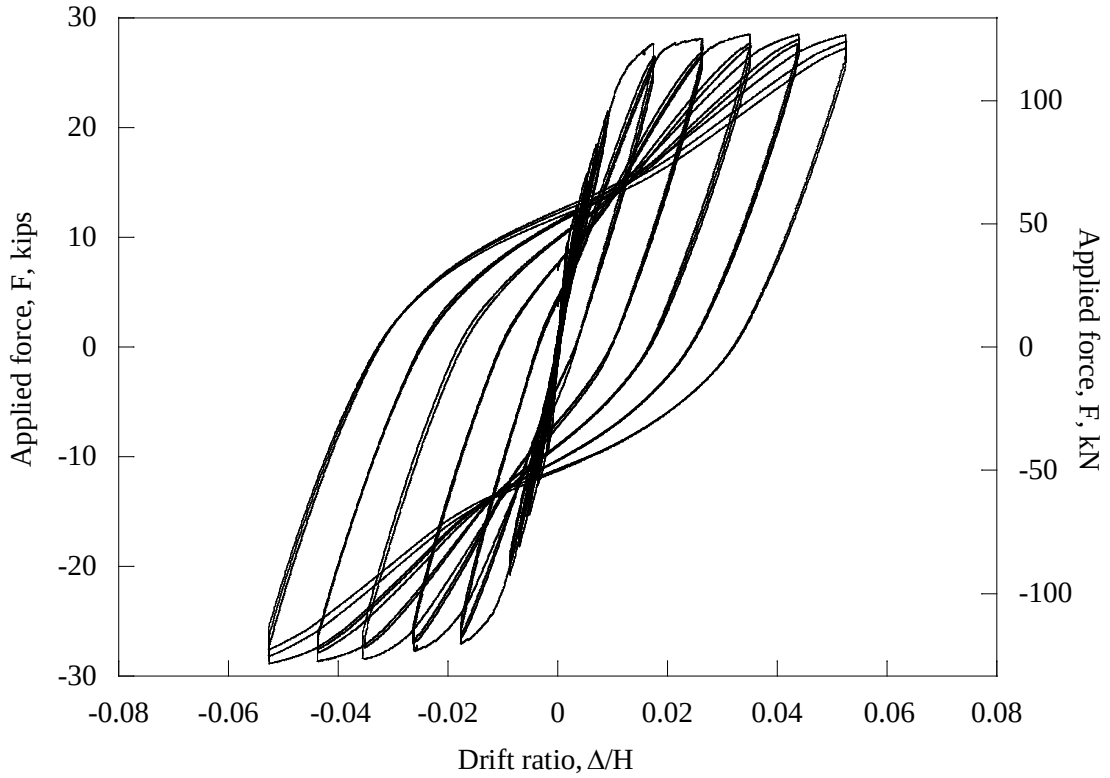

Figure 5.15: Drift ratio versus applied force of column C1

5.3 COLUMN C2 EXPERIMENTAL RESULTS

The experimental data of column C2 are presented in this section. Column C2 was designed to have approximately the same nominal moment capacity as column C1. However column C2 is reinforced with A706 Grade 80 whereas column C1 is reinforced with A706 Grade 60.

5.3.1 Concrete Cracking

As with column C1, crack mapping was performed at the final two peaks of each displacement cycle. Figure 5.16 shows two photographs of the crack mapping near the end of the testing. The figure shows that cracking was primarily dominated by flexure and progressed to shear dominated cracks towards larger displacement cycles. Cracking extended to approximately two thirds the column height.

Figure 5.16: Photograph of column C2 crack mapping

5.3.2 Concrete Spalling

The displacement cycles at the onset of concrete spalling, concrete delamination, and deep concrete spalling were observed and recorded. Table 5.3 shows a summary of the concrete spalling. As with column C1, all concrete spalling occurred after the longitudinal reinforcement yielded.

Table 5.3: Summary of column C2 concrete spalling

	Onset of concrete spalling	Concrete spalling	Deep concrete spalling
Displacement cycle in. (mm)	2.50 (63.5)	3.75 (95.3)	8.75 (222)
Drift ratio cycle	1.7%	2.6%	3.1%

5.3.3 Steel Reinforcing Bar Buckling

At the time of crack mapping, the column was also inspected to determine if any of the longitudinal bars had buckled. The first longitudinal bar buckled on the south side of the column during the 8.75 inch (222 mm) displacement cycle. Figure 5.17 shows a photograph of the first reinforcing bar that buckled. The apex of the buckled reinforcing bar was located approximately 8.5 inches (216 mm) from the base of the column.

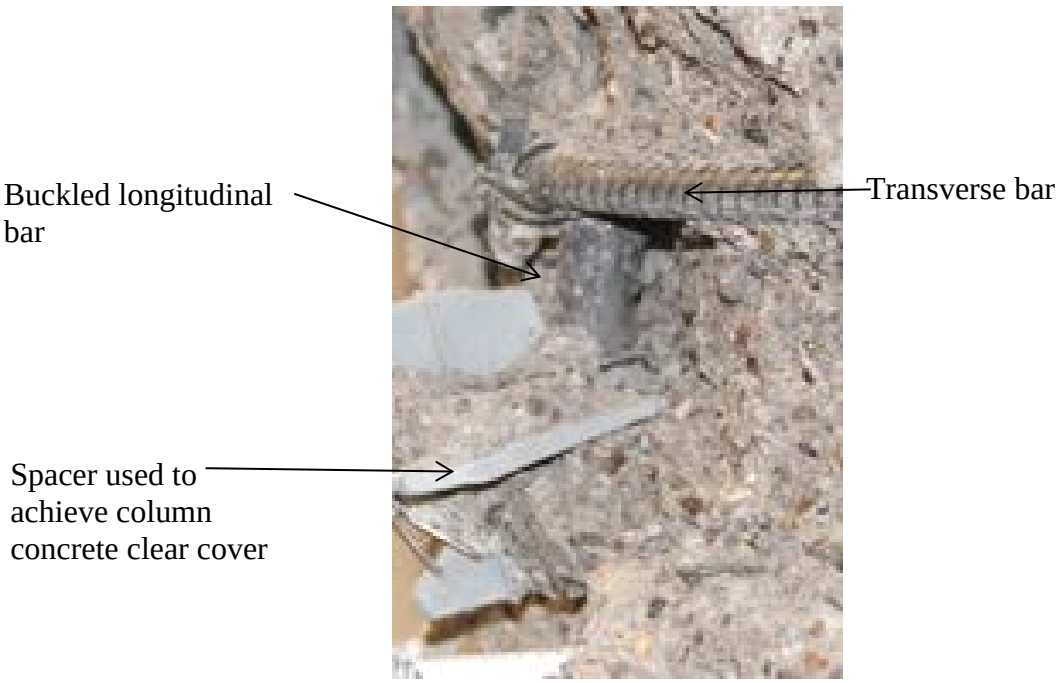

Figure 5.17: Photograph of first bar buckling in column C2

5.3.4 Steel Reinforcing Bar Fracture

The first longitudinal reinforcing bar that fractured occurred on the return cycle after the first peak of the 8.75 inch (222 mm) displacement cycle. The applied load was 10.94 kips (48.66 kN) and the tip displacement was 1.21 inches (30.7 mm). Post-failure observations indicate that the bar fractured after a microcrack formed due to the bar buckling. Figure 5.18 shows that the southernmost longitudinal reinforcing bar fractured at an elevation approximately 8.5 inches (216 mm) above the base of the column. The bar in this figure is the same bar shown in Figure 5.17.

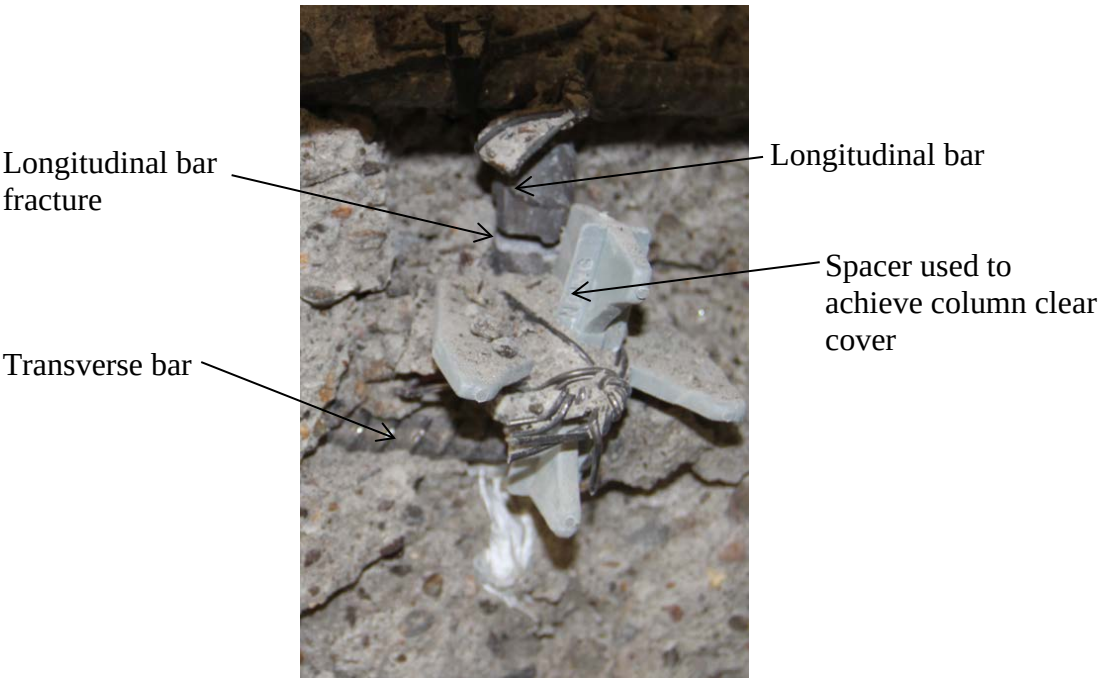

Figure 5.18: Photograph of first bar fracture in column C2

5.3.5 Column Tilt

The column tilt was measured in the same manner as column C1. Figure 5.19 shows a plot of the measured tilt and the calculated tilt versus the applied force. As seen in the plot there is an increasing difference between the measured tilt and the calculated tilt as the applied force reaches its maximum and minimum values. As with column C1, this is likely due to the positioning of the string pot that measures the tip displacement. As the column is being pushed horizontally the column also bends creating an additional vertical component measured by the string pot.

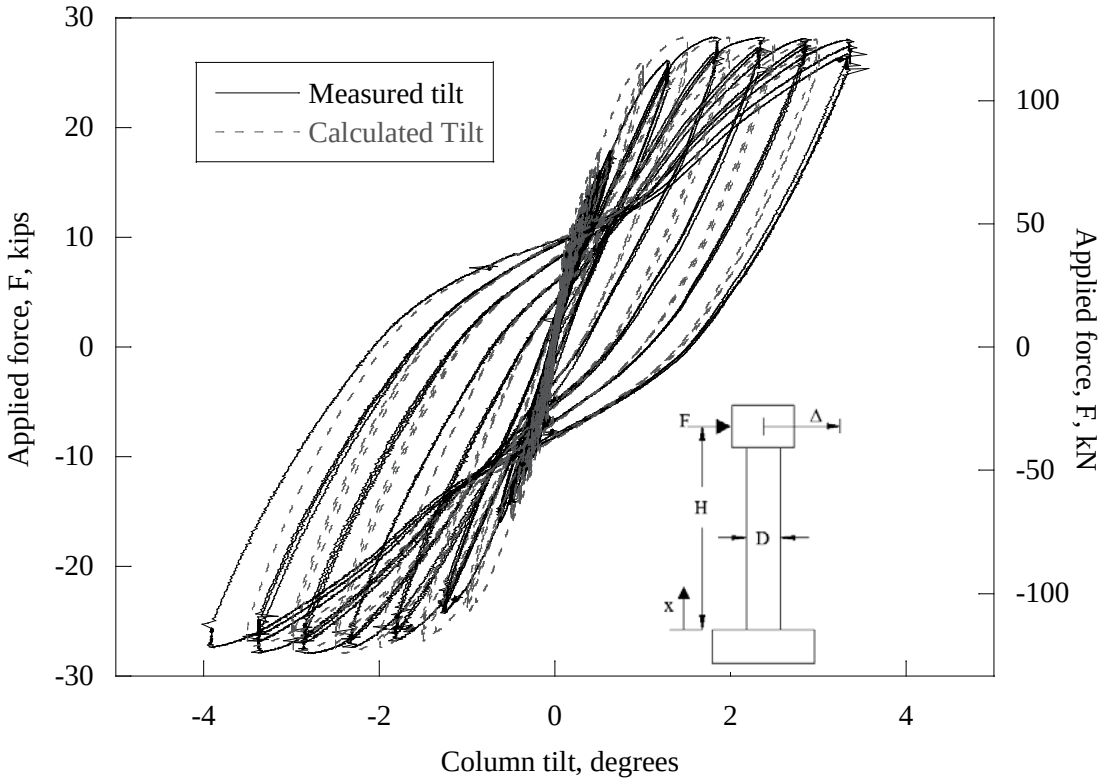

Figure 5.19: Tilt versus applied force of column C2

5.3.6 Vertical Load

The axial (vertical) load was applied in the same manner as described for column C1. The initial axial load was set to 90 kips (400 kN). The same procedure described for column C1 was used for column C2 to attempt to minimize the change in axial load during testing. As shown in Figure 5.20, the axial load increased as the applied horizontal load increased for column C2. The axial load for column C2 also dropped below the initial 90 kips (400 kN). The figure exhibits a similar shape as the figure for column C1, indicating that load histories were similar. The small differences in shape and the maximum axial load between columns C1 and C2 may be due to a slight difference in the pneumatic nitrogen accumulator pre charge.

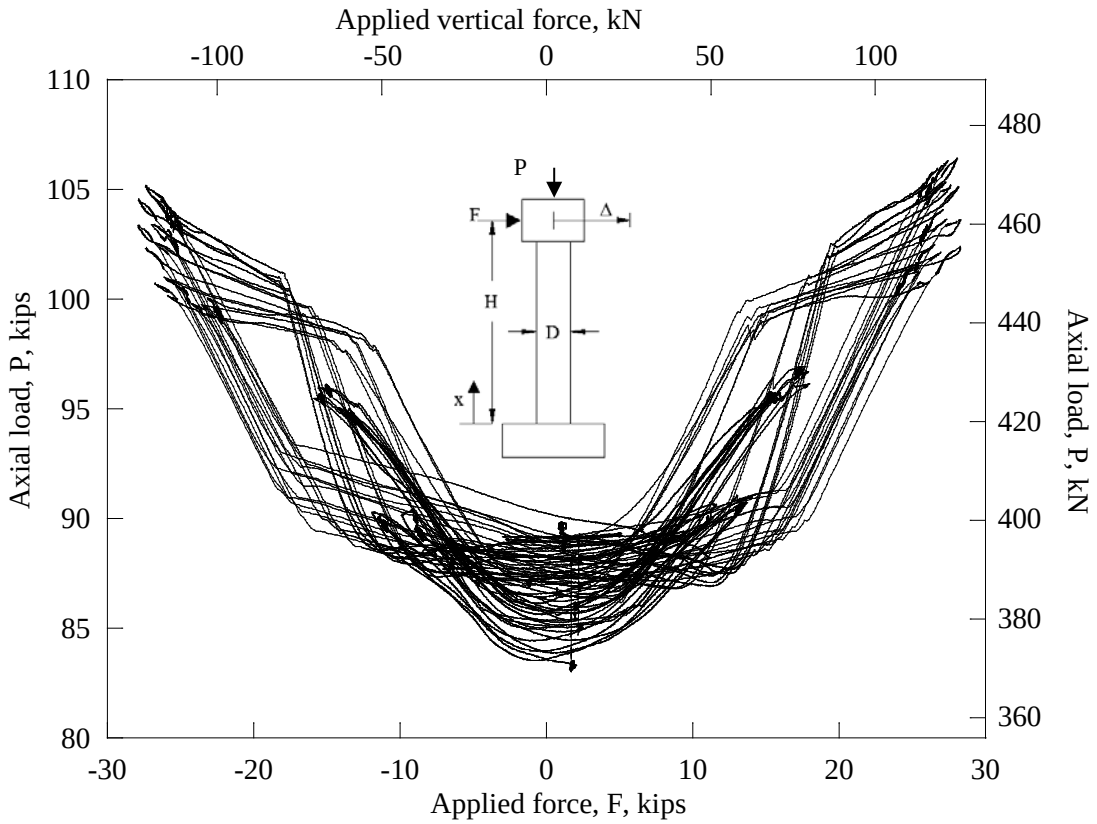

Figure 5.20: Applied force versus axial load of column C2

5.3.7 Footing Displacement and Strong Wall Displacement

The footing was instrumented with four vertical LVDTs at each corner of the top face of the footing and two LVDTs on the north face of the footing as discussed in Chapter 3 to determine if the footing rotated or displaced during the testing. The data from the six LVDTs showed that there was neither significant rotation nor horizontal displacement of the footing. No LVDT reading ever exceeded 0.05 inch (1.3 mm). The strong wall was instrumented with two string pots. The data from the string pots showed there was no significant displacement of the strong wall. The string pot recordings never exceeded 0.02 inches (0.51 mm).

5.3.8 Column Lateral Displacement

The lateral displacement of the column was measured at six points along the height of the column. Details of the point locations were discussed earlier. Figure 5.21 shows the maximum and minimum lateral deflections at the 6 points for the 12 displacement cycles. As with the data from column C1, the elevation is normalized with respect to the column diameter, D, and the lateral displacement, Δ, is normalized by the column test height, H. Figure 5.13 shows the

geometry and physical interpretation of the variables used in the column lateral displacement analysis, Δ, D, and H. Note that Δ, is taken at each of the 6 points along the height of the column.

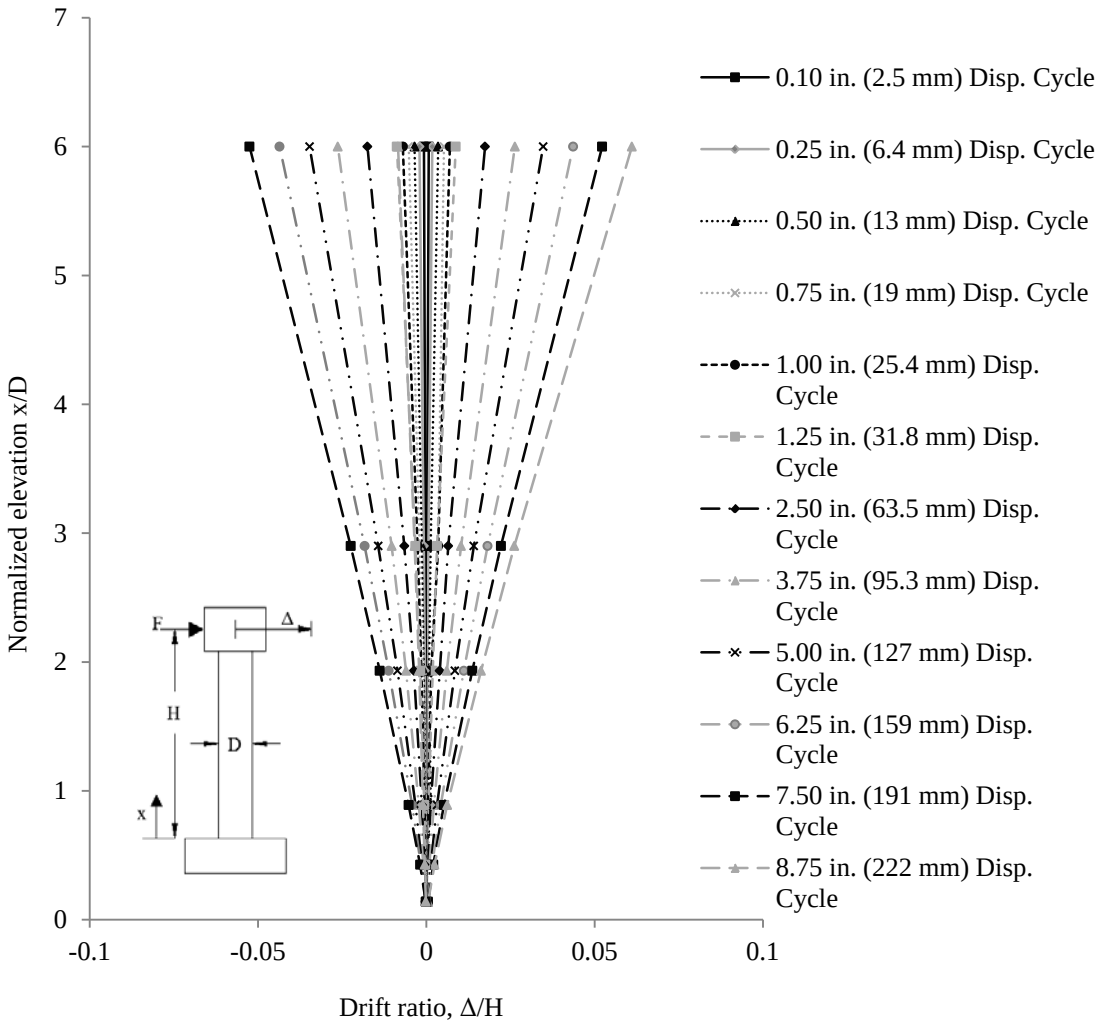

Figure 5.21: Normalized drift ratio versus normalized elevation of Column C2

5.3.9 Steel Reinforcement Strains

Steel reinforcing strains were recorded on both the longitudinal and transverse reinforcement. Locations of the strain gages for column C2 were provided in Chapter 3. Figure 5.22 shows the maximum transverse steel reinforcement strains for column C2 for each displacement cycle along the height of the column. The elevation is normalized by the column diameter, D, and the steel strain is normalized by the yield strain of the transverse reinforcement. The yield strain is defined in the same manner as described in section 5.2.6 for column C1. Note that the spiral

within the footing never went into tension during the final displacement cycle; the value shown in the figure is the minimum compression value.

As previously mentioned, occasionally a strain gage would electronically clip or get damaged and the data from the strain gage were no longer used. If this occurred at a location where there were two strain gages, the data from the damaged gage were no longer used, but data from the strain gage still functioning were used. The strain gage instrumentation level and displacement cycle where this occurred are:

1. level 3 during the 2.50-inch (63.5 mm) displacement cycle;

2. level 4 during the 6.25-inch (159 mm) displacement cycle, and;

3. level 2 during the 7.50-inch (191 mm) displacement cycle.

Once the longitudinal strains exceed the 3 percent strain capacity of the strain gages the value was reported as 3 percent for the tensile strains and the compression strain data was not used. The strains gage instrumentation level and the displacement cycle when the 3 percent limit occurred are:

1. level 3 during the 6.25-inch (159 mm) displacement cycle, and;

2. level 2 during the 8.25-inch (210 mm) displacement cycle.

Figure 5.23 shows the maximum longitudinal steel reinforcement strains of column C2 for each positive and negative displacement cycle along the height of the column. The maximum positive displacement cycle corresponds to the maximum tension strain. The maximum negative displacement cycle corresponds to the maximum compressive strain. The elevation is also normalized by the column diameter, D, and the steel strain is normalized by the yield strain of the longitudinal reinforcement. The yield strain was computed in the same manner as the transverse yield strain. Note that the transverse and longitudinal strains are stacked in terms of the displacement cycle, i.e. the lowest bar strains at each elevation represents 0.10 inch (2.5 mm) displacement cycle and the highest bar represents the 8.75 inch (0.222 m). Table 5.4 shows the experimental yield strain values used to determine the yield strain values used in the analysis. Note that the values in this table are different than the values used for column C1 because the grade of reinforcement is different between the two columns.

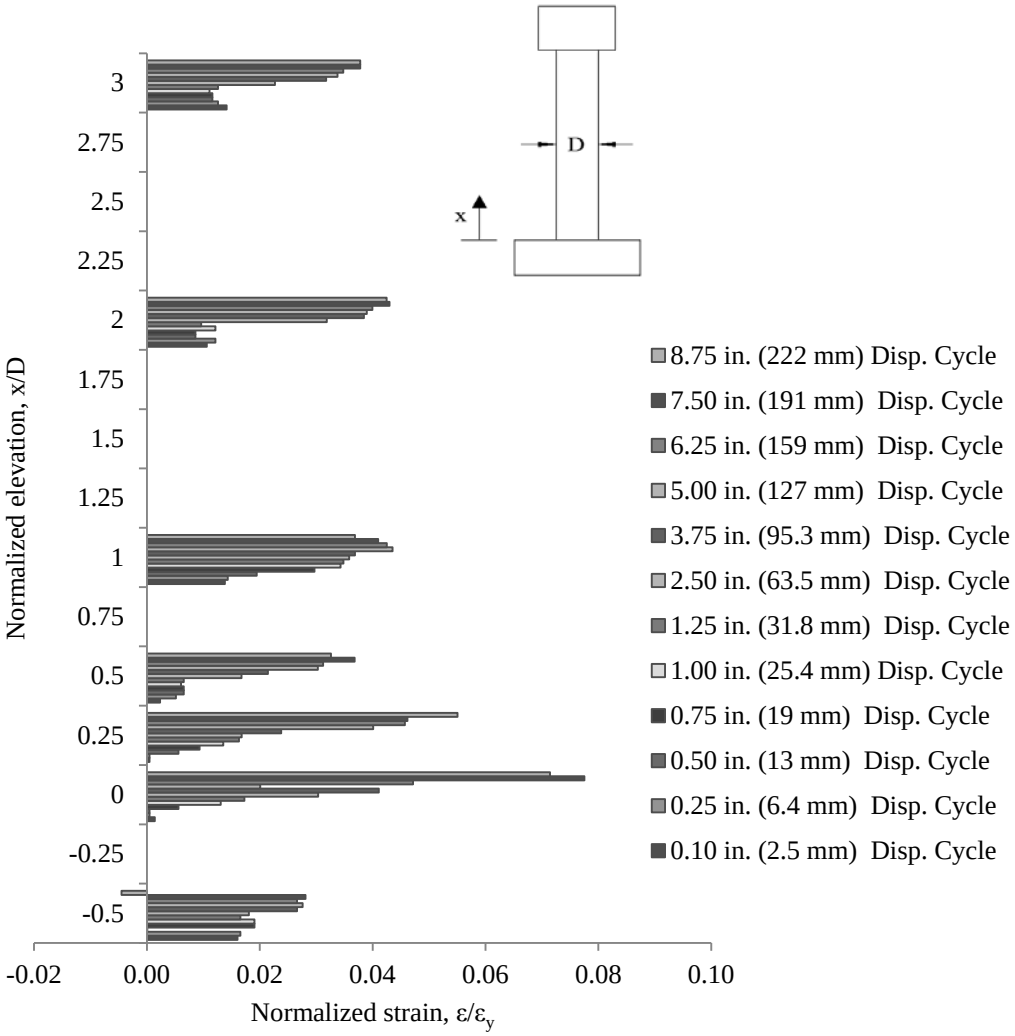

Figure 5.22: Transverse strains in Column C2

Table 5.4: Column C2 yield strains used in the strain analysis

Reinforcement	Calculated yield strain	Measured yield strain (0.2% OM)
#3 (#10M) Grade 80 ksi (550 MPa)	0.0035	0.0055
#5 (#16M) Grade 80 ksi (550 MPa)	0.0031	0.0051

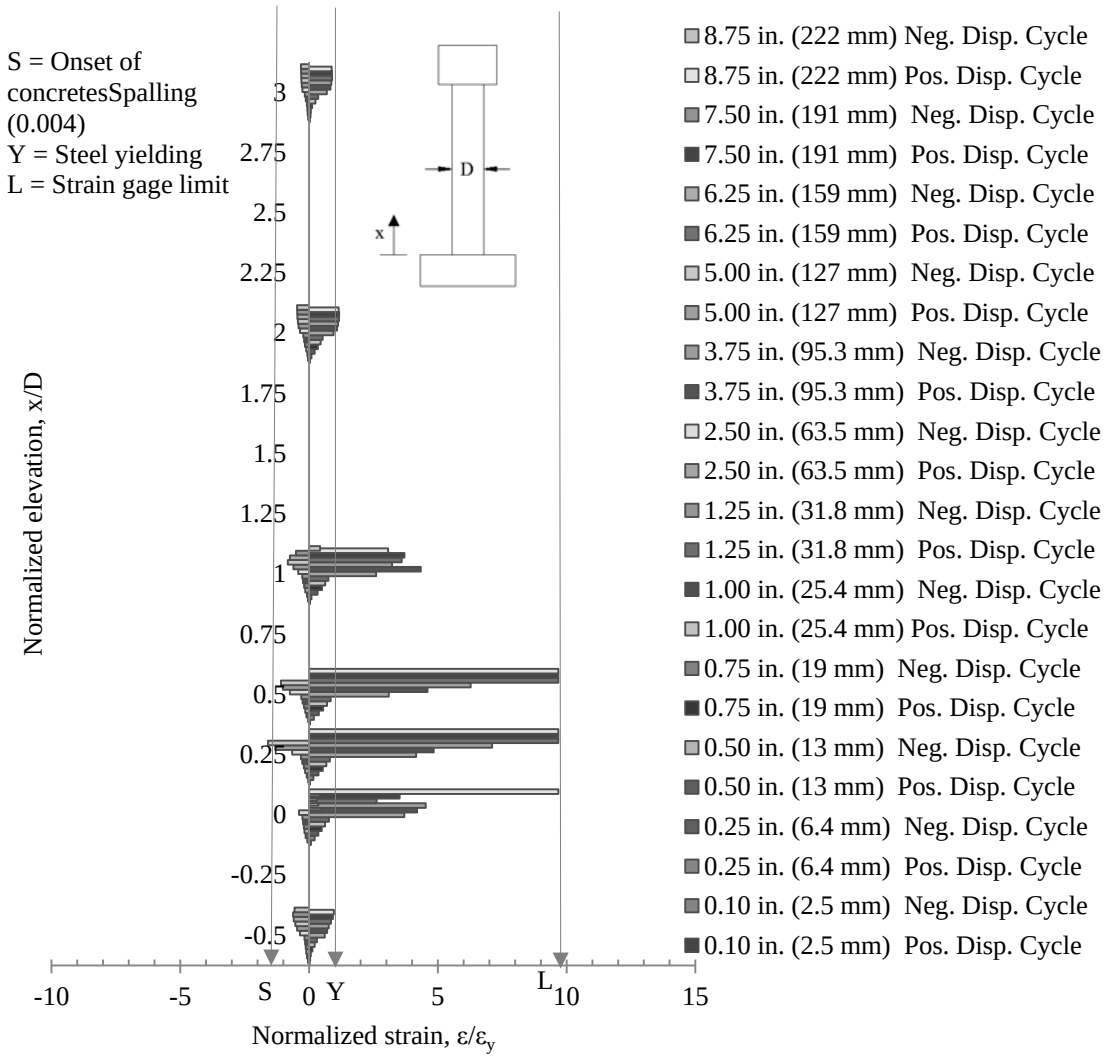

Figure 5.23: Longitudinal reinforcement strains in Column C2

5.3.10 Column Curvature

The curvature was computed at each of the five instrumentation levels for each displacement level. Figure 5.24 shows the curvature for each displacement cycle along the height of the column. The elevation and curvature are both normalized by the column diameter, *D*. The elevation is divided by the column diameter, *D*, and the curvature is multiplied by the column diameter, *D*. Figure 5.13 shows the physical representation of the variables used in the curvature computations. Calculations used to determine the curvature at each level, *i*, are the same as for column C1 shown in section 5.2.7.

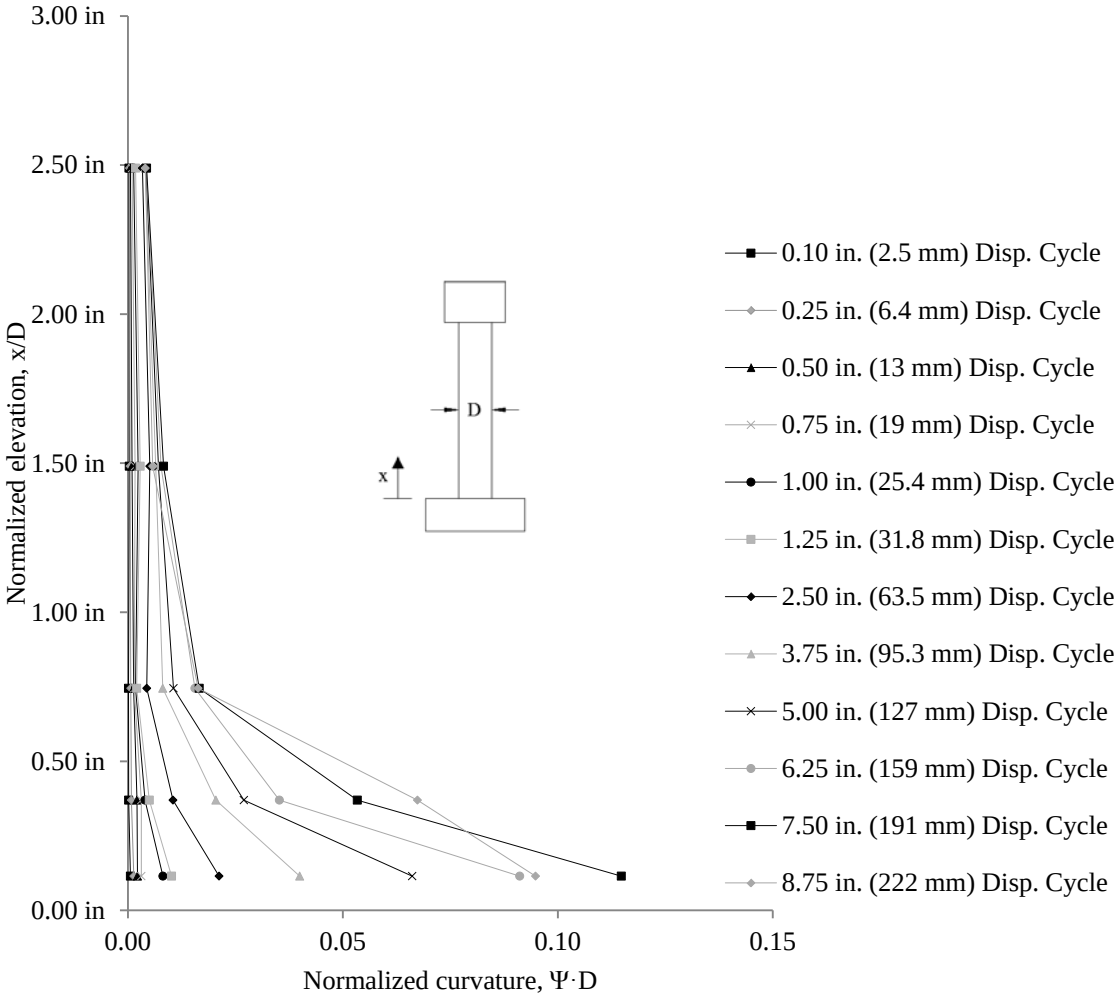

Figure 5.24: Normalized curvature versus normalized elevation of column C2

5.3.11 Applied Horizontal Load

The applied horizontal load was measured by a group of parallel load cells within the actuator. The applied load was plotted against the drift ratio and is shown in Figure 5.25**.** The maximum applied force was 28.24 kips (125.6 kN) and the maximum drift ratio was 6.1 percent.

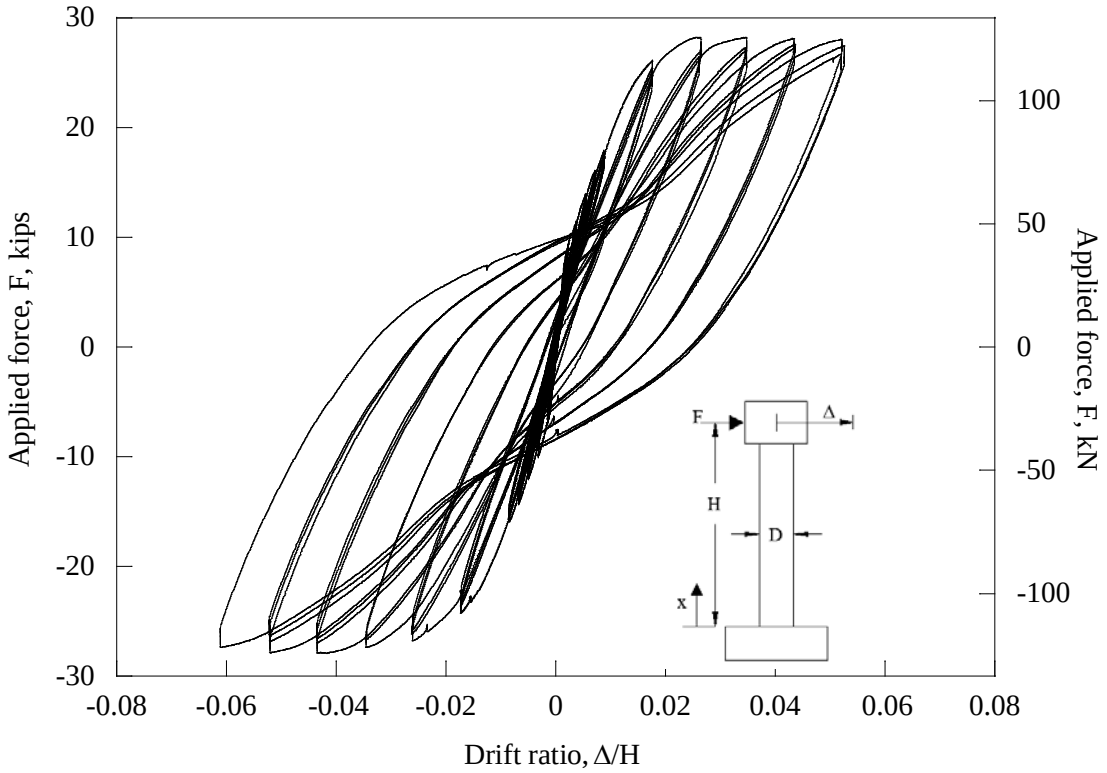

Figure 5.25: Drift ratio versus applied force of column C2

5.4 COLUMN C3 EXPERIMENTAL RESULTS

The experiment results of column C3 are presented in this section. Column C3 has the same moment-shear span ratio and reinforcement grade (Grade 60) as column C1 but has approximately double the longitudinal reinforcement ratio compared to column C1. This column is used as a baseline for comparison with column C4.

5.4.1 Concrete Cracking

Figure 5.26 shows two photographs of the crack mapping near the end of the testing. The figure shows that cracking was primarily dominated by flexure and progressed to shear dominated cracks towards larger displacement cycles. Cracking extended to approximately three-fourths the column height.

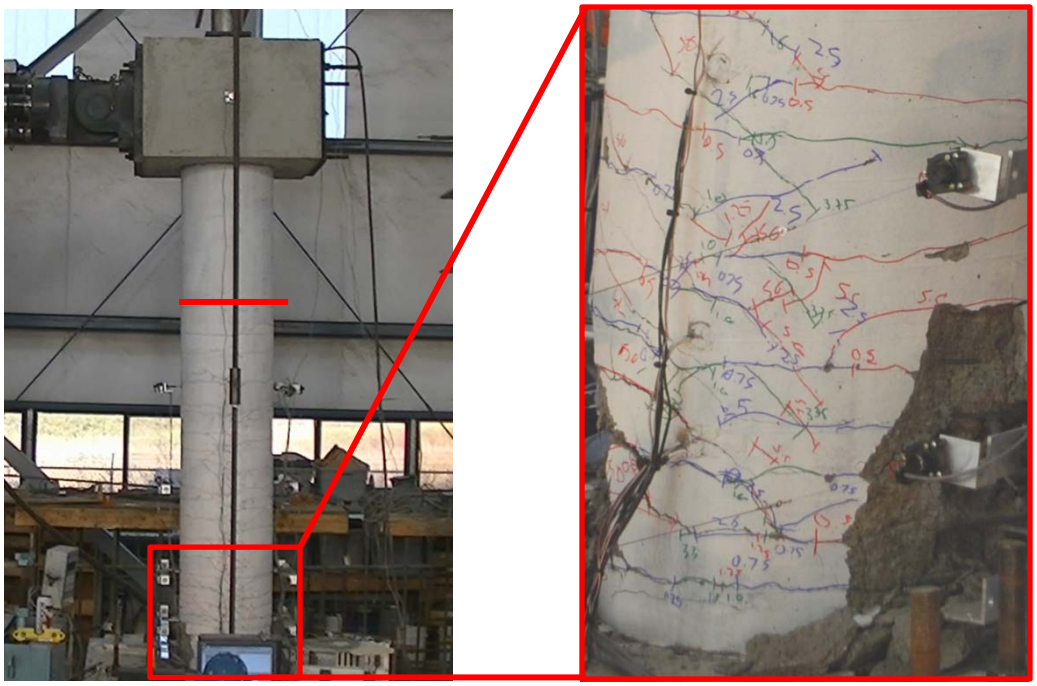

Figure 5.26: Photograph of column C3 crack mapping

5.4.2 Concrete Spalling

The displacement cycles at the onset of concrete spalling, concrete delamination, and deep concrete spalling were recorded. Table 5.5 provides a summary of the concrete spalling. As with column C1 and C2, all concrete spalling occurred after the longitudinal reinforcement yielded.

Table 5.5: Summary of column C3 concrete spalling

	Onset of concrete spalling	Concrete delamination	Deep concrete spalling
Displacement cycle in. (mm)	3.75 (95.3)	5.00 (127)	N.A.*
Drift ratio cycle	2.6%	3.5%	N.A.*

*N.A.: not available

5.4.3 Steel Reinforcing Bar Buckling

Figure 5.27 shows a photograph of the first reinforcing bars that buckled. The bar in the photograph is the longitudinal bar to the east of the southernmost longitudinal bar. Although not documented, the southernmost bar is believed to have buckled at or about the same time. The apex of the buckled reinforcing bar was located approximately 7.5 inches (190 mm) from the base of the column.

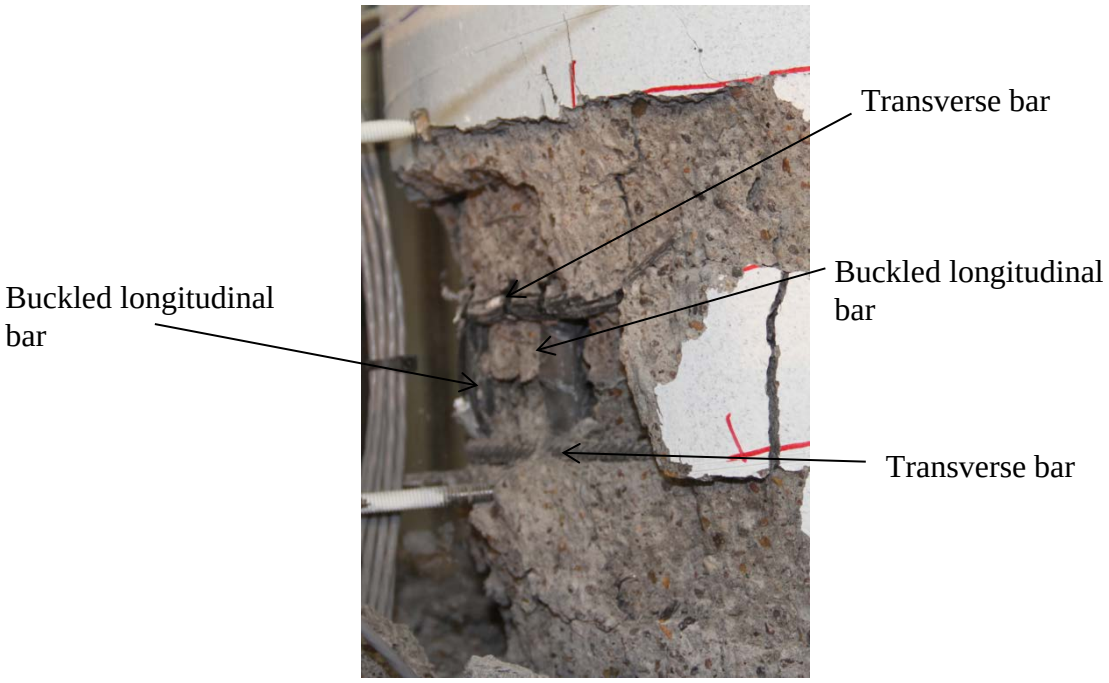

Figure 5.27: Photograph of initial bar buckling in column C3

5.4.4 Steel Reinforcing Bar Fracture

The first longitudinal reinforcing bar that fractured occurred on the return cycle after the final peak of the 10.0-inch (254 mm) displacement cycle. The applied load was 16.80 kips (74.73 kN) and the tip displacement was negative 3.10 inches (78.7 mm). Post-failure observations indicate that the bar fractured after a microcrack formed due to the bar buckling. Figure 5.28 shows that the southernmost longitudinal reinforcing bar fractured at an elevation of approximately 7.5 inches (190 mm) above the base of the column. The bar shown in this figure is also seen in Figure 5.27.

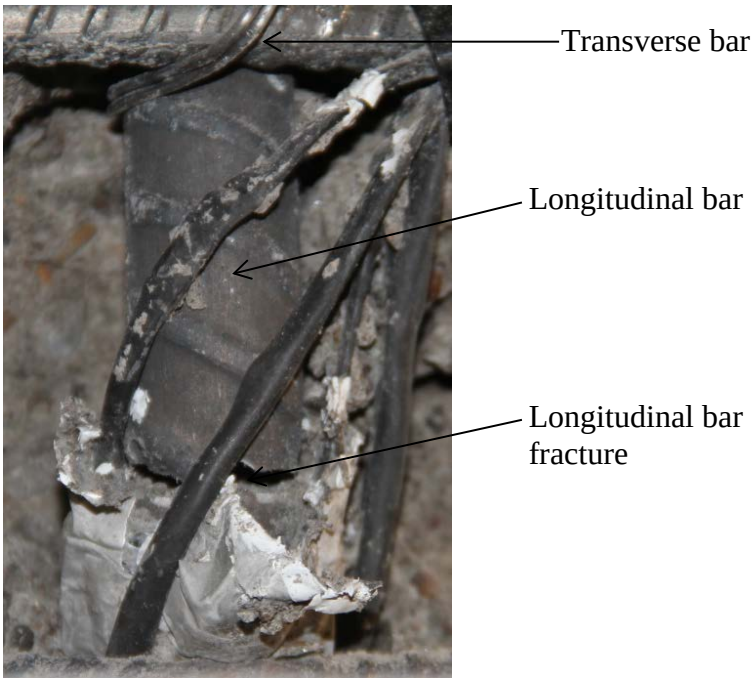

Figure 5.28: Photograph of column C3 first bar fracture

5.4.5 Column Tilt

Figure 5.29 shows a plot of the measured tilt and the calculated tilt versus the applied force. The calculated tilt was computed as the tip displacement divided by the column height converted into degrees. As with columns C1 and C2 there is an increasing difference between the measured tilt and the calculated tilt as the applied force reaches its maximum and minimum values.

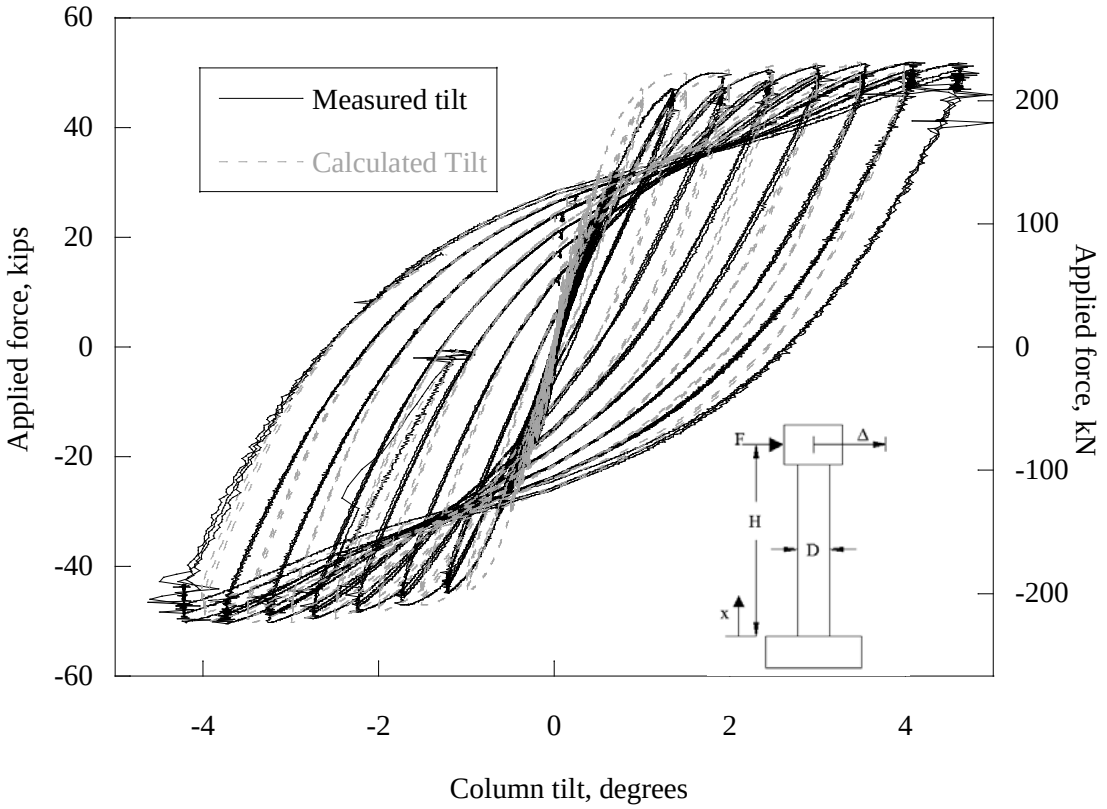

Figure 5.29: Tilt versus applied force of column C3

5.4.6 Vertical Load

As shown in Figure 5.30 the axial load increased as the applied horizontal load increased for column C3. The axial load for column C3 also dropped below the initial 90 kips (400 kN).

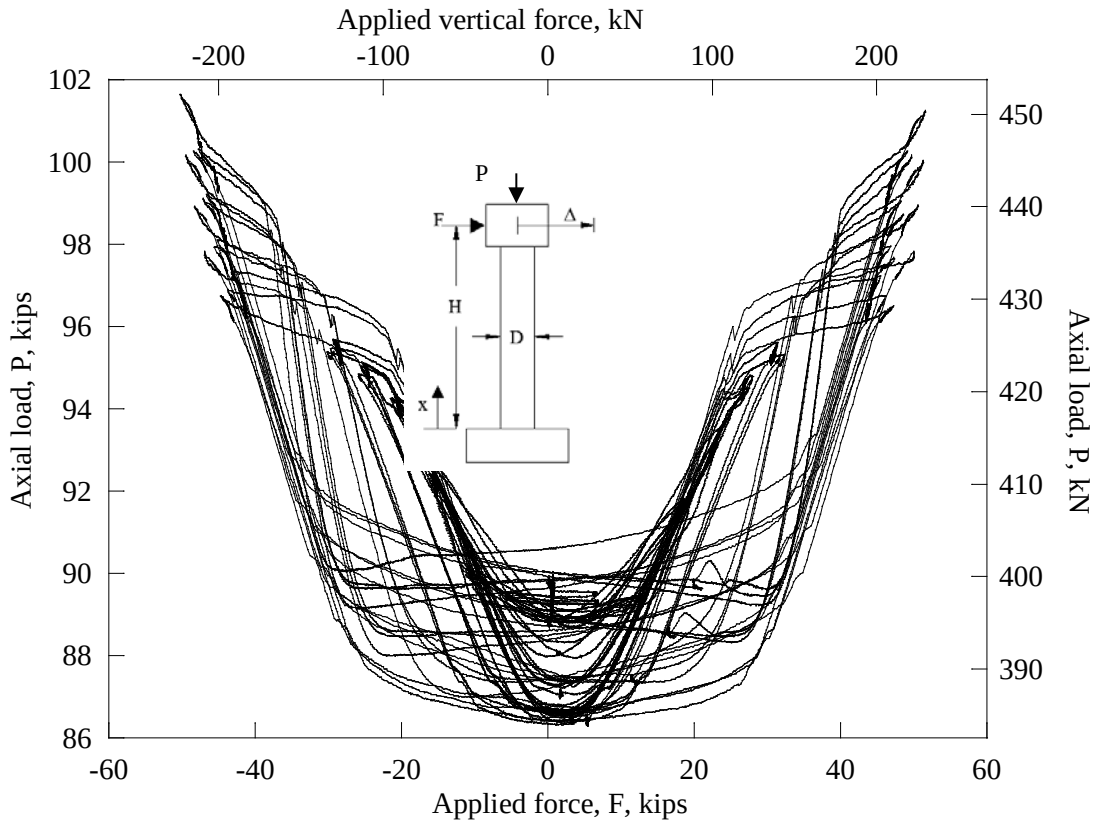

Figure 5.30: Applied force versus axial load of column C3

5.4.7 Footing displacement and Strong Wall Displacement

The footing was instrumented with four vertical LVDTs at each corner of the top face of the footing and two LVDTs on the north face of the footing as discussed in Chapter 3. These were used to determine if the footing rotated or displaced during the testing. The data from the six LVDTs showed that there was neither significant rotation nor horizontal displacement of the footing. No LVDT reading ever exceeded 0.07 inch (1.8 mm). The strong wall was instrumented with two string pots. The data from the string pots showed there was no significant displacement of the strong wall. The string pot recordings never exceeded 0.06 inches (1.5 mm).

5.4.8 Column Lateral Displacement

Figure 5.31 shows the maximum and minimum lateral deflections at the 6 points for the 13 displacement cycles. As with the data from the other columns, the elevation is normalized with respect to the column diameter, *D*, and the lateral displacement, Δ, is normalized by the column test height, *H*.

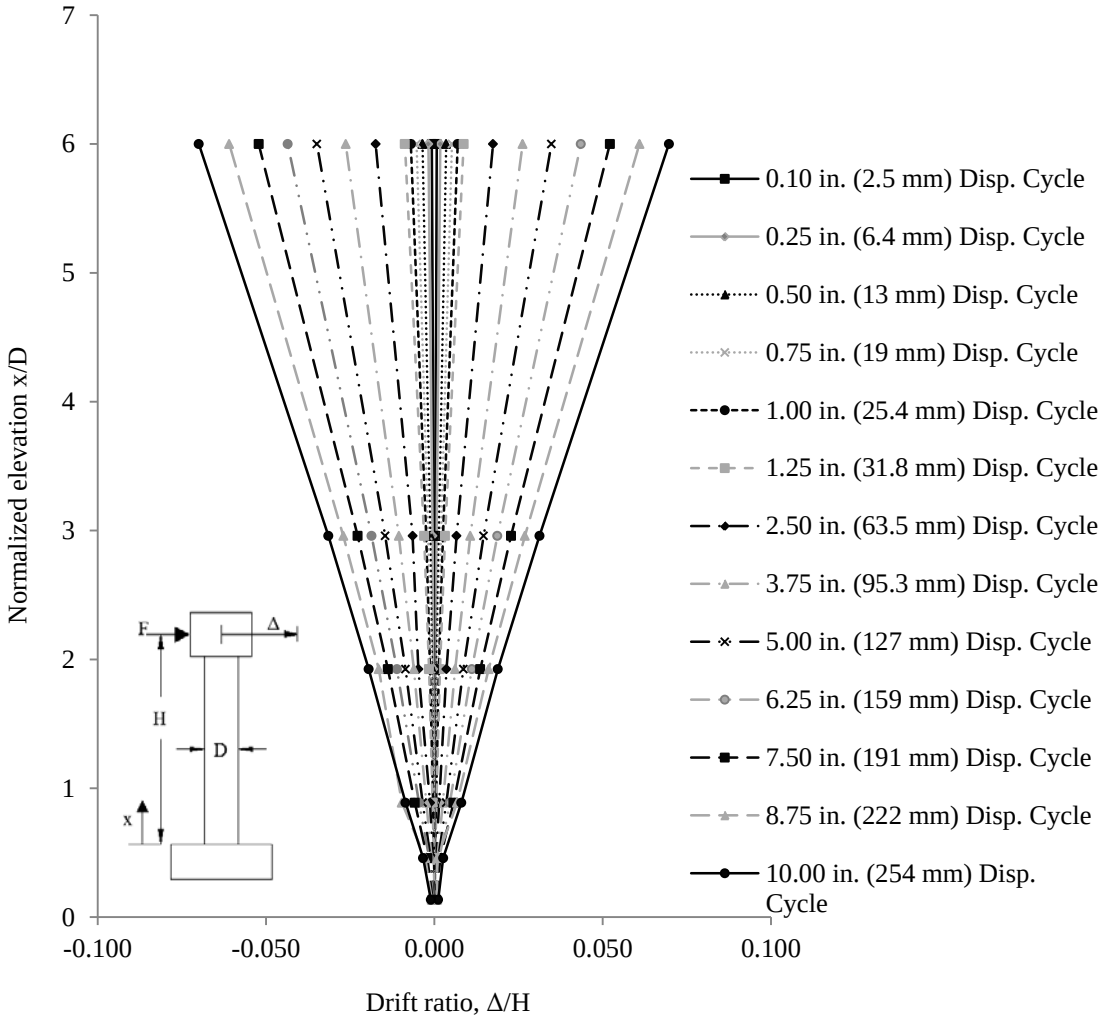

Figure 5.31: Drift ratio versus normalized elevation of Column C3

5.4.9 Steel Reinforcement Strains

Figure 5.32 shows the maximum transverse steel reinforcement strains for column C3 for each displacement cycle along the height of the column. The elevation is normalized by the column diameter, D, and the steel strain is normalized by the yield strain of the transverse reinforcement. The yield strain is defined in the same manner as described in section 5.2.6 for column C1.

As previously noted, occasionally a strain gage would electronically clip or get damaged. If this occurred at a location where there were two strain gages, the data from the damaged gage were no longer used, but data from the strain gage still functioning were used. The strain gage instrumentation level and displacement cycle where this occurred are:

1. level 2 during the 5.00-inch (127 mm) displacement cycle;

2. level 3 during the 6.25-inch (159 mm) displacement cycle, and;

3. levels 4 and 5 during the 7.50-inch (191 mm) displacement cycle.

Once the longitudinal strains exceed the 3 percent strain capacity of the strain gages the value was reported as 3 percent for the tensile strains and the compression strain data were not used. The strains gage instrumentation level and the displacement cycle when the 3 percent limit occurred are:

1. level 2 during the 7.50-inch (191 mm) displacement cycle;

2. level 4 during the 8.25-inch (210 mm) displacement cycle, and;

3. level 3 during the 10.00-inch (254 mm) displacement cycle.

Figure 5.33 shows the maximum longitudinal steel reinforcement strains for column C3 in the positive and negative displacement cycles along the height of the column. The maximum positive displacement cycle corresponds to the maximum tension strain and the maximum negative displacement cycle corresponds to the maximum compressive strain. The elevation is also normalized by the column diameter, *D*, and the steel strain is normalized by the yield strain of the longitudinal reinforcement. The yield strain was computed in the same manner as the transverse yield strain. Table 5.6 shows the experimental yield strain values used to determine the yield strain values used in the analysis. Note that the same values for column C1 for yield strain for the #3 (#10M) are used here. Because column C1 used #5 (#16M) longitudinal reinforcement, different yield strains values are used for the longitudinal reinforcement (#6 [#16M] for column C3). Note that the transverse and longitudinal strains are stacked in terms of the displacement cycle, i.e., the lowest bar strains at each elevation represents 0.10 inch (2.5 mm) displacement cycle and the highest bar represents the 8.75-inch (0.222 m).

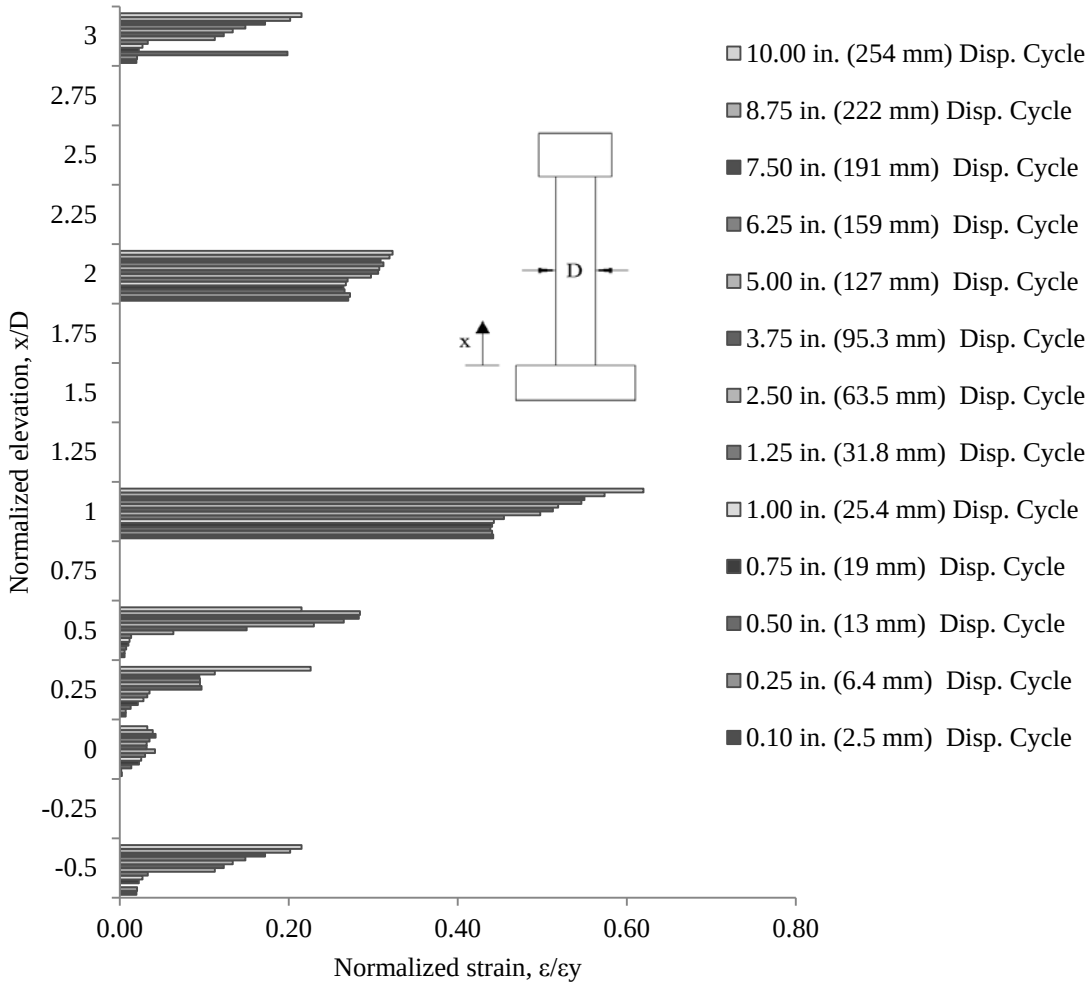

Figure 5.32: Transverse reinforcement strains in column C3

Table 5.6: Column C3 yield strains used in the strain analysis

Reinforcement	Calculated yield strain	Measured yield strain (0.2% OM)
#3 (#10M) Grade 60 ksi (420 MPa)	0.0025	0.0045
#6 (#19M) Grade 60 ksi (420 MPa)	0.0023	0.0043

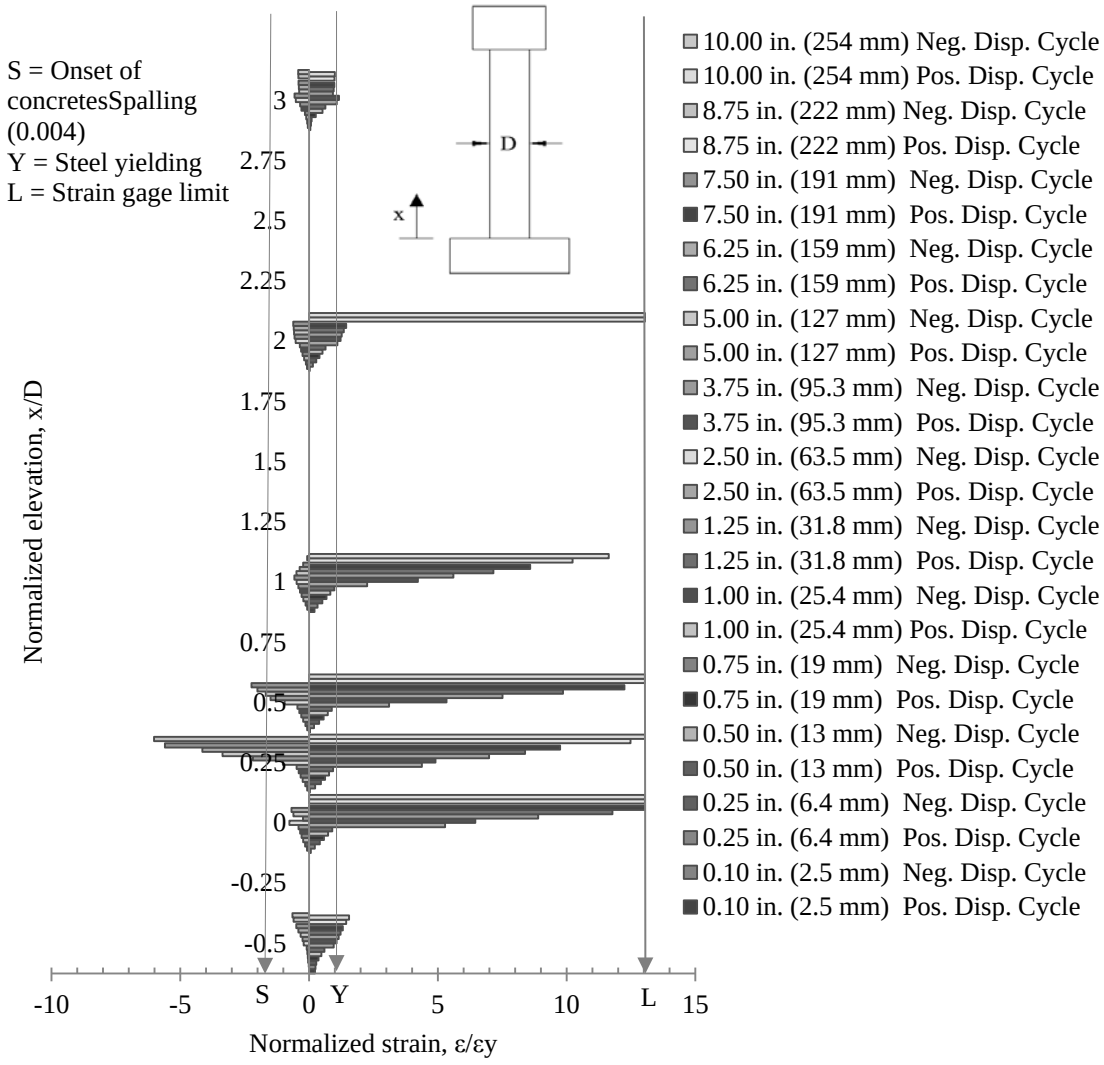

Figure 5.33: Longitudinal reinforcement strains in column C3

5.4.10 Column Curvature

The curvature was computed at each of the five instrumentation levels for each displacement level. Figure 5.34 shows the curvature for each displacement cycle along the height of the column. The data are normalized: the elevation is divided by the column diameter, *D*, and the curvature is multiplied by the column diameter, *D*. Figure 5.13 shows the physical representation of the variables used in the curvature computations. Calculations used to determine the curvature at each level, *i*, are the same as for column C1 shown in section 5.2.7.

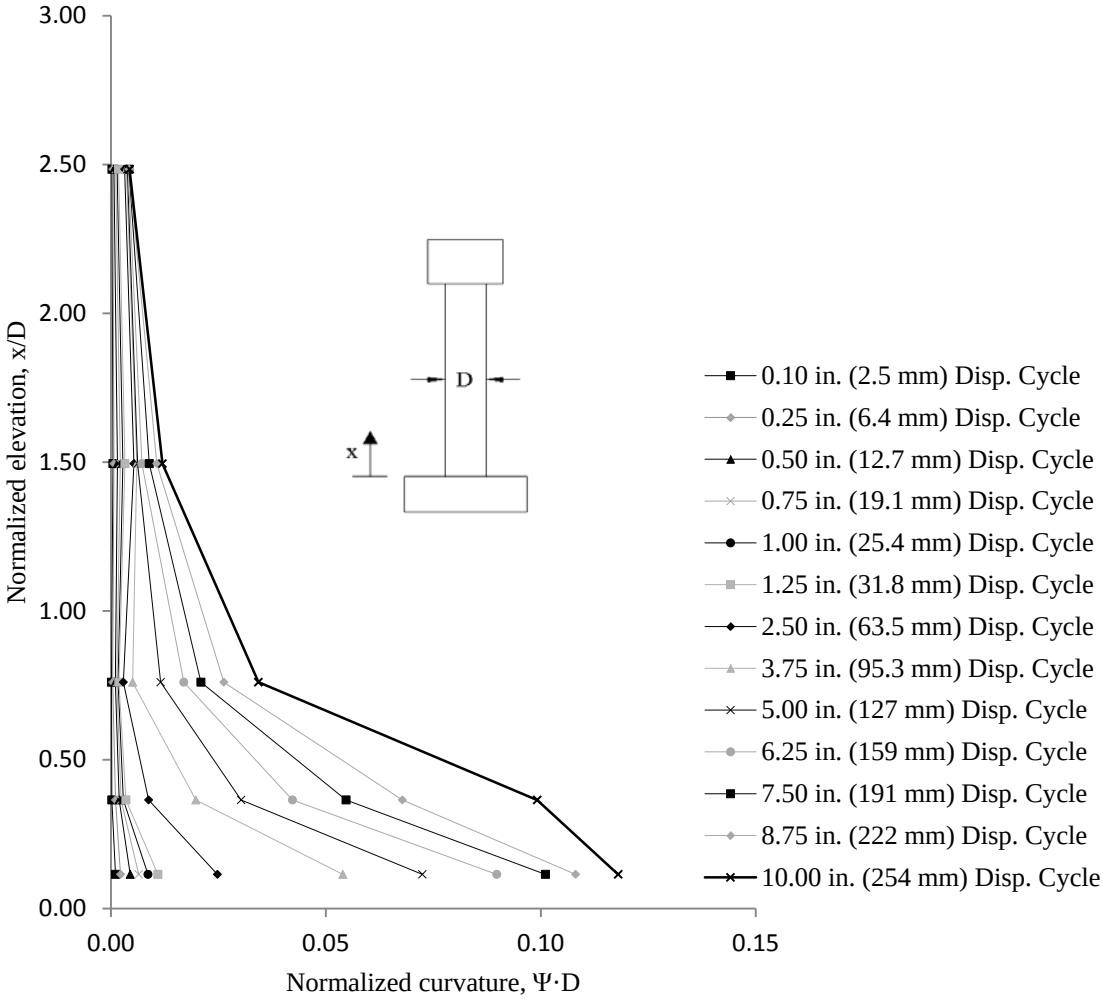

Figure 5.34: Normalized curvature versus normalized elevation of column C3

5.4.11 Applied Horizontal Load

The applied horizontal load is measured by a group of parallel load cells within the actuator. The applied load was plotted against the drift ratio as shown in Figure 5.35. The maximum applied force was 51.95 kips (231.1 kN) and the maximum drift ratio was 7.0 percent.

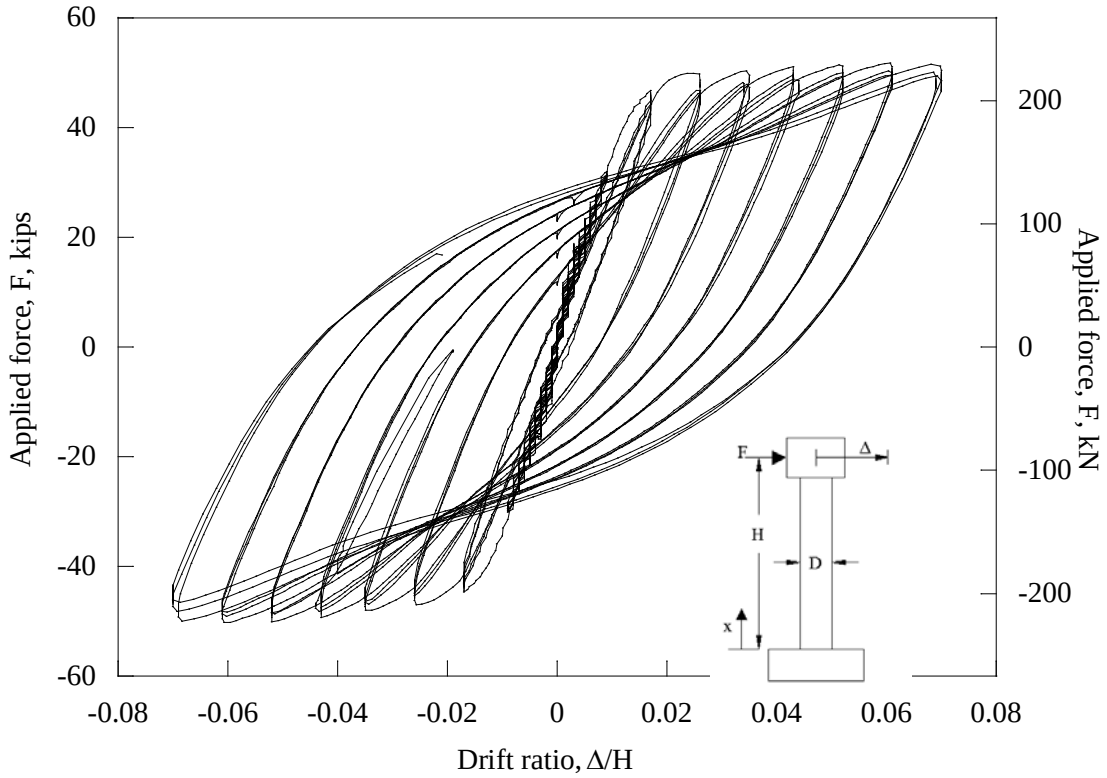

Figure 5.35: Drift ratio versus applied force of column C3

5.5 COLUMN C4 EXPERIMENTAL RESULTS

The experimental results of column C4 are presented in this section. Column C4 has a similar moment capacity as column C3 but is reinforced with A706 Grade 80. Column C4 and C3 both have a moment-shear span ratio of 6.

5.5.1 Concrete Cracking

Figure 5.36 shows two photographs of the crack mapping near the end of the testing. The figure shows that cracking was primarily dominated by flexure and progressed to shear dominated cracks towards larger displacement cycles. Cracking extended to approximately three-fourths the column height.

Figure 5.36: Photograph of column C4 crack mapping

5.5.2 Concrete Spalling

Table 5.7 provides a summary of the concrete spalling. As with column C1, C2 and C3, all concrete spalling occurred after the longitudinal reinforcement yielded.

Table 5.7: Summary of column C4 concrete spalling

	Onset of concrete spalling	Concrete spalling	Deep concrete spalling
Displacement cycle in. (mm)	3.75 (95.3)	5.00 (127)	N.A.*
Drift ratio cycle	2.6%	3.5%	N.A.*

*N.A.: not available

5.5.3 Steel Reinforcing Bar Buckling

Figure 5.37 shows a photograph of the first reinforcing bars that buckled. The bar in the photograph is the longitudinal bar to the west of the northern most longitudinal bar. The apex of the buckled reinforcing bar was located approximately 5 inches (127 mm) from the base of the column.

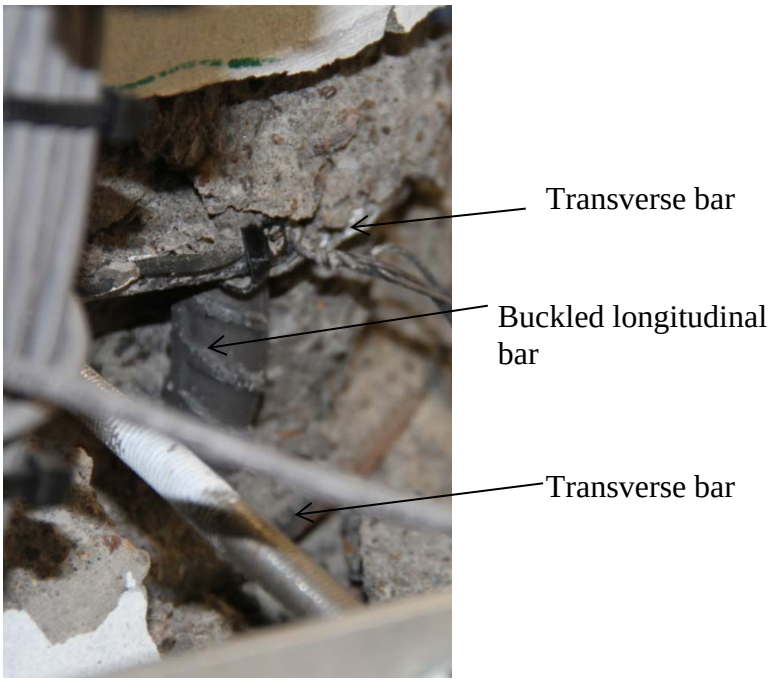

Figure 5.37: Photograph of initial bar buckling in column C4

5.5.4 Steel Reinforcing Bar Fracture

The first longitudinal reinforcing bar fractured approaching the fourth peak of the 10.00-inch (254 mm) displacement cycle. The applied load was negative 26.92 kips (119.7 kN) and the tip displacement was negative 3.64 inches (92.5 mm). Post-failure observations indicate that the bar fractured after a microcrack formed due to the bar buckling. Figure 5.38 shows that the northernmost longitudinal reinforcing bar fractured at an elevation approximately 5 inches (127 mm) above the base of the column.

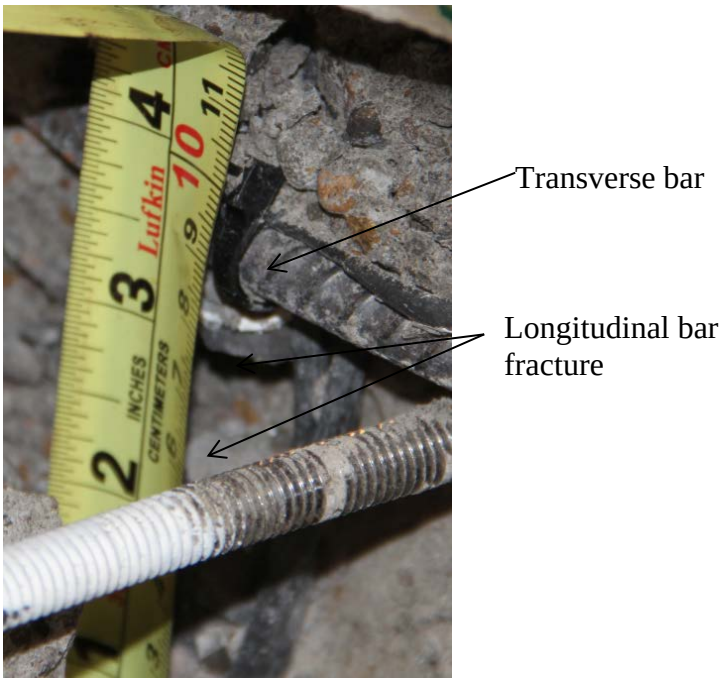

Figure 5.38: Photograph of first bar fracture in column C4

5.5.5 Column Tilt

Figure 5.39 shows a plot of the measured tilt and the calculated tilt versus the applied force. The calculated tilt was computed as the tip displacement divided by the column height converted into degrees. As seen in the plot there is an increasing difference between the measured tilt and the calculated tilt as the applied force reaches its maximum and minimum values. As with the other test columns, this is likely due to the positioning of the string pot that measures the tip displacement. As the column is being pushed horizontally the column also bends creating an additional vertical component measured by the string pot.

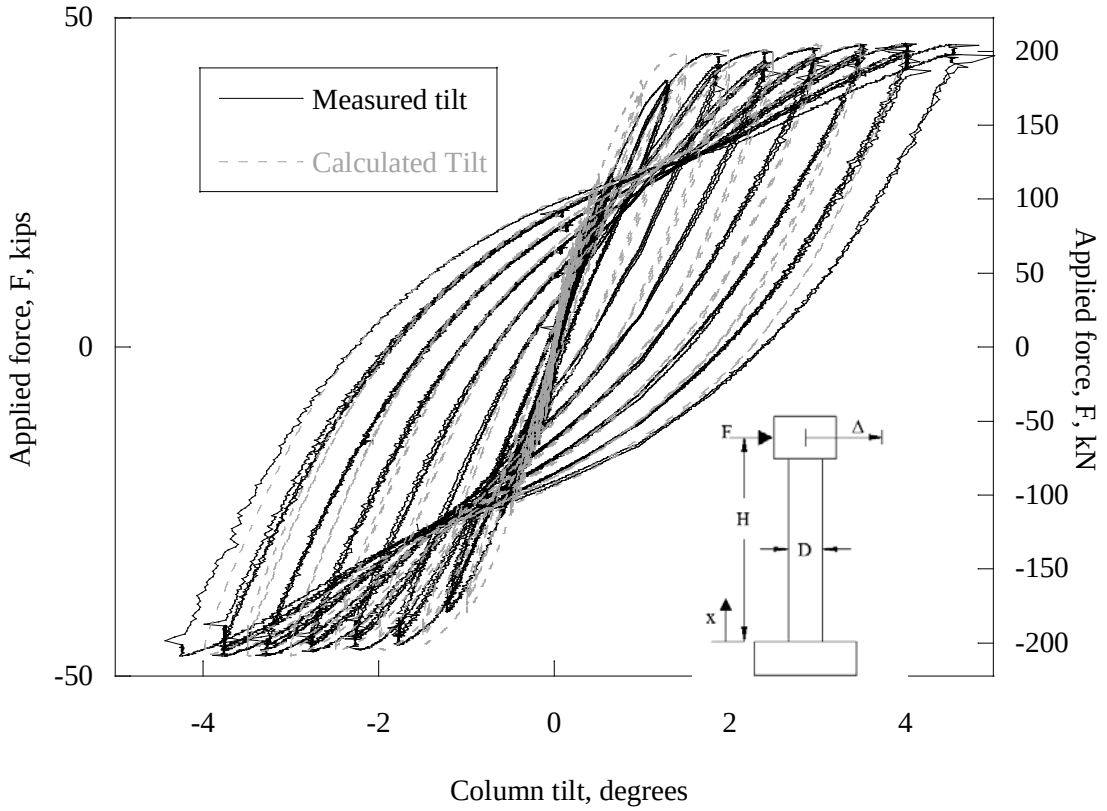

Figure 5.39: Tilt versus applied force of column C4

5.5.6 Vertical Load

As shown in Figure 5.40 the axial load increased as the applied horizontal load increased for column C4. The axial load for column C4 also dropped below the initial 90 kips (400 kN). The figure exhibits a similar shape as the figure for columns C3, however the slope is flatter in the middle region of the plot. The middle region of the plot also exhibits points with a higher axial load when the applied horizontal load is zero.

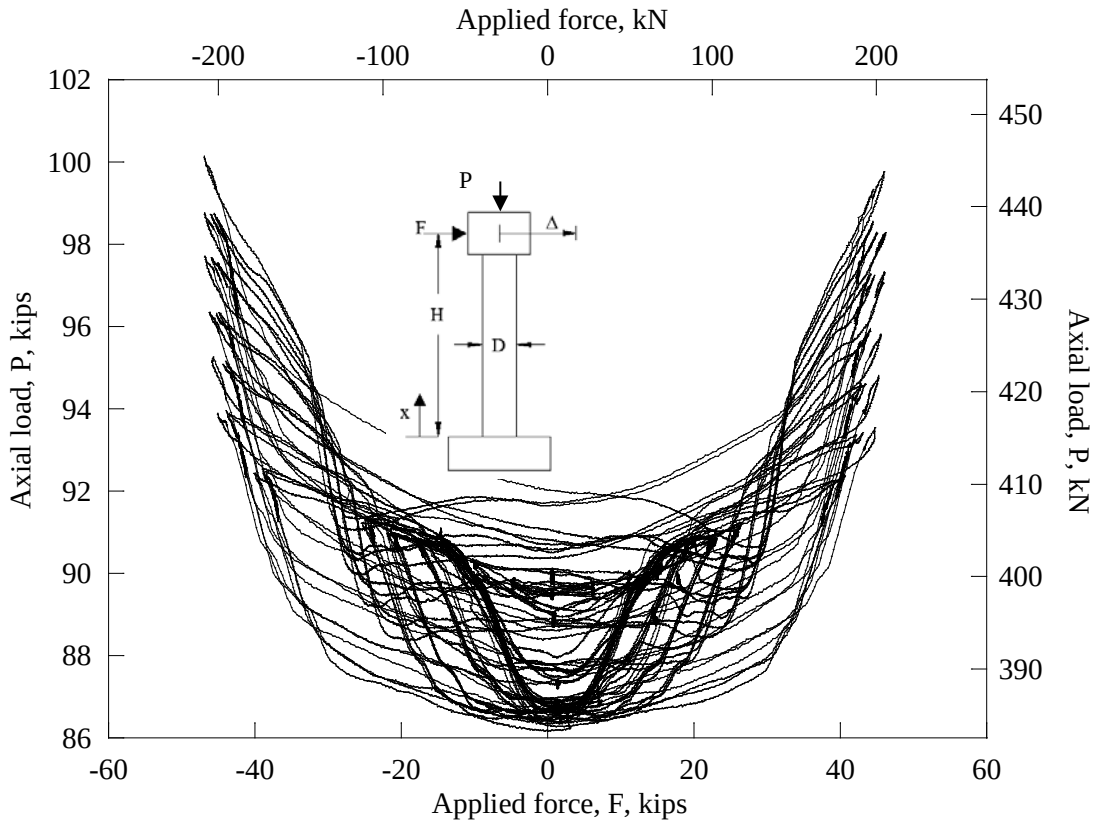

Figure 5.40: Applied force versus axial load of column C4

5.5.7 Footing Displacement and Strong Wall Displacement

The footing was instrumented with four vertical LVDTs at each corner of the top face of the footing and two LVDTs on the north face of the footing as discussed in Chapter 3 to determine if the footing rotated or displaced during the testing. The data from the six LVDTs showed that there was neither significant rotation nor horizontal displacement of the footing. No LVDT reading ever exceeded 0.01 inch (0.25 mm). The strong wall was instrumented with two string pots. The data from the string pots showed there was no significant displacement of the strong wall. The string pot recordings never exceeded 0.04 inches (1.0 mm).

5.5.8 Column Lateral Displacement

Figure 5.41 shows the maximum and minimum lateral deflections at the 6 points for the 13 displacement cycles. As with the data from the other columns, the elevation is normalized with respect to the column diameter, *D*, and the lateral displacement, Δ, is normalized by the column test height, *H*.

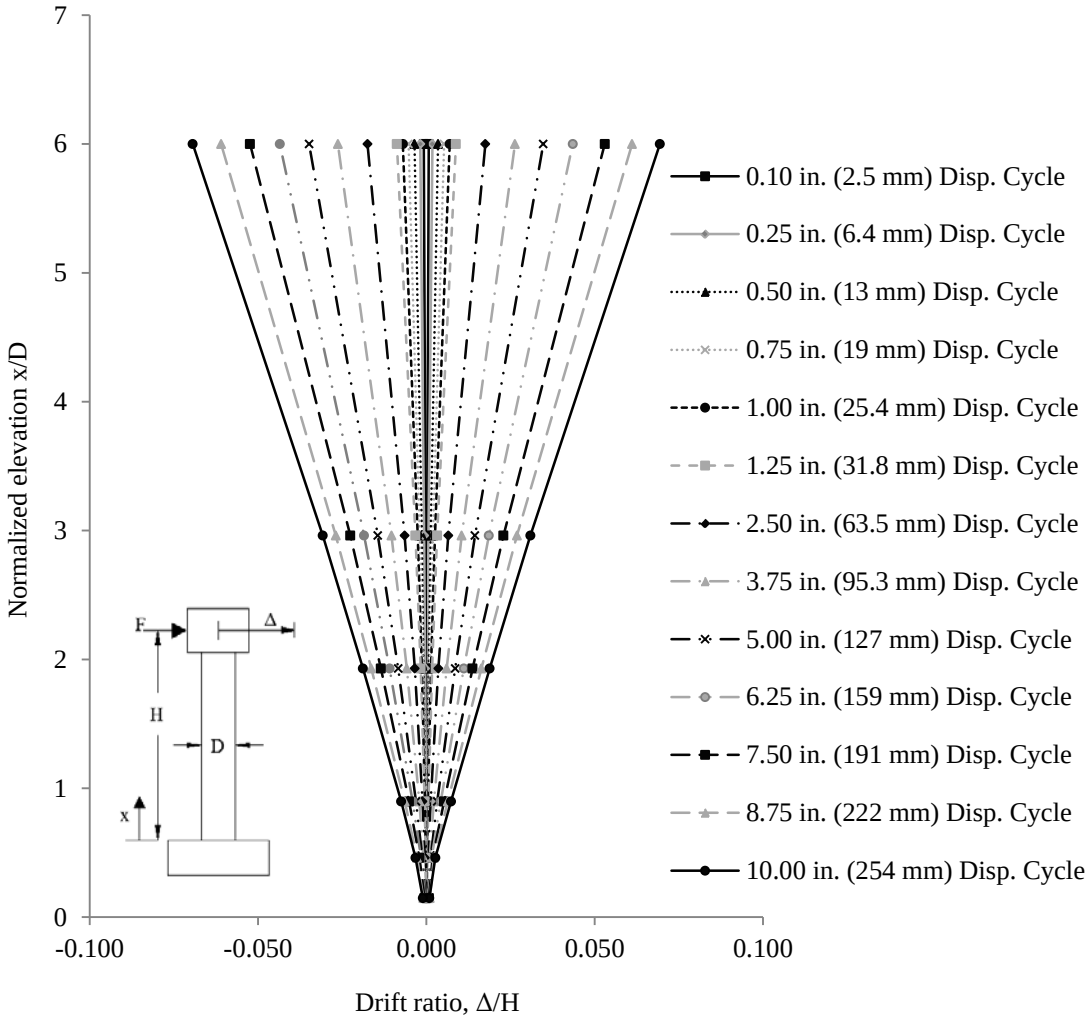

Figure 5.41: Drift ratio versus normalized elevation of column C4

5.5.9 Steel Reinforcement Strains

Figure 5.42 shows the maximum transverse steel reinforcement strains for column C4 for each displacement cycle along the height of the column. The elevation is normalized by the column diameter, D, and the steel strain is normalized by the yield strain of the transverse reinforcement. The yield strain is defined in the same manner as described in section 5.2.6 for column C1. Note that the transverse and longitudinal strains are stacked in terms of the displacement cycle, i.e., the lowest bar strains at each elevation represents 0.10-inch (2.5 mm) displacement cycle and the highest bar represents the 8.75-inch (0.222 m).

As previously noted, occasionally a strain gage would electronically clip or get damaged. Where this occurred at locations where two strain gages were present, the data from gage that was

damaged were no longer used, but data from the strain gage still functioning were used. The strain gage instrumentation level and displacement cycle where this occurred includes:

1. level 3 during the 5.00-inch (127 mm) displacement cycle, and;

2. level 2 during the 6.25-inch (159 mm) displacement cycle.

Once the longitudinal strains exceeded the 3 percent strain capacity of the strain gages the value was reported as 3 percent for the tensile strains and the compression strain data were not used. The strains gage instrumentation level and the displacement cycle when the 3 percent limit occurred include:

1. level 2 during the 6.25-inch (159 mm) displacement cycle, and;

2. level 3 during the 8.25-inch (210 mm) displacement cycle.

Figure 5.43 shows the maximum longitudinal steel reinforcement strains of column C4 for each positive and negative displacement cycle along the height of the column. The maximum positive displacement cycle corresponds to the maximum tension strain. The maximum negative displacement cycle corresponds to the maximum compressive strain. The elevation is also normalized by the column diameter, *D*, and the steel strain is normalized by the yield strain of the longitudinal reinforcement. The yield strain was computed in the same manner as the transverse yield strain.

Table 5.8 shows the experimental yield strain values used to determine the yield strain values used in the analysis. Note the values are different than those of column C3 due to the different grade of reinforcement in the column.

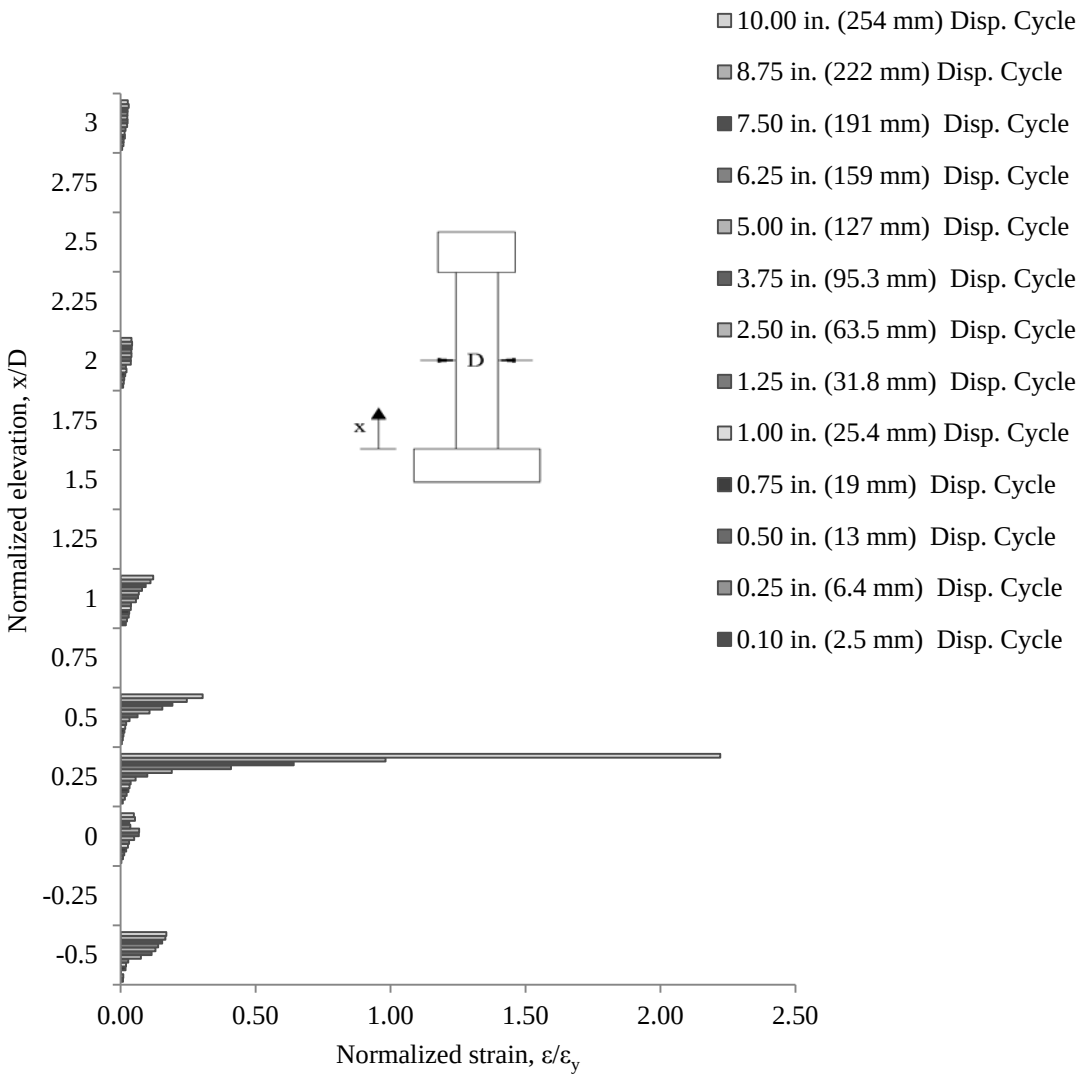

Figure 5.42: Transverse reinforcement strains in column C4

Table 5.8: Column C4 yield strains used in the strain analysis

Reinforcement	Calculated yield strain	Measured yield strain (0.2% OM)
#3 (#10M) Grade 80 ksi (550 MPa)	0.0035	0.0055
#6 (#19M) Grade 80 ksi (550 MPa)	0.0028	0.0048

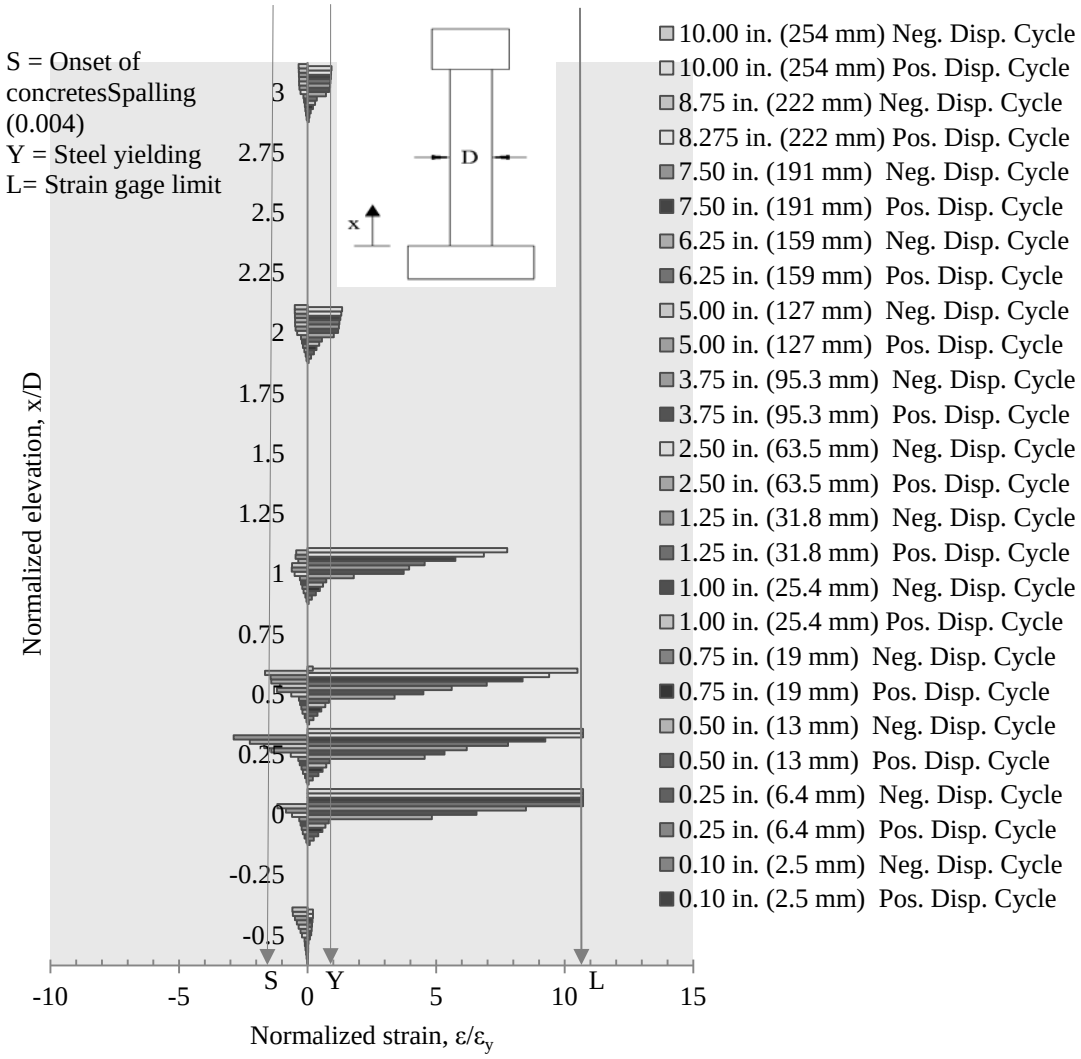

Figure 5.43: Longitudinal reinforcement strains in column C4

5.5.10 Column Curvature

The curvature was computed at each of the five instrumentation levels for each displacement level. Figure 5.44 shows the curvature for each displacement cycle along the height of the column. The elevation and curvature are both normalized by the column diameter, *D*. The elevation is divided by the column diameter, *D*, and the curvature is multiplied by the column diameter, *D*. Figure 5.13 shows the physical representation of the variables used in the curvature computations. Calculations used to determine the curvature at each level, *i*, are the same as for column C1 shown in section 5.2.7.

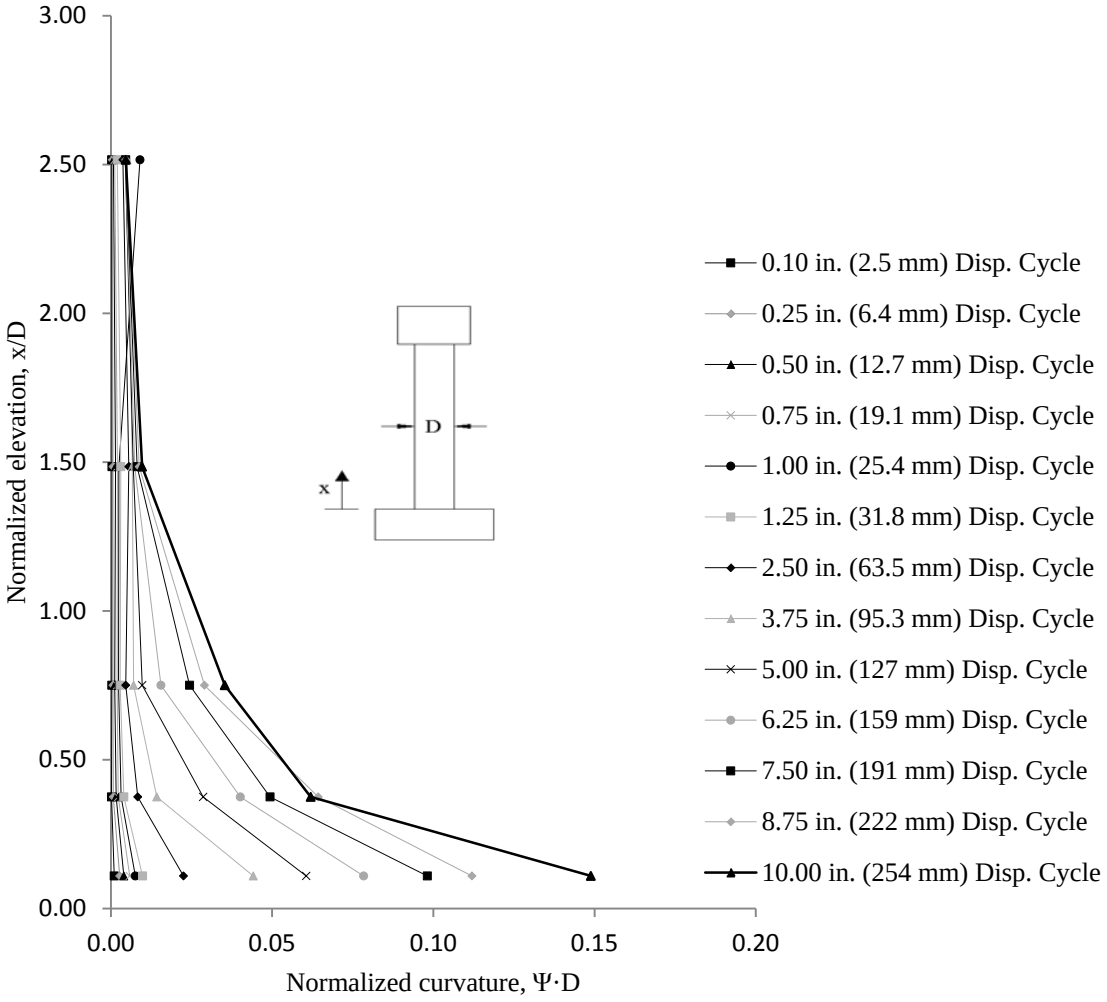

Figure 5.44: Normalized curvature versus normalized elevation of column C4

5.5.11 Applied Horizontal Load

The applied horizontal load was measured by a group of parallel load cells within the actuator. The applied load was plotted against the drift ratio as shown in Figure 5.45. The maximum applied force was negative 46.94 kips (119.7 kN) and the maximum drift ratio was 6.9 percent.

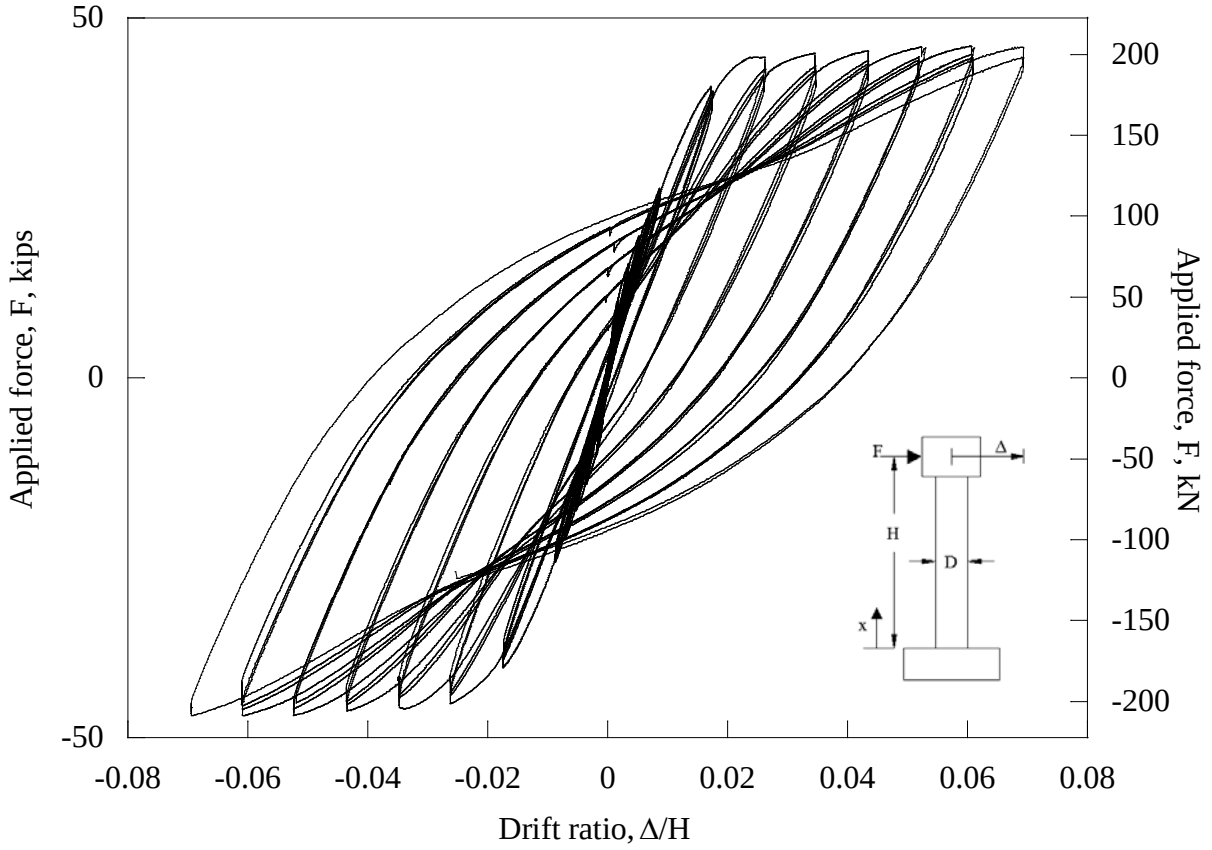

Figure 5.45: Drift ratio versus applied force of column C4

5.6 SUMMARY

This chapter presented both visual and measured observations for four columns: columns C1, C2, C3 and C4. Columns C1 and C2 have the equivalent of 1.11 percent Grade 60 longitudinal reinforcement ratio while columns C3 and C4 have the equivalent of 2.19 percent Grade 60 longitudinal reinforcement ratio. Columns C1 and C3 were reinforced with Grade 60 and columns C2 and C4 were reinforced with Grade 80. All four columns had a moment-shear span ratio of six. The visual observations included cracking, concrete spalling, bar buckling and bar fracture. The measured observations included column tilt, vertical applied load, footing and strong wall displacement, column lateral displacement, steel reinforcement strains, column curvature, and applied horizontal load. The measured observations were reported up to column failure which was defined as the first longitudinal bar fracture. The goal of this section was to present the data of the four columns under cyclic lateral loading. The next chapter, Chapter 6, presents the same visual and measured observations for columns C5 and C6. Chapter 7 contains the analysis of the data presented in this chapter and provides comparisons between the columns.

6.0 COLUMN C5 AND C6 EXPERIMENTAL RESULTS

6.1 INTRODUCTION

This chapter provides test results from two of the six column test specimens. First, a column reinforced with Grade 60 reinforcing bars (Column C5) and second, a column reinforced with Grade 80 reinforcing bars (Column C6). These two columns were half the height of the first four columns (Columns C1 through C4) corresponding to a moment-moment-shear span ratio of 3. The reduced moment-shear span ratio was chosen to represent the same bridge columns discussed in Chapter 5, but representing cyclic loading of a bridge in the longitudinal direction. Both columns were designed to have approximately the same moment capacity and were designed following the AASHTO and ODOT BDDM *(ODOT 2012*) standards.

The column testing procedure is described in Chapter 3. Results presented herein include visual and measured observations. Visual observations refer to cracking, concrete spalling, bar buckling, and bar fracture. Measured observations include column tilt, axial load, footing and strong wall displacement, column lateral displacement, steel reinforcement strains, column curvature, and horizontal applied load. Like the previous chapter, column failure was defined as the first bar fracture. In this chapter, the analysis procedures are similar to those described in Chapter 5. However, post first reinforcing bar fracture analysis was also conducted. The latter is presented in Chapter 7.

6.2 COLUMN C5 EXPERIMENTAL RESULTS

6.2.1 Concrete Cracking

Crack mapping was not performed on column C5 due to the density of the instrumentation around the column. However, photographs of the cracking were taken and the descriptions of the cracking were documented. Figure 6.1 shows a photograph of the cracking towards the end of testing. Initial cracking was observed at 0. 3 percent drift ratio level, which were flexural cracks, but shortly later shear cracks were observed at the 0.7 percent drift ratio level. Shear cracks became predominant at a drift ratio level of 1.7 percent. Shear cracking was distributed along the height of the column. Only the top 6 inches (150 mm) of the column exhibited no cracks.

Figure 6.1: Photograph of column C5 cracks

6.2.2 Concrete Spalling

Table 6.1 provides a summary of the displacement cycle at which concrete spalling was observed. Onset of concrete spalling, concrete spalling and deep concrete spalling are defined in Chapter 5 for column C1. As with the other test columns the onset of spalling and spalling occurred after the longitudinal reinforcement yielded.

Table 6.1: Summary of column C5 concrete spalling

	Onset of concrete spalling	Concrete spalling	Deep concrete spalling
Displacement cycle in. (mm)	1.88 (47.8)	1.88 (47.8)	4.38 (111)
Drift ratio cycle	2.6%	2.6%	6.1%

6.2.3 Steel Reinforcing Bar Buckling

Figure 6.2 shows a photograph of the first reinforcing bars that buckled. The bar in the photograph is the southernmost longitudinal bar. The bar buckled while approaching the final peak of the 4.38-inch (111 mm) displacement cycle, which corresponds to a 6.1 percent drift ratio. The apex of the buckled reinforcing bar was located approximately 5.5 inches (140 mm) from the base of the column. Note at this displacement level the two closest longitudinal bars to the southernmost bar on either side of the southernmost longitudinal bar also buckled. Thus, a total of five bars buckled during this displacement cycle.

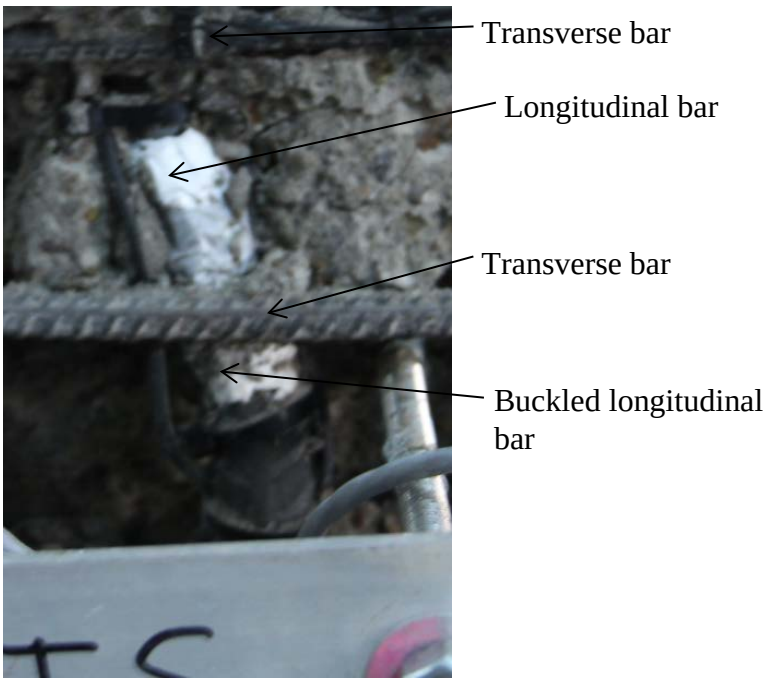

Figure 6.2: Column C5 initial buckling of longitudinal reinforcing bar

6.2.4 Steel Reinforcing Bar Fracture

The first longitudinal reinforcing bar fractured approaching the first peak of the 5.00 inch (127 mm) displacement cycle, which corresponds to a drift ratio of 6.9 percent. The applied load was 43.20 kips (192.2 kN) and the tip displacement was 0.19 inches (4.8 mm). Post-testing observations of the bar, it is believed that the reinforcing bar fractured after it formed a microcrack as a result of bar buckling. Figure 6.3 shows that the southernmost longitudinal reinforcing bar fractured at an elevation approximately 5 inches (127 mm) above the base of the column.

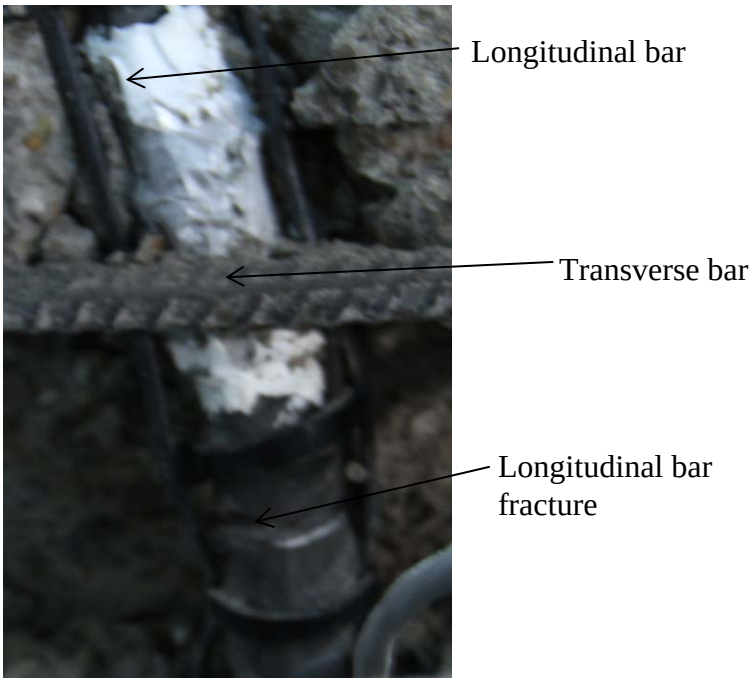

Figure 6.3: Photograph of column C5 first bar fracture

6.2.5 Column Tilt

Figure 6.4 shows a plot of the measured tilt and the calculated tilt versus the applied force. The calculated tilt was computed as the tip displacement divided by the column height. As seen in the plot there is an increasing difference between the measured tilt and the calculated tilt as the applied force reaches its maximum and minimum values. As with the other test columns, this is mainly due to the difference between rotations measured from the base of the column versus the tip rotation. The difference are then due to the fact that as the column is being pushed horizontally the column it also bends creating an additional vertical component measured by the string pot.

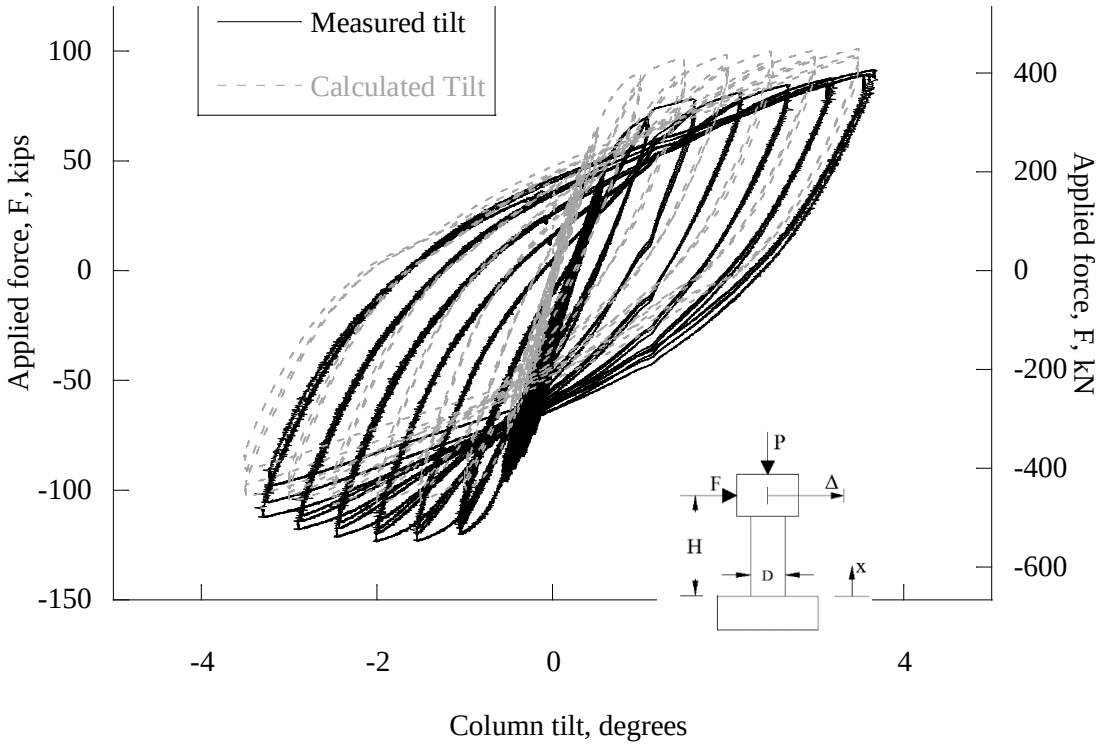

Figure 6.4: Drift ratio versus applied force of column C5

6.2.6 Vertical Load

Figure 6.5 shows the axial load increased as the applied horizontal load increased for column C5. The axial load for column C5 also dropped below the initial 90 kips (400 kN).

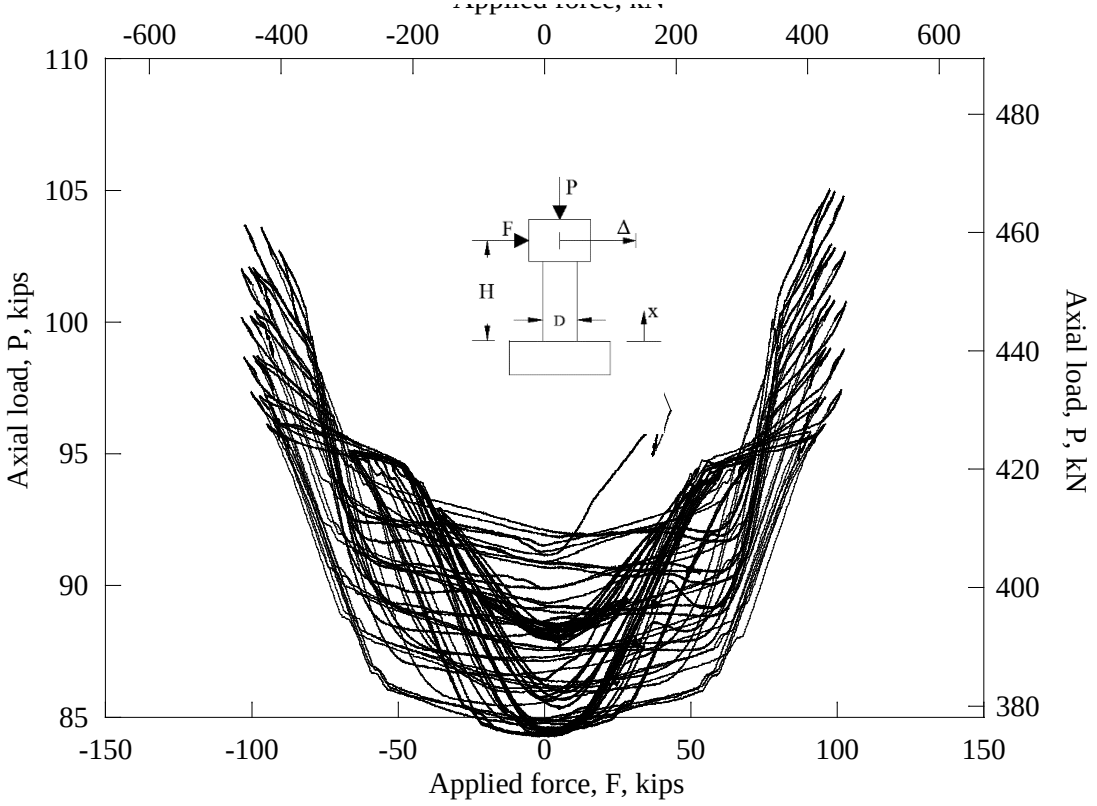

Figure 6.5: Axial load versus applied force of column C5

6.2.7 Footing Displacement and Strong Wall Displacements

As discussed in Chapter 3, the footing was instrumented with four vertical LVDTs at each corner of the top face of the footing and two LVDTs on the north face of the riser block and two string pots of the footing to determine if the footing rotated or displaced during the testing. The data from the six LVDTs and two string pots showed that the rotation and horizontal displacement of the footing were negligible. No LVDT reading ever exceeded 0.06 inch (1.5 mm).

The strong wall was also instrumented with two string pots. The data from the string pots showed there was no significant displacement of the strong wall. The string pot recordings also never exceeded 0.06 inches (1.5 mm).

6.2.8 Column Lateral Displacement

For column C5, Figure 6.6 shows the maximum and minimum lateral deflections at the 5 points for the 13 displacement cycles. In this figure, the elevation is normalized with respect to the column diameter, *D*, and the lateral displacement, Δ, is normalized by the column test height, *H*. Note that as the first instrumentation level (6 inches [152 mm] above the base of the column) lateral displacement was measure and hence the lines do not start at 0.000.

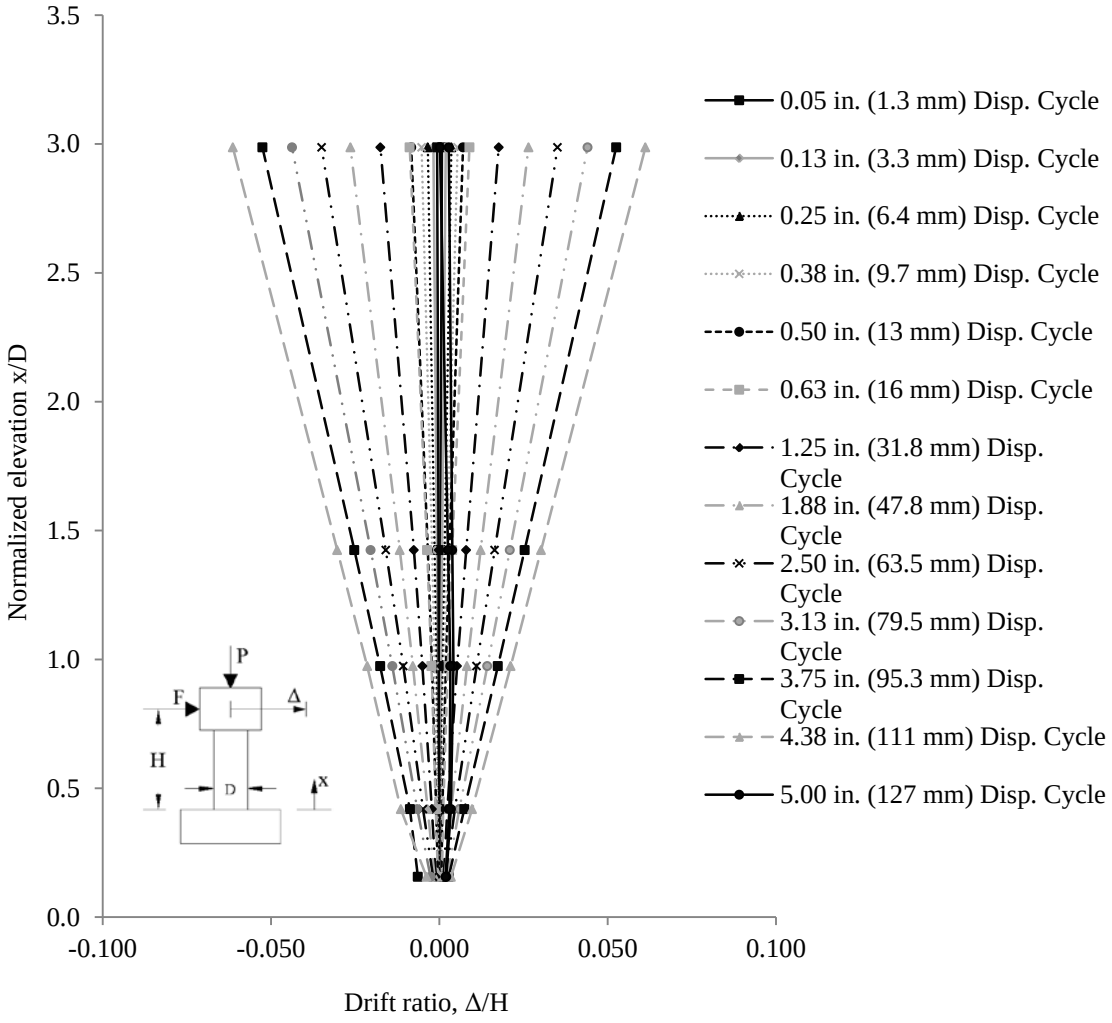

Figure 6.6: Drift ratio versus normalized elevation of column C5

6.2.9 Steel Reinforcement Strains

As previously mentioned, occasionally a strain gage would electronically clip or get damaged and the data from the strain gage was no longer used. If this occurred at a location where there were two strain gages, the data from the damaged gage was no longer used, but the strain gage still functioning was used. The strain gage instrumentation level and displacement cycle where this occurred are:

1. level 4 during the 0.63-inch (16 mm) displacement cycle;

2. level 2 during the 2.50-inch (64 mm) displacement cycle;

3. level 3 during the 3.13-inch (80 mm) displacement cycle, and;

4. level 1 during the 3.75-inch (95 mm) displacement cycle.

Once the longitudinal strains exceed the 3 percent strain capacity of the strain gages the value was reported as 3 percent for the tensile strains and the compression strain data was not used. The strains gage instrumentation level and the displacement cycle when the 3 percent limit was hit are:

1. levels 2 and 3 during the 3.75-inch (95 mm) displacement cycle, and;

2. level 4 during the 4.38-inch (111 mm) displacement cycle.

Figure 6.7 shows the maximum transverse steel reinforcement strains for column C5 for each displacement cycle along the height of the column. The elevation is normalized by the column diameter, D, and the steel strain is normalized by the yield strain of the transverse reinforcement. The yield strain is defined in the same manner as described in section 5.2.6 for column C1. It should also be noted that the transverse strain gage at the second instrumentation level was damaged during the fabrication of the column.

Figure 6.8 shows the maximum longitudinal steel reinforcement strains of column C5 for each positive and negative displacement cycle along the height of the column. The maximum positive displacement cycle corresponds to the maximum tension strain. The maximum negative displacement cycle corresponds to the maximum compressive strain. The elevation is also normalized by the column diameter, D, and the steel reinforcement strain is normalized by the yield strain of the reinforcement. Table 6.2 shows the experimental yield strain values used to determine the analytical yield strain values.. Note that the transverse and longitudinal strains are stacked in terms of the displacement cycle, i.e., the lowest bar strains at each elevation represents 0.05 inch (1.3 mm) displacement cycle and the highest bar represents the 5.00 inch (127 mm). Although the first bar to fracture in column C5 occurred during the 5.00-inch (127 mm) displacement cycle, the maximum tip displacement prior to the first longitudinal bar fracture was only 0.19 inches (4.8 mm). This resulted in small steel strains in column C5 during the final displacement cycle. Onset of spalling was observed when vertical cracks began to appear. The “S” shown in Figure 6.8 is equal to when the strain at the longitudinal reinforcement reached 0.004 strain.

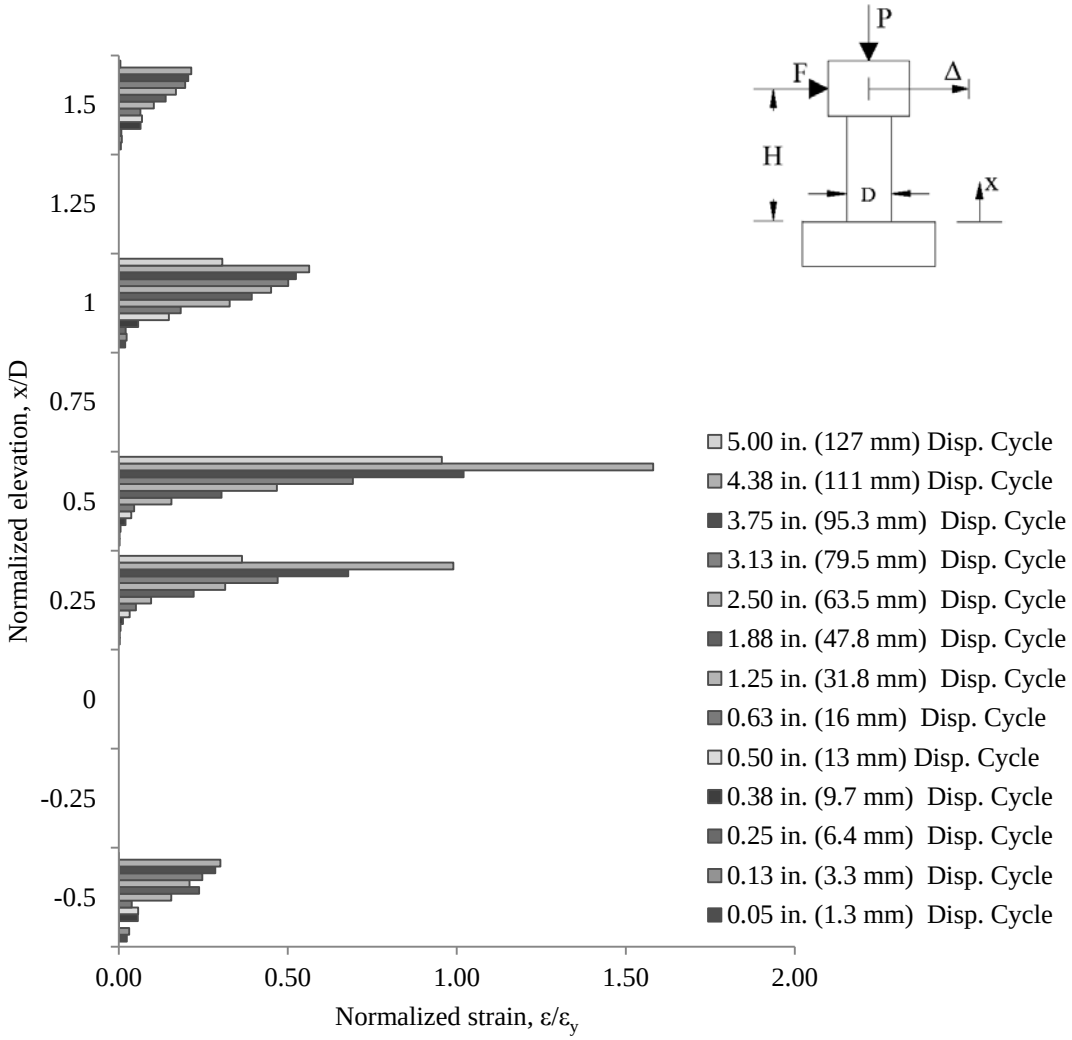

Figure 6.7: Transverse reinforcement strain in column C5

Table 6.2: Column C5 yield strains used in the strain analysis

Reinforcement	Calculated yield strain	Measured yield strain (0.2% OM)
#3 (#10M) Grade 60 ksi (420 MPa)	0.0025	0.0045
#6 (#19M) Grade 60 ksi (420 MPa)	0.0023	0.0043

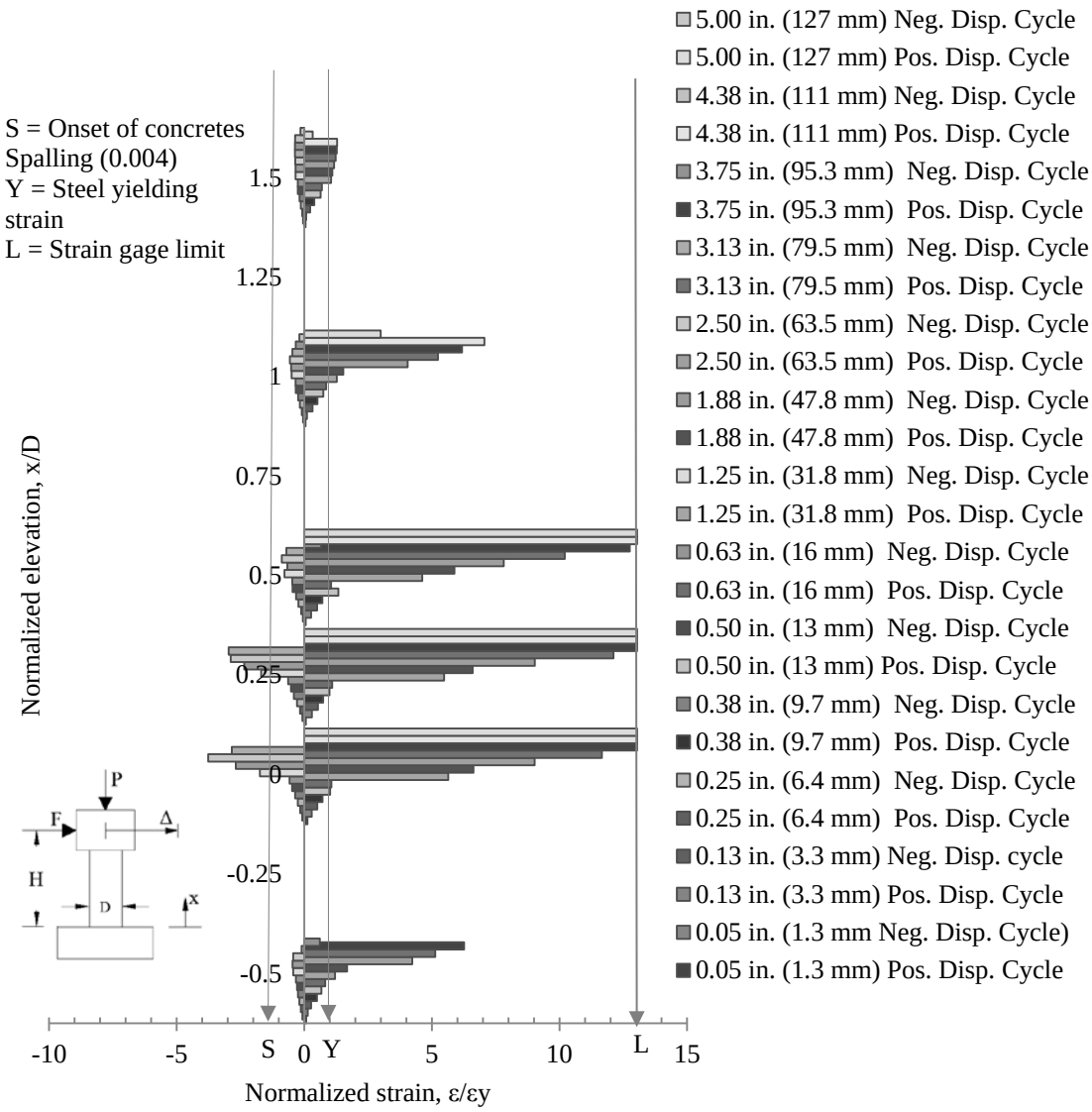

Figure 6.8: Longitudinal reinforcement strains in column C5

6.2.10 Column Curvature

The column curvature was computed at five levels between the five instrumentation levels and the footing for each displacement level. Figure 6.9 shows the curvature for each displacement cycle along the height of the column. The elevation and curvature are both normalized by the column diameter, D. Figure 5.13 shows the physical representation of the variables used in the curvature computations. Calculations used to determine curvatures at each level are shown in section 5.2.7. Note that the curvature corresponding to the 5.00-inch (127 mm) displacement cycle is not shown in the figure. The curvature is not shown for clarity because the column failed at a very small displacement during this cycle and did not reach the first peak.

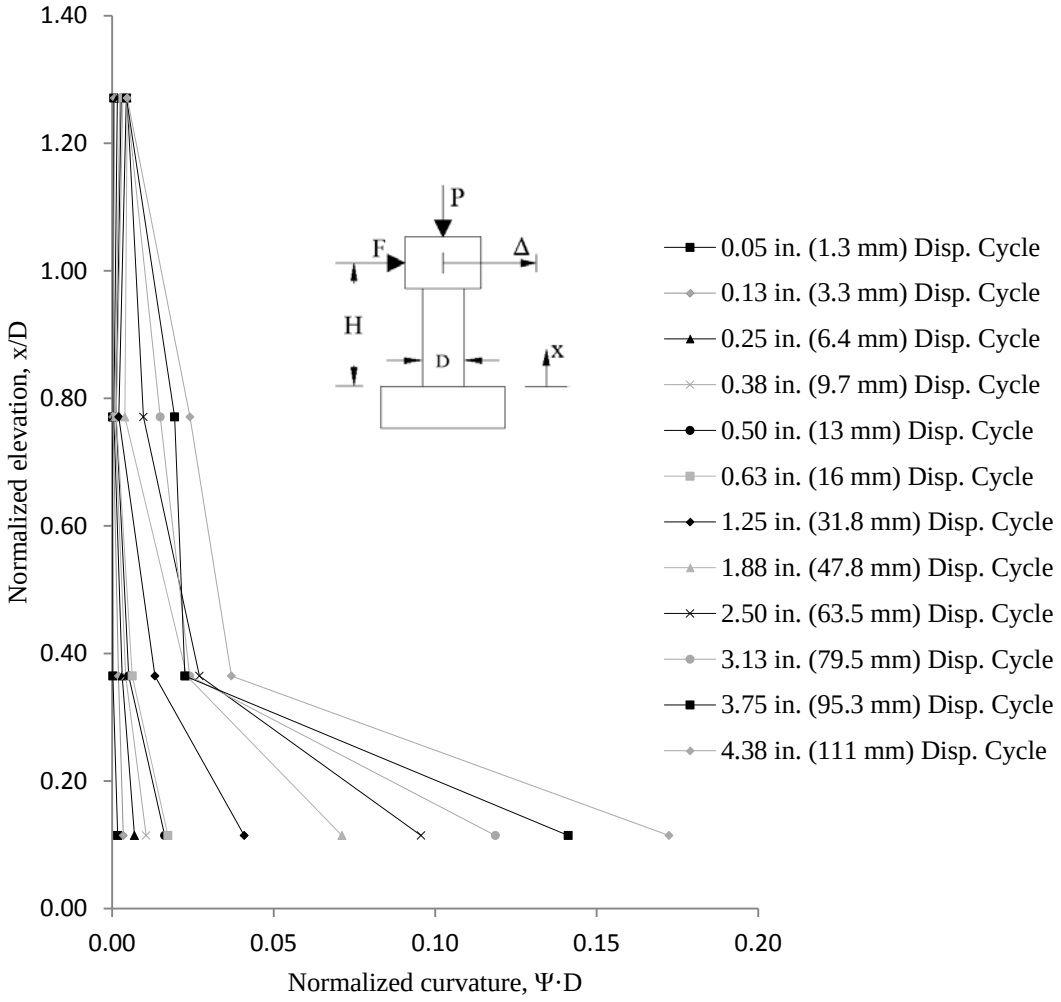

Figure 6.9: Normalized curvature versus normalized elevation of column C5

6.2.11 Applied Horizontal Load

The applied horizontal load is measured by a group of parallel load cells within the actuator. The applied load was plotted against the drift ratio as shown in Figure 6.10. The maximum applied force was negative 103.88 kips (462.1 kN) and the maximum drift ratio was 6.1 percent.

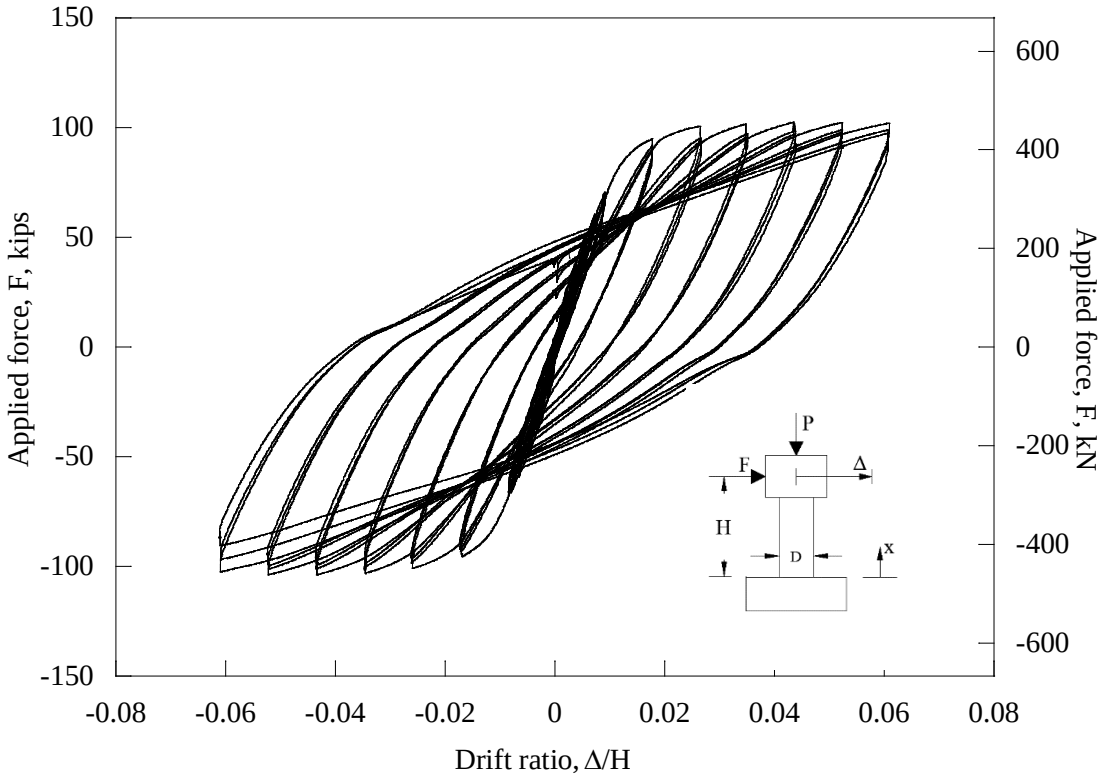

Figure 6.10: Drift ratio versus applied force of column C5

6.3 COLUMN C6 EXPERIMENTAL RESULTS

6.3.1 Concrete Cracking

Crack mapping was not performed on column C6 due to the density of the instrumentation around the column. However, photographs of the cracking were taken and the descriptions of the cracking were documented. Figure 6.11 shows a photograph of the cracking towards the end of testing. Initial cracking was observed at the 0.3 percent drift ratio level. These cracks are believed to be flexural cracks. Shortly later, at the 0.9 percent drift ratio level, shear cracks were observed. Shear cracks became dominate at the 1.7 percent drift ratio level. Shear cracking was distributed along the height of the column. Only the top 4 inches (102 mm) of the column exhibited no cracks. Cracking was similar to column C5.

Figure 6.11: Photograph of column C6 cracks

6.3.2 Concrete Spalling

Table 6.3 provides a summary of the displacement cycle at which concrete spalling was observed.

Table 6.3: Summary of column C6 concrete spalling

	Onset of concrete spalling	Concrete spalling	Deep concrete spalling
Displacement cycle inch (mm)	1.88 (47.8)	1.88 (47.8)	4.38 (111)
Drift ratio cycle	2.6%	2.6%	6.1%

6.3.3 Steel Reinforcing Bar Buckling

Figure 6.12 shows a photograph of the first reinforcing bars that buckled. The bar in the photograph is the southernmost longitudinal bar. The apex of the buckled reinforcing bar was located approximately 2 inches (51 mm) from the base of the column. The first bar buckled in column C6 during the 4.38-inch (111 mm) displacement cycle. The spiral seen in the photograph was bent outwards.

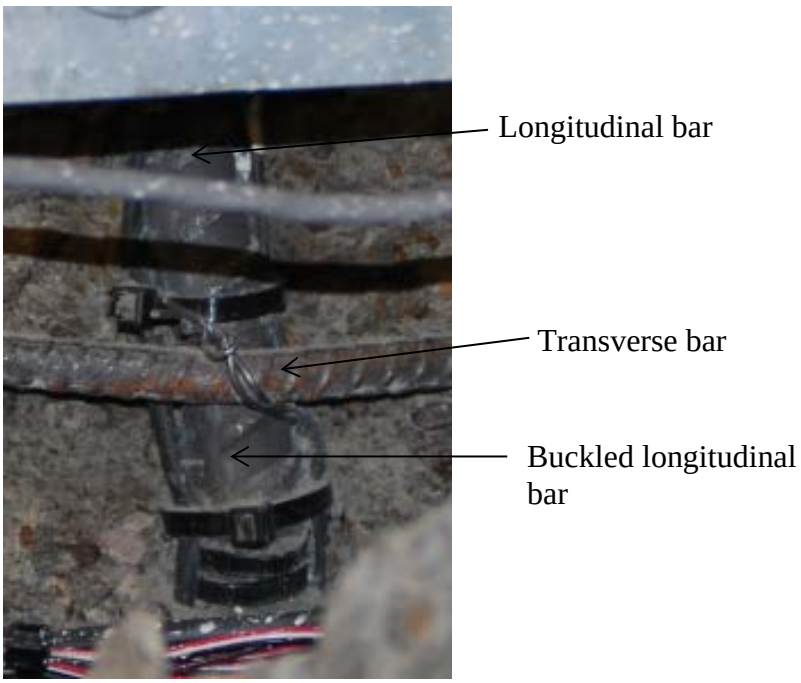

Figure 6.12: Photograph of column C6 initial buckling of longitudinal reinforcing bar

6.3.4 Steel Reinforcing Bar Fracture

The first longitudinal reinforcing bar fractured approaching the third peak of the 4.38 inch (111 mm) displacement cycle. The applied load was 76.93 kips (342.2 kN) and the tip displacement was 3.25 inches (82.6 mm). The first reinforcing bar to fracture was the southernmost bar which fractured at an elevation approximately 5 inches (127 mm) above the base of the column. Note this longitudinal bar may have buckled in two stages. The fracture occurred at the second buckling location, not the initial. It should be noted that the researchers are not sure whether the bar actually buckled twice or if the second apparent buckle location occurred after the bar fractured. It should also be noted that the concrete behind the longitudinal reinforcing bar had spalled. Figure 6.13 shows the first longitudinal reinforcing bar that fractured. Note the photograph shown was taken post testing. At the time of the fracture the bar was not as severely buckled as in the photograph.

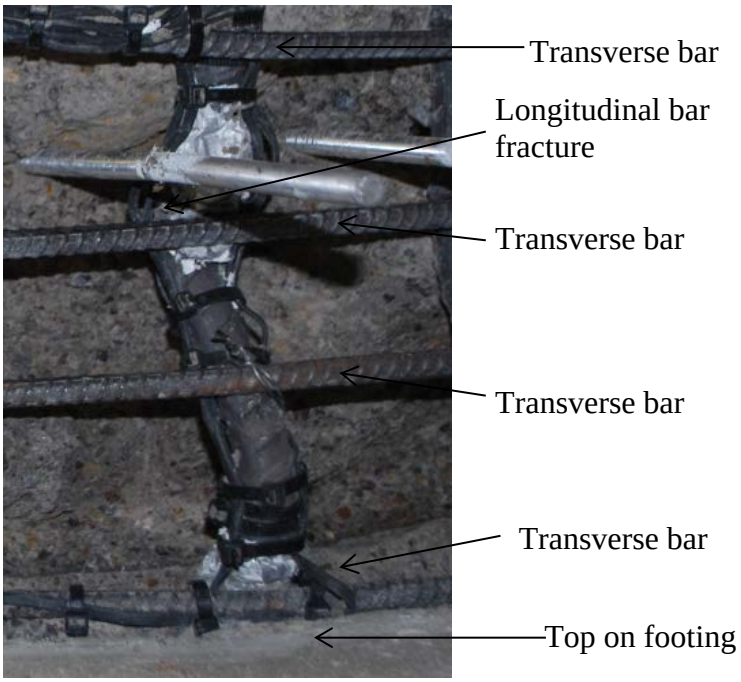

Figure 6.13: Photograph of column C6 first bar fracture

6.3.5 Column Lateral Displacement

For column C6, Figure 6.14 shows the maximum and minimum lateral deflections at the 5 points for the 12 displacement cycles. In this figure, the elevation is normalized with respect to the column diameter, *D*, and the lateral displacement, Δ, is normalized by the column test height, *H*.

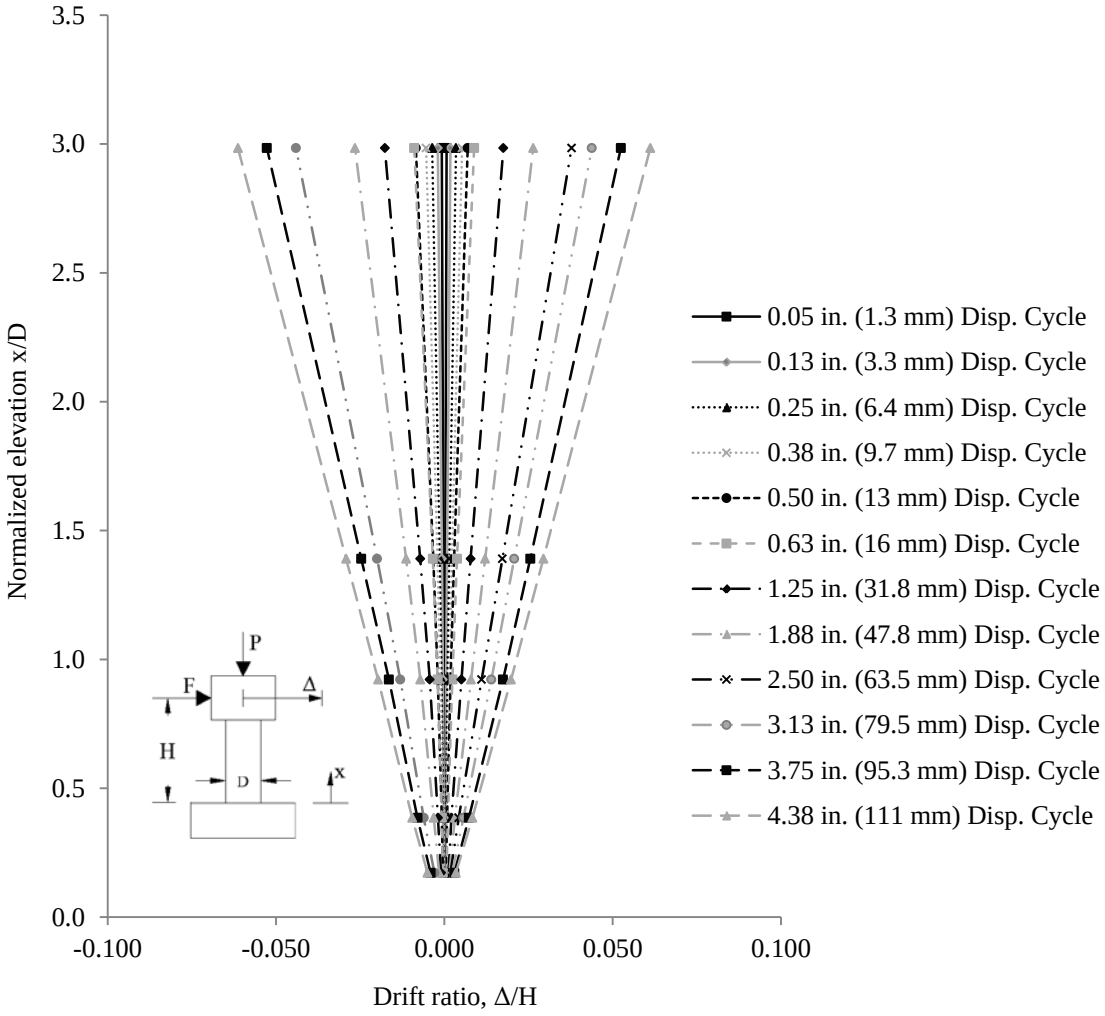

Figure 6.14: Drift ratio versus normalized elevation of column C6

6.3.6 Steel Reinforcement Strains

As previously mentioned, occasionally a strain gage would electronically clip or get damaged and the data from the strain gage was no longer used. If this occurred at a location where there were two strain gages, the data from the damaged gage was no longer used, but the strain gage still functioning was used. The strain gage instrumentation level and displacement cycle where this occurred are:

1. levels 2 and 3 during the 1.88-inch (48 mm) displacement cycle.

Once the longitudinal strains exceed the 3 percent strain capacity of the strain gages the value was reported as 3 percent for the tensile strains and the compression strain data was not used.

The strains gage instrumentation level and the displacement cycle when the 3 percent limit was hit are:

1. level 3 during the 2.50-inch (64 mm) displacement cycle;

2. level 2 during the 3.13-inch (80 mm) displacement cycle, and;

3. level 4 during the 3.75-inch (95 mm) displacement cycle.

Figure 6.15 shows the maximum transverse steel reinforcement strains for column C6 along the height of the column for each displacement cycle. The elevation is normalized by the column diameter, D, and the steel strain is normalized by the yield strain of the transverse reinforcement. The yield strain is defined in the same manner as described in section 5.2.6 for column C1.

Figure 6.16 shows the maximum longitudinal steel reinforcement strains of column C6 along the height of the column for each positive and negative displacement cycle. The maximum positive displacement cycle corresponds to the maximum tension strain. The maximum negative displacement cycle corresponds to the maximum compressive strain. The elevation is also normalized by the column diameter, D, and the steel strain is normalized by the yield strain of the longitudinal reinforcement. Note that in this figure it appears that the concrete did not spall, however this is due to the strain gage hitting the 3 percent strain limit. It should also be noted that the strains shown are of the longitudinal reinforcement and not the outer edge of the concrete.

The yield strain was computed in the same manner as the transverse yield strain. Table 6.4 shows the experimental yield strain values used to determine the yield strain values used in the analysis. Note that the transverse and longitudinal strains are stacked in terms of the displacement cycle, i.e., the lowest bar strains at each elevation represents 0.05 inch (1.3 mm) displacement cycle and the highest bar represents the 4.38 inch (111 mm).

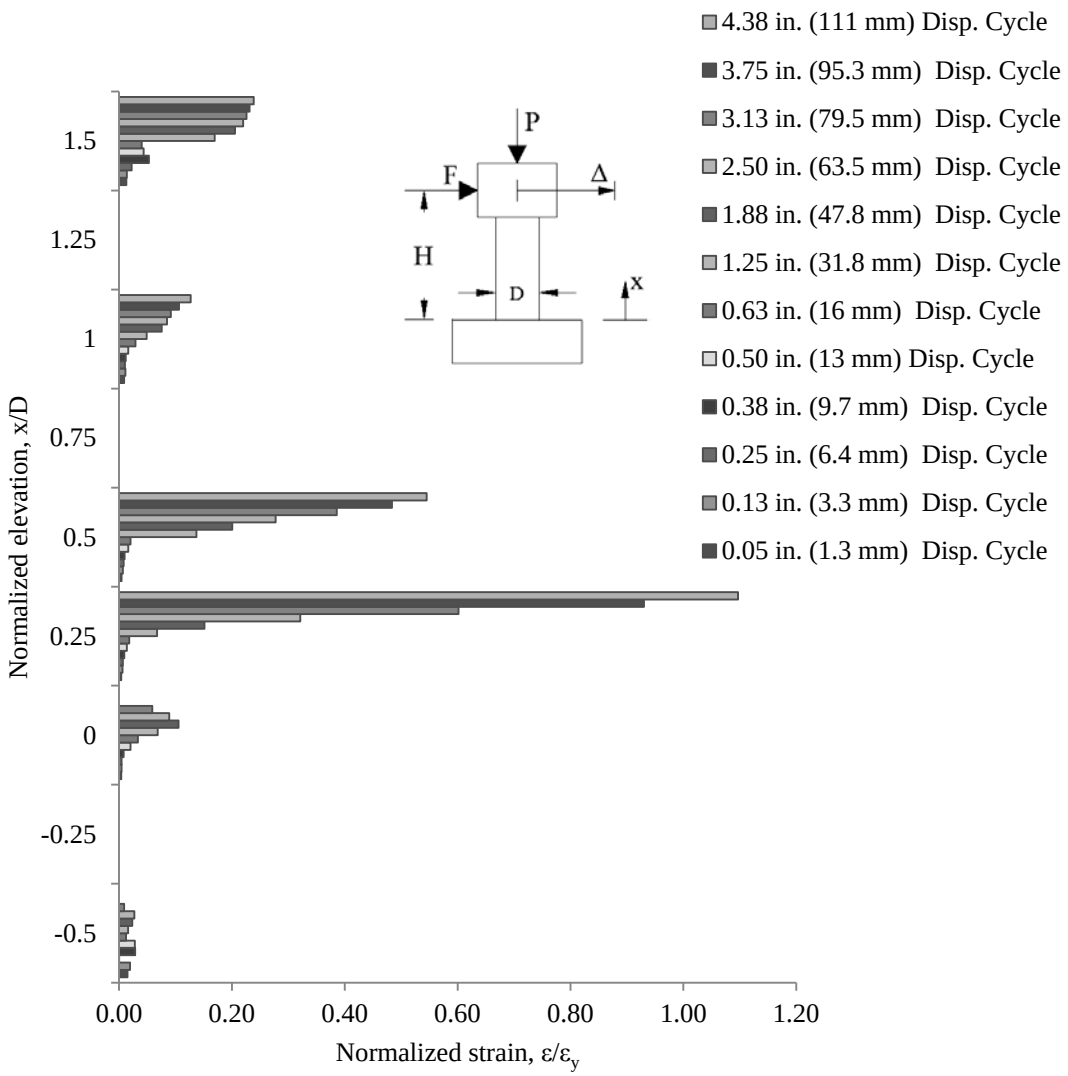

Figure 6.15: Transverse reinforcement strains in column C6

Table 6.4: Column C6 yield strains used in the strain analysis

Reinforcement	Calculated yield strain	Measured yield strain (0.2% OM)
#3 (#10M) Grade 80 ksi (550 MPa)	0.0035	0.0055
#6 (#19M) Grade 80 ksi (550 MPa)	0.0028	0.0048

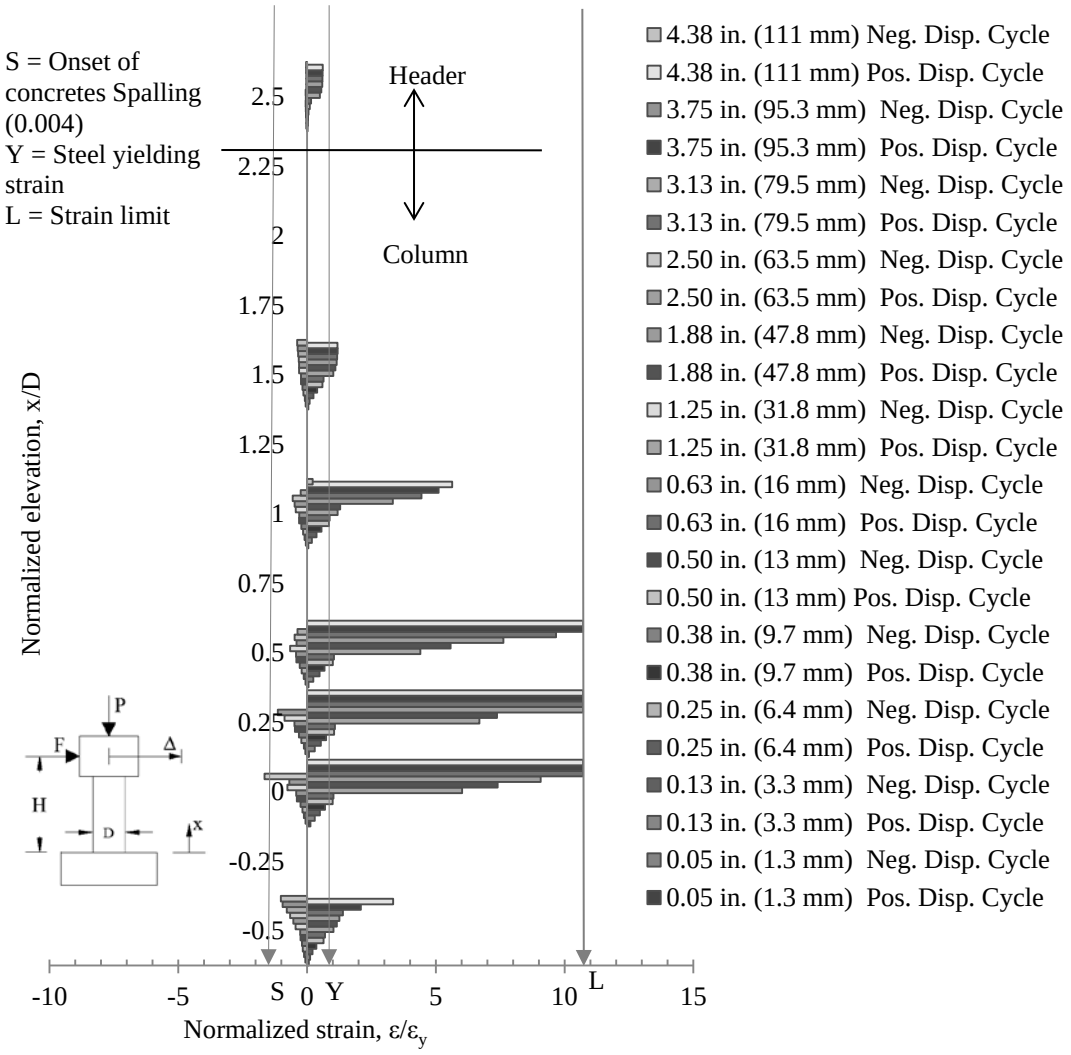

Figure 6.16: Longitudinal reinforcement strains in column C6

6.3.7 Column Tilt

Figure 6.17 shows a plot of the measured tilt and the calculated tilt versus the applied force. The calculated tilt was computed as the tip displacement divided by the column height (in degrees). As seen in the plot there is an increasing difference between the measured tilt and the calculated tilt as the applied force reaches its maximum and minimum values. As with the other columns, this is likely due to the positioning of the string pot that measures the tip displacement as well as the differences between rotations measured from the base of the column versus the tip rotation. As the column is being pushed horizontally the column also bends creating an additional vertical component measured by the string pot.

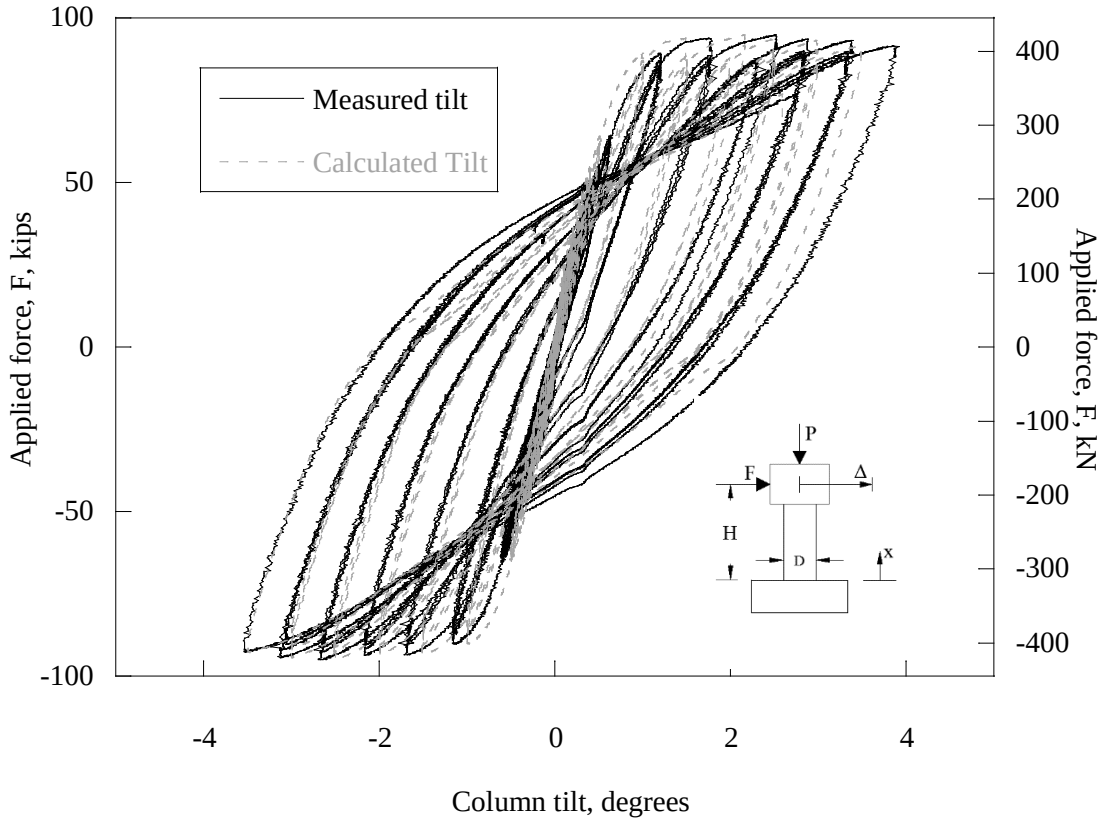

Figure 6.17: Tilt versus applied force of column C6

6.3.8 Vertical Load

Figure 6.18 the axial load increased as the applied horizontal load increased for column C6. The axial load for column C6 also dropped below the initial 90 kips (400 kN).

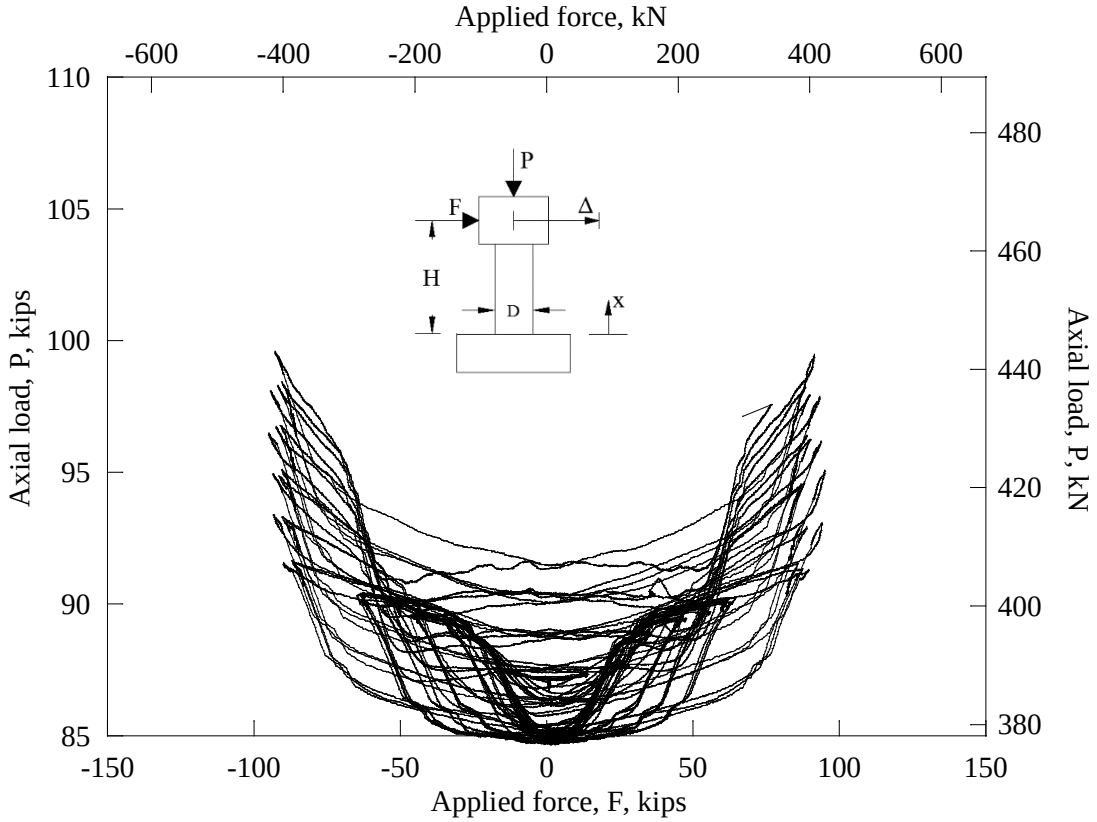

Figure 6.18: Applied force versus axial load of column C6

6.3.9 Footing Displacement and Strong Wall Displacements

The footing was instrumented with four vertical LVDTs at each corner of the top face of the footing and two LVDTs on the north face of the riser block and two string pots of the footing as discussed in Chapter 3 to determine if the footing rotated or displaced during the testing. The data from the six LVDTs and two string pots showed that there was neither significant rotation nor horizontal displacement of the footing. No LVDT reading ever exceeded 0.04 inch (1.0 mm). The strong wall was instrumented with two string pots. The data from the string pots showed there was no significant displacement of the strong wall. The string pot recordings never exceeded 0.01 inches (0.3 mm).

6.3.10 Column Curvature

The curvature was computed between the five instrumentation levels as well as between the footing and the first instrumentation level for each displacement level. Figure 6.19 shows the curvature for each displacement cycle along the height of the column. Figure 5.13 shows the physical representation of the variables used in the curvature computations. Calculations used to determine the curvature at each level, shown in section 5.2.7.

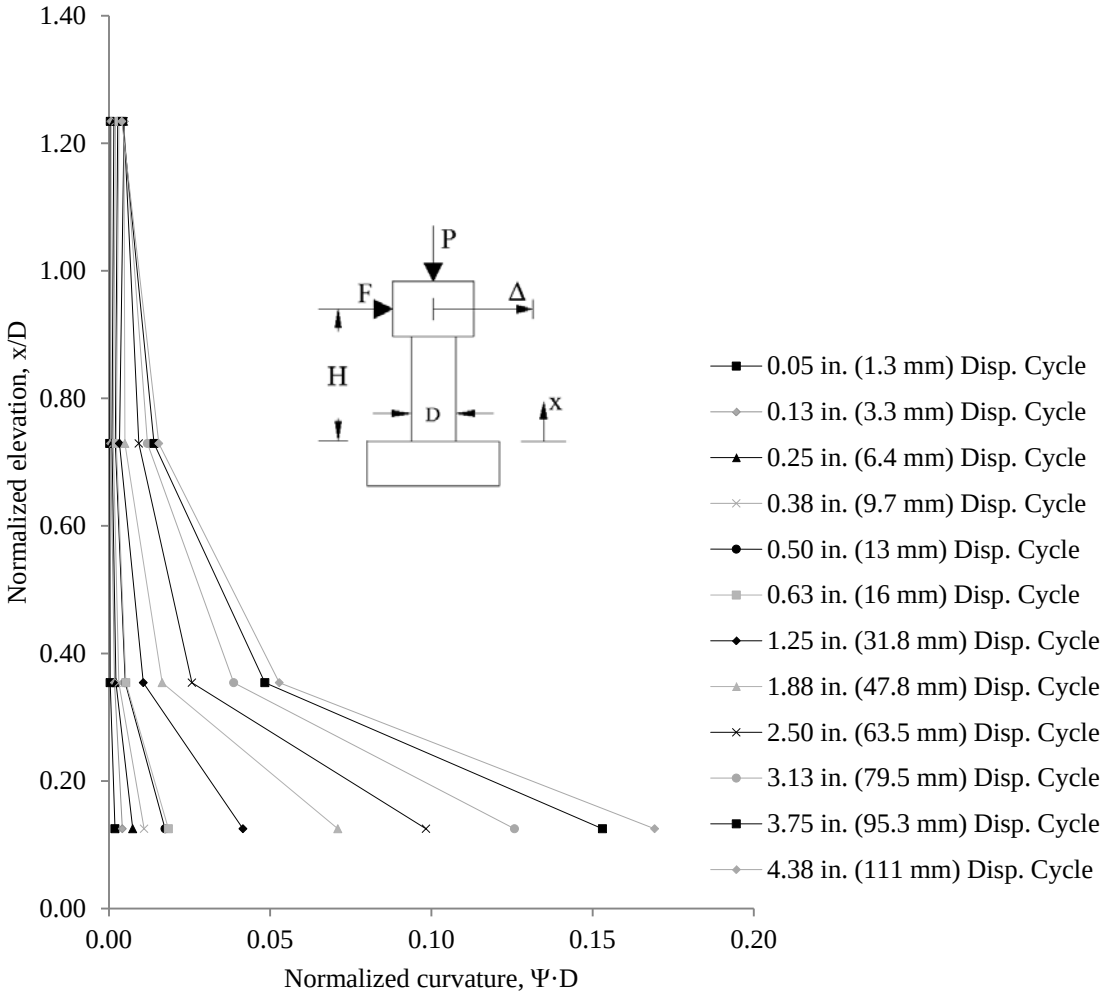

Figure 6.19: Normalized curvature versus normalized elevation of column C6

6.3.11 Applied Horizontal Load

The applied horizontal load is measured by a group of parallel load cells within the actuator. The applied load was plotted against the drift ratio as shown in Figure 6.20. The maximum applied force was negative 95.01 kips (422.6 kN) and the maximum drift ratio was 6.1 percent.

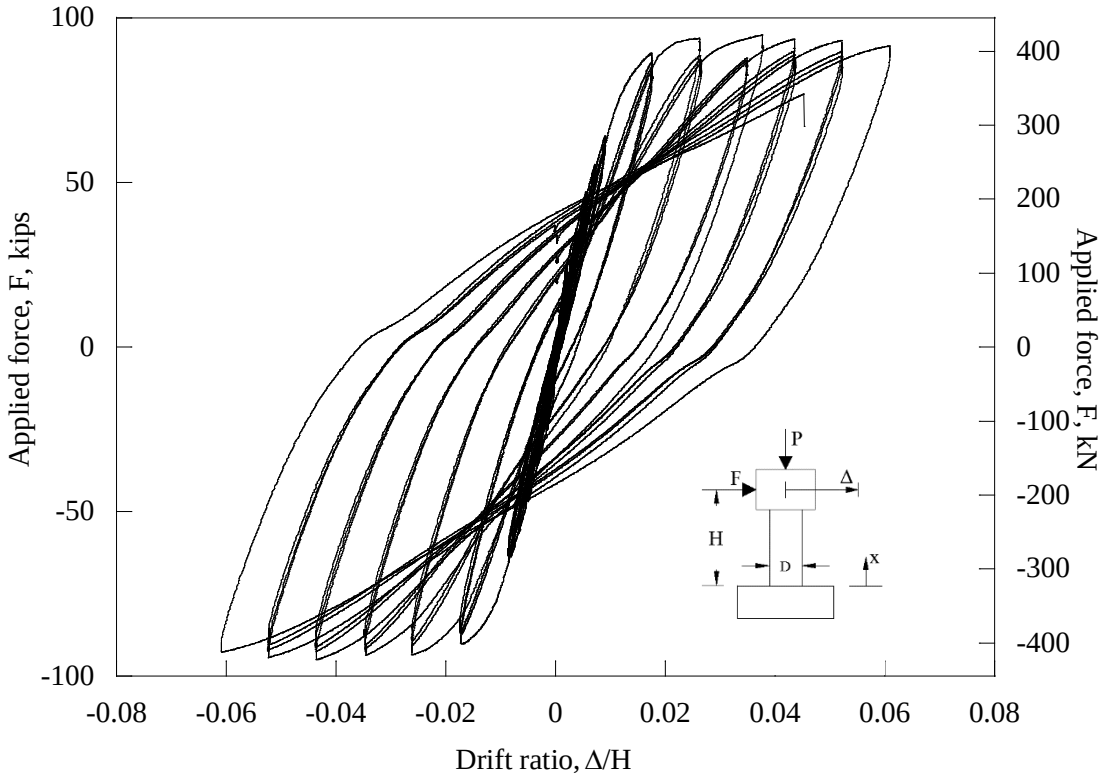

Figure 6.20: Drift ratio of applied force of column C6

6.4 SUMMARY

This chapter presented both visual and measured observations for two columns (C5 and C6). The visual observations included cracking, concrete spalling, bar buckling and bar fracture. The measured observations included column lateral displacement, steel reinforcement strains, column curvature, column tilt, horizontal applied load, vertical applied load, footing displacement and strong wall displacements. The measured observations were reported up to column failure which was defined as the first longitudinal bar fracture. The goal of this section was to present the data of the two columns under cyclic lateral loading. Chapter 7 contains the analysis of the data presented in this chapter as well as post failure performance.

7.0 ANALYSIS OF EXPERIMENTAL DATA

7.1 INTRODUCTION

Analyses were conducted using experimental data presented in Chapters 5 and 6. For the analyses in this report the initial bar fracture is defined as the point of column failure. Therefore, only data collected until the first bar fracture is included for columns C1, C2, C3, and C4. Results for columns C5 and C6 are analyzed up to first bar fracture as well, but analysis of post failure performance is also presented.

The effect of steel reinforcement grade, longitudinal reinforcement ratio, and column moment-shear span ratio are evaluated based on the visual observations, column lateral displacement, column steel reinforcement strains, column curvature, column forces, energy dissipation, and column ductility.

7.2 EFFECT OF STEEL REINFORCEMENT GRADE

In this section three sets of columns are compared. Columns C1 and C2, columns C3 and C4, and columns C5 and C6. Each pair consists of one column reinforced with Grade 60 (columns C1, C3, and C5) and one column reinforced with Grade 80 (columns C2, C4, and C6).

7.2.1 Column C1 and C2

Columns C1 and C2 are compared to determine the effects of reinforcement grade for columns designed with the minimum reinforcement ratio and a moment-shear span ratio equal to six. Note that both columns have approximately 1.11 percent equivalent Grade 60 longitudinal reinforcement ratio. The purpose of this section is to compare the performance of a column reinforced with A706 Grade 80 with the aforementioned properties against one reinforced with A706 Grade 60.

7.2.1.1 Visual Observations

Columns C1 and C2 exhibited similar crack distributions. However, the cracks in column C2 seem to appear over a larger height than column C1. This difference is approximately 2 feet (0.61 m). It is not clear whether this is a result of the reinforcement grade or a result of fewer longitudinal reinforcing bars in column C2. Figure 7.1 shows a side-by-side comparison of the cracking of columns C1 and C2. The larger development length of the Grade 80 may also contribute to this. Note that these photographs were not taken at the same displacement ratio cycle.

Figure 7.1: Photographs of column C1 (left) and C2 (right) cracking

Columns C1 and C2 exhibited the onset of concrete spalling during the same displacement cycles. Deep concrete spalling for column C2 occurred 2 displacement cycles later than column C1. Deep concrete spalling occurred for column C2 on the 8.75-inch (0.222 m) displacement cycle and at the 6.25-inch (0.159 m) displacement cycle for column C1. The location of the longitudinal reinforcing bar that buckled and ruptured was the same for both columns—this bar was the bar furthest to the south (closest to the strong wall). Thus, the mode of failure of the columns was flexural with bar buckling followed by tension fracture. The first longitudinal reinforcing bar to buckle and fracture in column C2 occurred at a height of approximately 2.5 inches (0.064 m) further from the base of the column when compared with column C1. The bar fractured in column C1 was approximately 6 inches (0.152 m) from the base of the column at the final peak of the 7.50-inch (0.191 m) displacement cycle. The column C2 bar fractured approximately 8.5 inches away from the base of the column on the return from the first peak of the 8.75-inch (0.222 m) displacement cycle. The first longitudinal reinforcing bar in column C2 ruptured one displacement cycle later than column C1. Columns C1 and C2 both exhibited initial bar buckling in the direction of the applied load.

From the visual observation results of columns C1 and C2, column C2 similar performance, crack pattern, and mode of failure. The visual observations suggest that Grade 80 reinforcement meeting ASTM A706 specifications can be used as an alternative to Grade 60 reinforcement for columns with a relatively small reinforcement ratio (near 1 percent). It should be noted that because the bar fracture in column C2 occurred at a higher elevation than the bar fracture in

column C1, the plastic hinge zone may need to be extended and/or additional development length provided. Although further research is needed to assess this, longitudinal bar buckling and fracture higher in the column may be an advantage for post-earthquake rehabilitation.

7.2.1.2 Maximum Lateral Displacement

Displacements at the level of the horizontal actuator force were recorded for all tests. Column C2 exhibited a maximum displacement of 8.79 in (0.223 m) and column C1 exhibited a maximum displacement of 7.53 in (0.191 m). Figure 7.2 shows the drift ratio vs. elevation for the 7.5 inch (0.191 m) and 8.75 inch (0.222 m) displacement cycles for columns C1 and C2. The maximum drift ratio of column C1 was 5.23 percent and 6.11 percent for column C2.

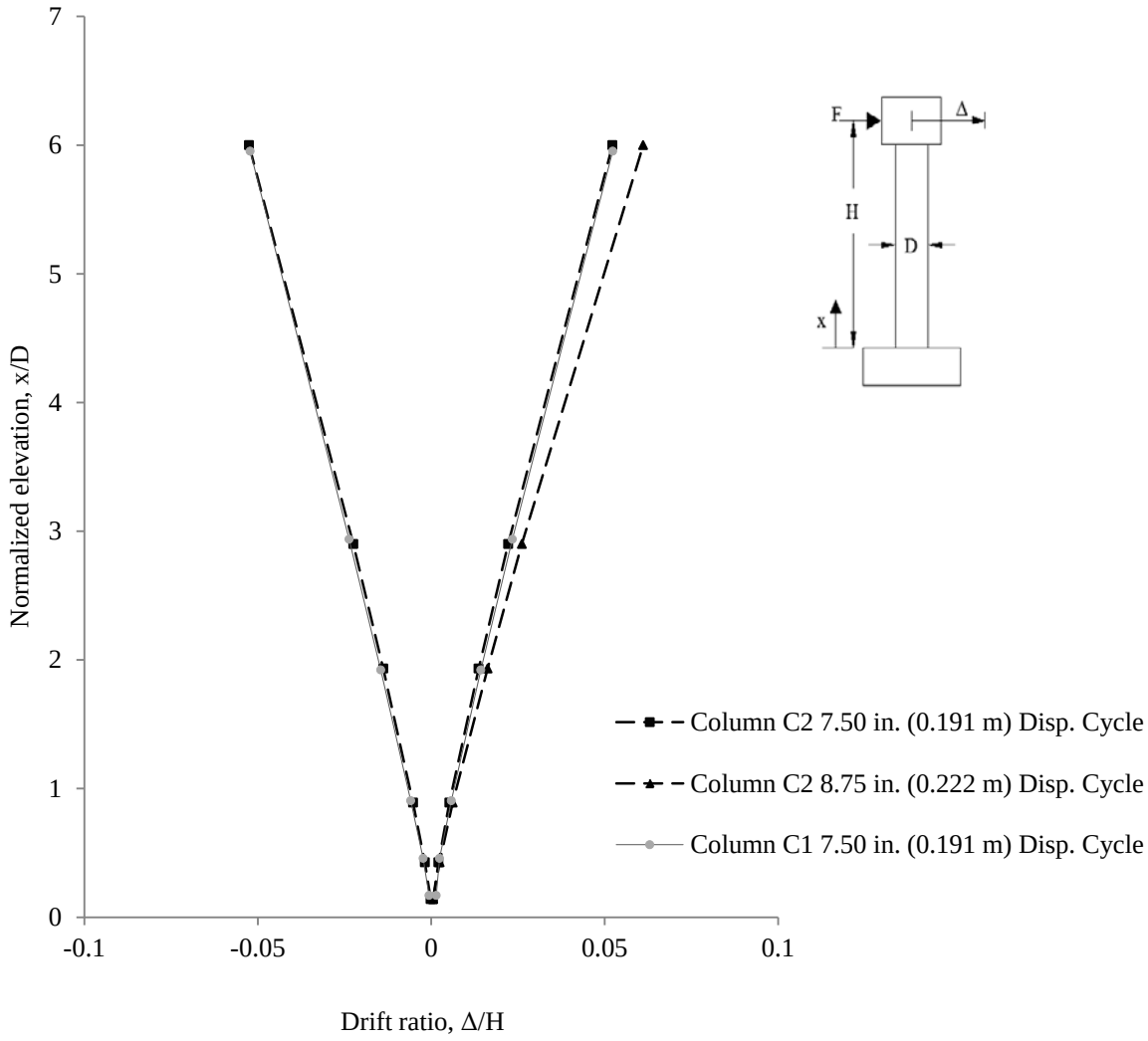

Figure 7.2: Drift ratio versus normalized elevation of columns C1 and C2

Figure 7.2 shows the drift ratios for columns C1 and C2 along the normalized elevation of the column. It can be seen that the profile of the drift ratios are very similar for the 7.50 inch (0.191 m) displacement cycle (equivalent to a drift ratio of 5.2 percent). It is also seen that column C2 did not fail until the 8.75 inch (0.222 m) displacement cycle (equivalent to a drift ratio of 6.1 percent).

7.2.1.3 Steel Reinforcement Strains

Columns C1 and C2 had strain gages attached at similar locations to compare the strains in the steel reinforcement during loading. Figure 3.10 shows the locations of the strain gages and the levels at which these were installed. The

longitudinal reinforcing bars in column C1 yielded first at a tip displacement of 1.17 inches (29.7 mm). This occurred at the base of the column, level 2, where the strain is largest during the approach to the first peak of the 1.25 inch (31.8 mm) displacement cycle. The steel reinforcing bar also yielded at levels 3 and 4 during this displacement cycle. The longitudinal bars in column C2 first yielded at a tip displacement of 1.52 inches (38.6 mm). This occurred at instrumentation level 3 during the approach to the first peak of the 2.50 inch (63.5 mm) displacement cycle. The reinforcement at the base of the column, level 2, through level 5 also yielded later in this same displacement cycle. Note that the longitudinal reinforcing bar in column C2 first yielded 6 inches (152 mm) above the base of the column while the longitudinal reinforcing bar in column C1 first yielded at the base of the column. This may indicate that additional details are required to develop the Grade 80 reinforcing bars at the base of the column and that development lengths are larger for Grade 80 reinforcement.

The longitudinal steel in column C1 yielded in the footing (level 1) on the 3.75 inch (95.3 mm) displacement cycle and the longitudinal steel in column C2 did not yield in the footing (level 1) until the 8.75 inch (222 mm) displacement cycle. This indicates that the contribution of strain penetration is not as critical for column C2 as compared to column C1. Table 7.1 shows the transverse strains for columns C1 and C2 for 3 displacement cycles. All the transverse strains were very small in magnitude and never reached yielding. However, it can be seen in Table 7.1 that the transverse strains in column C2 were typically larger than those of column C1. This may be due to the larger spacing between the longitudinal reinforcing bars embedded in column C2 compared to column C1. Note that column C1 does not have transverse strains for level 1(in the footing) because the lead wires were damaged during fabrication of the footing.

Table 7.1: Summary of maximum transverse steel reinforcement strains of columns C1 and C2

Level	Elevation in. (mm)	2.50 inch (63.5 mm) displacement cycle		5.00 inch (127 mm) displacement cycle		7.50 inch (191 mm) displacement cycle	
		C1 max % strain	C2 max % strain	C1 max % strain	C2 max % strain	C1 max % strain	C2 max % strain
1	-12.00 (-304.8)	N.A.*	0.0063	N.A.*	0.0097	N.A.*	0.0098
2	0.00 (0.00)	0.0067	0.0106	0.0093	0.0070	0.0172	0.0271
3	6.00 (152)	0.0020	0.0059	0.0031	0.0140	0.0136	0.0162
4	12.00 (304.8)	0.0066	0.0059	0.0133	0.0106	0.0329	0.0129
5	24.00 (609.6)	0.0078	0.0125	0.0120	0.0152	0.0145	0.0143
6	48.00 (1,219)	0.0062	0.0112	0.0070	0.0136	0.0067	0.0150
7	72.00 (1,829)	0.0069	0.0079	0.0083	0.0118	0.0097	0.0132

* N.A. Not available because lead wires were damaged during the footing concrete placement.

Table 7.2 shows the longitudinal tensile strains for columns C1 and C2 for 3 displacement cycles. For all displacement cycles prior to reaching the maximum three percent strain, column C1 had larger longitudinal tensile strains at instrumentation levels two and three when compared to column C2. Also worth noting is that column C1 exhibits maximum strains at level 2 (at the base of the column) while column C2 exhibits maximum strains at level 3 (6 inches [152 mm] from the base of the column). This may suggest that column C2 reinforcement (Grade 80 reinforcement) may require additional detailing to ensure the bar is fully developed at the base of the column, as already noted. At instrumentation levels four and five the data indicate that the columns exhibited similar performance and reinforcement tensile strains. The data indicate that at higher elevations (levels 6 and 7) column C2 has larger longitudinal tensile strains compared to column C1.

Table 7.3 shows the longitudinal compressive strains for columns C1 and C2 for 3 displacement cycles. The compressive strains were very similar for the vast majority of locations and displacement cycles, except at levels 2 and 3 at and past the 2.50-inch (63.5 mm) displacement cycle where column C1 exhibited significantly larger compressive strains.

Table 7.2: Summary of maximum longitudinal tensile steel strains of columns C1 and C2

Level	Elevation in. (mm)	2.50 inch (63.5 mm) displacement cycle		5.00 inch (127 mm) displacement cycle		7.50 inch (191 mm) displacement cycle	
		C1 max % strain	C2 max % strain	C1 max % strain	C2 max % strain	C1 max % strain	C2 max % strain
1	-12.00 (-304.8)	0.12	0.19	0.29	0.24	0.35	0.30
2	0.00 (0.00)	1.57	1.15	3.00	1.40	3.00	3.00
3	6.00 (152)	1.33	1.29	2.28	2.20	3.00	3.00
4	12.00 (304.8)	0.30	0.96	2.33	1.95	3.00	3.00
5	24.00 (609.6)	0.34	0.81	1.38	1.00	1.52	0.95
6	48.00 (1,219)	0.27	0.30	0.30	0.35	0.30	0.36
7	72.00 (1,829)	0.17	0.21	0.20	0.27	0.20	0.27

Table 7.3: Summary of maximum longitudinal compressive steel strains of columns C1 and C2

Level	Elevation in. (mm)	2.50 inch (63.5 mm) displacement cycle		5.00 inch (127 mm) displacement cycle		7.50 inch (191 mm) displacement cycle	
		C1 max % strain	C2 max % strain	C1 max % strain	C2 max % strain	C1 max % strain	C2 max % strain
1	-12.00 (-304.8)	-0.14	-0.11	-0.07	-0.17	-0.09	-0.17
2	0.00 (0.00)	-0.23	-0.12	N.A.*	0.11**	N.A.*	N.A.*
3	6.00 (152)	-0.64	-0.20	-1.14	-0.50	N.A.*	N.A.*
4	12.00 (304.8)	-0.21	-0.23	-0.23	-0.34	N.A.*	N.A.*
5	24.00 (609.6)	-0.14	-0.13	-0.19	-0.26	-0.32	0.13**
6	48.00 (1,219)	-0.12	-0.11	-0.13	-0.13	-0.14	-0.14
7	72.00 (1,829)	-0.07	-0.08	-0.08	-0.09	-0.08	-0.10

*N.A. equals not available, the data was not used because the strain gage had reached the 3 percent maximum strain limit in tension
** The data showed that the gage never went into compression

7.2.1.4 Column Curvature

The normalized curvature data were shown in Chapter 5. The curvature was normalized by multiplying the value by the diameter, D, of the column. The largest curvatures occurred closest to the base of the column and reduced in magnitude along the height of the column. Table 7.4 shows the curvature for 3 of the larger displacement cycles for columns C1 and C2. It can be seen that the curvatures at instrumentation levels other than level 1 are very similar for the two columns. However, at level 1, for all displacement cycles, column C1 exhibited larger values of curvature when compared to column C2. These results indicate that Grade 80 and Grade 60 reinforced columns have similar curvatures resulting from flexural deformations (i.e., from levels 2 through 5). The curvature at level 1 is composed of flexural deformations and strain penetration. It is not possible to state exactly which of the two contributions is making the curvature values at the lower level for column C1 larger than those of column C2. However, analysis of the data of the longitudinal strains at the same elevations, indicate that column C1 exhibits larger strain penetration effects, which explains the larger curvature values measured at level 1.

Nonetheless, since at all other levels both columns show similar curvatures it can be said that columns with Grade 80 reinforcement achieve similar curvature demands and therefore a substantial shift of the neutral axis is not expected.

Table 7.4: Summary of column C1 and C2 curvature

Level	Approx. elevation in. (mm)	2.50 inch (63.5 mm) displacement cycle		5.00 inch (127 mm) displacement cycle		7.50 inch (191 mm) displacement cycle	
		C1 max normalized curvature	C2 max normalized curvature	C1 max normalized curvature	C1 max normalized curvature	C1 max normalized curvature	C2 max normalized curvature
1	3.00 (76)	0.031	0.021	0.085	0.066	0.119	0.115
2	9.00 (229)	0.008	0.010	0.029	0.027	0.050	0.053
3	18.00 (457)	0.005	0.004	0.010	0.011	0.021	0.017
4	36.00 (914)	0.004	0.005	0.005	0.007	0.005	0.008
5	60.00 (1,524)	0.003	0.003	0.004	0.004	0.004	0.004

7.2.1.5 Column Forces

The applied horizontal load was measured using a load cell in the actuator while the tip displacement was measured using a string pot. The geometry effects of the applied axial load due to the experimental setup, is a follower load affecting the shear and moment demands of the column. To remove this effect, the following steps were done.

1. Compute the axial force angle with respect to the vertical axis, θ;

$$\theta = \frac{\Delta}{H + d_f} \tag{7.1}$$

   where d_f is the distance from the top of the footing to the location where the axial load rod is tied to.

2. Compute the horizontal and vertical components of the applied follower (axial) load, P_H and P_V, respectively;

$$P_H = P \sin(\theta) \text{ and } P_V = P \cos(\theta) \tag{7.2}$$

3. Compute the current moment demand of the column, *M*;

$$M = \left(F - P_H\right) H + P_V \Delta \tag{7.3}$$

4. Compute the current column shear force of the column, *V*;

$$V = F - P_H \tag{7.4}$$

Table 7.5 shows the column forces and moment demands for both columns. These define the moment capacity and the associated horizontal forces. The associated plastic shear force is the expect shear force associated with the expected moment capacity. As shown in the table, the maximum applied forces of the two columns are very similar, and the maximum applied column shear forces are the same. The moment capacity of column C2 is slightly smaller than the moment capacity of column C1. The main difference in this moment capacity is likely due to the different material overstrength factors for the ASTM A706 Grade 60 and ASTM A706 Grade 80. The percent difference between the actual moment capacities of columns C1 and C2 is 3.2 percent. The percent differences suggest that no special considerations are needed to predict the moment capacity of a concrete column reinforced with Grade 80 with a moment-shear span ratio of 6 and near the minimum longitudinal reinforcement ratio compared to a column reinforced with Grade 60.

Table 7.5: Moment and force capacity of columns C1 and C2

Column	Maximum applied force kip (kN)	Column shear force kip (kN)	Associated plastic shear kip (kN)	Nominal moment capacity (Response 2000)	Tested moment capacity kip-ft (kN-m)	Expected moment capacity kip-ft (kN-m)
C1	28.9 (128.4)	25.9 (115.1)	33.58 (149.4)	288 (390)	354 (480)	403 (546)
C2	28.2 (125.6)	25.9 (115.1)	33.22 (147.8)	285 (386)	344 (466)	399 (541)

In the design stage the nominal moment capacities were computed using Response 2000® and assuming elastic perfectly-plastic steel stress strain models with nominal material properties. It is worth nothing that ODOT BDDM *(ODOT 2012*) suggests the use of expected plastic material properties. Other more advanced material models are used in the next chapter to improve the prediction capability of the models. The experimental computed overstrength factor was taken as the ratio of the tested moment capacity to the nominal moment capacity based on nominal material properties. For column C1, the overstrength factor of 1.23 is obtained, and for column C2 the overstrength factor of 1.20 is obtained.

Figure 7.3 shows the applied horizontal force versus the drift ratio for columns C1 and C2 up to the first longitudinal bar fracture. It can be seen that the overall shape of the hysteretic loops are similar, but column C1 has more area in between the loading and unloading curves resulting in greater energy dissipation. This is discussed in more detail in section 7.2.1.6.

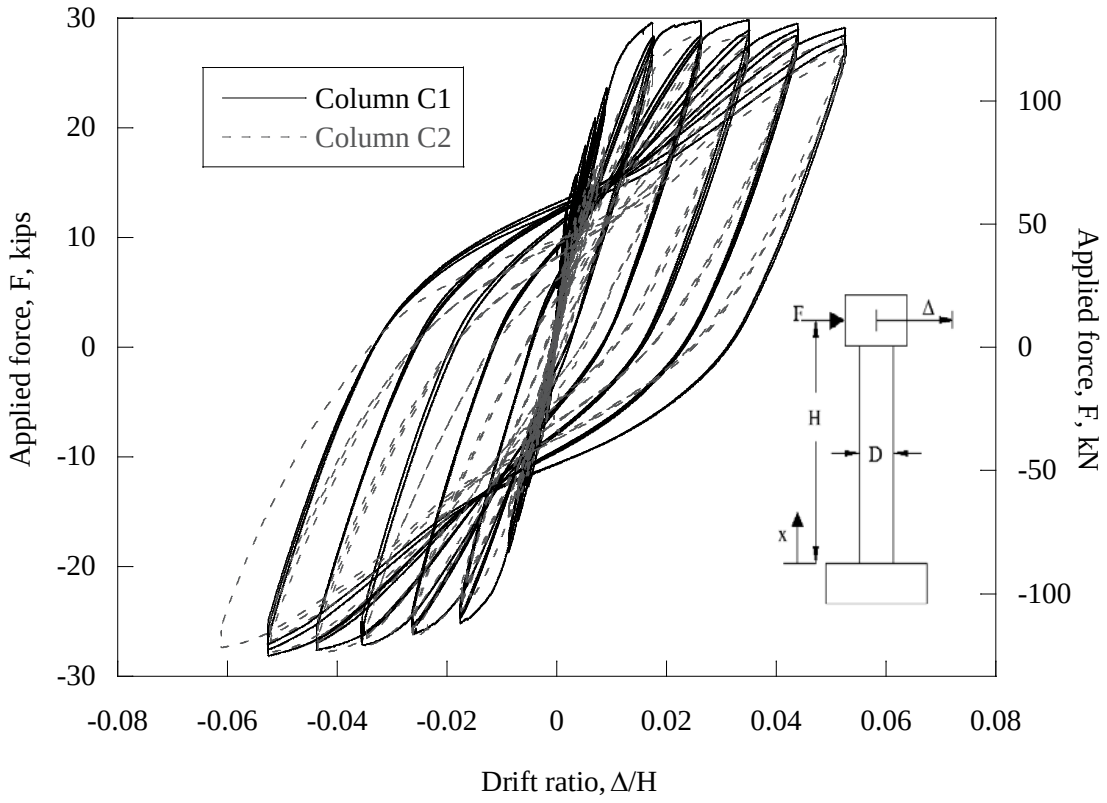

Figure 7.3: Drift ratio versus applied force of columns C1 and C2

Figure 7.4 shows a plot of the shear force versus drift ratio for columns C1 and C2. It can be seen from this plot that the response of the two columns are very similar except that when unloading column C1 is stiffer than column C2. It is worth noting that with increasing the level of displacement, the shear forces decrease due to P-Δ effects.

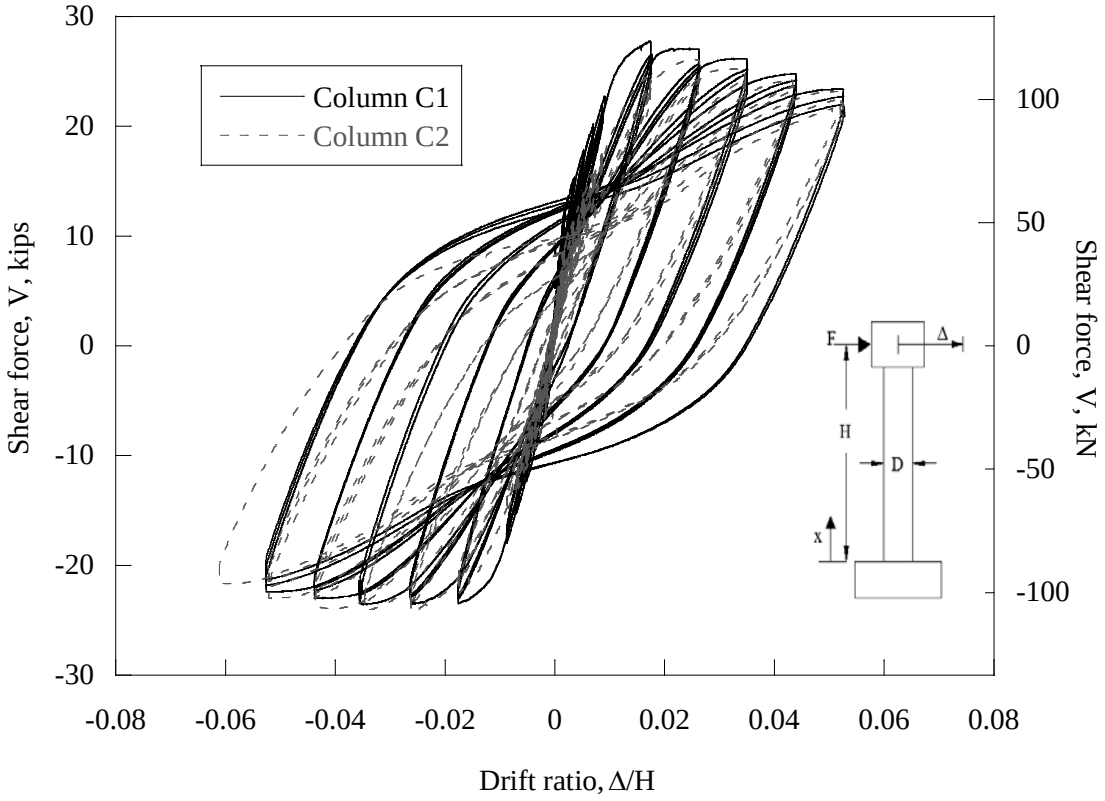

Figure 7.4: Columns C1 and C2 shear force versus drift ratio

7.2.1.6 Hysteretic Energy Dissipation

The energy dissipated was determined for each column. The value was determined by taking the area within the applied force versus displacement hysteretic loops for each displacement cycle. This was computed by numeric integration using the Simpson Rule. It is worth noting that for each drift ratio level there was 3 cycles each having a north and south displacement peak equal to the value of the given drift ratio level. Also, note that for the final displacement cycle for column C2 only two peaks were reached before the first reinforcing bar fractured.

As shown in Figure 7.5, column C1 exhibited greater energy dissipation until the failure cycle when compared to column C2. This was expected because column C1 had more reinforcing bars and therefore was stiffer than column C2. Table 7.6 shows the total energy dissipated up to the first reinforcing bar fracture, first yield, and reference yield. It can be seen in this table that overall column C1 dissipated more energy when compared to column C2 prior to failure. However, column C2 dissipated more energy at the column first yield and reference yield compared to column C1.

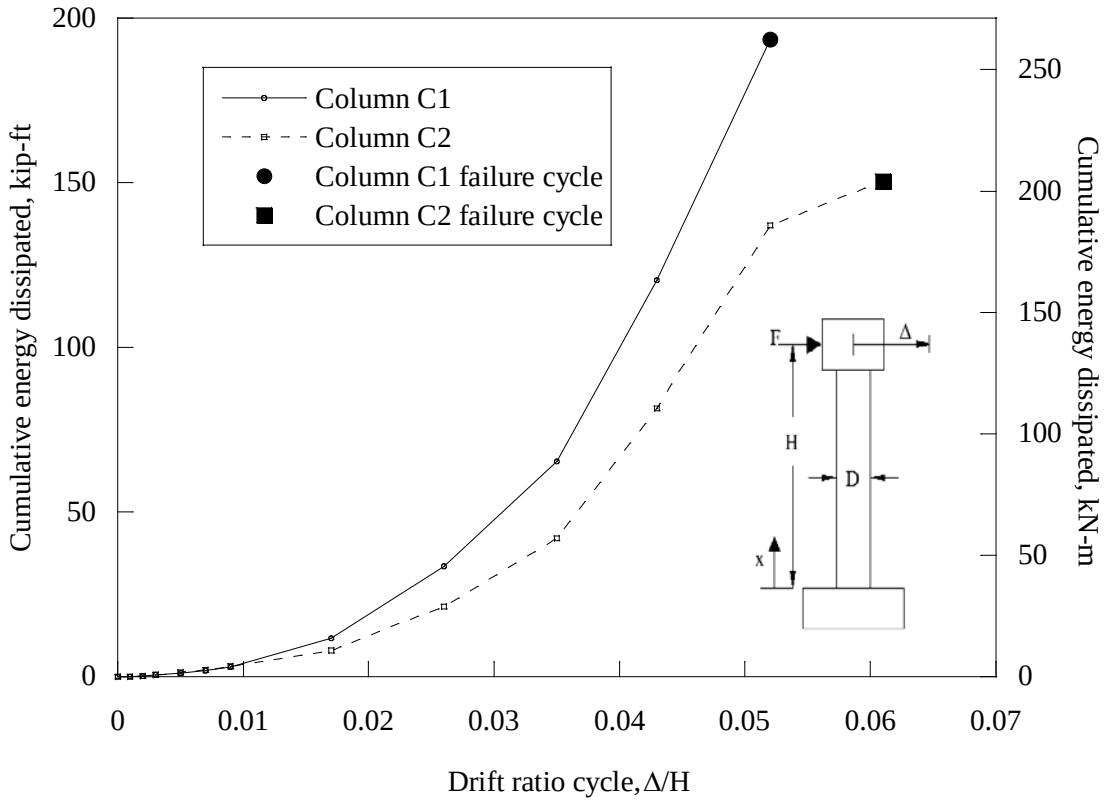

Figure 7.5: Cumulative energy dissipated of columns C1 and C1

Table 7.6: Energy dissipated for columns C1 and C2

	Column C1	**Column C2**
Energy dissipated at first yield, kip-ft (kN-m)	3.24 (4.39)	4.78 (6.48)
Energy dissipated at reference yield, kip-ft (kN-m)	5.48 (7.43)	5.80 (7.86)
Total energy dissipated at column failure, kip-ft (kN-m)	193.48 (262.32)	150.33 (203.82)

Energy dissipation is not a primary parameter used in design, however, it becomes an important parameter when predicting the performance of structures and also when modeling structures to collapse. It should be noted that most codes do not require a minimum energy dissipation value.

7.2.1.7 Column Ductility

Herein, column ductility is defined in terms of displacement ductility and curvature ductility. The displacement ductility is computed as the ratio of the maximum tip displacement to the tip displacement at a reference yield value.

Note that different reference yield definitions are possible. The reference yield was defined as the point when the longitudinal reinforcement bars reach a strain of 1 percent. Displacement ductility was also computed using the first yield displacement of the column as the reference value. The first yield is defined as the displacement at which the longitudinal reinforcement first yields. The curvature ductility is computed as the ratio of the maximum curvature and the reference yield curvature. The reference yield curvature was defined Priestley *(Priestley 2003)* as:

$$\phi_y = \frac{2.25\varepsilon_y}{D} \tag{7.5}$$

where ε_y is the yield strain of the longitudinal reinforcement and D is the column diameter. An associated curvature ductility is computed at each of the five curvature instrumentation levels, with level 1 corresponding to the lowest elevation and level 5 corresponding to the highest elevation.

Table 7.7 summarizes the displacement and curvature ductility values of columns C1 and C2. The results indicate that when using the reference yield, the displacement ductility is larger for column C2 when compared to column C1. However, it should be noted that C1 has larger displacement ductility when using the first yield displacement. The curvature ductility of column C1 at instrumentation levels 1, 3, 4, and 5 are larger than those of column C2. At instrumentation level 2 column C2 had larger curvature ductility values when compared to column C1. For both columns the curvature ductility was largest at the base of the column (level 1).

Table 7.7: Summary of ductility values of columns C1 and C2

	Displacement ductility, μΔ		**Curvature ductility, μψ**				
	Reference yield	**First yield**	**Level 1**	**Level 2**	**Level 3**	**Level 4**	**Level 5**
Column C1	3.95	5.83	20.34	8.54	3.54	0.93	0.69
Column C2	4.13	5.51	16.45	9.66	2.38	1.19	0.63
% Difference	4.455	5.64	21.15	12.31	39.19	24.53	9.09

The curvature ductility is typically the most critical towards the base of the column where the majority of the damage occurs. In this case, the data indicate that the curvature ductility value of columns C1, at 6 inches (152 mm) from the base of the column (level 1) which includes the effects of strain penetration is larger than the value for C2. However, at 12 inches (305 mm) from the base of the column (level 2) column C2 exhibited a larger curvature ductility value when compared to column C1.

7.2.2 Column C3 and Column C4

Performance of columns C3 and C4 are compared in this section. Column C3 is reinforced with Grade 60 and has a longitudinal reinforcement ratio of 2.19 percent. Column C4 is reinforced with Grade 80 and has a longitudinal reinforcement ratio of 1.56 percent. Note that the longitudinal reinforcement ratio of columns C3 and C4 are approximately twice that of the longitudinal reinforcement ratio of columns C1 and C2, respectively.

7.2.2.1 Visual Observations

Columns C3 and C4 exhibited similar crack distributions. Figure 7.6 shows a side-by-side comparison of the cracking of columns C3 and C4. Note that these photographs were not taken at the exact same displacement ratio cycle.

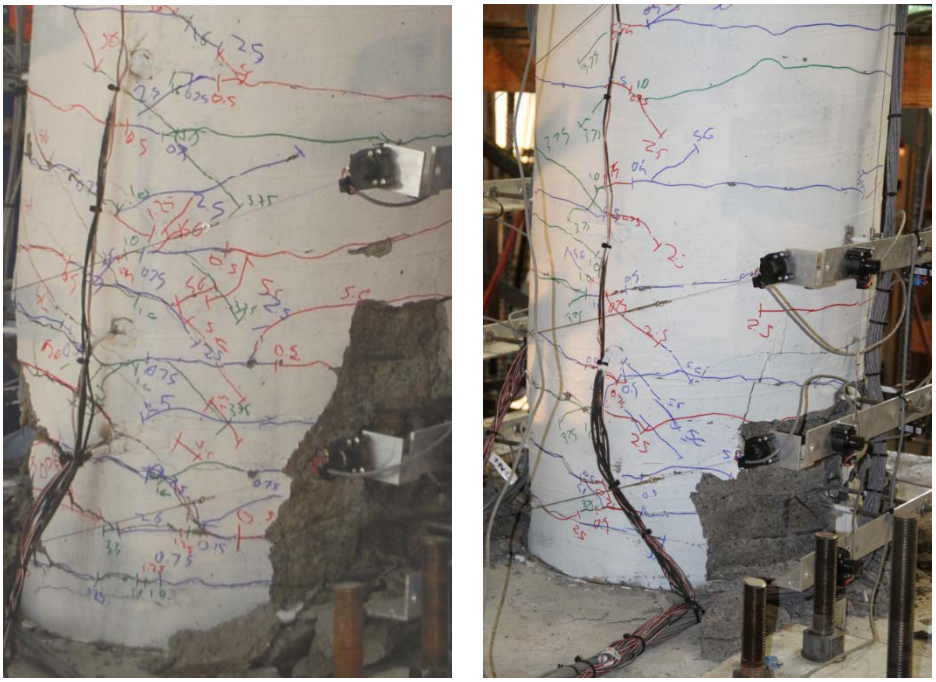

Figure 7.6: Photographs of column C3 (left) and C4 (right) cracking

Columns C3 and C4 exhibited the onset of concrete spalling and concrete spalling at the same displacement cycles. The mode of failure of both columns was flexural governed by reinforcing bar buckling followed by tension fracture of the reinforcement. The first longitudinal reinforcing bar to buckle and fracture in column C3 occurred at approximately 2.5 inches (63.5 mm) further from the base of the column when compared with column C4. Both columns failed during the same displacement cycle, however, column C3 hit all six peaks before failing where column C4 failed prior to the fourth peak. The bar fracture in column C3 was approximately 7.5 inches (191 mm) from the base of the column and occurred when the column was returning from the final peak of the

10.00-inch (254 mm) displacement cycle. The bar in column C4 fractured approximately 5.00 inches (127 mm) away from the base of the column when it was approaching the fourth peak of the 10.00-inch (254 mm) displacement cycle.

In summary from visual observations of columns C3 and C4, the performance of the columns was similar, except that column C3 was able to reach three more peaks in the 10.00-inch (254 mm) displacement cycle compared to column C4. This indicates that columns constructed with Grade 80 reinforcement meeting ASTM A706 specifications may perform similarly to columns constructed with Grade 60 reinforcement.

7.2.2.2 Maximum Lateral Displacement

Displacements at the level of the applied horizontal force were recorded for all tests. Columns C3 and column C4 reached the same tip displacement prior to column failure. Figure 7.7 shows the drift ratio versus elevation for the 10.00-inch (254 mm) displacement cycle for columns C3 and C4.

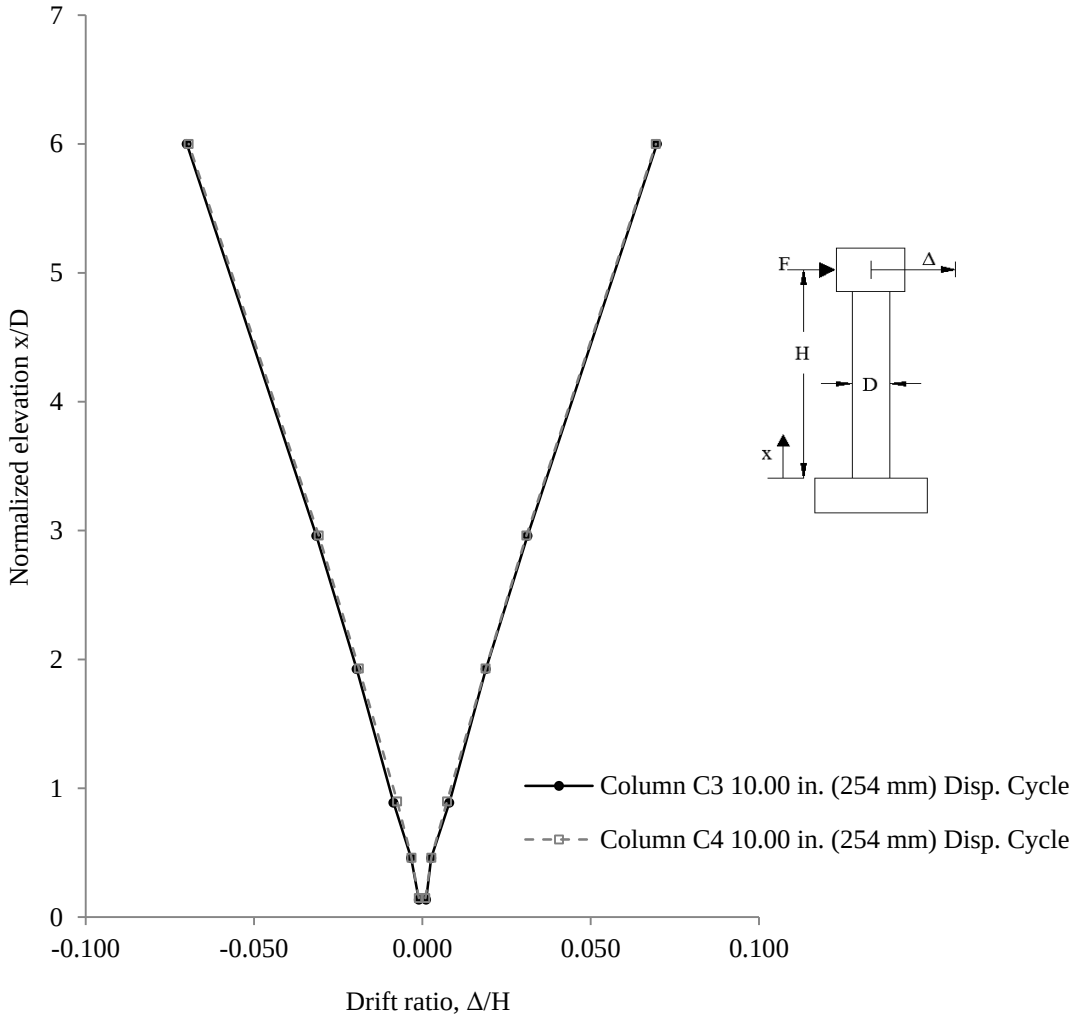

Figure 7.7: Drift ratio versus normalized elevation of columns C3 and C4

As seen in Figure 7.7, the drift ratios along the normalized elevation of the column are almost identical for the 10.00-inch (254 mm) displacement cycle for columns C3. The data indicates that columns reinforced with A706 Grade 80 reinforcement performed similarly to columns reinforced with A706 Grade 60 reinforcement.

7.2.2.3 Steel Reinforcement Strains

Columns C3 and C4 had strain gages attached at similar elevations to the longitudinal and transverse reinforcement. Figure 3.10 shows the locations of the strain gages and the levels at which these were installed.

The longitudinal reinforcing bars in column C3 yielded first at a tip displacement of 1.44 inches (36.6 mm). This occurred at the base of the column, level 2, where the strain is largest during the approach to the first peak of the 2.50-inch (63.5 mm) displacement cycle. The bar also yielded during this displacement cycle at all levels except for level one which is inside the footing. The longitudinal bars in column C4 first yielded at a tip displacement of 1.58 inches (40.1 mm). This occurred during the approach to the first peak of the 2.50-inch (63.5 mm) displacement cycle and occurred at the base of the column (level 2) where the strain is largest.

The longitudinal steel in column C3 yielded in the footing (level 1) on the 3.75 inch (95.3 mm) displacement cycle and the longitudinal steel in column C4 never yielded in the footing (level 1). This indicates that the contribution of strain penetration may not be as critical for a column reinforced with Grade 80 bars. Table 7.8 shows the transverse strains for columns C3 and C4 for 3 displacement cycles. All the transverse strains were small in magnitude and never approached yielding, except for column C4 at level 3 where on the final displacement cycle the spiral did yield. The transverse strains at levels 2 and 3 in column C4 were larger than those of column C3 for all displacement cycles. However, the transverse strains at levels 5, 6, and 7 in column C3 were larger than those of column C4 for all displacement cycles. Column C4 may have larger stresses applied to the spiral within the plastic hinge zone due to localized concentrations of the longitudinal forces because it had fewer bars than column C3. Outside the plastic hinge zone (levels 5 to 7) column C3 had slightly larger shear forces, which implies larger shear strains, but the increase in shear force does not justify the larger difference in the spiral strains.

Table 7.8: Summary of maximum transverse steel strains of columns C3 and C4

Level	Elevation in. (mm)	2.50 inch (63.5 mm) displacement cycle		5.00 inch (127 mm) displacement cycle		7.50 inch (191 mm) displacement cycle	
		C3 max % strain	C4 max % strain	C3 max % strain	C4 max % strain	C3 max % strain	C4 max % strain
1	-12.00 (-304.8)	0.0281	0.0262	0.0334	0.0452	0.0430	0.0539
2	0.00 (0.00)	0.0104	0.0175	0.0080	0.0240	0.0106	0.0111
3	6.00 (152)	0.0088	0.0194	0.0237	0.0664	0.0235	0.2244
4	12.00 (304.8)	0.0159	0.0116	0.0574	0.0375	0.0707	0.0672
5	24.00 (609.6)	0.1244	0.0198	0.1297	0.0236	0.1375	0.0325
6	48.00 (1,219)	0.0743	0.0131	0.0768	0.0140	0.0772	0.0146
7	72.00 (1,829)	0.0281	0.0085	0.0334	0.0086	0.0430	0.0092

Table 7.9 shows the longitudinal tensile strains for columns C3 and C4 for 3 displacement cycles. Table 7.10 shows the longitudinal tensile strains for columns C3 and C4 for 3 displacement cycles. For all displacement cycles, column C4 had larger longitudinal strains at the base of the column (level 2) and at level 3 when compared to column C3 prior to the strain gages reaching the three percent strain limit. Column C3 had larger tensile strains in the footing (level 1) compared to column C4 at all displacement cycles. This may suggest that column C4 (containing Grade 80 reinforcement) may require additional detailing to ensure the bar is fully developed at the base of the column, as already noted for columns C1 and C2. In general, the compressive strains were similar between the two columns, except for at levels 2 and 3 at and past the 3.75-inch (95.3 mm) displacement cycle. At level 2 column C3 exhibited larger compressive strains and at level 3 column C4 exhibited larger compressive strains at the for mentioned displacement cycles. Other than that there does not seem to be any significant differences between the strains in the longitudinal reinforcing bars between column C3 reinforced with Grade 60 bars and column C4 reinforced with Grade 80 bars.

Table 7.9: Summary of maximum longitudinal tensile steel strains of columns C3 and C4

Level	Elevation in. (mm)	2.50 inch (63.5 mm) displacement cycle		5.00 inch (127 mm) displacement cycle		7.50 inch (191 mm) displacement cycle	
		C3 max % strain	C4 max % strain	C3 max % strain	C4 max % strain	C3 max % strain	C4 max % strain
1	-12.00 (-304.8)	0.22	0.03	0.26	0.05	0.30	0.05
2	0.00 (0.00)	1.21	1.35	2.05	2.38	3.00	3.00
3	6.00 (152)	1.01	1.28	1.61	1.73	2.24	2.59
4	12.00 (304.8)	0.72	0.95	1.73	1.57	2.82	2.34
5	24.00 (609.6)	0.52	0.50	1.29	1.11	1.97	1.61
6	48.00 (1,219)	0.25	0.29	0.29	0.34	0.33	0.36
7	72.00 (1,829)	0.25	0.20	0.21	0.25	0.23	0.25

Table 7.10: Summary of maximum longitudinal compressive steel strains of columns C3 and C4

Level	Elevation in. (mm)	2.50 inch (63.5 mm) displacement cycle		5.00 inch (127 mm) displacement cycle		7.50 inch (191 mm) displacement cycle	
		C3 max % strain	C4 max % strain	C3 max % strain	C4 max % strain	C3 max % strain	C4 max % strain
1	-12.00 (-304.8)	-0.05	-0.06	-0.08	-0.10	-0.11	-0.17
2	0.00 (0.00)	-0.17	-0.17	-0.14	-0.33	N.A.*	N.A.*
3	6.00 (152)	-0.23	-0.18	-0.77	-0.47	-1.29	-0.81
4	12.00 (304.8)	-0.22	-0.18	-0.39	-0.30	-0.51	-0.40
5	24.00 (609.6)	-0.11	-0.14	-0.11	-0.17	-0.05	-0.13
6	48.00 (1,219)	-0.12	-0.11	-0.13	-0.14	-0.14	-0.14
7	72.00 (1,829)	-0.12	-0.08	-0.09	-0.09	-0.09	-0.10

*N.A.: Not available

7.2.2.4 Column Curvature

The normalized curvature data were shown in Chapter 5. The curvature was normalized by multiplying the value by the diameter, D, of the column. The largest curvatures occurred closest to the base of the column and reduced in magnitude along the height of the column. Table 7.11 shows the curvature for 3 of the larger displacement cycles for columns C3 and C4. It can be seen that the curvatures at all instrumentation levels are similar between the two columns. These results indicate that reinforced columns containing Grade 60 and Grade 80 have similar curvatures, which is an indication that columns constructed with Grade 80 reinforcement may exhibit similar performance to columns containing Grade 60 reinforcement.

Table 7.11: Summary of column C3 and C4 curvature

Level	Approx. elevation in. (mm)	2.50 in. (63.5 mm) displacement cycle		5.00 in. (127 mm) displacement cycle		7.50 in. (191 mm) displacement cycle	
		C3 max normalized curvature	C4 max normalized curvature	C3 max normalized curvature	C4 max normalized curvature	C3 max normalized curvature	C4 max normalized curvature
1	3.00 (76)	0.025	0.023	0.072	0.061	0.101	0.098
2	9.00 (229)	0.009	0.008	0.030	0.029	0.055	0.049
3	18.00 (457)	0.003	0.005	0.012	0.010	0.021	0.024
4	36.00 (914)	0.005	0.006	0.006	0.007	0.009	0.008
5	60.00 (1,524)	0.003	0.004	0.004	0.004	0.004	0.005

7.2.2.5 Column Forces

Following the procedure presented in section 7.2.1.5, geometry effects of the applied axial load were removed to establish test shear and moment demands. factor of 1.20 is obtained.

Table 7.12 shows the maximum applied force, shear force, and moment demands for columns C3 and C4. The differences in maximum applied force and shear force between columns C3 and C4 was expected since the columns nominal moment capacity was slightly different. The difference in nominal moment capacity was due to being unable to exactly match the increase in yield strength (80/60 = 1.33) of the longitudinal reinforcing bars with the reduction of the number of longitudinal reinforcing bars (22/16 = 1.38).

Table 7.12: Column C3 and C4 moment capacity

Column	Maximum applied force kip (kN)	Column shear force kip (kN)	Associated plastic shear kip (kN)	Nominal moment capacity (Response 2000) kip-ft (kN-m)	Tested moment capacity kip-ft (kN-m)	Expected moment capacity kip-ft (kN-m)
C3	52.0 (231)	47.9 (213)	54.0 (240)	463 (628)	631 (856)	649 (880)
C4	46.9 (209)	43.1 (192)	52.3 (233)	448 (607)	572 (776)	628 (851)

For column C3, an overstrength factor of 1.36 is obtained. For column C4, an overstrength factor was computed to be 1.28. Note that the percent difference between the expected moment capacities of columns C3 and C4 is 3.29 percent. The percent difference between the tested moment capacities of columns C3 and C4 is 9.81 percent. The nominal moment capacities were computed using Response 2000® and assuming elastic perfectly-plastic steel stress strain models.

Figure 7.8 shows the applied horizontal force versus the drift ratio for columns C3 and C4 up to the first longitudinal bar fracture. It can be seen that the overall shape of the hysteretic loops are similar, but column C3 has larger area between the loading and unloading curves resulting in greater hysteretic energy dissipation. This is discussed in more detail in section 7.2.2.6. The difference in applied force capacities between the two columns can also be seen in this figure.

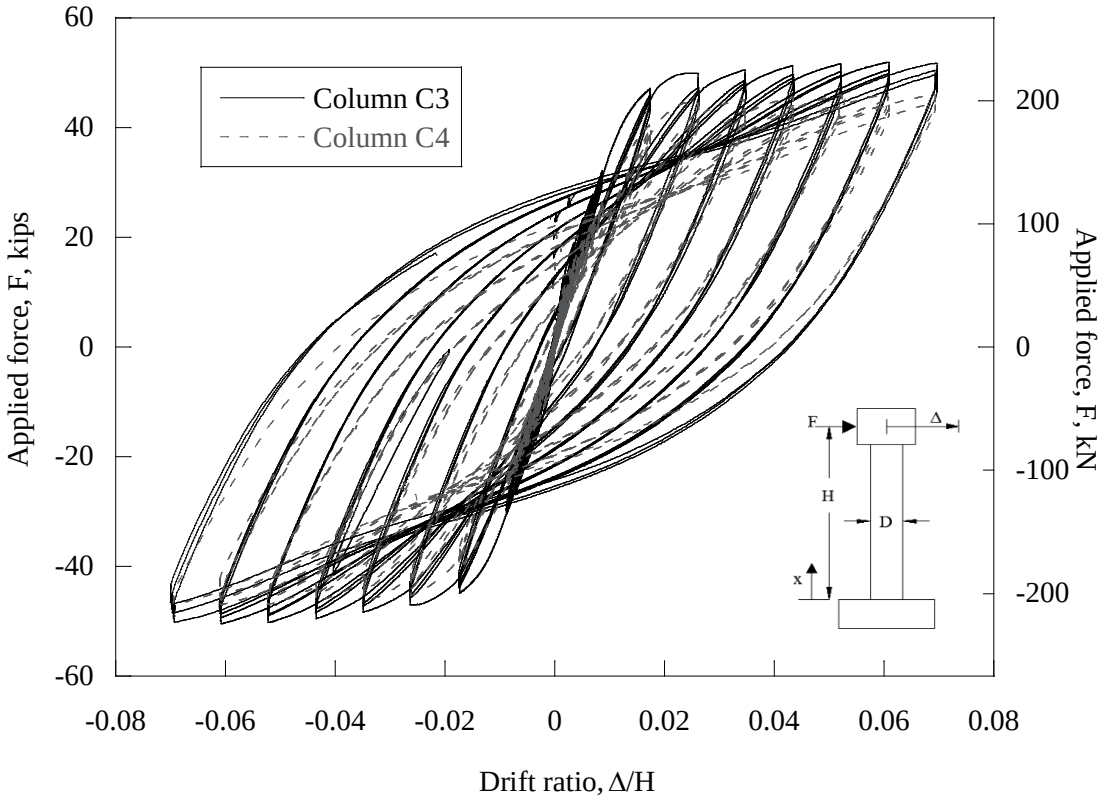

Figure 7.8: Drift ratio versus applied force of columns C3 and C4

Figure 7.9 shows a plot of the shear force versus drift ratio for columns C3 and C4. It can be seen from this plot that the response of the two columns are similar. However, column C3 has a larger applied force capacity and dissipates more hysteretic energy during unloading compared to column C4. It is also clear that column C3 has larger stiffness in the initial loading and unloading.

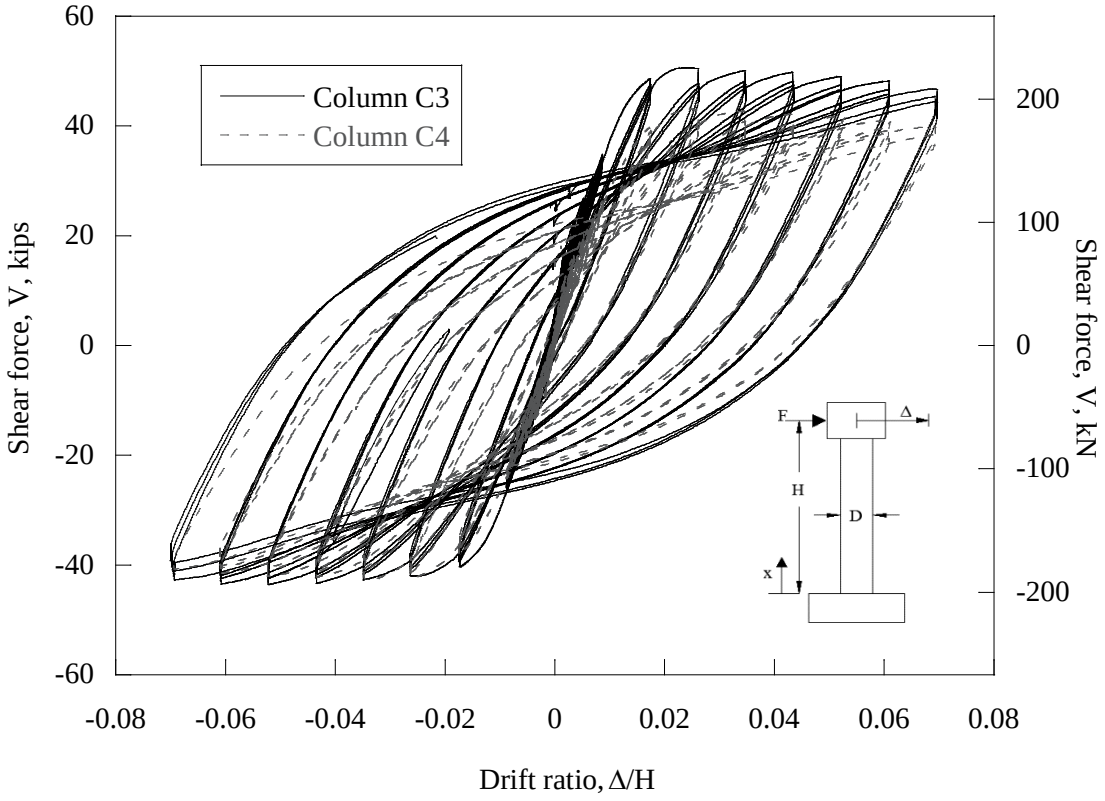

Figure 7.9: Shear force versus drift ratio of columns C3 and C4

7.2.2.6 Hysteretic Energy Dissipation

The hysteretic energy dissipation was determined for each column. The value was determined by taking the area within the hysteretic loops for the applied force-displacement curves for each displacement cycle. This was computed by numeric integration using the Simpson rule. Each drift ratio cycle there was typically 3 cycles each having a north and south displacement peak equal to the value of the given drift ratio cycle. Also, note that for the final displacement cycle for column C4 only four peaks were reached before the column failed.

As shown in Figure 7.10, column C3 exhibited greater hysteretic energy dissipation when compared to column C4. This was expected because column C3 had more reinforcing bars to absorb the energy even though the reinforcing bars yielded at a lower stress when compared with the Grade 80 reinforcing bars in column C4. More importantly the stiffness of the column is larger and therefor produces “taller” hysteretic loops. Table 7.13 shows the total energy dissipated up to the first reinforcing bar fracture, first yield, and reference yield. It can be seen that column C3 dissipated more energy compared to column C4. This is most likely due to the reduction in the area of steel in column C4, which

results in lower column stiffness, which in turn lowers its energy dissipation capacity. Column C4 dissipated less energy prior to and after the longitudinal reinforcement yielding when compared to column C3.

Energy dissipation is not a primary parameter used in design, however, it becomes an important parameter when predicting the performance of structures and also when modeling structures to collapse. It should be noted that most codes do not require a minimum energy dissipation value.

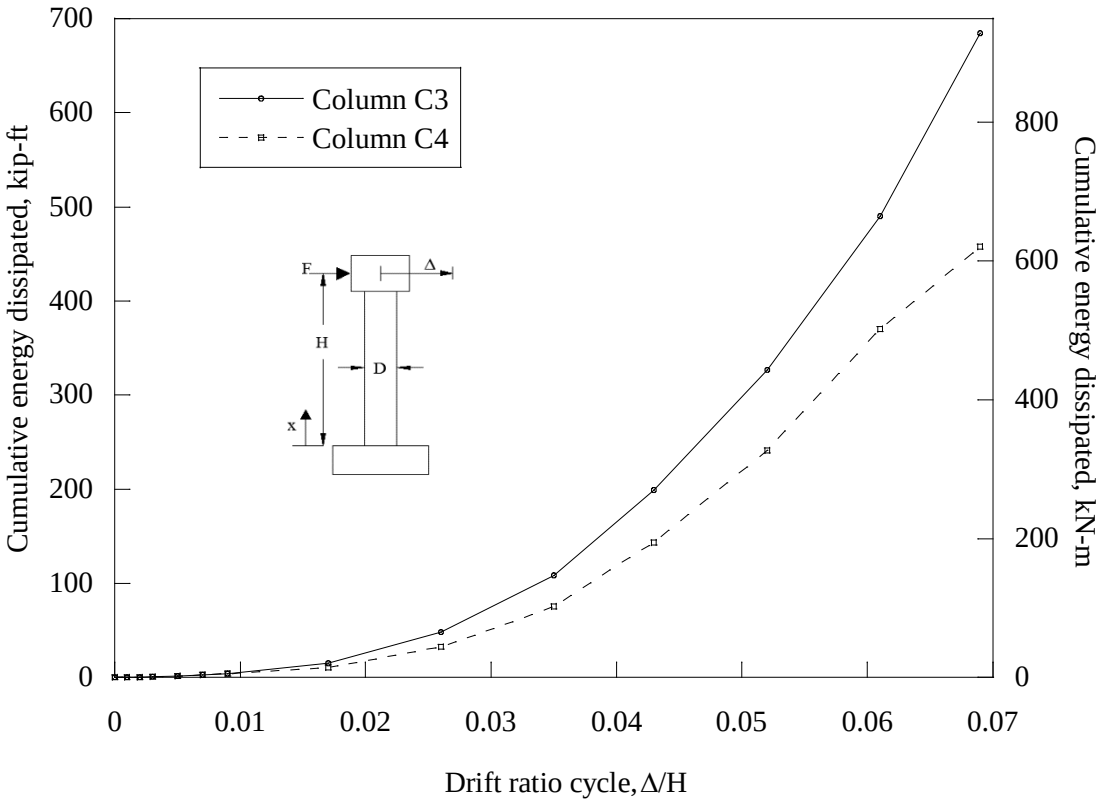

Figure 7.10: Cumulative energy dissipated of columns C3 and C4

Table 7.13: Energy dissipated for columns C3 and C4

	Column C3	**Column C4**
Energy dissipated at first yield, kip-ft (kN-m)	6.43 (8.72)	5.97 (8.09)
Energy dissipated at reference yield, kip-ft (kN-m)	9.01 (12.2)	8.07 (10.9)
Total energy dissipated, kip-ft (kN-m)	684.24 (927.71)	457.67 (620.52)

7.2.2.7 Column Ductility

Table 7.14 summarizes the displacement and curvature ductility values for columns C3 and C4. The results indicate that when the reference and first yield criteria is used, the displacement ductility is larger for column C3 when compared to column C4. The percent difference between the displacement ductility values using the reference yield criteria between columns C3 and C4 is 5.15 percent. For such small differences it can be concluded that similar performance for both columns was achieved. The curvature ductility of column C3 at instrumentation levels 2, 3, and 4 are larger than those of column C4. At instrumentation level 1 and 5 column C4 exhibited larger curvature ductility values when compared to column C3. For both columns the curvature ductility was largest at the base of the column (level 1). The curvature ductility is typically more critical towards the base of the column where the majority of the curvature occurs. In this case, the data indicate that a column reinforced with Grade 80 reinforcement exhibits a larger curvature ductility value compared to a column reinforced with Grade 60 reinforcement at the base of the base of the column (level 1). However at the next lowest level, column C3 exhibited a significantly larger curvature ductility compared to column C4. Note that at level 1 the effects of strain penetration affects the curvature.

Table 7.14: Summary of column C3 and C4 ductility

	Displacement ductility, μ_Δ		**Curvature ductility, μ_ψ**				
	Reference yield	**First yield**	**Level 1**	**Level 2**	**Level 3**	**Level 4**	**Level 5**
Column C3	4.58	7.00	20.89	19.16	6.63	2.32	0.84
Column C4	4.35	6.33	23.63	10.21	5.61	1.54	1.43
% Difference	5.15	10.05	12.31	60.95	16.67	40.41	51.98

7.2.3 Column C5 and Column C6

Columns C5 and C6 are compared in this section to determine the effects of reinforcement grade on column performance. Columns were designed with a typical longitudinal reinforcement ratio used in bridges in California, Oregon, and Washington and a shear span ratio equal to three. Column C5 is reinforced with Grade 60 reinforcement and has a longitudinal reinforcement ratio of 2.19 percent. Column C6 is reinforced with Grade 80 corresponding to a longitudinal reinforcement ratio of 1.58 percent. Both columns were designed to have similar nominal moment capacities. The longitudinal reinforcement ratios of columns C5 and C6 are identical to columns C3 and C4, respectively. The post column failure performance of columns C5 and C6 is also analyzed in this section.

7.2.3.1 Visual Observations

Columns C5 and C6 exhibited similar crack distributions. Both columns initially exhibited flexure cracking then soon after shear cracks were also clearly visible forming a shear fan. Both columns also had cracking over nearly the entire

height of the column. Figure 7.11 shows a side-by-side comparison of the cracking of columns C5 and C6. Note that these photographs were not taken at the same displacement ratio cycle.

Figure 7.11: Photographs of columns C5 (left) and C6 (right) cracking

Columns C5 and C6 exhibited the onset of concrete spalling and concrete spalling during the 1.88-inch (47.8 mm) displacement cycle (2.6 percent drift ratio). The mode of failure of both columns was flexural with bar buckling followed by tension fracture of the longitudinal bars. The first longitudinal reinforcing bar to buckle in column C5 occurred at approximately 3.5 inches (89 mm) further from the base of the column when compared with column C6, which failed at 2 inches (51 mm) above the base of the column. Both columns first longitudinal bars to fracture were the southernmost bar at an elevation of approximately 5.0 inches (127 mm) from the base of the column. The first bar to fracture in column C5 occurred when approaching the first peak of the 5.00-inch (127 mm) displacement cycle. The applied load was 43.20 kips (192.2 kN) and the corresponding tip displacement was 0.19 inches (4.8 mm). The first bar to fracture in column C6 occurred when approaching the third peak of the 4.38-inch (111 mm) displacement cycle. The applied load was 76.93 kips (342.2 kN) and the corresponding tip displacement was 3.25 inches (82.6 mm).

Unlike columns C1 through C4, for columns C5 and C6, loading was continued until six bars fractured. Table 7.15 provides a summary of the bar fracture information of columns C5 and C6. It can be seen that although the first bar to fracture in column C6 occurred one displacement cycle earlier than column C5, the final bar fracture of column C6 occurred only a half cycle earlier than the

final bar fracture of column C5. From the visual observations of columns C5 and C6, the performance of the columns seem to be similar, except that column C5 achieved a 5.00-inch (127 mm) displacement cycle prior to the first bar fracture.

Table 7.15: Column C5 and C6 bar fracture summary

Bar fracture	Column C5				Column C6			
	Disp. cycle, inch (mm)	Total # of cycles prior to fracture	Load kip (kN)	Tip disp. inch (mm)	Disp. cycle, inch (mm)	Total # of cycles prior to fracture	Load kip (kN)	Tip disp. inch (mm)
First	5.00 (127)	36	43.20 (192.2)	0.19 (4.8)	4.38 (111)	35	76.93 (342.2)	3.25 (82.6)
Second	5.00 (127)	36	62.84 (279.5)	2.69 (68.3)	4.38 (111)	35.5	-40.79 (-181.4)	-0.74 (-19)
Third	5.00 (127)	36	72.51 (322.5)	3.44 (87.4)	5.00 (127)	36	65.62 (291.9)	3.59 (91.2)
Fourth	5.00 (127)	37	66.86 (297.4)	4.65 (118)	5.00 (127)	37	34.21 (152.2)	2.19 (55.6)
Fifth	5.00 (127)	38	34.81 (154.8)	1.61 (40.9)	5.00 (127)	37.5	-9.83 (-43.7)	1.07 (27.2)
Sixth	5.00 (127)	38	41.87 (186.2)	3.37 (85.6)	5.00 (127)	37.5	-47.40 (-210.8)	-4.54 (115)

Note that for this table a positive load represents a bar fracture on the south side of the column and a negative load represents a bar fracture on the north side of the column.

7.2.3.2 Maximum Lateral Displacement

Displacements at the level of the applied horizontal force as well as the other four instrumentation levels were recorded for all tests. Figure 7.12 shows the drift ratio versus normalized elevation for the 4.38-inch (111 mm) and 5.00-inch (127 mm) displacement cycles of columns C5 and C6. The maximum drift ratio of both columns was 6.1 percent. As seen from the figure, the maximum lateral displacement of column C5 occurred during the 4.38-inch (111 mm) displacement cycle even though it did not fail until the 5.00-inch (127 mm) displacement cycle. This was because column C5 failed very early in the 5.00-inch (127 mm) displacement cycle.

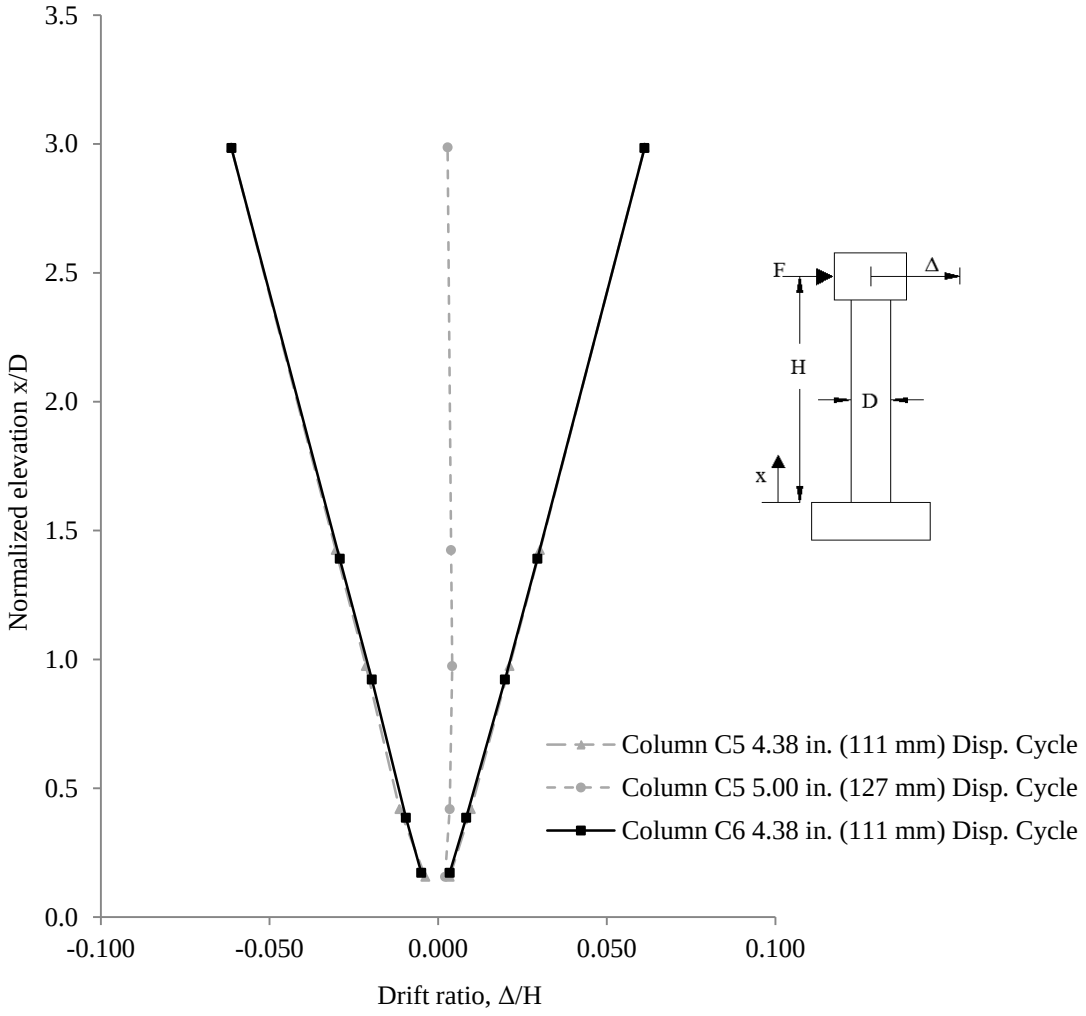

Figure 7.12: Drift ratio versus normalized elevation of columns C5 and C6

As seen in Figure 7.12 the drift ratios along the normalized elevation of the columns are almost identical for the 4.38-inch (111 mm) displacement cycle. The data suggests that columns reinforced with A706 Grade 80 reinforcement exhibit similar performance to columns reinforced with A706 Grade 60 reinforcement.

7.2.3.3 Steel Reinforcement Strains

Columns C5 and C6 had strain gages at similar locations to compare the strains of the steel reinforcement. Figure 3.10 shows the locations of the strain gages and the levels at which these were installed. The longitudinal reinforcement in columns C5and C6 yielded during the 0.7 percent drift ratio cycle. The

longitudinal reinforcement in column C5 initially yielded at a tip displacement of -0.50 inches (-13 mm). Yielding occurred at 12 inches (305 mm) from the base of the column (level 4), which corresponds to a drift ratio of 0.69 percent. The longitudinal reinforcement in column C6 initially yielded at a tip displacement of -0.56 inches (-14 mm), 6 inches (152 mm) from the base of the column (level 3), which corresponds to a rift ratio of 0.78 percent.

The longitudinal steel in column C5 and C6 yielded in the footing (level 1) on the 1.25-inch (31.8 mm) displacement cycle. During this displacement cycle the longitudinal bar yielded at all instrumentation levels within the column. Table 7.16 shows the transverse strains for columns C5 and C6 for 3 displacement cycles. The spiral in column C5 yielded 12 inches (305 mm) above the base of the column (level 4) at the 3.75-inch (95.3 mm) displacement cycle. The spiral in column C6 yielded 6 inches (152 mm) above the base of the column (level 3) at the 4.38-inch (111 mm) displacement cycle. Column C5 exhibited larger tensile strains in the spiral within the footing (level 1) and level 5 for all displacement cycles compared to column C6. The strains at the top level (level 6) were similar between the columns; the maximum difference in percent strain was 0.037 percent. The strains were also similar between the columns at levels 3 and 4 up to the 1.88-inch (47.8 mm) displacement cycle. After the 1.88-inch (47.8 mm) displacement cycle, column C5 exhibited larger strains at level 4 and column C6 exhibited larger strains at level 3.

Table 7.16: Summary of maximum transverse steel strains of columns C5 and C6

Level	Elevation inch (mm)	1.25 inch (31.8 mm) displacement cycle		2.50 inch (63.5 mm) displacement cycle		3.75 inch (95.3 mm) displacement cycle	
		C5 max % strain	C6 max % strain	C5 max % strain	C6 max % strain	C5 max % strain	C6 max % strain
1	-12.00 (-304.8)	0.0389	0.0056	0.0523	0.0094	0.0713	N.A.*
2	0.00 (0.00)	N.A.*	0.0240	N.A.*	0.0311	N.A.*	N.A.*
3	6.00 (152)	0.0239	0.0236	0.0554	0.1124	0.1698	0.3255
4	12.00 (304.8)	0.0389	0.0480	0.0760	0.0971	0.2550	0.1692
5	24.00 (609.6)	0.0820	0.0171	0.0983	0.0297	0.1311	0.0371
6	36.00 (914.4)	0.0259	0.0593	0.0347	0.0770	0.0514	0.0810

*N.A.-not available due to the strain gage being damaged

Table 7.17 shows the longitudinal tensile strains for columns C5 and C6 for 3 displacement cycles. Table 7.18 shows the longitudinal compressive strains for columns C5 and C6 for 3 displacement cycles. For the majority of locations and displacement cycles, column C6 had larger tensile strains in the longitudinal bars when

compared to column C5. However, in the footing (level 1), column C5 exhibited larger tensile strains after the 1.25-inch (31.8 mm) displacement level compared to column C6. Column C6 had slightly larger compression strains in the longitudinal bars compared to column C5 for the majority of locations and displacement cycles. However, at levels 2 and 3 after the 1.25-inch (31.8 mm) displacement cycle, column C5 exhibited larger compression strains compared to column C6. Note that the differences in compressive strains were small in magnitude except at levels 2 and 3 at and past the 1.25-inch (31.8 mm) displacement cycle.

Table 7.17: Summary of maximum longitudinal tensile steel strains of columns C5 and C6

Level	Elevation inch (mm)	1.25 inch (31.8 mm) displacement cycle		2.50 inch (63.5 mm) displacement cycle		3.75 inch (95.3 mm) displacement cycle	
		C5 max % strain	C6 max % strain	C5 max % strain	C6 max % strain	C5 max % strain	C6 max % strain
1	-12.00 (-304.8)	0.28	0.29	0.97	0.35	1.44	0.58
2	0.00 (0.00)	1.30	1.69	2.08	2.54	3.00	3.00
3	6.00 (152)	1.26	1.87	2.08	3.00	3.00	3.00
4	12.00 (304.8)	1.06	1.23	1.80	2.13	2.93	3.00
5	24.00 (609.6)	.29	0.33	0.93	0.93	1.42	1.43
6	36.00 (914.4)	.24	0.29	0.27	0.32	0.29	0.33

Table 7.18: Summary of maximum longitudinal compressive steel strains of columns C5 and C6

Level	Elevation inch (mm)	1.25 inch (31.8 mm) displacement cycle		2.50 inch (63.5 mm) displacement cycle		3.75 inch (95.3 mm) displacement cycle	
		C5 max % strain	C6 max % strain	C5 max % strain	C6 max % strain	C5 max % strain	C6 max % strain
1	-12.00 (-304.8)	-0.10	-0.13	-0.10	-0.18	0.14**	-0.27
2	0.00 (0.00)	-0.40	-0.21	-0.87	-0.46	N.A.*	N.A.*
3	6.00 (152)	-0.39	-0.24	-0.66	N.A.*	N.A.*	N.A.*
4	12.00 (304.8)	-0.18	-0.18	-0.20	-0.14	0.15**	N.A.*
5	24.00 (609.6)	-0.11	-0.12	-0.13	-0.16	-0.08	0.01**
6	36.00 (914.4)	-0.08	-0.09	-0.08	-0.09	-0.08	-0.10

*N.A. equals not available, at this location the strain gage reached its maximum tensile strain limit

** The data shows the strain gage never went into compression

7.2.3.4 Column Curvature

The normalized curvature data was shown in Chapter 6. The curvature was normalized by multiplying the value by the diameter, D, of the column. Table 7.19 shows the curvature for 3 of the larger displacement cycles for columns C5 and C6. It can be seen that the curvatures at all instrumentation levels are similar between the columns. These results indicate that Grade 80 and Grade 60 reinforced columns exhibit similar curvatures. These results suggest that columns containing Grade 80 reinforcement may exhibit similar performance as columns containing Grade 60 reinforcement.

Table 7.19: Summary of column C5 and C6 normalized curvature

Level	Approx. elevation inch (mm)	1.25 inch (31.8 mm) displacement cycle		2.50 inch (63.5 mm) displacement cycle		3.75 inch (95.3 mm) displacement cycle	
		C5 max normalized curvature	C6 max normalized curvature	C5 max normalized curvature	C6 max normalized curvature	C5 max normalized curvature	C6 max normalized curvature
1	3.00 (76)	0.043	0.048	0.101	0.114	0.150	0.177
2	9.00 (229)	0.007	0.005	0.015	0.011	0.012	0.020
3	18.00 (457)	0.001	0.002	0.005	0.005	0.010	0.007
4	30.00 (762)	0.001	0.001	0.001	0.001	0.001	0.001

7.2.3.5 Column Forces

The shear force and moment at the base of the column was computed for columns C5 and C6. The same calculations were performed to remove the geometry effects of the applied axial load that was discussed in section 7.2.1.5 for columns C1 and C2.

Table 7.20 shows the maximum applied force, shear force, and moment capacity for columns C5 and C6. The differences in maximum applied force and shear between columns C5 and C6 was expected because the columns nominal moment capacities were slightly different. The difference in nominal moment capacities was due to being unable to exactly match the increase in yield strength of the longitudinal bars (80/60 = 1.33) with the reduction of the number of longitudinal bars (22/16 = 1.38).

Table 7.20: Summary of force and moment capacities of columns C5 and C6

Column	Maximum applied force kip (kN)	Column shear force kip (kN)	Associated plastic shear kip (kN)	Nominal moment capacity (Response 2000) kip-ft (kN-m)	Tested moment capacity kip-ft (kN-m)	Expected moment capacity kip-ft (kN-m)
C5	103.9 (462.2)	100.4 (446.6)	108.1 (480.8)	463 (628)	629 (853)	649 (879)
C6	95.0 (422.6)	92.0 (409.2)	104.6 (465.3)	448 (608)	575 (780)	628 (851)

For column C5, an overstrength factor of 1.36 is obtained. For column C6, an overstrength factor of 1.28 is obtained. The percent difference between the tested moment capacities of columns C5 and C6 is 8.97 percent.

Figure 7.13 shows the applied horizontal force versus the drift ratio for columns C5 and C6 up to the first longitudinal bar fracture. It can be seen that the overall shape of the hysteretic loops are similar, but column C5 has a slightly larger applied force capacity and greater hysteretic energy dissipation.

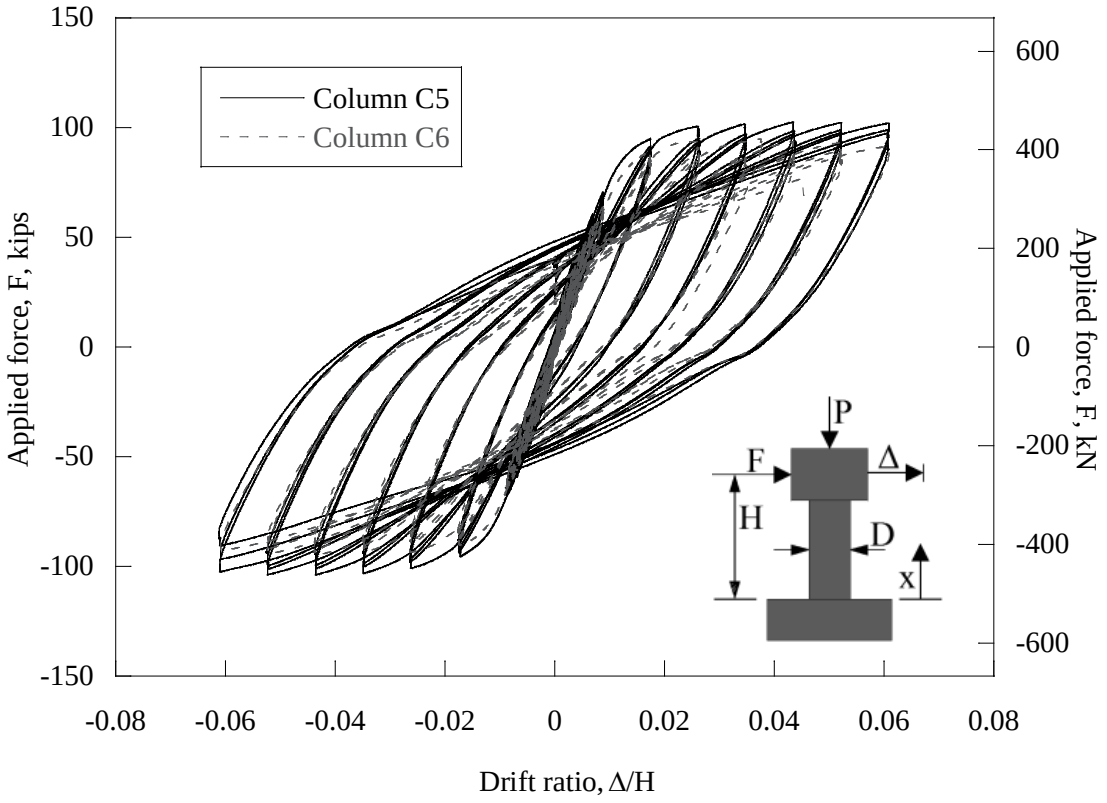

Figure 7.13: Applied force versus drift ratio of columns C5 and C6

Figure 7.14 shows a plot of the shear force versus drift ratio for columns C5 and C6. It can be seen from this plot that the response of the two columns are similar, except that hysteretic loops of column C5 contain a larger area compared to column C6. In addition, column C5 exhibits increased associated shear force.

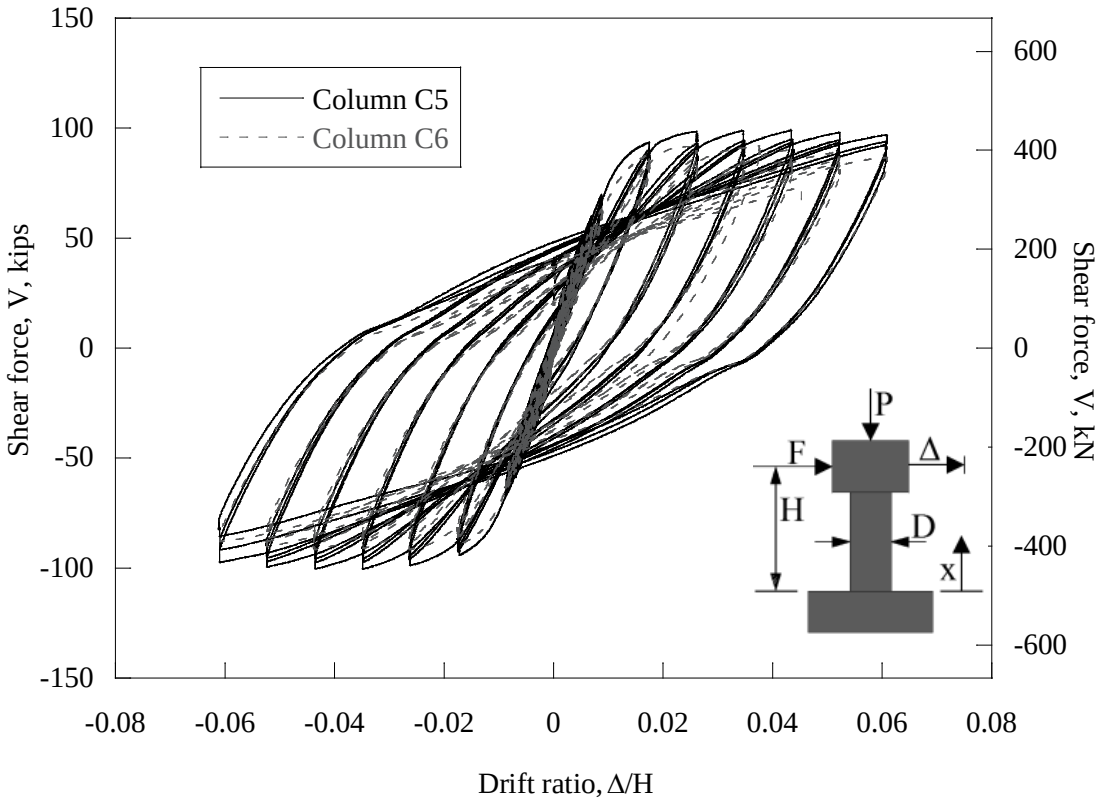

Figure 7.14: Shear force versus drift ratio of columns C5 and C6

7.2.3.6 Hysteretic Energy Dissipation

As shown in Figure 7.15, column C5 exhibited greater energy dissipation compared to column C6. This was expected because column C5 has more reinforcing bars to absorb the energy compared to column C6. Table 7.21 shows the total energy dissipated up the first yield, reference yield, and at each of the six bar fractures. It can be seen in this table that column C5 dissipated more energy when compared to column C6. This is most likely due to the reduction in the area of steel in column C6, which results in lower column stiffness, which in turn lowers its energy dissipation capacity. Column C5 dissipated less energy prior to the longitudinal reinforcement yielding when compared to column C6. However, column C6 dissipated less energy prior to the reference yield of the column when compared to column C5. It should be noted that both of these differences were small.

Energy dissipation is not a primary parameter used in design, however it becomes an important parameter when predicting the performance of structures and also when modeling structures to collapse. It should be noted that most codes do not require a minimum energy dissipation value.

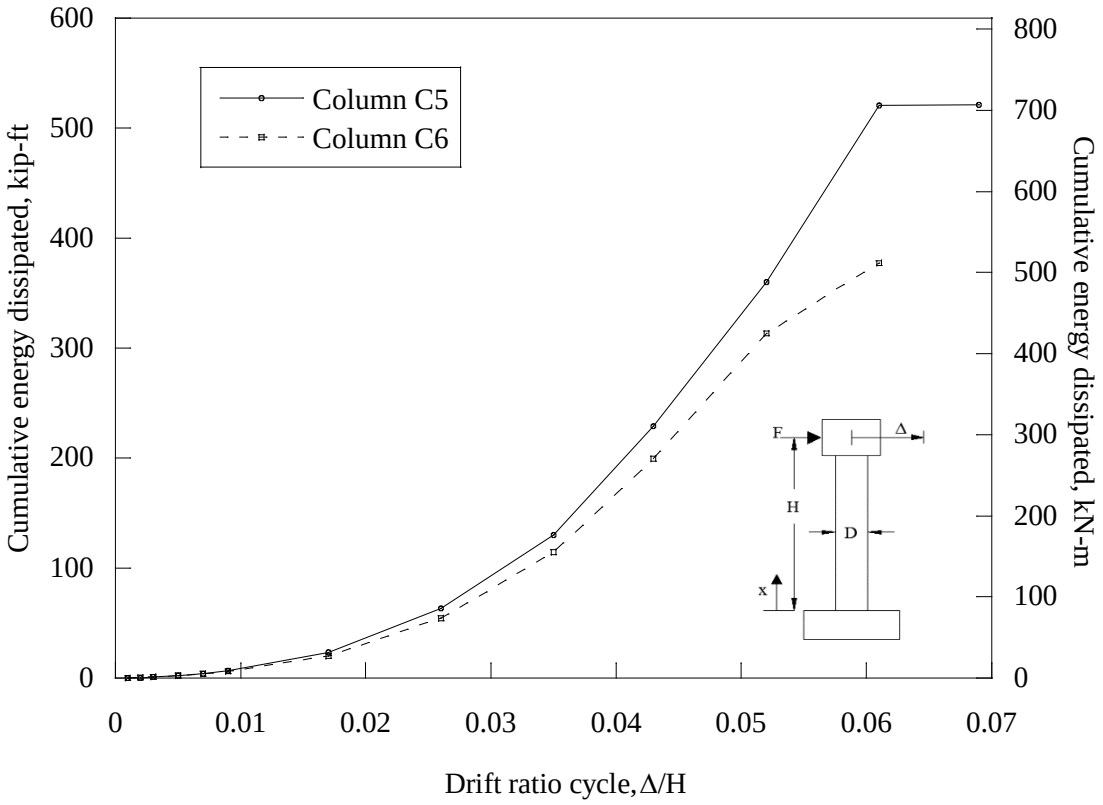

Figure 7.15: Cumulative energy dissipation of columns C5 and C6

Table 7.21: Energy dissipated of columns C5 and C6

	Column C5	Column C6
Energy dissipated at first yield, kip-ft (kN-m)	4.37 (5.92)	4.57 (6.20)
Energy dissipated at reference yield, kip-ft (kN-m)	10.39 (14.09)	9.66 (13.10)
Total energy dissipated at first bar fracture, kip-ft (kN-m)	521.22 (706.68)	377.43 (511.73)
Total energy dissipated at second bar fracture, kip-ft (kN-m)	532.84 (722.44)	428.98 (581.62)
Total energy dissipated at third bar fracture, kip-ft (kN-m)	537.21 (728.36)	460.10 (623.81)
Total energy dissipated at fourth bar fracture, kip-ft (kN-m)	593.04 (804.06)	494.81 (670.87)
Total energy dissipated at fifth bar fracture, kip-ft (kN-m)	619.08 (839.36)	502.45 (681.23)
Total energy dissipated at sixth bar fracture, kip-ft (kN-m)	624.55 (846.78)	514.10 (697.03)

7.2.3.7 Column Ductility

Table 7.22 summarizes the displacement and curvature ductility values of columns C5 and C6. The results indicate that when using the reference yield criteria, the displacement ductility values are similar (0.61 percent difference). This indicates the performance of the columns is similar. However, when using the first yield criteria, the displacement ductility is larger (12.95 percent difference) for column C5 when compared to column C6. The curvature ductility of column C5 at instrumentation levels 1, 3, and 4 are larger than those of column C6. At instrumentation level 1 column C6 exhibited larger curvature ductility values when compared to column C5. For both columns the curvature ductility was largest at the base of the column (level 1).

Table 7.22: Summary of column C5 and C6 ductility

	Displacement ductility, μ_Δ		Curvature ductility, μ_ψ			
		First yield	Level 1	Level 2	Level 3	Level 4
Column C5		8.88	33.31	7.14	4.46	0.91
Column C6	4.90	7.80	26.86	8.38	2.45	0.74
% Difference	0.61	12.95	21.44	15.98	58.18	20.61

The curvature ductility is typically more critical towards the base of the column where the majority of the curvature occurs. In this case, the data indicates that the curvature ductility value of columns C5 at 6 inches (152 mm) from the base

of the column (level 1) which includes the effects of strain penetration is larger than the value for C6. However at 12 inches (305 mm) from the base of the column (level 2) column C6 exhibited a larger curvature ductility value compared to column C5.

7.3 EFFECT OF LONGITUDINAL REINFORCEMENT RATIO

In this section the effect of the longitudinal reinforcement ratio is evaluated. First, the two columns constructed with Grade 60 reinforcement with a moment-shear span ratio of 6 (C1 and C3) are evaluated. Column C1 has a longitudinal reinforcement ratio of 1.11 percent and column C3 has a longitudinal reinforcement ratio of 2.19 percent. Next, the two columns with a moment-shear span ratio of 6 and constructed with Grade 80 reinforcement are evaluated and compared against the differences between columns C1 and C3. Column C2 has a longitudinal reinforcement ratio of 0.83 percent and column C4 has a longitudinal reinforcement ratio of 1.58 percent. The purpose of this section is to compare whether the effects of the longitudinal reinforcement ratio are similar for columns reinforced with A706 Grade 60 and Grade 80 reinforcement.

7.3.1 Column C1 and Column C3

In this section, columns C1 and C3 are compared to examine the effects on the longitudinal reinforcement ratio for columns constructed with Grade 60 reinforcement. Column C1 has a longitudinal reinforcement ratio of 1.11 percent and column C3 has a longitudinal reinforcement ratio of 2.19 percent. The effects of the longitudinal reinforcement ratio between columns C1 and C3 will be used as a base line to compare the effects of the longitudinal reinforcement ratio between columns C2 and C4 presented in section 7.3.2.

7.3.1.1 Visual Observations

Columns C1 and C3 exhibited similar cracking except column C1 only exhibited cracking along half the height of the column whereas column C3 exhibited cracking along three fourths of the column height. Figure 7.16 shows a side-by-side comparison of the cracking of columns C1 and C3. Note that these photographs were not taken at the same displacement ratio cycle.

Figure 7.16: Photographs of columns C1 (left) and C3 (right) cracking

Column C3 exhibited the onset of concrete spalling and concrete spalling one displacement cycle later than column C1. This suggests that the increase in longitudinal reinforcement ratio delays the onset of concrete spalling and concrete spalling. However it should be noted that this may not be directly due to increase in the area of longitudinal reinforcement but rather due to the spacing of the longitudinal bars. The mode of failure of both columns was flexural with reinforcing bar buckling followed by tension fracture of the longitudinal reinforcing bar. The first longitudinal reinforcing bar to buckle and fracture in column C3 occurred approximately 1.25 inches (31.8 mm) further from the base of the column when compared with column C1. Column C3 failed at the 10.00-inch (254 mm) displacement cycle whereas column C1 failed at the 7.50-inch (191 mm) displacement cycle. This suggests that the increase in longitudinal reinforcement ratio increases the columns drift ratio capacity. However it should be noted that both columns are well below the balance point in the moment-axial load interaction curve. For columns with larger axial loads this may not be true. The first bar fractured in column C1 approximately 6.0 inches (152 mm) from the base of the column during the final peak of the 7.50-inch (191 mm) displacement cycle. The first bar fractured in column C3 approximately 7.50 inches (127 mm) away from the base of the column during the return from the final peak of the 10.00-inch (254 mm) displacement cycle. Columns C1 and C3 both exhibited initial reinforcing bar buckling in the direction of the applied load.

From the visual observations of columns C1 and C3, the performance of column C3 was superior to column C1. This indicates that for columns constructed with

Grade 60 reinforcement, an increase in the longitudinal reinforcement ratio with result in superior column performance.

7.3.1.2 Maximum Lateral Displacement

Column C1 and column C3 exhibited very similar lateral displacements along the height of the column until column C1 failed. Figure 7.17 shows the normalized elevation versus drift ratio for the 2.50-inch (63.5 mm), 5.00-inch (127 mm), 7.50-inch (191 mm), 8.75-inch (222 mm), and the 10.00-inch (254 mm) displacement cycle for columns C1and C3. Note column C1 failed during the 7.50-inch (191 mm) displacement cycle.

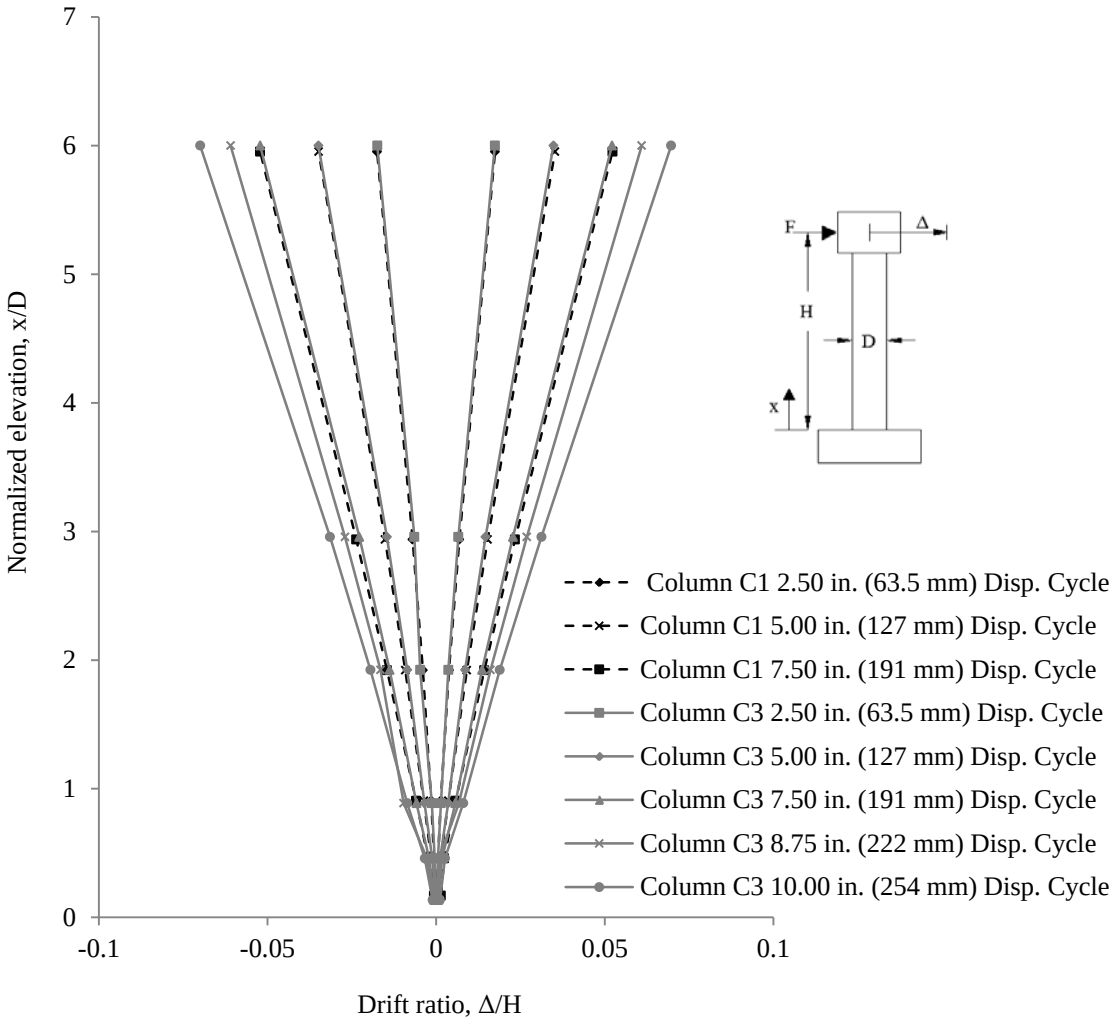

Figure 7.17: Normalized elevation versus drift ratio of columns C1 and C3

As seen in Figure 7.17 the drift ratios along the normalized elevation of the column are almost identical for the 2.50-inch (63.5 mm), 5.00-inch (127 mm), and 7.50-inch (191 mm) displacement cycles for columns C1 and C3. The data suggest that the reinforcement ratio does not affect the lateral displacement along the columns height for the comparable displacements cycles.

7.3.1.3 Steel Reinforcement Strains

The longitudinal reinforcing bars in column C1 first yielded at a tip displacement of 1.29 inches (32.8 mm) during the approach to the first peak of the 1.25-inch (31.8 mm) displacement cycle at the base of the column, level 2. The reinforcing bar did not yield at any other levels during this displacement

cycle. The longitudinal reinforcing bars in column C3 first yielded at a tip displacement of 1.44 inches (36.6 mm). This occurred one displacement cycle later than column C1 during the approach to the first peak of the 2.50-inch (63.5 mm) displacement cycle at the base of the column, level 2. The bar also yielded at all other levels except level 1 which is within the footing during this displacement cycle.

The longitudinal reinforcement in column C1 yielded in the footing (level 1) on the 5.00 inch (127 mm) displacement cycle and the longitudinal reinforcement in column C3 yielded in the footing (level 1) on the 3.75-inch (95.3 mm) displacement cycle. This suggests that the contribution of strain penetration is not as critical for column C1 as compared to column C3. Table 7.23 shows the transverse strains for columns C1 and C3 for 3 displacement cycles. All the transverse strains were small in magnitude and never approached yielding. For the vast majority of displacement cycles and instrumentation levels the transverse strains in column C3 were slightly larger than those of column C1.

Table 7.23: Summary of maximum transverse steel strains of columns C1 and C3

Level	Elevation inch (mm)	2.50 inch (63.5 mm) displacement cycle		5.00 inch (127 mm) displacement cycle		7.50 inch (191 mm) displacement cycle	
		C1 max % strain	C3 max % strain	C1 max % strain	C3 max % strain	C1 max % strain	C3 max % strain
1	-12.00 (-304.8)	N.A.*	0.0281	N.A.*	0.0334	N.A.*	0.0430
2	0.00 (0.00)	0.0067	0.0104	0.0093	0.0080	0.0172	0.0106
3	6.00 (152)	0.0020	0.0088	0.0031	0.0237	0.0136	0.0235
4	12.00 (304.8)	0.0066	0.0159	0.0133	0.0574	0.0329	0.0707
5	24.00 (609.6)	0.0078	0.1244	0.0120	0.1297	0.0145	0.1375
6	48.00 (1,219)	0.0062	0.0743	0.0070	0.0765	0.0067	0.0772
7	72.00 (1,829)	0.0069	0.0281	0.0084	0.0308	0.0097	0.0430

*N.A. stands for not available; the strain gage was damaged during construction

Table 7.24 shows the longitudinal tensile strains for columns C1 and C3 for 3 displacement cycles. Table 7.25 shows the longitudinal compressive strains for columns C1 and C3 for 3 displacement cycles. For all displacement cycles, column C1 had larger longitudinal tensile strains at the base of the column (level 2) and at level 3 when compared to column C3 prior to the strain gages reaching the three percent strain limit. Column C1 also had larger longitudinal tensile strains at level 4 compared to column C3 for all displacement cycles other than 2.50-inch (63.5 mm) displacement cycle. For the majority of

locations and displacement cycles the compressive strains between the two columns were similar except at level 3 at and past the 2.50-inch (63.5 mm) displacement cycle where column C1 exhibited significantly larger compressive strains compared to column C3.

The data suggest that for columns reinforced with A706 Grade 60 reinforcement an increase in the longitudinal reinforcement ratio results in larger transverse strains and smaller longitudinal tensile strains.

Table 7.24: Summary of maximum longitudinal tensile steel strains of columns C1 and C3

Level	Elevation inch (mm)	2.50 inch (63.5 mm) displacement cycle		5.00 inch (127 mm) displacement cycle		7.50 inch (191 mm) displacement cycle	
		C1 max % strain	C3 max % strain	C1 max % strain	C3 max % strain	C1 max % strain	C3 max % strain
1	-12.00 (-304.8)	0.12	0.22	0.29	0.26	0.35	0.30
2	0.00 (0.00)	1.57	1.21	3.00	2.05	3.00	3.00
3	6.00 (152)	1.33	1.01	2.28	1.61	3.00	2.87
4	12.00 (304.8)	0.30	0.72	2.33	1.73	3.00	3.00
5	24.00 (609.6)	0.34	0.52	1.38	1.29	1.72	2.35
6	48.00 (1,219)	0.27	0.25	0.30	0.29	0.31	3.00
7	72.00 (1,829)	0.17	0.25	0.20	0.21	0.20	0.23

Table 7.25: Summary of maximum longitudinal compressive steel strains of columns C1 and C3

Level	Elevation inch (mm)	2.50 inch (63.5 mm) displacement cycle		5.00 inch (127 mm) displacement cycle		7.50 inch (191 mm) displacement cycle	
		C1 max % strain	C3 max % strain	C1 max % strain	C3 max % strain	C1 max % strain	C3 max % strain
1	-12.00 (-304.8)	-0.14	-0.05	-0.07	-0.08	-0.09	-0.11
2	0.00 (0.00)	-0.23	-0.17	N.A.*	-0.14	N.A.*	N.A.*
3	6.00 (152)	-0.64	-0.23	-1.14	-0.77	N.A.*	-1.29
4	12.00 (304.8)	-0.21	-0.22	-0.23	-0.39	N.A.*	-0.51
5	24.00 (609.6)	-0.14	-0.11	-0.19	-0.11	-0.32	-0.05
6	48.00 (1,219)	-0.12	-0.12	-0.13	-0.13	-0.14	-0.14
7	72.00 (1,829)	-0.07	-0.12	-0.08	-0.09	-0.08	-0.09

* N.A. equals not available because the strain gage reached its 3 percent maximum tensile strain limit

7.3.1.4 Column Curvature

Table 7.26 shows the curvature for three of the larger displacement cycles for columns C1 and C3. It can be seen that the curvatures at all instrumentation levels are similar between the two columns. These results indicate that for columns constructed with Grade 60 reinforcement the longitudinal reinforcement ratio does not have a significant influence on the curvature of the column.

Table 7.26: Summary of column C1 and C3 curvatures

Level	Approx. elevation inch (mm)	2.50 inch (63.5 mm) displacement cycle		5.00 inch (127 mm) displacement cycle		7.50 inch (191 mm) displacement cycle	
		C1 max normalized curvature	C3 max normalized curvature	C1 max normalized curvature	C3 max normalized curvature	C1 max normalized curvature	C3 max normalized curvature
1	3.00 (76)	0.031	0.025	0.085	0.072	0.119	0.101
2	9.00 (229)	0.008	0.009	0.029	0.030	0.050	0.055
3	18.00 (457)	0.005	0.003	0.010	0.012	0.021	0.021
4	36.00 (914)	0.004	0.005	0.005	0.006	0.005	0.009
5	60.00 (1,524)	0.003	0.003	0.004	0.004	0.004	0.004

7.3.1.5 Column Forces

The same calculations were performed to remove the geometry effects of the applied axial load that was discussed in section 7.2.1.5. Table 7.27 shows the maximum applied force, shear force, and moment demands for columns C1 and C3. The large percent differences shown in the table were expected since column C3 has approximately twice the longitudinal reinforcement ratio as column C1. These values will be used to compare against the percent differences between columns C2 and C4 which are constructed with Grade 80 reinforcement.

Table 7.27: Column C1 and C3 moment capacity

Column	Maximum applied force kip (kN)	Column shear force kip (kN)	Associated plastic shear kip (kN)	Nominal moment capacity (Response 2000) kip-ft (kN-m)	Tested moment capacity kip-ft (kN-m)	Expected moment capacity kip-ft (kN-m)
C1	28.9 (128.4)	25.9 (115.1)	33.58 (149.4)	288 (390)	354 (480)	403 (546)
C3	52.0 (231)	47.9 (213)	54.0 (240)	463 (628)	631 (856)	649 (880)
% Diff.	57.11	59.62	46.63	46.63	56.24	46.77

The computed overstrength factor of column C1 was 1.23 and the computed overstrength factor of column C3 was 1.36. The data suggest that for columns constructed with Grade 60 reinforcement the longitudinal reinforcement ratio increases the overstrength factor.

Figure 7.18 shows the applied horizontal force versus the drift ratio for columns C1 and C3 up to the first longitudinal bar fractures. It can be seen that column C3 has a much larger applied force as well as a larger drift ratio capacity. This was expected since column C3 has approximately twice the area of longitudinal reinforcement compared to column C1. Figure 7.19 shows a plot of the shear force vs. drift ratio for columns C1 and C3. The comparisons are identical to those of Figure 7.14.

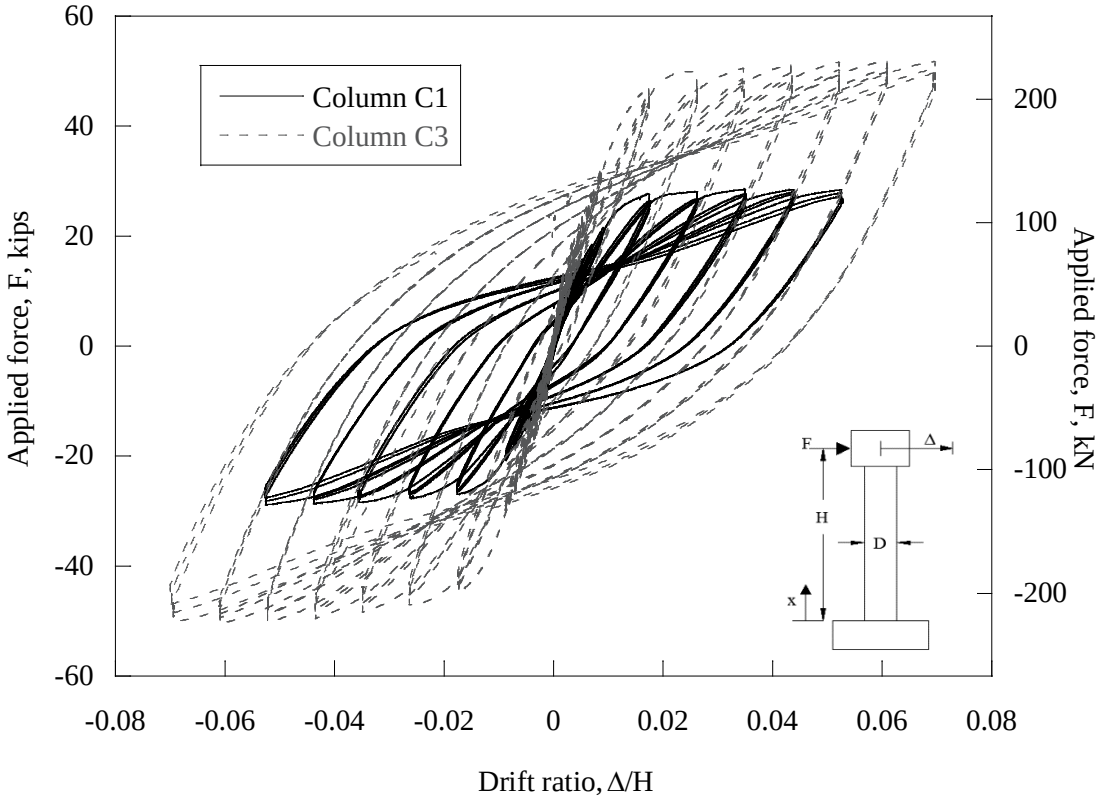

Figure 7.18: Applied force versus drift ratio of columns C1 and C3

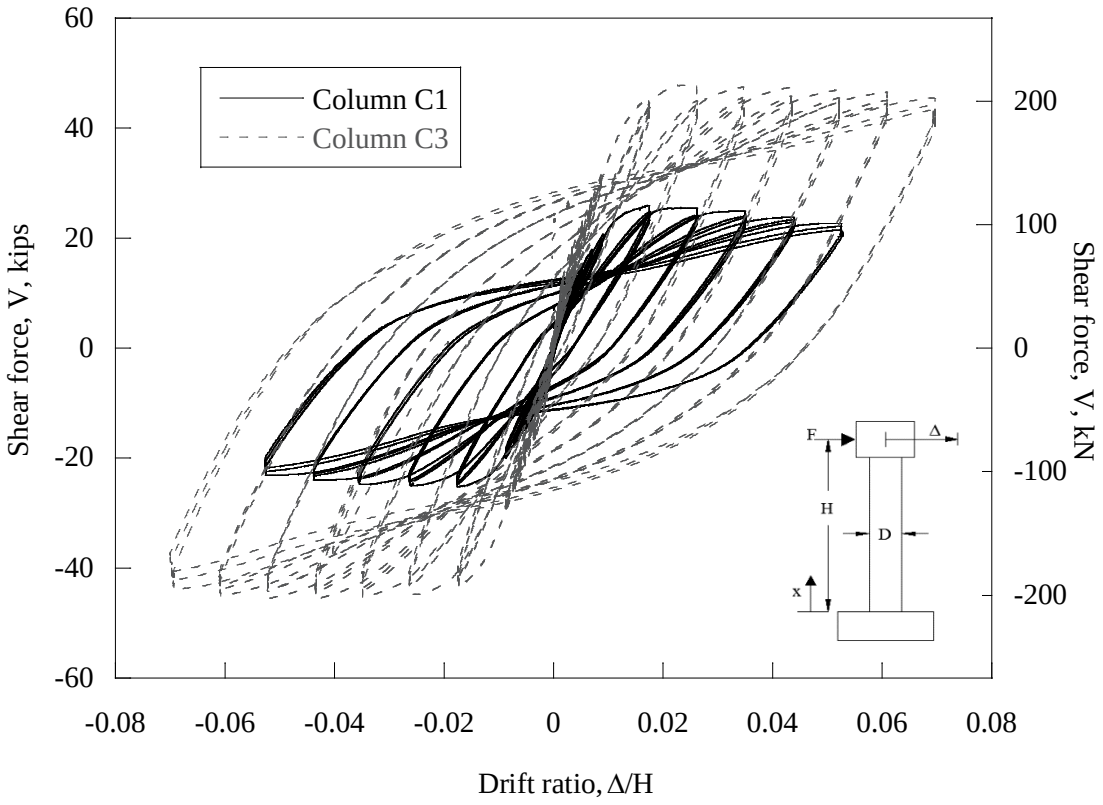

Figure 7.19: Shear force versus drift ratio of columns C1 and C3

7.3.1.6 Hysteretic Energy Dissipation

As shown in Figure 7.20, column C3 exhibited greater hysteretic energy dissipation when compared to column C1. This was expected because column C3 had approximately twice the area of longitudinal reinforcement to absorb the energy compared to column C1. Table 7.28 shows the total hysteretic energy dissipated up to the first reinforcing bar fracture, first yield, reference yield, and the percent differences between the columns. The percent differences will be used to compare against the percent differences between columns C2 and C4. It can be seen in this table that column C3 dissipated significantly more hysteretic energy when compared to column C1. This is most likely due to the reduction in the area of reinforcement in column C1, which results in lower column stiffness, which in turn lowers its hysteretic energy dissipation capacity. Column C1 dissipated less energy prior to the longitudinal reinforcement yielding and the column reference yield when compared to column C3. This validates the assumption that the difference in energy dissipated at the first bar fracture of the three pairs of columns (C1 and C2, C3 and C4, C5 and C6) shown in section 7.2 may be due to the difference in the area of reinforcement rather than the grade of reinforcement.

Energy dissipation is not a primary parameter used in design, however it becomes an important parameter when predicting the performance of structures and also when modeling structures to collapse. It should be noted that most codes do not require a minimum energy dissipation value.

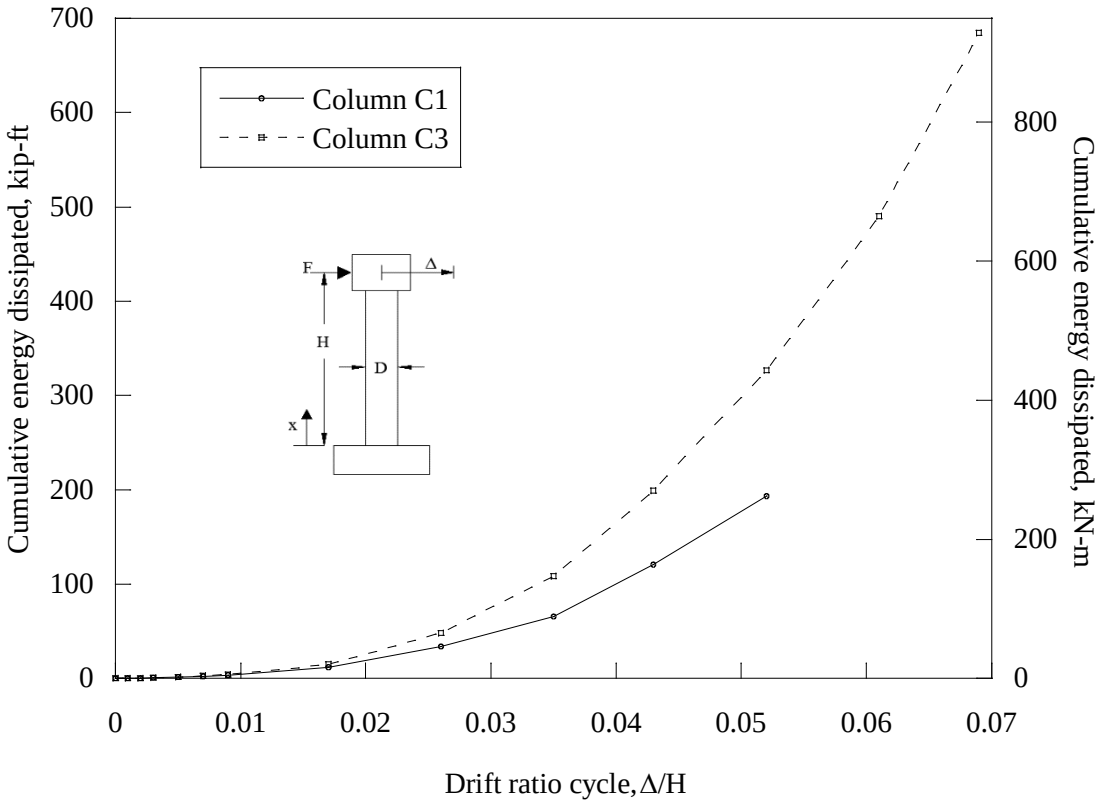

Figure 7.20: Cumulative energy dissipated of columns C1 and C3

Table 7.28: Energy dissipated of columns C1 and C3

	Column C1	Column C3	Percent difference
Energy dissipated at first yield, kip-ft (kN-m)	3.24 (4.39)	6.43 (8.72)	65.98
Energy dissipated at reference yield, kip-ft (kN-m)	5.48 (7.43)	9.01 (12.2)	48.72
Total energy dissipated, kip-ft (kN-m)	193.48 (262.32)	684.24 (927.71)	111.83

7.3.1.7 Column Ductility

Table 7.29 summarizes the displacement and curvature ductility values of columns C1 and C3. The results indicate that when using both the reference yield and first yield criteria, the displacement ductility is larger for column C3 when compared to column C1. This suggests that with an increase in the amount of longitudinal reinforcement the displacement ductility is also increased for columns constructed with Grade 60 reinforcement. Column C3 exhibited larger curvature ductility values at all levels when compared to column C1. At level 1, the curvature ductility values of the two columns were similar (2.67 percent difference). The data suggests that an increase in the area of longitudinal reinforcement results in a large increase in curvature ductility values not affected by strain penetration effects (all levels except level 1) and a slight increase in curvature ductility which is also affected by strain penetration.

Table 7.29: Summary of ductility values of columns C1 and C3

	Displacement ductility, μ_Δ		Curvature ductility, μ_ψ				
	Reference yield	First yield	Level 1	Level 2	Level 3	Level 4	Level 5
Column C1	3.95	5.83	20.34	8.54	3.54	0.93	0.69
Column C3	4.58	7.00	20.89	19.16	6.63	2.32	0.84
% Difference	14.77	18.24	2.67	76.68	60.77	85.54	19.61

7.3.2 Column C2 and Column C4

In this section columns C2 and C4 are compared to examine the effects of the longitudinal reinforcement ratio on columns constructed with Grade 80 reinforcement. Both columns have a moment-shear span ratio equal to six. Column C2 has a longitudinal reinforcement ratio of 0.83 percent and column C4 has a longitudinal reinforcement ratio of 1.58 percent. The results of this section are compared with the results of section 7.3.1 where columns C1 and C3 are compared to determine if the effects of the longitudinal reinforcement ratio are similar with columns constructed with Grade 60 reinforcement and columns constructed with Grade 80 reinforcement.

7.3.2.1 Visual Observations

Columns C2 and C4 exhibited similar crack distributions. Figure 7.21 shows a side-by-side comparison of the cracking of columns C2 and C4. Note that these photographs were not taken at the same displacement ratio cycle.

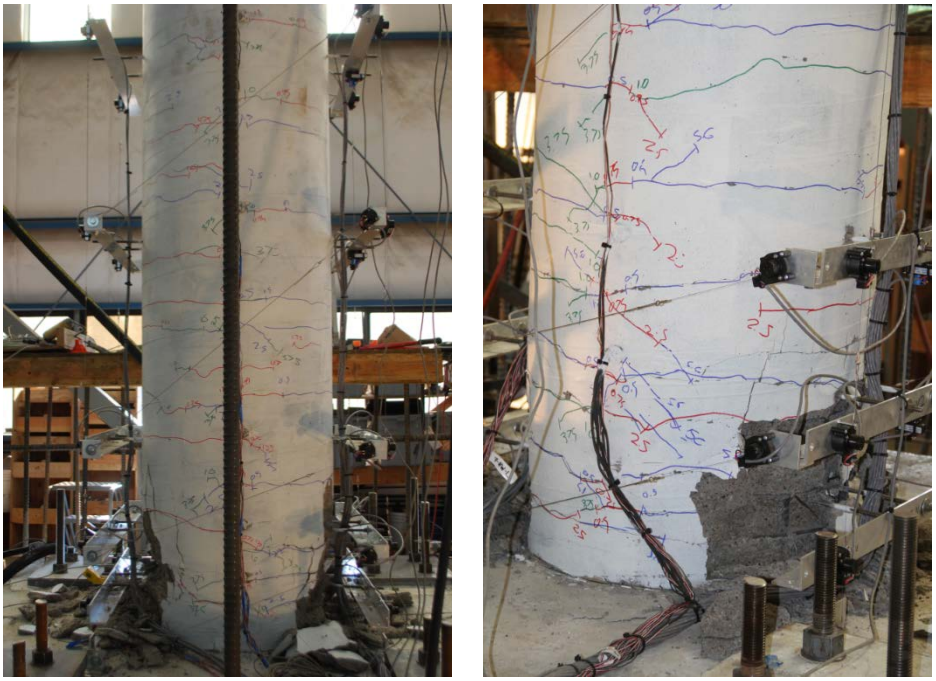

Figure 7.21: Photographs of columns C2 (left) and C4 (right) cracking

Columns C4 exhibited the onset of concrete spalling and concrete spalling one displacement cycle later than column C2. This is similar to the comparison of columns C1 and C3 suggesting that the delay in concrete spalling due to an increase in the amount of longitudinal reinforcement is similar for columns constructed with Grade 60 or Grade 80 reinforcement. However, as previously stated this may be due to the decrease in spacing between the longitudinal reinforcing bars rather than the increase in the amount of longitudinal reinforcement. The mode of failure of both columns was flexural due to reinforcing bar buckling followed by tension fracture of the reinforcing bar. The first longitudinal reinforcing bar to buckle and fracture in column C2 occurred at approximately 3.5 inches (88.9 mm) further from the base of the column when compared to column C4. The reinforcing bar fractured in column C2 was approximately 8.5 inches (216 mm) from the base of the column occurring during the return from the final peak of the 8.75-inch (222 mm) displacement cycle. Column C4 first reinforcing bar fractured approximately 5.00 inches (127 mm) away from the base of the column occurring during the approach to the fourth peak of the 10.00-inch (254 mm) displacement cycle. The delay in the first bar fracture is similar to the delay between columns C1 and C3. This

indicates that an increase in the amount of longitudinal reinforcement may delay reinforcing bar fracture for columns reinforced with Grade 60 or Grade 80 reinforcement. However, as previously stated this may be due to the spacing of the longitudinal reinforcing bars rather than the increase in area of the longitudinal reinforcement.

7.3.2.2 Maximum Lateral Displacement

Figure 7.22 shows the normalized elevation versus drift ratio for the 2.50-inch (63.5 mm), 5.00-inch (127 mm), 7.50-inch (191 mm), and the 10.00-inch (254 mm) displacement cycle for columns C2 and C4. Note that only column C4 reached the 10.00-inch (254 mm) displacement cycle prior to the first longitudinal reinforcing bar fracture.

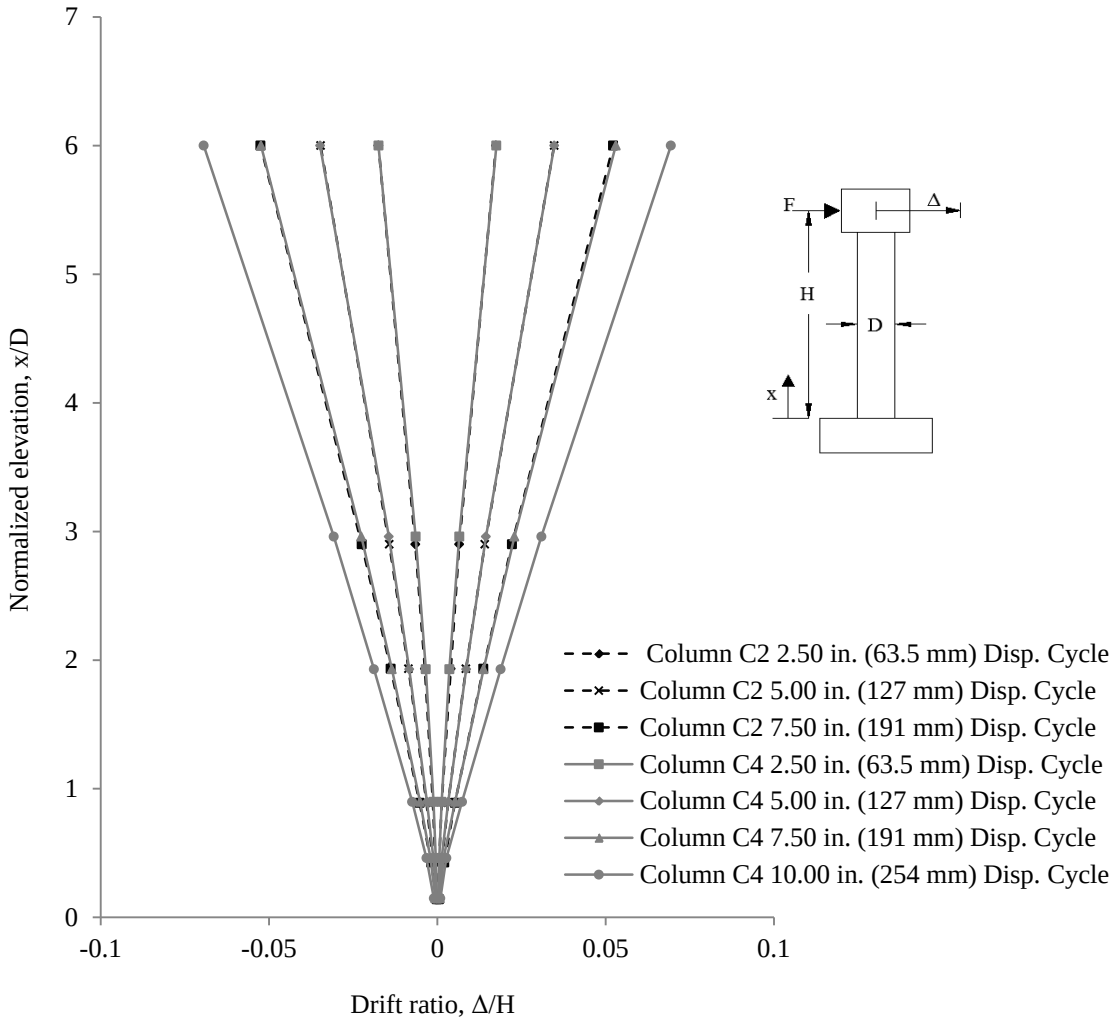

Figure 7.22: Drift ratio versus normalized elevation of columns C2 and C4

As seen in Figure 7.22 the drift ratios along the normalized elevation of the column are almost identical for the 2.50-inch (63.5 mm), 5.00-inch (127 mm), and the 7.50-inch (191 mm) displacement cycle for columns C2 and C4. This result is very similar to the results between columns C1 and C3. This suggests that the increase in longitudinal reinforcement does not affect the lateral displacement along the height of the column for comparable displacement cycles. This conclusion was the same for columns C1 and C3 suggesting that for columns constructed with Grade 60 or Grade 80 reinforcement the increase in longitudinal reinforcement ratio does not significantly affect the lateral displacements of comparable displacement cycles but does increase the maximum lateral displacements.

7.3.2.3 Steel Reinforcement Strains

The longitudinal reinforcing bars in column C2 first yielded at a tip displacement of 1.60 inches (40.6 mm). This occurred during the approach to the first peak of the 2.50-inch (63.5 mm) displacement cycle at level 3. The longitudinal bars in column C4 first yielded at a tip displacement of 1.58 inches (40.1 mm). This occurred during the approach to the first peak of the 2.50-inch (63.5 mm) displacement cycle at the base of the column, level 2. The longitudinal reinforcing bars first yielded in columns C2 and C4 at very similar displacements.

The longitudinal reinforcement in column C2 and C4 never yielded in the footing (level 1). This indicates that the contribution of strain penetration is not as important for columns C2 and C4 (constructed with Grade 80 reinforcement) compared to columns C1 and C3 (constructed with Grade 60 reinforcement). Table 7.30 shows the transverse strains for columns C2 and C4 for 3 displacement cycles. All the transverse strains were small in magnitude and never yielded, except for column C4 at level 3 where the spiral did yield during the final displacement cycle due to longitudinal reinforcing bar buckling. The transverse strains in both columns were very similar for the vast majority of locations and displacement cycles. This conclusion is different than that of columns C1 and C3 where column C3 generally exhibited larger transverse strains.

Table 7.30: Summary of maximum transverse steel strains of columns C2 and C4

Level	Elevation inch (mm)	2.50 inch (63.5 mm) displacement cycle		5.00 inch (127 mm) displacement cycle		7.50 inch (191 mm) displacement cycle	
		C2 max % strain	C4 max % strain	C2 max % strain	C4 max % strain	C2 max % strain	C4 max % strain
1	-12.00 (-304.8)	0.0063	0.0262	0.0097	0.0452	0.0098	0.0539
2	0.00 (0.00)	0.0106	0.0175	0.0070	0.0240	0.0271	0.0111
3	6.00 (152)	0.0059	0.0194	0.0140	0.0664	0.0162	0.2244
4	12.00 (304.8)	0.0059	0.0116	0.0106	0.0375	0.0129	0.0672
5	24.00 (609.6)	0.0125	0.0198	0.0152	0.0236	0.0143	0.0325
6	48.00 (1,219)	0.0112	0.0131	0.0136	0.0140	0.0150	0.0146
7	72.00 (1,829)	0.0079	0.0085	0.0118	0.0086	0.0132	0.0092

Table 7.31 shows the longitudinal tensile strains for columns C2 and C4 for 3 displacement cycles. Table 7.32 shows the longitudinal compressive strains for columns C2 and C4 for 3 displacement cycles. For the majority of locations and displacement cycles column C2 exhibited larger longitudinal tensile strains compared to column C4. At level 2, the longitudinal tensile strains were larger in column C4 when compared to column C2. This suggests that increasing the amount of longitudinal reinforcement may reduce the magnitude of tensile strains in the longitudinal reinforcement. The compressive strains were similar between the two columns. This conclusion is similar to that for columns C1 and C3 which are constructed with Grade 60 reinforcement. The longitudinal reinforcement in column C2 and C4 never yielded in the footing (level 1). However, at level 2, larger strains were observed for column C4 than column C2, which is at the interface between the column and footing. This indicates that the strain penetration length was smaller for columns C4 than for column C2. Furthermore, comparison with results for columns C1 and C3 indicate that the contribution of strain penetration is not as important for columns C2 and C4 (constructed with Grade 80 reinforcement) compared to columns C1 and C3 (constructed with Grade 60 reinforcement).

Table 7.31: Summary of maximum longitudinal tensile steel strains of columns C2 and C4

Level	Elevation inch (mm)	2.50 inch (63.5 mm) displacement cycle		5.00 inch (127 mm) displacement cycle		7.50 inch (191 mm) displacement cycle	
		C2 max % strain	C4 max % strain	C2 max % strain	C4 max % strain	C2 max % strain	C4 max % strain
1	-12.00 (-304.8)	0.19	0.03	0.24	0.05	0.30	0.05
2	0.00 (0.00)	1.15	1.35	1.40	2.38	3.00	3.00
3	6.00 (152)	1.29	1.28	2.20	1.73	3.00	2.59
4	12.00 (304.8)	0.96	0.95	1.95	1.57	3.00	2.34
5	24.00 (609.6)	0.81	0.50	1.00	1.11	0.95	1.61
6	48.00 (1,219)	0.30	0.29	0.35	0.34	0.36	0.36
7	72.00 (1,829)	0.21	0.20	0.27	0.25	0.27	0.25

Table 7.32: Summary of maximum longitudinal compressive steel strains of columns C2 and C4

Level	Elevation inch (mm)	2.50 inch (63.5 mm) displacement cycle		5.00 inch (127 mm) displacement cycle		7.50 inch (191 mm) displacement cycle	
		C2 max % strain	C4 max % strain	C2 max % strain	C4 max % strain	C2 max % strain	C4 max % strain
1	-12.00 (-304.8)	-0.11	-0.06	-0.17	-0.10	-0.19	-0.14
2	0.00 (0.00)	-0.12	-0.17	0.11**	-0.33	0.13**	N.A.*
3	6.00 (152)	-0.20	-0.18	-0.50	-0.47	N.A.*	-0.81
4	12.00 (304.8)	-0.23	-0.18	-0.34	-0.30	N.A.*	-0.40
5	24.00 (609.6)	-0.13	-0.14	-0.26	-0.17	-0.16	-0.13
6	48.00 (1,219)	-0.11	-0.11	-0.13	-0.14	-0.14	-0.14
7	72.00 (1,829)	-0.08	-0.08	-0.09	-0.09	-0.10	-0.10

*N.A. equals not available because the strain gage had reached its 3 percent maximum tensile strain limit

**The data shows the strain gage never went into compression

7.3.2.4 Column Curvature

Table 7.33 shows the normalized curvatures for 3 of the larger displacement cycles for columns C2 and C4. It can be seen that the curvatures at all instrumentation levels were similar between the two columns. This conclusion is similar to that for columns C1 and C3. This suggests that for columns constructed with Grade 60 or Grade 80 reinforcement the amount of longitudinal reinforcement does not significantly affect the curvature of the column.

Table 7.33: Summary of column C2 and C4 curvature

Level	Approx. elevation in. (mm)	2.50 in. (63.5 mm) displacement cycle		5.00 in. (127 mm) displacement cycle		7.50 in. (191 mm) displacement cycle	
		C2 max normalized curvature	C4 max normalized curvature	C2 max normalized curvature	C4 max normalized curvature	C2 max normalized curvature	C4 max normalized curvature
1	3.00 (76)	0.021	0.023	0.066	0.061	0.115	0.098
2	9.00 (229)	0.010	0.008	0.027	0.029	0.053	0.049
3	18.00 (457)	0.004	0.005	0.011	0.010	0.017	0.024
4	36.00 (914)	0.005	0.006	0.007	0.007	0.008	0.008
5	60.00 (1,524)	0.003	0.004	0.004	0.004	0.004	0.005

7.3.2.5 Column Forces

The same calculations were performed to remove the geometry effects of the applied axial load that was discussed in section 7.2.1.5.

Table 7.34 shows the maximum applied force, shear force and moment demands for columns C2 and C4. The large percent differences shown in the table is expected since column C4 has approximately twice the longitudinal reinforcement ratio as column C2. Column C2 has a computed overstrength factor of 1.21 and column C4 has a computed overstrength factor of 1.28. The data suggest that for columns constructed with Grade 60 or Grade 80 reinforcement the calculated overstrength factor increases with an increase in the longitudinal reinforcement ratio.

The percent difference between columns C2 and C4 shear and moment capacity was larger when compared to the percent difference between C1 and C3. The difference in percent difference in associated shear force at failure was 9.76 percent. The difference in percent difference in moment capacity was 6.46 percent.

Table 7.34: Column C2 and C4 moment capacity

Column	Maximum applied force kip (kN)	Column shear force kip (kN)	Associated plastic shear kip (kN)	Nominal moment capacity (Response 2000) kip-ft (kN-m)	Tested moment capacity kip-ft (kN-m)	Expected moment capacity kip-ft (kN-m)
C2	28.2 (125.6)	25.9 (115.1)	33.22 (147.8)	285 (386)	344 (466)	399 (541)
C4	46.9 (209)	43.1 (192)	52.3 (233)	448 (607)	572 (776)	628 (851)
% Diff.	49.80	49.86	44.62	44.47	49.78	44.60

Figure 7.23 shows the drift ratio versus applied horizontal force for columns C2 and C4 up to the first longitudinal bar fracture. The increase in applied force and drift ratio capacity of column C4 is expected due to the increase in the amount of longitudinal reinforcement. Figure 7.24 shows a plot of the drift ratio versus shear force for columns C2 and C4. Again the increase in shear force and drift ratio capacity of column C4 is expected due to the increase in the amount of longitudinal reinforcement.

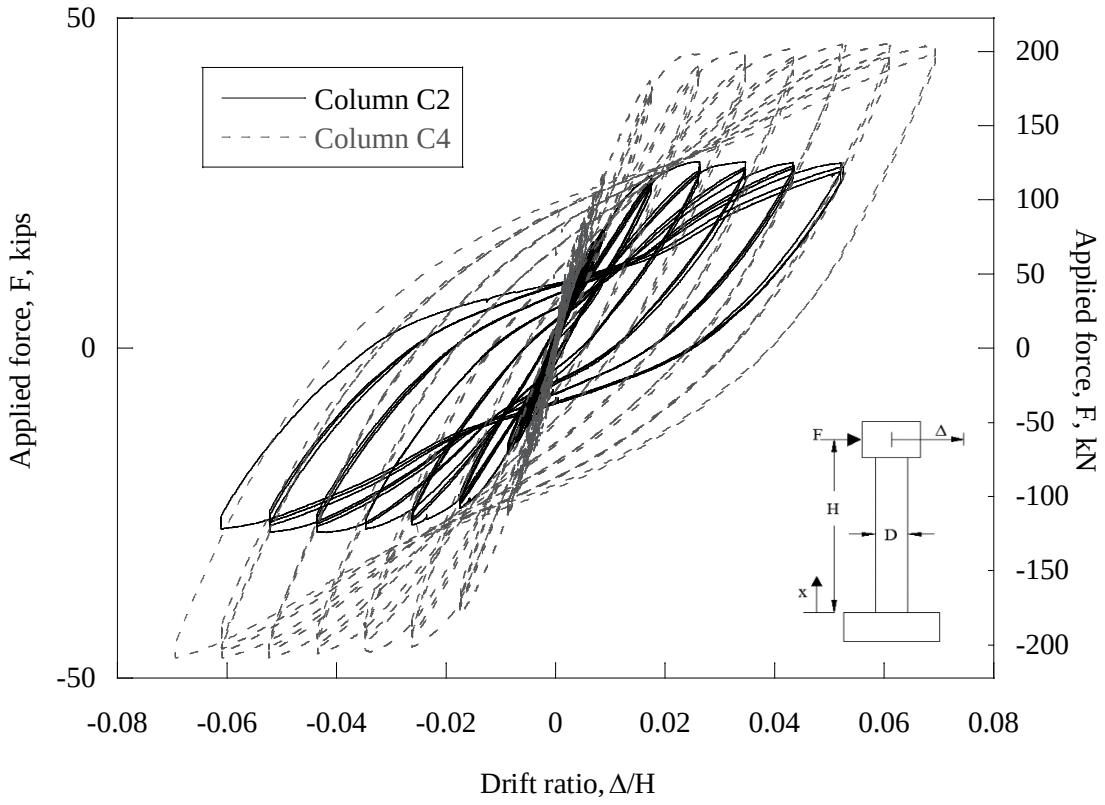

Figure 7.23: Drift ratio versus applied force of columns C2 and C4

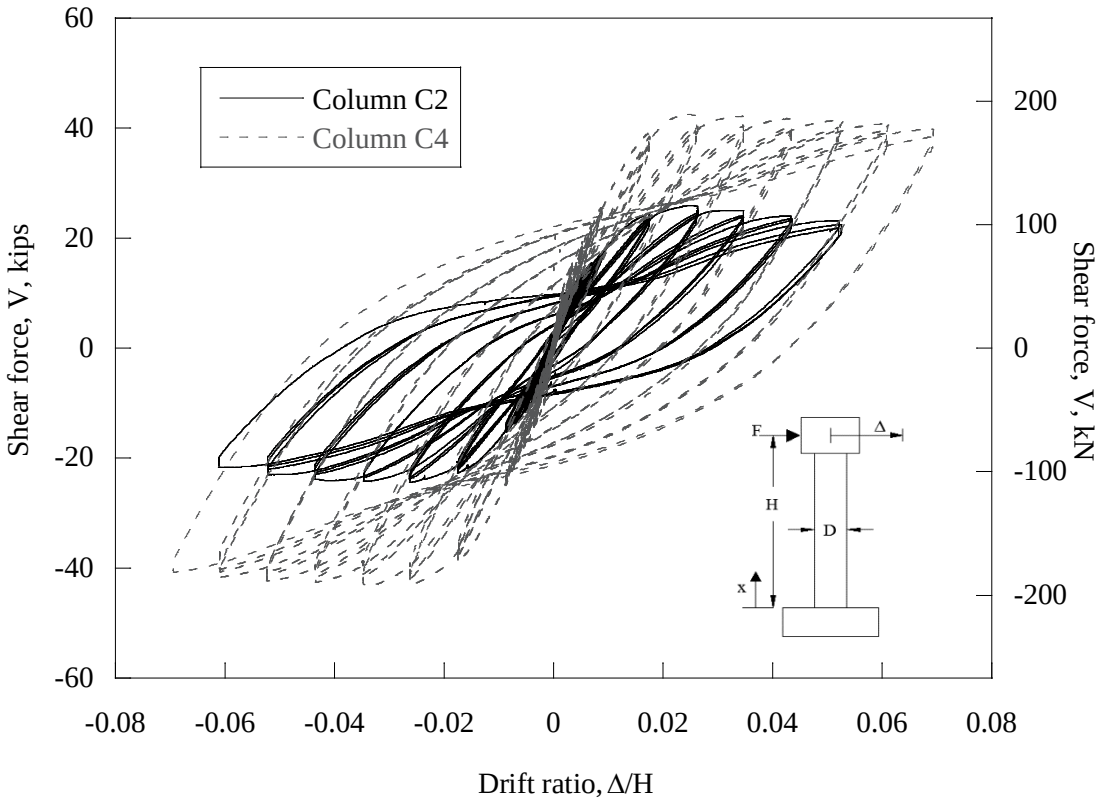

Figure 7.24: Drift ratio versus shear force of columns C2 and C4

7.3.2.6 Hysteretic Energy Dissipation

As shown in Figure 7.25, column C4 exhibited greater hysteretic energy dissipation when compared to column C2. This was expected because column C4 has more reinforcing bars to absorb the hysteretic energy compared to column C2. Table 7.35 shows the total hysteretic energy dissipated up to the first reinforcing bar fracture, first yield and reference yield. It can be seen in this table that column C4 dissipated more hysteretic energy at the first yield, reference yield, and first bar fracture when compared to column C2. This is most likely due to the reduction in the area of reinforcement in column C2, which results in lower column stiffness, which in turn lowers its hysteretic energy dissipation capacity. This was also seen in the comparison in columns C1 and C3 which were constructed with Grade 60 reinforcement. This supports the claim that the reduction in hysteretic energy dissipation capacity is primarily a function of the amount of longitudinal reinforcement rather than the grade of reinforcement. The percent differences in hysteretic energy dissipated at the first yield and reference yield between columns C2 and C4 was smaller than the percent differences between columns C1 and C3. However the percent

difference in hysteretic energy dissipated to first bar fracture between columns C2 and C4 was larger than that of column C1 and C3.

Again it should be noted that hysteretic energy dissipation is not a primary parameter used in design, however it becomes an important parameter when predicting the performance of structures and also when modeling structures to collapse. It should be noted that most codes do not require a minimum energy dissipation value.

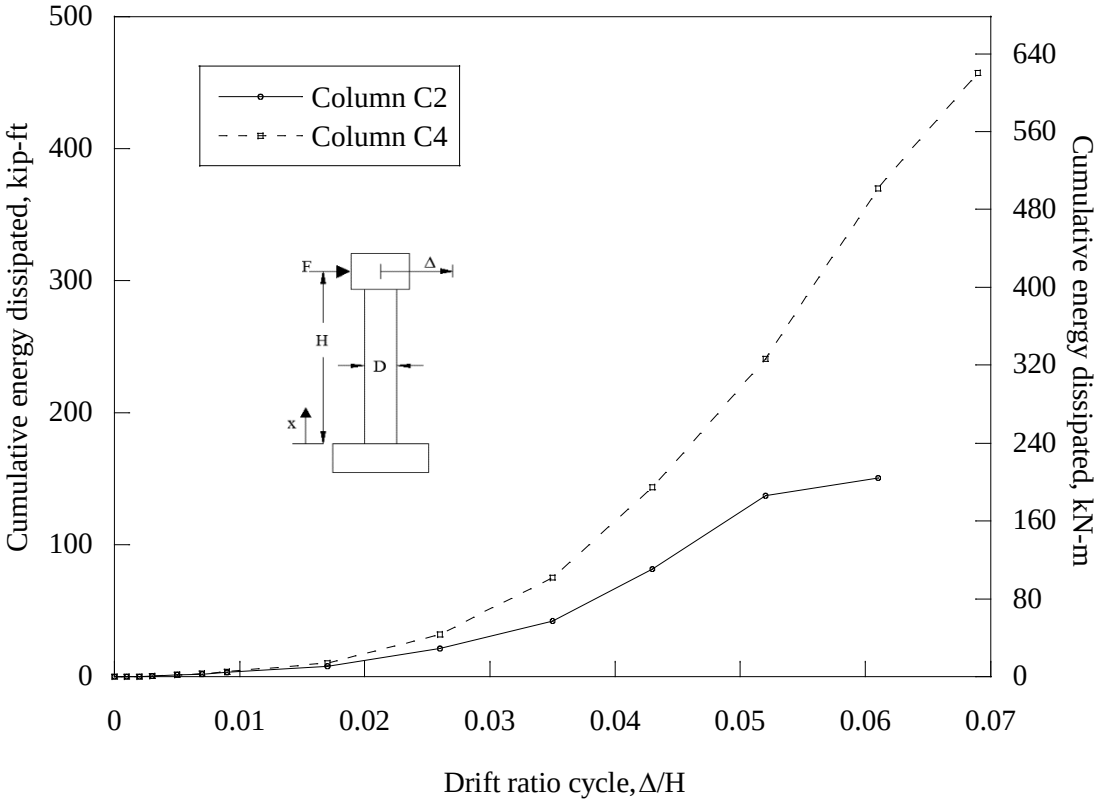

Figure 7.25: Cumulative energy dissipation of column C2 and C4

Table 7.35: Cumulative energy dissipation of column C2 and C4

	Column C2	Column C4	Percent difference
Energy dissipated at first yield, kip-ft (kN-m)	3.24 (4.39)	5.97 (8.09)	59.28
Energy dissipated at reference yield, kip-ft (kN-m)	5.48 (7.43)	8.07 (10.9)	38.23
Total energy dissipated, kip-ft (kN-m)	193.48 (262.32)	457.67 (620.52)	117.19

7.3.2.7 Column Ductility

Table 7.36 summarizes the displacement and curvature ductility values of columns C2 and C4. The results indicate that when using both the reference yield and first yield criteria, the displacement ductility values are larger for column C4 when compared to column C2. This result was also the case for the comparison for columns C1 and C3. This suggests that an increase in the longitudinal reinforcement ratio results in a larger displacement ductility values for columns constructed with Grade 60 or Grade 80 reinforcement. However, it may be more due to the decrease in spacing of the longitudinal bars rather than solely on the increase in the longitudinal reinforcement ratio.

The curvature ductility values of column C4 at all elevations were larger than those of column C2. This was also the result for the comparison of columns C1 and C3. However the increase in curvature ductility values at levels 1 and 2 were different between the columns constructed with Grade 60 reinforcement and the columns constructed with Grade 80 reinforcement. The difference at level 1 is influenced by strain penetration effects as well as the actual flexural deformations. The percent difference between the displacement ductility using both the first yield and the reference yield between columns C2 and C4 is smaller than that of columns C1 and C3. This was also the case for curvature ductility at all levels other than the top level, level 5. This suggests that increase in the amount of longitudinal reinforcement affects the ductility of the column constructed with Grade 60 or Grade 80 reinforcement similarly.

Table 7.36: Summary of columns C2 and C4 ductility values

	Displacement ductility, μ_Δ		Curvature ductility, μ_ψ				
	Reference yield	First yield	Level 1	Level 2	Level 3	Level 4	Level 5
Column C2	4.13	5.51	16.45	9.66	2.38	1.19	0.63
Column C4	4.35	6.33	23.63	10.21	5.61	1.54	1.43
% Difference	5.19	13.85	35.83	5.54	80.85	25.64	77.67

7.4 EFFECT OF COLUMN MOMENT-SHEAR SPAN RATIO

In this section the effect of the moment-shear span ratio is evaluated. Columns C3 and C5 are first compared to determine the effects of the moment-shear span ratio for columns constructed with Grade 60 reinforcement. Both columns have identical transverse and longitudinal reinforcement; however column C3 has a moment-shear span ratio of 6 whereas column C5 has a moment-shear span ratio of 3. Next, columns C4 and C6 will be compared to determine the effects of the moment-shear span ratio for columns constructed with Grade 80 reinforcement. Both columns have identical transverse and longitudinal reinforcement; however column C4 has a moment-shear span ratio of 6 whereas column C6 has a moment-shear span ratio of 3. The results between columns C4 and C6 will be compared against the results between columns C3 and C5 to determine if the moment-shear span ratio affects columns constructed with Grade 80 reinforcement differently than columns constructed with Grade 60 reinforcement.

7.4.1 Column C3 and Column C5

Columns C3 and C5 have the identical longitudinal and transverse reinforcement. Column C3 has a moment-shear span ratio of 6 and column C5 has a moment-shear span ratio of 3. The purpose of this section is to determine the effect of the moment-shear span ratio on the performance of columns constructed with Grade 60 reinforcement. Note that the magnitude in displacement cycles are different for the two columns, however the drift ratio at each cycle are identical for the two columns. The time per cycle was also the same.

7.4.1.1 Visual Observations

Columns C3 and C5 exhibited different crack distribution. Column C3 only exhibited cracking over three fourths of the height of the column. The cracks in column C3 were predominately flexural and then progressed into shear cracks at larger displacements. Column C5 exhibited cracking over nearly the entire height of the column. The cracks in column C5 started off as flexural but soon after shear cracks were the predominant form of cracking and were seen along the entire height of the column. Figure 7.26 shows a side-by-side comparison of the cracking of columns C3 and C5. Note that these photographs were not taken at the same drift ratio cycle.

Figure 7.26: Photographs of columns C3 (left) and C5 (right) cracking

Columns C3 and C5 exhibited the onset of concrete spalling at the same drift ratio cycle. Column C3 exhibited concrete spalling one drift ratio cycle past the cycle where the onset of spalling occurred whereas column C5 exhibited onset of spalling and concrete spalling on the same cycle. The mode of failure of both columns was flexural due to reinforcing bar buckling followed by tension fracture of the reinforcement. The first longitudinal reinforcing bar to buckle and fracture in column C3 occurred approximately 2 inches (51 mm) further from the base of the column when compared to column C5. Both columns failed during the same drift ratio cycle, however column C3 hit all six peaks before failing where column C5 failed prior to reaching the first peak.

From the visual observations of columns C3 and C5, the performance was similar, except for that column C3 was able to hit six more peaks at the 6.9 percent drift ratio cycle compared to column C5. In essence column C3 was able to complete a full drift ratio cycle more compared to column C5.

7.4.1.2 Maximum Lateral Displacement

Column C3 reached a maximum drift ratio of 7.0 percent while column C5 reached a maximum drift ratio of 6.1 percent. Figure 7.27 shows the normalized elevation versus drift ratio for the 1.7 percent, 3.5 percent, 5.2 percent, and 6.9 percent drift ratio cycles.

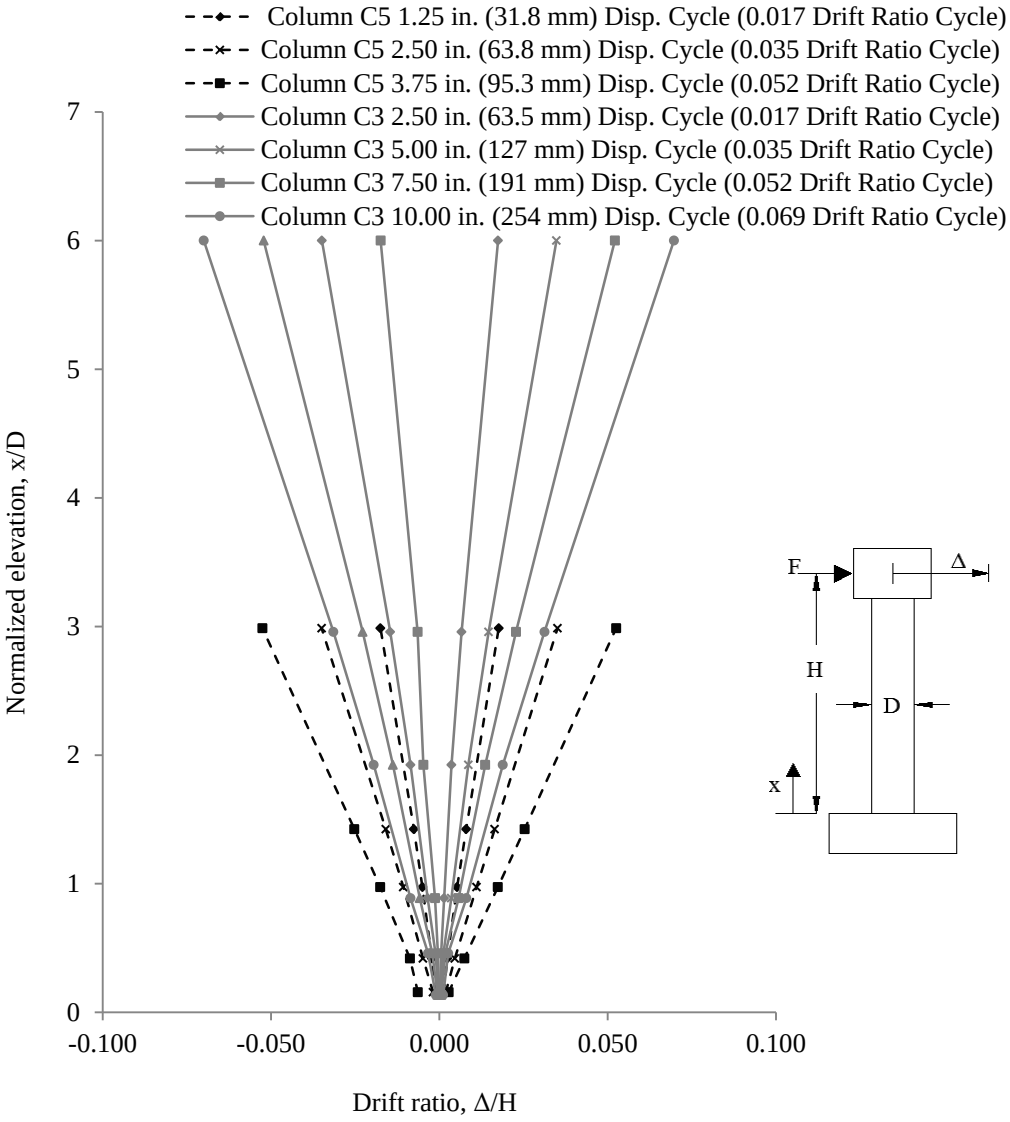

Figure 7.27: Normalized elevation of columns C3 and C5

As seen in Figure 7.27 the drift ratios along the normalized elevation of the column are larger for column C5 compared to column C3. It should be noted that the tip (roof) drift ratios are the same for both columns up to the 6.1 percent drift ratio cycle. The results suggest that a column with a smaller moment-shear span ratio is able to achieve larger drift ratios along the height of the column.

7.4.1.3 Steel Reinforcement Strains

Columns C3 and C5 have strain gages at similar locations up to level 5 to compare the strains in the steel reinforcement. The longitudinal reinforcing bars in column C3 first yielded at a tip displacement of 1.44 inches (36.6 mm). This occurred during the approach to the first peak of the 1.7 percent drift ratio cycle

at the base of the column, level 2. The longitudinal reinforcing bars in column C5 first yielded at a tip displacement of negative 0.50 inches (13 mm). This occurred at the fourth peak of the 0.7 percent drift ratio cycle at 12 inches (305 mm) from the base of the column, level 4. The data indicate that a decrease in the moment-shear span ratio of columns constructed with Grade 60 reinforcement may cause the longitudinal reinforcement to yield earlier.

The longitudinal reinforcement in column C3 yielded in the footing (level 1) on the 2.6 percent drift ratio cycle and the longitudinal steel in column C5 yielded in the footing (level 1) on the 1.7 percent drift ratio cycle. Note that for both columns all locations along the height of column yield during the drift ratio cycle at which the longitudinal reinforcing bar yielded in the footing.

Table 7.37 shows the transverse strains for columns C3 and C5 for 3 drift ratio cycles. The transverse strains in the footing, level 1, of column C5 were larger when compared to column C3 at all drift ratio cycles. The transverse strains at level 5 of column C3 were larger when compared to column C5 at all drift ratio cycles. After the 0.5 percent drift ratio cycle column C5 exhibited larger transverse strains at levels 3 and 4 when compared to column C3.

Table 7.37: Summary of maximum transverse steel strains of columns C3 and C4

Level	Elevation inch (mm)	0.017 Drift ratio cycle		0.035 Drift ratio cycle		0.052Drift ratio cycle	
		C3 max % strain	C5 max % strain	C3 max % strain	C5 max % strain	C3 max % strain	C5 max % strain
1	-12.00 (-304.8)	0.0281	0.0389	0.0334	0.0523	0.0430	0.0713
2	0.00 (0.00)	0.0104	N.A.*	0.0080	N.A.*	0.0106	N.A.*
3	6.00 (152)	0.0088	0.0239	0.0237	0.0554	0.0235	0.1698
4	12.00 (304.8)	0.0159	0.0389	0.0574	0.0760	0.0707	0.2550
5	24.00 (609.6)	0.1244	0.0820	0.1297	0.0983	0.1375	0.1311

*N.A. stands for not available due to the strain gage being damaged

Table 7.38 shows the longitudinal tensile strains for columns C3 and C5 for 3 drift ratio cycles. Table 7.39 shows the longitudinal compressive strains for columns C3 and C5 for 3 drift ratio cycles. At all drift ratio cycles column C3 exhibit larger longitudinal tensile strains at level 5 when compared to column C5. At all drift ratio cycles column C5 exhibit larger longitudinal tensile strains at level 2, level 3, and level 4 when compared to column C3 up to the three percent strain limit except at level 2 during the 4.3 percent drift ratio cycle. For the majority of locations and drift ratio cycles the longitudinal compressive strains were similar except at levels 3 and 4 at and past the 2.6 percent drift ratio

cycle where column C3 exhibited larger compressive strains compared to column C5.

Table 7.38: Summary of maximum longitudinal tensile steel strains of columns C3 and C5

Level	Elevation inch (mm)	0.017 Drift ratio cycle		0.035 Drift ratio cycle		0.052Drift ratio cycle	
		C3 max % strain	C5 max % strain	C3 max % strain	C5 max % strain	C3 max % strain	C5 max % strain
1	-12.00 (-304.8)	0.22	0.28	0.26	0.97	0.30	1.44
2	0.00 (0.00)	1.21	1.30	2.05	2.08	3.00	3.00
3	6.00 (152)	1.01	1.26	1.61	2.08	2.24	3.00
4	12.00 (304.8)	0.72	1.06	1.73	1.80	2.82	2.93
5	24.00 (609.6)	0.52	0.29	1.29	0.93	1.97	1.42

Table 7.39: Summary of maximum longitudinal compressive steel strains of columns C3 and C5

Level	Elevation inch (mm)	0.017 Drift ratio cycle		0.035 Drift ratio cycle		0.052Drift ratio cycle	
		C3 max % strain	C5 max % strain	C3 max % strain	C5 max % strain	C3 max % strain	C5 max % strain
1	-12.00 (-304.8)	-0.05	-0.10	-0.08	-0.10	-0.11	0.14**
2	0.00 (0.00)	-0.17	-0.40	-0.14	-0.87	N.A.*	N.A.*
3	6.00 (152)	-0.23	-0.39	-0.77	-0.66	-1.29	N.A.*
4	12.00 (304.8)	-0.22	-0.18	-0.39	-0.20	-0.51	0.15**
5	24.00 (609.6)	-0.11	-0.11	-0.11	-0.13	-0.05	-0.08

*N.A. equals not available because the strain gage had reached its 3 percent maximum tensile strain limit

**The data shows the strain gage never went into compression

7.4.1.4 Column Curvature

Table 7.40 shows the curvature for 3 of the larger drift ratio cycles of columns C3 and C5. Column C5 exhibited larger curvature values at the base of the

column, level 1, for all the drift ratio cycles except the final cycle where column C5 failed prior to reaching the first peak when compared to column C3. However column C3 exhibited larger curvature values at all other instrumentation levels at all drift ratio cycles when compared to column C5.

Table 7.40: Summary of column C3 and C5 curvature

Level	Approx. elevation inch (mm)	0.017 Drift ratio cycle		0.035 Drift ratio cycle		0.052Drift ratio cycle	
		C3 max normalized curvature	C5 max normalized curvature	C3 max normalized curvature	C5 max normalized curvature	C3 max normalized curvature	C5 max normalized curvature
1	3.00 (76)	0.025	0.043	0.072	0.101	0.101	0.150
2	9.00 (229)	0.009	0.007	0.030	0.015	0.055	0.012
3	18.00 (457)	0.003	0.001	0.012	0.005	0.021	0.010

7.4.1.5 Column Forces

The same calculations were performed to remove the geometry effects of the applied axial load that was discussed in section 7.2.1.5. Table 7.41 shows the maximum applied force, shear force and moment demands for both columns. The differences in maximum applied force and shear force between columns C3 and C5 is expected since the applied force of column C5 was approximately twice the value of column C3. It is also seen in the table that both columns have identical nominal and expected moment capacities which is expected since they have identical cross-sections.

Both columns have a computed overstrength value of 1.36. This suggests that for columns constructed with Grade 60 reinforcement the moment-shear span ratio does not affect the overstrength factor. The percent differences in associated plastic shear and column shear force capacity between columns C3 and C5 are similar suggesting that the change in moment-shear span ratio does not affect the prediction of the shear force of columns constructed with Grade 60 reinforcement.

Table 7.41: Summary of force and moment capacities of columns C3 and C5

Column	Maximum applied force kip (kN)	Column shear force kip (kN)	Associated plastic shear kip (kN)	Nominal moment capacity (Response 2000) kip-ft (kN-m)	Tested moment capacity kip-ft (kN-m)	Expected moment capacity kip-ft (kN-m)
C3	52.0 (231)	47.9 (213)	54.0 (240)	463 (628)	631 (856)	649 (880)
C5	103.9 (462.2)	100.4 (446.6)	108.1 (480.8)	463 (628)	629 (853)	649 (879)
% Diff.	66.58	70.80	66.75	0.00	0.32	0.00

Figure 7.28 shows the applied force versus drift ratio of columns C3 and C5 up to the first longitudinal reinforcing bar fracture. It can be seen from this figure that column C5 has a much greater applied force, but exhibited smaller maximum drift ratios compared to column C3. Figure 7.29 shows a plot of the shear force versus drift ratio of columns C3 and C5. The conclusion of this figure is the same as for previous figure.

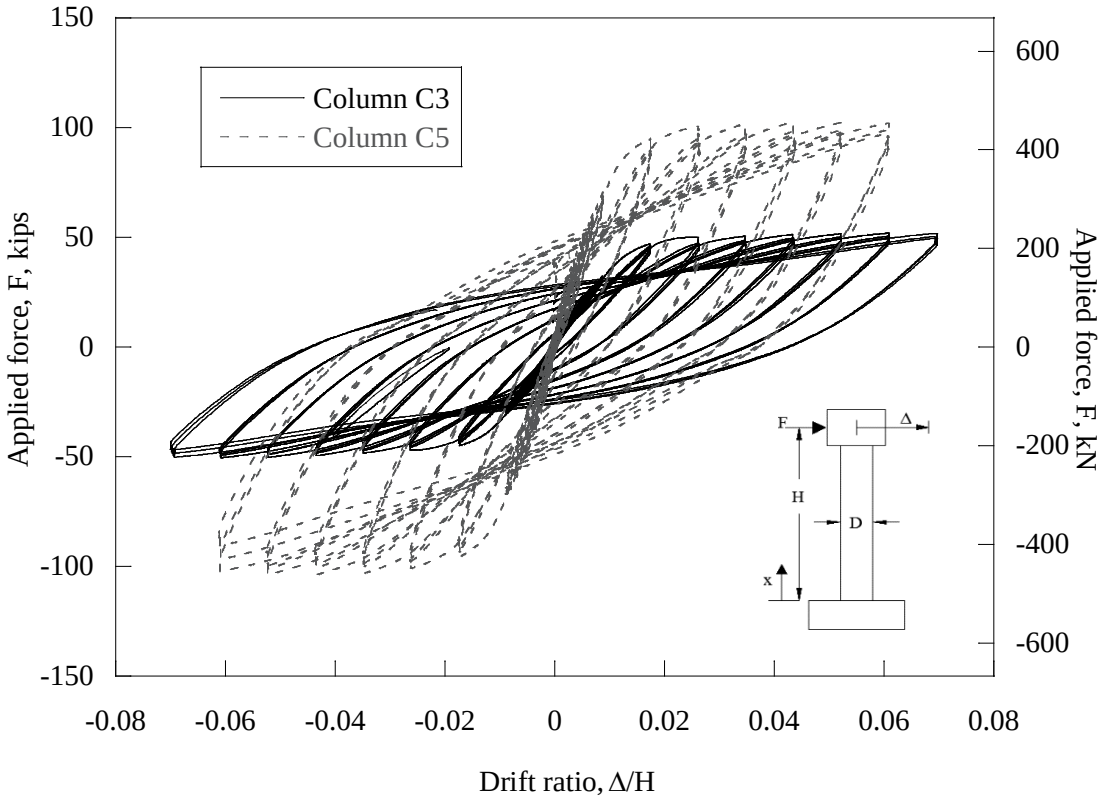

Figure 7.28: Drift ratio versus applied force of columns C3 and C5

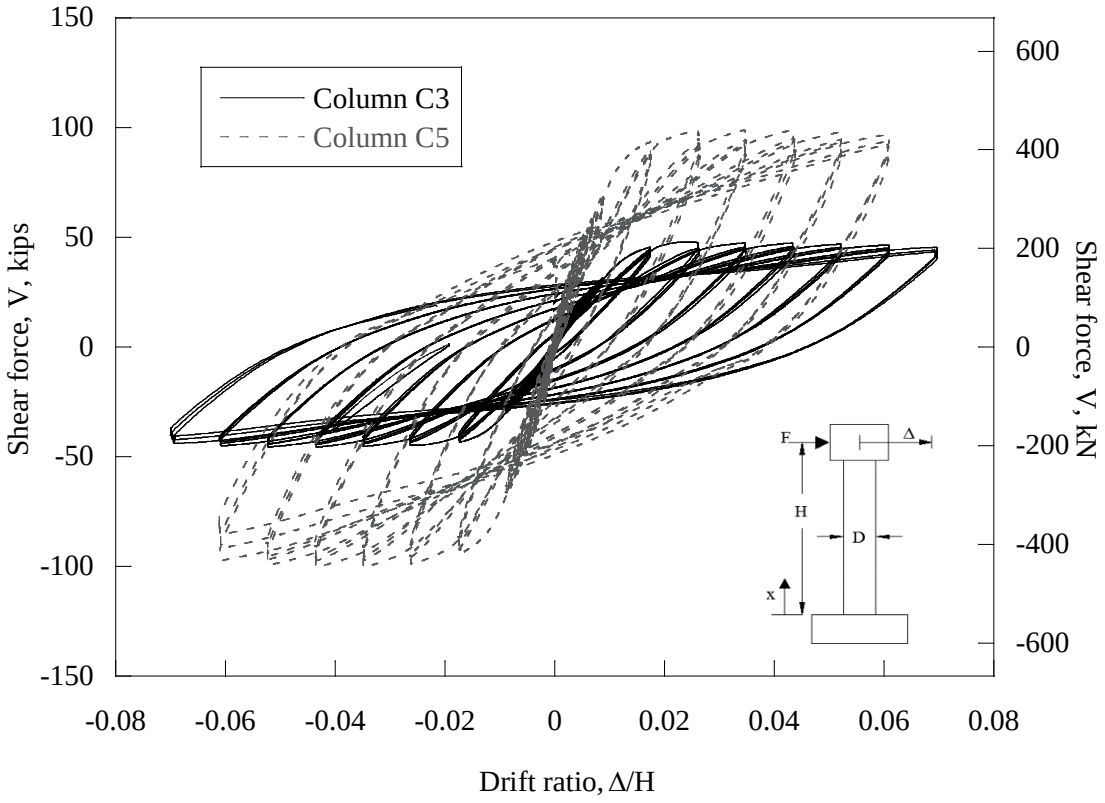

Figure 7.29: Drift ratio versus shear force of columns C3 and C5

7.4.1.6 Hysteretic Energy Dissipation

As shown in Figure 7.30, column C5 exhibited greater hysteretic energy dissipation when compared to column C3 prior to the failure drift ratio cycle. This is due to the greater force capacity of column C5 resulting in a greater area within the hysteretic loops. The results suggest that as the moment-shear span ratio is reduced for columns constructed with Grade 60 reinforcement the hysteretic energy dissipation capacity after the column has yielded and prior to the failure drift ratio cycle is increased. Table 7.42 shows the total hysteretic energy dissipated up to the first reinforcing bar fracture, first yield and reference yield. It can be seen in this table that column C3 dissipated more hysteretic energy at the first yield and column failure when compared to column C5. Column C5 dissipated more hysteretic energy at the reference yield when compared to column C6. It should be noted that first yield and the reference yield occur early in the testing process. It should also be noted that column C5 did not reach a single peak of the 6.9 percent drift ratio cycle resulting in a very small increase in dissipated hysteretic energy from the previous cycle.

As previously noted hysteretic energy dissipation is not a primary parameter used in design, however it becomes an important parameter when predicting the performance of structures and also when modeling structures to collapse. It should be noted that most codes do not require a minimum energy dissipation value.

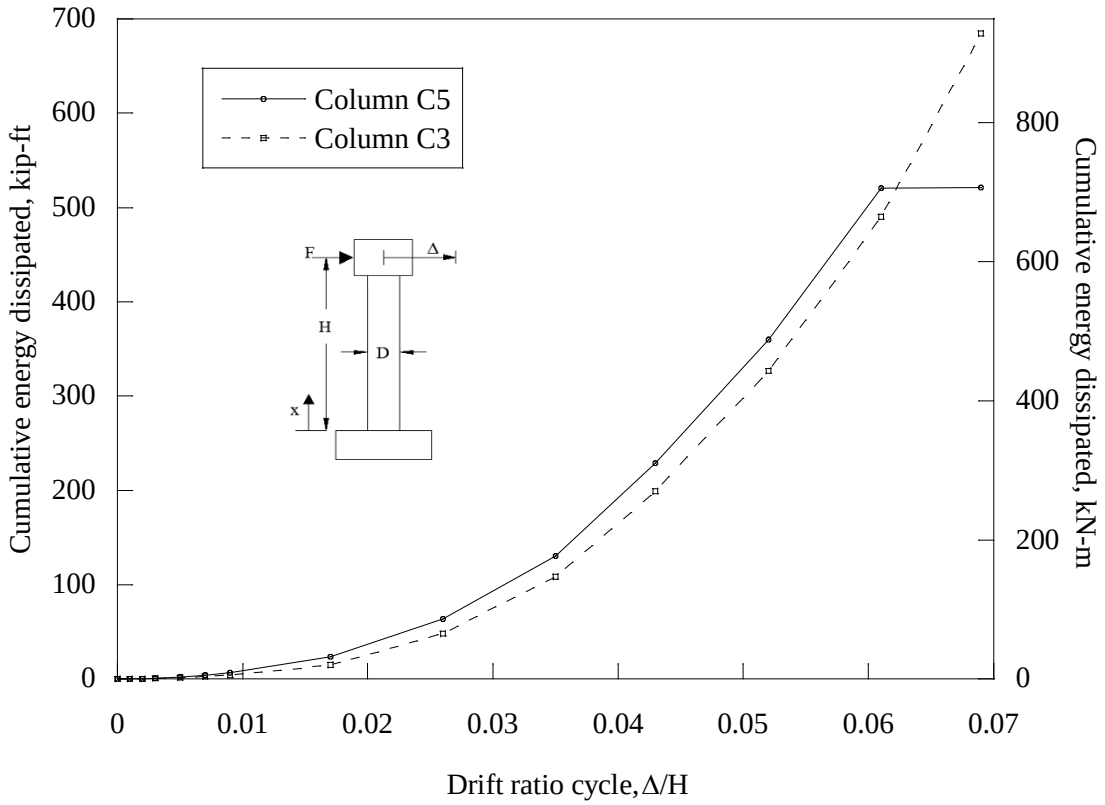

Figure 7.30: Energy dissipation of columns C3 and C5

Table 7.42: Energy dissipation of columns C3 and C5

	Column C3	Column C5	Percent difference
Energy dissipated at first yield, kip-ft (kN-m)	6.43 (8.72)	4.37 (5.92)	38.15
Energy dissipated at reference yield, kip-ft (kN-m)	9.01 (12.2)	10.39 (14.09)	14.23
Total energy dissipated, kip-ft (kN-m)	684.24 (927.71)	521.22 (706.68)	27.05

7.4.1.7 Column Ductility

Table 7.43 summarizes the displacement and curvature ductility values of columns C3 and C5. The results indicate that when using both the reference yield and first yield criteria, the displacement ductility values are larger for column C5 when compared to column C3. This suggests for columns constructed with Grade 60 reinforcement a decrease in the moment-shear span ratio results in an increase in displacement ductility. Column C5 also exhibited a larger curvature ductility value at the base of the column, level 1, compared to column C3. However column C3 exhibited larger curvature ductility values at levels two and three when compared to column C5. Note that at instrumentation levels two and three the curvature ductility values are a result of only flexural deformations whereas at the base of the column, level one, the curvature ductility value is also effected by strain penetration effects. This may suggest that a reduction in the moment-shear span ratio of columns constructed with Grade 60 reinforcement reduces the curvature ductility resulting from only flexural deformations but increases the curvature ductility resulting from the contributions of strain penetration as well as flexural deformations.

Table 7.43: Summary of Ductility values of columns C3 and C5

	Displacement ductility, μ_Δ		**Curvature ductility, μ_ψ**		
	Reference yield	**First yield**	**Level 1**	**Level 2**	**Level 3**
Column C3	4.58	7.00	20.89	19.16	6.63
Column C5	4.93	8.88	33.31	7.14	4.46
% Difference	7.36	23.68	45.83	91.41	39.13%

7.4.2 Column C4 and Column C6

Columns C4 and C6 have identical longitudinal and transverse reinforcement. Column C4 has a moment-shear span ratio equal 6 and column C6 has a moment-shear span ratio equal 3. The goal of this section is to compare the effect of the moment-shear span ratio of columns constructed with Grade 80 reinforcement (columns C4 and C6) against columns constructed with Grade 60 reinforcement (columns C3 and C5). Note that the magnitudes of the displacement cycles are different for columns C4 and C6, however the drift ratios at each cycle are identical for the two columns. The time per cycle is also identical.

7.4.2.1 Visual Observations

Columns C4 and C6 exhibited different crack distributions. Column C4 only exhibited cracking over three fourths of the height of the column. The cracks in column C4 were predominately flexural and then progressed into shear cracks at larger displacements. Column C6 exhibited cracking over nearly the entire height of the column. The cracks in column C6 started off as flexural but shortly after shear cracks were the predominant mode of cracking and were seen along

the entire height of the column. The difference in cracking between columns C4 and C6 was similar to the difference between columns C3 and C5. This suggests that the moment-shear span ratio affects the cracking of the columns constructed with Grade 60 or Grade 80 reinforcement similarly. Figure 7.31 shows a side-by-side comparison of the cracking of columns C4 and C6. Note that these photographs were not taken at the same drift ratio cycle.

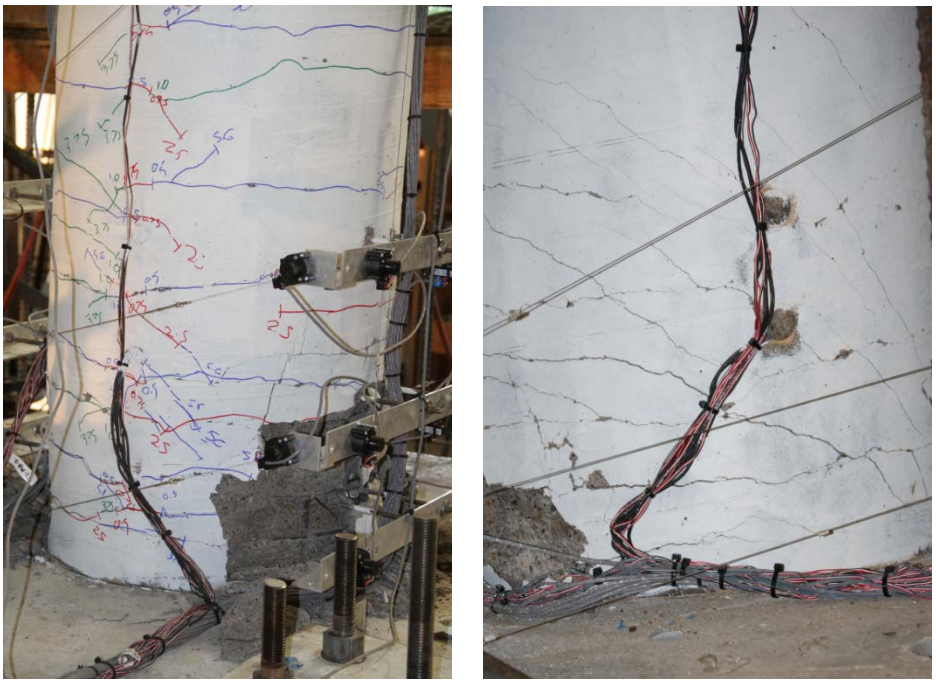

Figure 7.31: Photographs of columns C4 (left) and C6 (right) cracking

Columns C4 and C6 exhibited the onset of concrete spalling at the same drift ratio cycle (2.6 percent). Column C4 exhibited concrete spalling one drift ratio cycle past the cycle when the onset of spalling occurred whereas column C6 exhibited the onset of spalling and spalling on the same drift ratio cycle. This was the same result as column C3 and C5. This suggests that the moment-shear span ratio affects concrete spalling of columns constructed with Grade 60 or Grade 80 reinforcement similarly. The mode of failure of both columns was flexural due to reinforcing bar buckling followed by tension fracture of the reinforcement. The first longitudinal reinforcing bar to buckle in column C4 occurred at approximately 3 inches (76.2 mm) further from the base of the column when compared with column C6. The first reinforcing bar that fracture in both columns occurred 5 inches (127 mm) from the base of the column. Column C4 first reinforcing bar fractured on the 6.9 percent drift ratio cycle whereas column C6 failed one drift cycle prior on the 6.1 percent drift ratio cycle. The first reinforcing bar to fracture in column C4 occurred approaching the fourth peak of the 6.9 percent drift ratio cycle. The first bar to fracture in column C6 occurred approaching the third peak of the 6.1 percent drift cycle

ratio. Column C4 was able to hit a total of six more peaks (3 cycles) compared to C6, which was the same result between columns C3 and C5. This suggests that the moment-shear span ratio affects the lateral cyclic capacity of constructed with Grade 60 or Grade 80 reinforcement similarly.

7.4.2.2 Maximum Lateral Displacement

Lateral displacements along the height of the column were recorded for columns C4 and C6. Figure 7.32 shows the normalized elevation versus the drift ratio for the 1.7 percent, 3.5 percent, 5.2 percent, and 6.9 percent drift ratio cycles. Note column C6 did reach the 6.1 percent drift ratio cycle prior to failure but is not shown in the figure for clarity. Column C4 reach a maximum tip (roof) drift ratio of 6.9 percent whereas column C6 only reached a maximum roof drift ratio of 6.1 percent. This was the same result for columns C3 and C5. This suggests that the moment-shear span ratio affects the maximum tip (roof) drift ratio of columns constructed with Grade 60 or Grade 80 similarly.

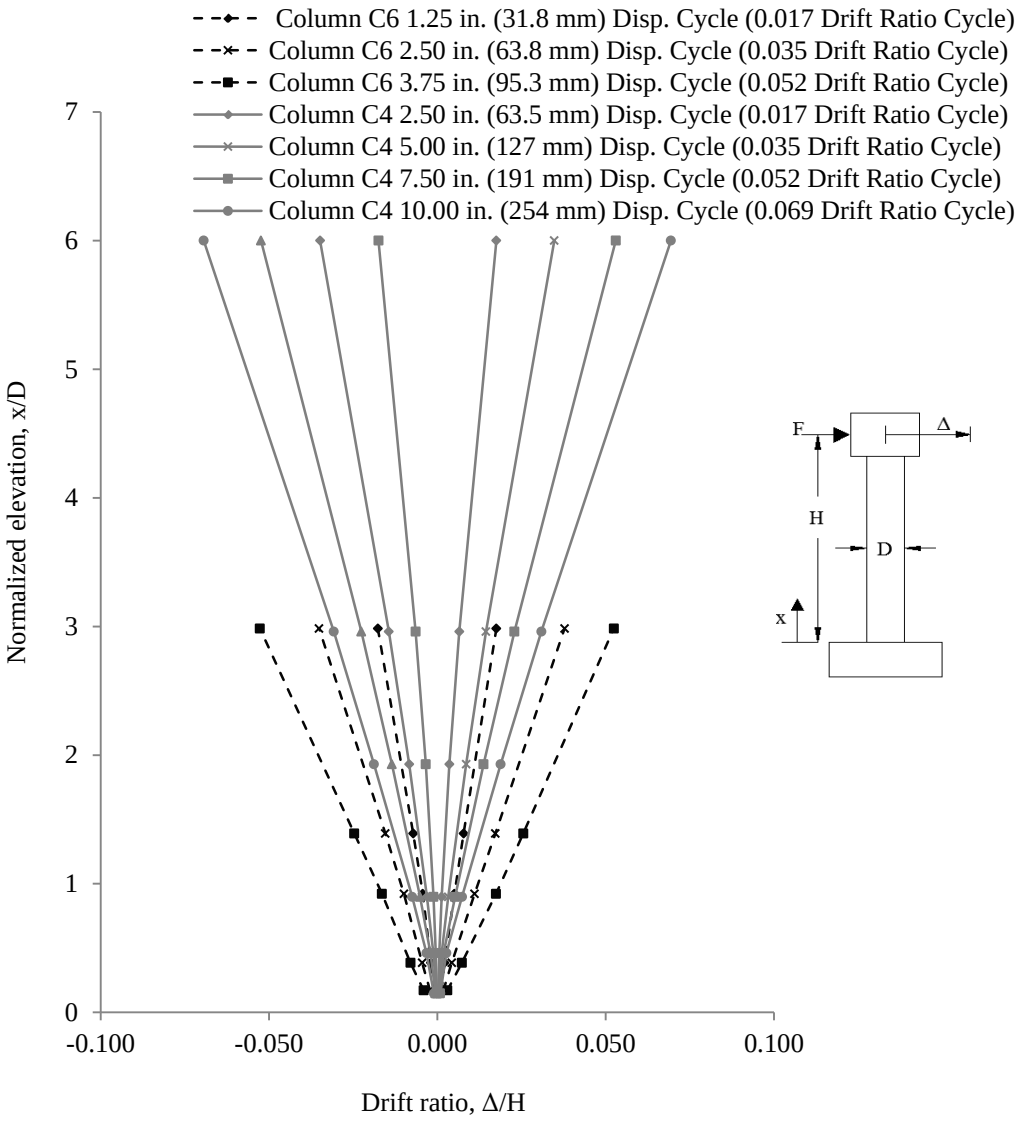

Figure 7.32: Normalized elevation versus drift ratio of columns C4 and C6

As seen in Figure 7.32 the drift ratios along the normalized elevation of the column are larger for column C6 when compared to column C4. This is the same result for columns C3 and C6. The data indicates that a reduction in moment-shear span ratio may result in larger lateral drifts at comparable drift ratio cycles for columns constructed with Grade 60 or Grade 80 reinforcement.

7.4.2.3 Steel Reinforcement Strains

Columns C4 and C6 had strain gages at similar locations up to level 5 to compare the strains in the reinforcement. The longitudinal reinforcing bars in column C4 yielded during the 1.7 percent drift ratio cycle at the base of the

column, level 2. The longitudinal reinforcing bars in column C6 yielded during the 0.7 percent drift ratio cycle at level 3. Column C4 was able to complete 2 more drift ratio cycles prior to yielding when compared to column C6. This result was identical to difference between columns C3 and C5. This suggests that a decrease in the moment-shear span ratio causes the longitudinal reinforcing bars to yield earlier for columns constructed with Grade 60 or Grade 80 reinforcement.

The longitudinal reinforcement in column C6 yielded in the footing (level 1) on the 0.7 percent drift ratio cycle and the longitudinal steel in column C4 never yielded in the footing (level 1). The data indicates that the contribution of strain penetration is not as important for column C4 when compared to column C6. This was not the same case for columns C3 and C5. This may suggest that the effect of the moment-shear span ratio on strain penetration for columns constructed with Grade 60 or Grade 80 reinforcement is different.

Table 7.44 shows the transverse reinforcement strains for columns C4 and C6 for 3 drift ratio cycles. Column C4 transverse reinforcement yielded during the 6.9 percent drift ratio cycle at level 3. Column C6 transverse reinforcement also yielded at level 3 but earlier during the 6.1 percent drift ratio cycle. Column C6 exhibited larger transverse strains at the base of the column, level 2, for all drift ratio cycles compared to column C4. At and past the 2.6 percent drift ratio cycle column C6 exhibited larger transverse strains at levels 2 through 4 compared to column C4. The results are similar to columns C3 and C5; however the trends were slightly different. Future research is needed to determine if the moment-shear span ratio affects the transverse strains of columns constructed with Grade 60 or Grade 80 reinforcement differently or similarly.

Table 7.44 Summary of maximum transverse reinforcement strains of columns C4 and C6

Level	Elevation inch (mm)	0.017 Drift ratio cycle		0.035 Drift ratio cycle		0.052 Drift ratio cycle	
		C4 max % strain	C6 max % strain	C4 max % strain	C6 max % strain	C4 max % strain	C6 max % strain
1	-12.00 (-304.8)	0.0262	0.0056	0.0452	0.0094	0.0539	N.A.*
2	0.00 (0.00)	0.0175	0.0240	0.0240	0.0311	0.0111	N.A.*
3	6.00 (152)	0.0194	0.0236	0.0664	0.1124	0.2244	0.3255
4	12.00 (304.8)	0.0116	0.0480	0.0375	0.0971	0.0672	0.1692
5	24.00 (609.6)	0.0198	0.0171	0.0236	0.0297	0.0325	0.0371

*N.A. stands for not available due to the strain gage being damaged

Table 7.45 shows the longitudinal tensile strains for columns C4 and C6 for 3 drift ratio cycles. Table 7.46 shows the longitudinal compressive strains for columns C4 and C6 for 3 drift ratio cycles. Column C6 exhibited larger longitudinal tensile strains at all levels other than level 5 compared to column C4. Column C4 exhibited larger longitudinal tensile strains at level 5 at and past the 1.7 percent drift ratio cycle compared to column C6. These results were very similar to columns C3 and C5. This suggests that the moment-shear span ratio affects the longitudinal tensile strains of columns constructed with Grade 60 or Grade 80 reinforcement similarly. For the majority of locations and displacement cycles the longitudinal compressive strains were similar for both columns except at and past the 2.6 percent drift ratio cycle at level 4, where column C6 exhibited larger compressive strains compared to column C4. This was similar to columns C3 and C5. This suggests that the moment-shear span ratio affects the longitudinal compressive strains of columns constructed with Grade 60 or Grade 80 reinforcement similarly.

Table 7.45: Summary of maximum longitudinal tensile reinforcement strains of columns C5 and C6

Level	Elevation inch (mm)	0.017 Drift ratio cycle		0.035 Drift ratio cycle		0.052 Drift ratio cycle	
		C4 max % strain	C6 max % strain	C4 max % strain	C6 max % strain	C4 max % strain	C6 max % strain
1	-12.00 (-304.8)	0.03	0.29	0.05	0.35	0.05	0.58
2	0.00 (0.00)	1.35	1.69	2.38	2.54	3.00	3.00
3	6.00 (152)	1.28	1.87	1.73	3.00	2.59	3.00
4	12.00 (304.8)	0.95	1.23	1.57	2.13	2.34	3.00
5	24.00 (609.6)	0.50	0.33	1.11	0.93	1.61	1.43

Table 7.46: Summary of maximum longitudinal compressive reinforcement strains of columns C5 and C6

Level	Elevation inch (mm)	0.017 Drift ratio cycle		0.035 Drift ratio cycle		0.052 Drift ratio cycle	
		C4 max % strain	C6 max % strain	C4 max % strain	C6 max % strain	C4 max % strain	C6 max % strain
1	-12.00 (-304.8)	-0.06	-0.13	-0.10	-0.18	-0.14	-0.27
2	0.00 (0.00)	-0.17	-0.21	-0.33	-0.46	N.A.*	N.A.*
3	6.00 (152)	-0.18	-0.24	-0.47	N.A.*	-0.81	N.A.*
4	12.00 (304.8)	-0.18	-0.18	-0.30	-0.14	-0.40	N.A.*
5	24.00 (609.6)	-0.14	-0.12	-0.17	-0.16	-0.13	0.01**

*N.A. equals not available because the strain gage had reached its 3 percent maximum tensile strain limit

**The data shows the strain gage never went into compression

7.4.2.4 Column Curvature

Table 7.47 shows the normalized curvature values for 3 of the larger drift ratio cycles for columns C4 and C6. The curvature values of column C6 were larger at the base of the column when compared to column C4. However, the curvature at all other levels were larger in column C4 when compared to column C6. This was the same result for columns C3 and C5. This suggests that a decrease in the moment-shear span ratio decreases the curvature ductility caused by only flexural deformations and increases the curvature ductility at the base of the column which is affected by strain penetration as well as flexural deformations for columns constructed with Grade 60 or Grade 80 reinforcement. Note that this may also be due to an increase in shear deformations.

Table 7.47: Summary normalized curvature values of columns C4 and C6

Level	Approx. elevation inch (mm)	0.017 Drift ratio cycle		0.035 Drift ratio cycle		0.052 Drift ratio cycle	
		C4 max normalized curvature	C6 max normalized curvature	C4 max normalized curvature	C6 max normalized curvature	C4 max normalized curvature	C6 max normalized curvature
1	3.00 (76)	0.023	0.048	0.061	0.114	0.098	0.177
2	9.00 (229)	0.008	0.005	0.029	0.011	0.049	0.020
3	18.00 (457)	0.005	0.002	0.010	0.005	0.024	0.007

7.4.2.5 Column Forces

The same calculations were performed to remove the geometry effects of the applied axial load that was discussed in section 7.2.1.5. Table 7.48 shows the maximum applied force, shear force and moment demands for columns C4 and C6. Both columns have identical moment capacities since they have identical cross-sections. The difference in maximum applied force and shear force is expected due to the test heights of the columns being different by a factor of two.

Both columns have a computed overstrength factor of 1.28. As with columns C3 and C5 the change in moment-shear span ratio showed no effect on the overstrength factor used to predict the moment capacity in this research. This suggests that for columns constructed with Grade 60 or Grade 80 reinforcement the moment-shear span ratio has no effect on the computed overstrength factor. The percent differences in maximum applied force and shear force between columns C4 and C6 were similar to the percent differences between columns C3 and C5. This suggests that the moment-shear span ratio does not affect the prediction of the shear force of columns constructed with Grade 60 or Grade 80 reinforcement. However it should be noted that these columns were very well detailed for confinement and shear forces were not an issue. It does not suggest that shear would not be an issue for columns with larger moment capacities. Future testing of columns with larger reinforcement ratios (i.e. 3 percent and 4 percent) is needed to confirm this.

Table 7.48: Summary of force and moment capacity of columns C4 and C6

Column	Maximum applied force kip (kN)	Column shear force kip (kN)	Associated plastic shear kip (kN)	Nominal moment capacity (Response 2000) kip-ft (kN-m)	Tested moment capacity kip-ft (kN-m)	Expected moment capacity kip-ft (kN-m)
C4	46.9 (209)	43.1 (192)	52.3 (233)	448 (607)	572 (776)	628 (851)
C6	95.0 (422.6)	92.0 (409.2)	104.6 (465.3)	448 (608)	575 (780)	628 (851)
% Diff.	67.58	72.39	66.67	0.00	0.52	0.00

Figure 7.33 shows the applied force versus drift ratio for columns C4 and C6 up to the first longitudinal reinforcing bar fracture. It can be seen in the figure that column C6 has a much greater applied force capacity compared to column C4. However, column C4 was able to achieve larger drift ratios. Figure 7.34 shows a plot of the shear force versus drift ratio for columns C4 and C6. The conclusions

from this figure are the same as for the previous figure. The differences in both plots between columns C4 and C6 were similar to columns C3 and C5.

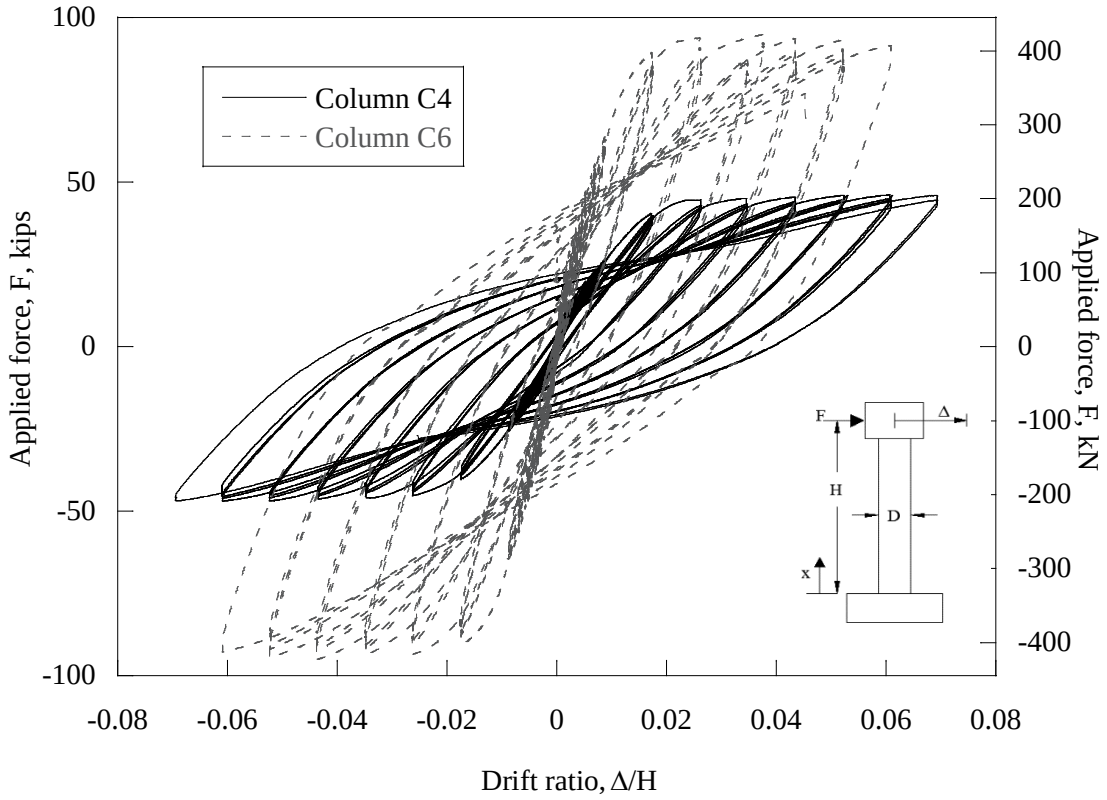

Figure 7.33: Drift ratio versus applied force of columns C4 and C6

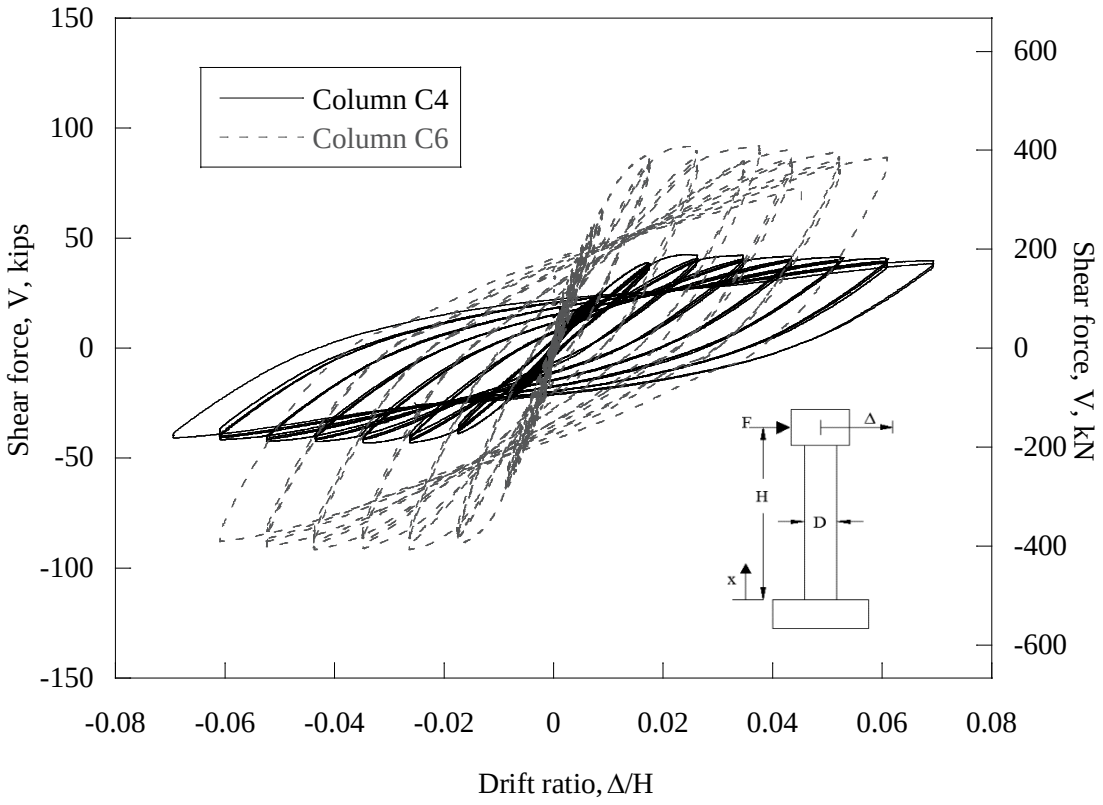

Figure 7.34: Drift ratio versus shear force of columns C4 and C6

7.4.2.6 Hysteretic Energy Dissipation

As shown in Figure 7.35, column C6 exhibited greater hysteretic energy dissipation when compared to column C4 prior to the failure of column C4. This is due to the greater force capacity of column C6 resulting in more area within the hysteretic loops. Table 7.49 shows the total hysteretic energy dissipated up to the first reinforcing bar fracture, first yield and reference yield. It can be seen in this table that column C4 dissipated more hysteretic energy at the first yield and at column failure when compared to column C6. However, Column C6 dissipated more hysteretic energy at the reference yield when compared to C4. These results were the same for columns C3 and C5. This suggests that a reduction in the moment-shear span ratio results in an increase in hysteretic energy dissipation capacity after the first yield of columns constructed with Grade 60 or Grade 80 reinforcement. However, it should be noted that the columns with a larger moment-shear span ratio (columns C3 and C4) were able to achieve larger roof drift ratios prior to failure resulting in an overall increase in hysteretic energy dissipation capacity at column failure compare to columns with a smaller moment-shear span ratio (columns C5 and C6). The increase in

hysteretic energy dissipation of the columns with smaller moment-shear span ratios may be due to the increased stiffness of the columns due to the shorter column height.

As previously noted, hysteretic energy dissipation is not a primary parameter used in design, however it becomes an important parameter when predicting the performance of structures and also when modeling structures to collapse. It should be noted that most codes do not require a minimum energy dissipation value.

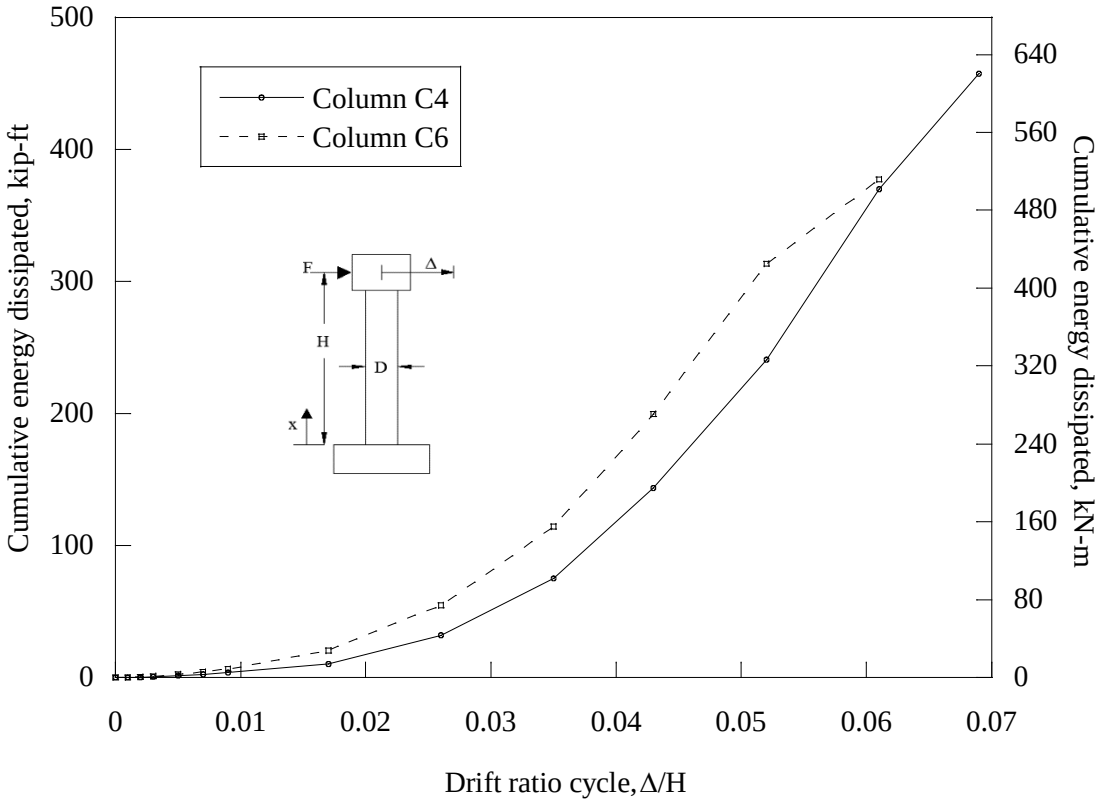

Figure 7.35: Energy dissipation of columns C4 and C6

Table 7.49: Energy dissipation of columns C4 and C6

	Column C4	Column C6	Percent difference
Energy dissipated at first yield, kip-ft (kN-m)	5.97 (8.09)	4.57 (6.20)	26.57
Energy dissipated at reference yield, kip-ft (kN-m)	8.07 (10.9)	9.66 (13.10)	17.94
Total energy dissipated, kip-ft (kN-m)	457.67 (620.52)	377.43 (511.73)	19.22

7.4.2.7 Column Ductility

Table 7.50 summarizes the displacement and curvature ductility values of columns C4 and C6. The results indicate that column C6 exhibits larger displacement ductility values when using both the first yield and reference yield criteria when compared to column C4. This was the same result with columns C3 and C5. This suggests that with a reduction in the moment-shear span ratio an increase in the displacement ductility values is expected for columns constructed with Grade 60 or Grade 80 reinforcement. Column C6 exhibited a larger curvature ductility value at the base of the column, level 1, when compared to column C4. Column C4 exhibited larger curvature ductility values at levels 2 and 3 when compared to column C6. This was the same result as from the comparison between columns C3 and C5. However, the percent differences were different between the two pairs of columns. The data indicate that moment-shear span ratio affects the curvature ductility similarly between columns constructed with Grade 60 or Grade 80 reinforcement.

Table 7.50: Summary Ductility values of columns C4 and C6

	Displacement ductility, μ_Δ		Curvature ductility, μ_ψ		
	Reference yield	First yield	Level 1	Level 2	Level 3
Column C4	4.35	6.33	23.63	10.21	5.61
Column C6	4.90	7.80	26.86	8.38	2.45
% Difference	11.89	20.81	12.79	19.69	78.41

7.5 SUMMARY

In this chapter the effects of the reinforcement grade, longitudinal reinforcement ratio, and the moment-shear span ratio were examined for columns constructed with Grade 60 reinforcement and columns constructed with Grade 80 reinforcement. To examine the effects of the reinforcement grade, the performance of all three pairs of columns were analyzed (C1 versus C2, C3 versus C4, and C5 versus C6). To examine the effect of longitudinal reinforcement ratio, the performance of columns C1 and C3 were compared to establish a baseline. The performance of columns C2 and C4 were then compared to the baseline to determine if the longitudinal reinforcement ratio has the

same affect for Grade 60 and Grade 80 reinforced concrete columns. Similarly the performance of columns C3 and C5 were analyzed to set a baseline for the effect of the moment-shear span ratio. Following this the performance of columns C4 and C6 were compared to the baseline to determine if the moment-shear span ratio has the same affect for Grade 60 and Grade 80 reinforced concrete columns.

Analyzing the data to determine the effects of reinforcement grade on column performance of the three pairs of columns showed consistent trends. The trends observed are as follows:

1. time of concrete spalling was similar between each pair of columns;

2. columns constructed with Grade 80 reinforcement exhibited equal or greater maximum drift ratios when compared to columns constructed with Grade 60 reinforcement;

3. each pair of columns exhibited very similar lateral displacements along the height of the columns;

4. for all three pairs of columns, the curvature at all levels were similar between the columns constructed with Grade 60 reinforcement and the columns constructed with Grade 80 reinforcement, except at the base of the column (level 1) between columns C1 and C2;

5. the three columns constructed with Grade 60 reinforcement all exhibited significantly larger hysteretic energy dissipation compared to the corresponding columns constructed with Grade 80 reinforcement. This is believed to be a result of the increase cross-sectional area of reinforcement in the columns constructed with Grade 60 reinforcement, resulting in stiffer columns, which increases the hysteretic energy dissipation capacity. However hysteretic energy dissipation is not a primary parameter used in design, however it becomes an important parameter when predicting the performance of structures and also when modeling structures to collapse. It should be noted that most codes do not require a minimum energy dissipation value;

6. when using the reference yield previously defined, the displacement ductility of columns constructed with Grade 60 or Grade 80 were similar;

7. for the first pair (C1 and C2) and third pair (C5 and C6) of columns the curvature ductility values closest to the base of the column (level 1) which are effected by strain penetration were larger for the columns containing Grade 60 reinforcement (C1 and C5) when compared to the columns containing Grade 80 reinforcement (C2 and C6). At the second lowest instrumentation level (level 2) the columns containing Grade 80 reinforcement (C2 and C6) exhibited larger curvature ductility values compared to the columns containing Grade 60 reinforcement (C1 and C5). However for the second pair of columns (C3 and C4) the previously described observation were opposite, and;

8. the computed overstrength factor of the columns constructed with Grade 80 reinforcement were smaller than that of the columns constructed with Grade 60 reinforcement. However, for columns C1 and C2 the value was only slightly larger (1.23 and 1.20 respectively).

Consistent trends were also observed when determining the effect of the longitudinal reinforcement ratio on column performance. Trends observed are as follows:

1. an increase in the longitudinal reinforcement ratio resulted in delaying concrete spalling and first reinforcing bar fracture in columns constructed with Grade 60 or Grade 80 reinforcement. However it should be noted that this may be due to the decrease in longitudinal reinforcing bar spacing rather than solely on the increase in the longitudinal reinforcement ratio;

2. for both grades of reinforcement the increase in longitudinal reinforcement ratio resulted in larger drift ratios prior to column failure. Again it should be noted that this may be due to the decrease in longitudinal reinforcing bar spacing rather than solely on the increase in the longitudinal reinforcement ratio;

3. the lateral drift at comparable cycles was similar between the two columns constructed with Grade 60 reinforcement and also between the two columns constructed with Grade 80 reinforcement, suggesting that the increase in the longitudinal reinforcement ratio does not affect the lateral drifts along the column height of comparable cycles;

4. for both grades of reinforcement the longitudinal reinforcement ratio did not significantly affect the curvature of the columns;

5. for both grades of reinforcement the increase in longitudinal reinforcement ratio appears to increase the computed overstrength factor;

6. the displacement and curvature ductility values were larger for the columns with larger longitudinal reinforcement ratios for both grades of reinforcement, and;

7. the hysteretic energy dissipation capacity was also larger for columns with larger longitudinal reinforcement ratios for both grades of reinforcement.

In addition to the previous two parameters examined, consistent trends were also observed when determining the effect of the moment-shear span ratio on column performance. The observed trends are as follows:

1. for both grades of reinforcement the decrease in moment-shear span ratio resulted in more shear cracks and cracking over a larger portion of the column;

2. the decrease in moment-shear span ratio resulted in a decrease in maximum roof (tip) drift ratio but increased drift ratio at lower elevations of the column for both grades of reinforcement;

3. the data indicated that a decrease in the moment-shear span ratio decreases the curvature caused by only flexural deformations and increases the curvature at the base of the column (level 1) which is also influenced by strain penetration as well as flexural deformations for columns constructed with Grade 60 or Grade 80 reinforcement;

4. for both grades of reinforcement the decrease in moment-shear span ratio resulted in the longitudinal reinforcing bars yielding sooner;

5. the moment-shear span ratio did not affect the computed overstrength factor for either grade of reinforcement;

6. the reduction in moment-shear span ratio resulted in an increase in hysteretic energy dissipation capacity after the reinforcement in the column first yielded for both grades of reinforcement. However, because the columns with larger moment-shear span ratios exhibited larger roof (tip) drift ratios prior to failure they were also able to dissipate more hysteretic energy prior to failure;

7. for both grades of reinforcement the reduction in moment-shear span ratio increased the displacement ductility values, and;

8. for both grades of reinforcement the reduction in moment-shear span ratio increased the curvature ductility closest to the base of the column (level 1) which is effected by the contributions of strain penetration. However at the other instrumentation levels which are not affected by strain penetration the reduction in moment-shear span ratio decreased the curvature ductility values.

8.0 COMPUTATIONAL MODELING

Seismic design and analysis of reinforced concrete bridges requires that columns and their models accurately capture the cyclic force and deformation demands. Accurately capturing the inelastic response of reinforced concrete elements is difficult and simplified design and analysis methods are required in practice.

The main goal of this section is to accurately predict the performance of concrete columns reinforced with A706 Grade 60 as well as concrete columns reinforced with A706 Grade 80 under lateral loading, focusing specifically on the performance in terms of strength and force-displacement response envelope. Design and analysis models of varying complexity have been developed in this study. Design methods reviewed include ODOT's BDDM plastic moment equations and overstrength factors. The analysis methods include moment-curvature analyses and nonlinear static pushover analysis. These analysis methods are validated through comparison of numerical results obtained using the Open System for Earthquake Engineering Simulation *(OpenSees 2012)* against global and local experimental results described in the previous chapters for columns C1 to C6.

OpenSees is used as the analysis software. The analyses performed include nonlinear fiber-section moment-curvature analysis and nonlinear static pushover analysis. The techniques used include nonlinear material properties and nonlinear geometry of beam-column element formulations available in the OpenSees version 2.4.3 (release r5645, 2013). OpenSees is an open source software framework used for earthquake engineering using advanced nonlinear finite element methods. It's written primarily in the object-oriented programming language C++. Because it is an open-source software, being primarily developed at UC Berkeley and Oregon State University, new components are continuously being developed to improve its modeling capabilities. One of the many benefits of OpenSees is the ability to efficiently model a structural component at the element level, section level, and fiber level allowing for use of physics-based and phenomenological nonlinear hysteretic stress-strain material models of concrete and reinforcing steel. Moreover, OpenSees has a wide community of users and its development has been supported through research projects of several State Highway Agencies, such as Caltrans, WashDOT, and ODOT, which makes it particularly attractive as an analysis tool for seismic applications. It is worth noting that other tools such as Response-2000 may be used.

8.1 PLASTIC HINGE STRENGTH

In bridge columns the maximum moments are observed at column ends, which are then transferred to the foundations or bent-caps. The current design philosophy for bridge systems is to concentrate the nonlinear behavior at the column ends, thus allowing these to form plastic hinges. These regions then have to be detailed appropriately so they

exhibit ductile flexural failures. The flexural strength of bridge column plastic hinges is given in common design standards including ODOT's BDDM *(ODOT 2012)*. All other elements connecting to the columns are designed to remain essentially elastic. Thus, for example, ODOT's Section 1.1.5.5(12), states that the moment to be transferred from the column to top of the shaft is the lesser of the overstrength plastic moment (M_{po}) of the column or the elastic moment of the shaft. Thus, for reinforced concrete members:

$$M_{po} = \lambda_{mo} M_p \tag{8.1}$$

where:

M_p is plastic moment capacity of the column

λ_{mo} is an overstrength factor taken between 1.2 and 1.4 as determined by AASHTO Article 8.5

ODOT also refers to Section 8.5 of the AASHTO Guide Specifications for LRFD Seismic Bridge Design for determination of the overstrength plastic moment. Additionally, as stated in the BDDM, plastic hinging capacity should be determined from column interaction curves with axial and moment ϕ values of 1.0, in which the unfactored dead load is considered and is entered in the interaction diagram, and the plastic moment obtained from this interaction diagram is then multiplied by 1.3 to estimate the plastic moment capacity.

8.2 MOMENT-CURVATURE ANALYSIS

8.2.1 Overview

Design standards specify methods for determining nominal and ultimate flexural strengths of elements that can develop plastic hinging. In this report, the nominal moment strength, M_n, is determined using nominal material properties, and the plastic moment capacity, M_p, is then determined by multiplying the nominal moment by an overstrength factor, λ_{mo}. Comparisons of results of moment-curvature analyses with results from the testing program were used to assess the overstrength factor, as described in Chapter 7. Table 8.1 shows the computed overstrength factors from the experimental results as well as from the cross-sectional moment-curvature analysis when using *Concrete07* for the concrete material model and *reinforcingSteel* for the steel material model in OpenSees for each column. As seen from this table the predicted overstrength factor from the OpenSees analysis over predicts moment capacity of all the columns. The analysis does agree with the experimental results in the sense that the columns reinforced with Grade 80 result in smaller computed

overstrength factors. In addition the analysis results also agree with the experimental results that the increase in longitudinal reinforcement ratio also increases the computed overstrength factor. Hence, the experimental computed overstrength factor was taken as the ratio of the tested moment capacity to the nominal moment capacity based on nominal material properties.

Table 8.1: Computed overstrength factors of all test columns

Overstrength factor	C1	C2	C3	C4	C5	C6
Experimental	1.23	1.20	1.36	1.28	1.36	1.28
Analysis	1.37	1.30	1.47	1.34	1.47	1.34
Percent difference	10.77	8.00	7.78	4.58	7.78	4.58

AASHTO Guide Specifications for LRFD Seismic Bridge Design states that the plastic moment capacity needs to be determined using a moment-curvature section analysis, taking into account the expected yield strength of the materials, the confined concrete properties, and any strain hardening effects of the longitudinal reinforcement. In this study, OpenSees was the software used to perform the moment-curvature analysis. A fiber-section model was defined to capture the cross-section moment-curvature response. The discretization of the column cross-section was selected to optimize accuracy and efficiency of the model. A large number of fibers will lead to larger accuracy, but in lieu of efficiency due to the increased computational demand. To capture the strain hardening effects, different uniaxial material models can be defined for each fiber.

8.2.2 Material Models

For the reinforcing steel models two different material models were tested:

1. the Menegotto-Pinto material model with modifications proposed by Filippou and Bertero *(Filippou and Bertero 1983)* (Steel02 in OpenSees), and;

2. the *(Kunnath et al. 2009)* material model (*ReinforcingSteel* in OpenSees).

For the concrete models, two different models were tested were:

1. the Yassin *(Yassin 1994)* model, which is based on the Kent-Scott-Park model *(Scott et al. 1982)* and includes a linear tension stiffening component (*Concrete02* in OpenSees), and;

the Chang and Mander *(Chang and Mander 1994*) model (*Concrete07* in OpenSees).

Figure 8.1 shows the response of the *Steel02* and *ReinforcingSteel* material models to an idealized cyclic strain history. From Figure 8.1, it can be observed that the *ReinforcingSteel* model allows for modeling of a yield plateau, whereas *Steel02* does not. Furthermore, the *ReinforcingSteel* model captures the increase in strength of the bars in compression, which is phenomenon that has been described in the literature (e.g. Mander, Panthaki, and Kasalanati *(Mander et al. 1994a*), Rodriguez, Botero, and Villa *(Rodriguez et al. 1999)*). For reference, a monotonic stress-strain response of a tested ASTM A706 Grade 80 #5 (#16M) reinforcing bar is also shown in this figure. From comparison of the testing curve with the numerical models, it can be seen that the *ReinforcingSteel* model predicts the stress-strain response better than the *Steel02* model. This has to do with the fact that the *ReinforcingSteel* model has a curved strain-hardening envelope which follows a yield plateau, both of which are typically observed in rebar test results, unlike the *Steel02* model which considers a linear strain hardening and does not model the yield plateau region. The *ReinforcingSteel* model is therefore used in moment-curvature and shear force-drift analysis described next.

Figure 8.2 shows results of cyclic testing for *Concrete02* and *Concrete07* concrete models. It can be observed that there are slight differences in the envelopes in tension and compression of both models. However, the main difference between the two models is observable in the loading from tension to compression strains, i.e. in the fourth quadrant of the stress-strain Cartesian plane. When unloading or loading from tension to compression strains, the stress-strain curve of the *Concrete02* model passes through the origin before it continues on to compression strains. In the *Concrete07* model the stress-strain curve does not pass through the origin, gaining compression strength at a reference positive strain. This gradual increase in compressive stresses when transitioning from positive to negative strains, with an accompanying gradual change in stiffness, is related to concrete crack closure effects. The *Concrete07* model is a more realistic model than the *Concrete02* model, which assumes that cracks close in a single step.

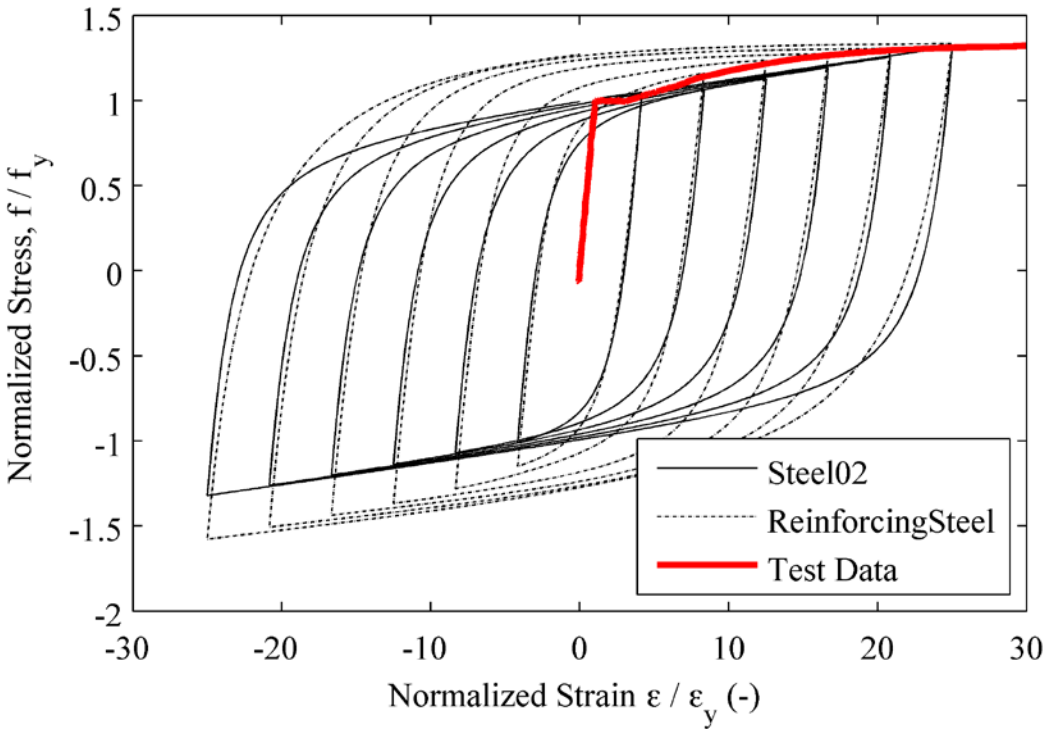

Figure 8.1: Normalized cyclic stress-strain response of *Steel02* and *ReinforcingSteel* materials, and ASTM A706 Grade 80 #5 (#16M) tension test data.

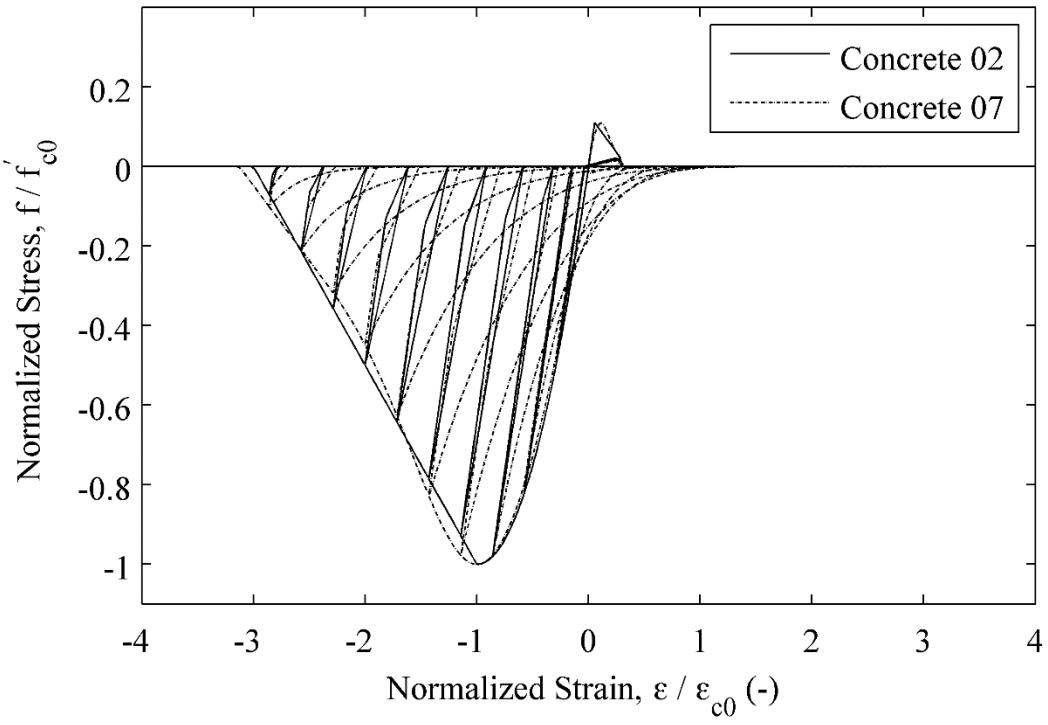

Figure 8.2: Normalized cyclic stress-strain response of Concrete02 and Concrete07 unconfined concrete material models.

8.2.3 Section Modeling

The column cross sections were discretized into fibers that represent the concrete and reinforcing steel. Figure 8.3 illustrates the discretized fiber sections of column C1 and C2. On both cross-sections, three different regions can be observed from the figure. First, a tighter mesh is defined near the outside perimeter of the column to model the unconfined concrete. The uniaxial stress-strain material model assigned to these fibers simulates the cover concrete that follows the behavior of unconfined concrete. Second, in the inner core, a stress-strain relation that accounts for increased concrete strength and increased concrete ultimate strain is used. The effect of confinement was determined based on equations provided in Mander, Priestley, and Park *(Mander et al. 1988)* and Karthik and Mander *(Karthik and Mander 2011*). Finally, the black filled circles (fibers) correspond to reinforcing steel bars, which are positioned according to their nominal position.

The discretization used for the column cross section is 32 theta divisions in the core and cover, 16 radial divisions in the core and 4 radial divisions in the cover. The number of fibers used was defined following a parametric study in which the number of fibers was increased until no significant change was observed in the moment-curvature response, thus allowing for a compromise between accuracy and computational efficiency. Note that the same discretization of the column cross section was used for columns C3, C4, C5, and C6, except for the longitudinal reinforcement. The longitudinal reinforcement was adjusted to match bar size and number of bars for each column.

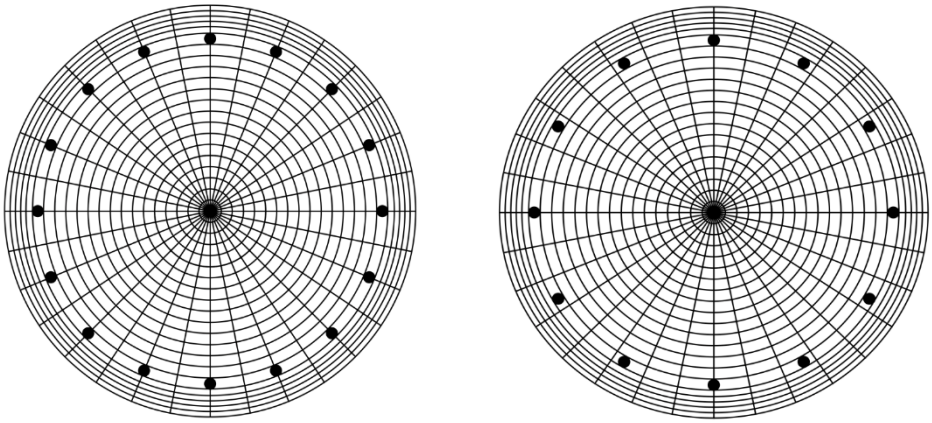

(a) **(b)**

Figure 8.3: Fiber-section for: (a) Column C1, and (b) Column C2

Figure 8.4 illustrates the normalized curvature versus normalized moment response for column C1 using the four combinations of material models from the two steel material models and the two concrete material models discussed in section 8.2.1. The moment was normalized by dividing the computed moment by the nominal moment of the column. The nominal moment capacity, M_n, was determined in Chapter 3. The curvature was normalized by dividing the computed curvature by a calculated reference yield curvature of the column. The reference yield curvature is computed following equation (3.1) defined by Priestley *(Priestley 2003)*. This yield strain used in this equation was computed as the yield strain determined by the 0.2 percent offset method shown in Chapter 4 minus 0.2 percent strain. This was the same calculation used in the reinforcement strain analysis in Chapters 5 and 6.

From Figure 8.4**,** the main observations worth highlighting are:

1. up to yield, the material models produce the same results;

2. after yield differences are observable when different steel models are used;

3. after yield differences are observable when different concrete models are used, however, these differences diminish after curvatures approximately ten times the yield curvature, and;

4. peak overstrength factors (normalized moment values), for very high curvature demands, are below 1.4.

Figure 8.5 illustrates the normalized curvature versus normalized moment response for column C2 using the four combinations of material models from the two steel material models and the two concrete material models. The moment and curvature were normalized following the procedure stated for column C1. All the main observations

that were made for column C1, made by inspecting Figure 8.4, are applicable for the plot shown in Figure 8.5.

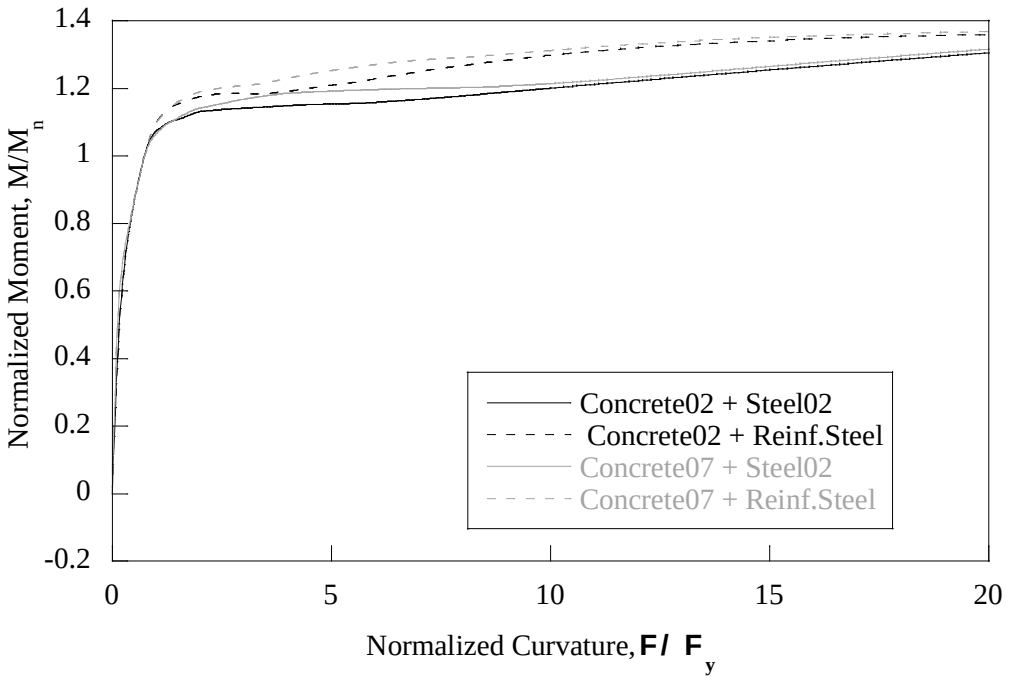

Figure 8.4: Moment-curvature response of column C1

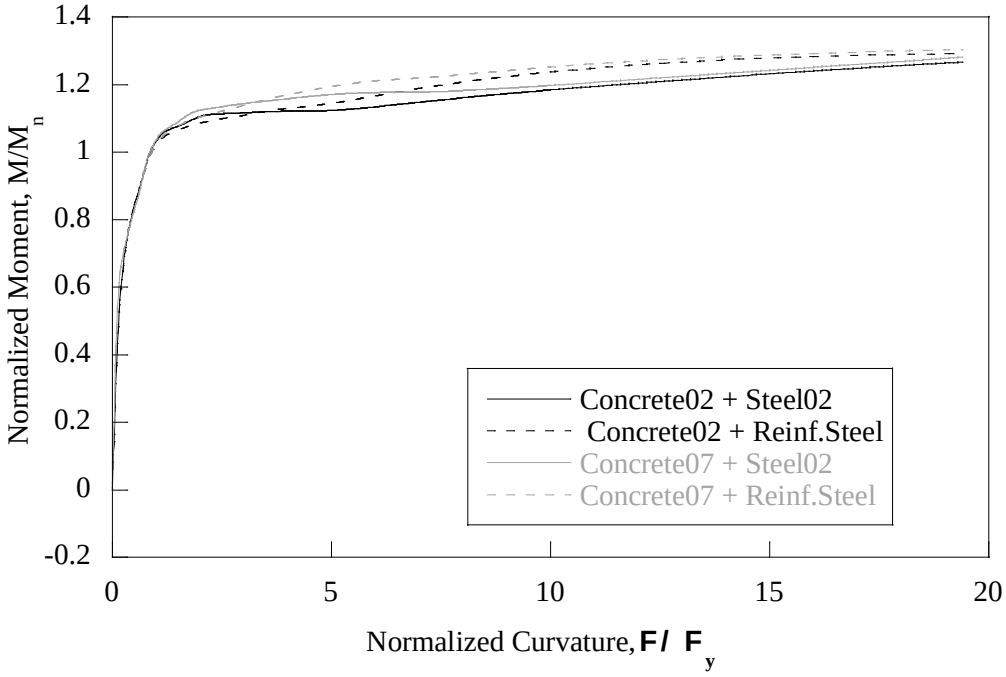

Figure 8.5: Moment-curvature response of column C2

Figure 8.6 shows the responses for columns C1 and C2 using the *Concrete07* concrete material model and the *ReinforcingSteel* steel material model. From these figures it can be seen that:

1. even though the nominal moment capacity is similar for column C1 and C2, the value of the moment at reference yield is larger for the column C1 than for column C2. This is due to the fact that the ratio of the actual yield strength to the nominal yield strength of the Grade 60 reinforcing steel is larger than the Grade 80 reinforcing steel, and;

2. after yielding column C1 exhibits larger strengths than column C2. This is due to the fact that the longitudinal Grade 60 reinforcing steel exhibits larger ratios of ultimate to yield strength than the Grade 80 reinforcing steel.

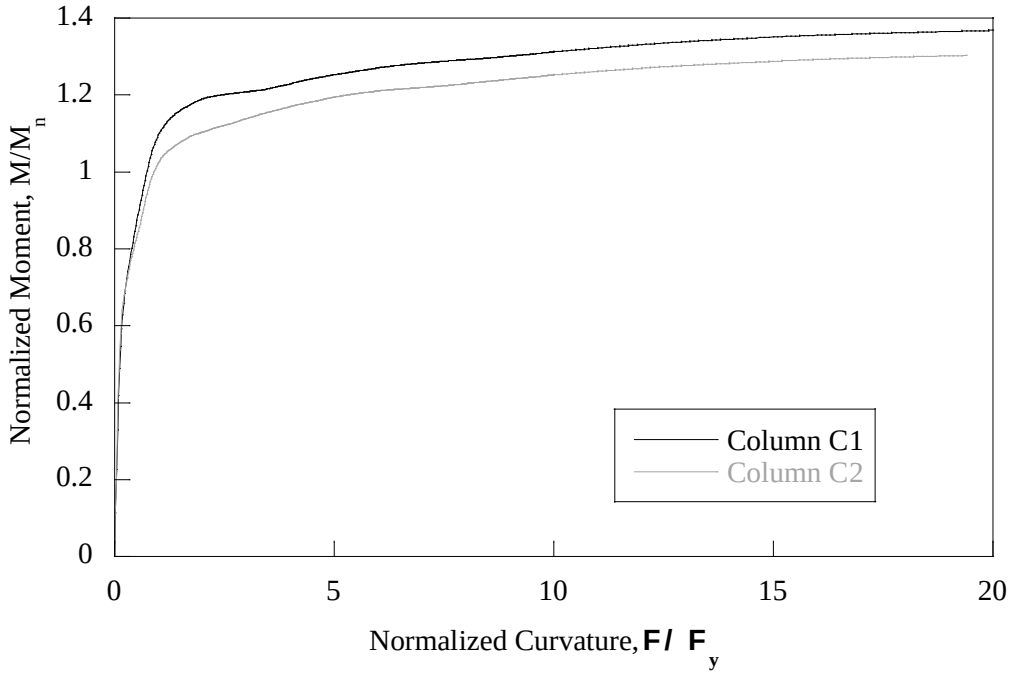

Figure 8.6: Moment-curvature response of columns C1 and C2 using *Concrete07* and *ReinforcingSteel*

Figure 8.7 illustrates the normalized curvature versus normalized moment response for column C3/C5 using the four combinations of material models from the two steel material models and the two concrete material models. Note that this figure represents both columns C3 and C5 because they have identical cross-sections in terms of outer dimensions and reinforcement ratios. The moment and curvature were normalized following the procedure stated for column C1. Main observations worth highlighting are:

1. up to yield, the material models produce the very similar results;

2. when *Steel02* is used, the ultimate moment capacity of the columns is the same for either concrete material model. However when *ReinforcingSteel* is used, results obtained using the two different concrete material models yield different peak strengths;

3. after yield large differences are observable when different steel models are used;

4. after yield differences are observable when different concrete models are used;

5. when *Concrete07* and *ReinforcingSteel* are used peak overstrength factors (normalized moment values), for very high curvature demands are larger than 1.4, and;

6. peak overstrength factors (normalized moment values), for very high curvature demands are larger than those observed for columns C1.

Figure 8.8 illustrates the normalized curvature versus normalized moment response for column C4/C6 using the four combinations of material models from the two steel material models and the two concrete material models. Note that the figure represents both columns C4 and C6 because they have identical cross sections. The moment and curvature were normalized following the procedure stated for column C1. Main observations worth highlighting are:

1. up to yield, the material models produce the very similar results;

2. after yield differences are observable when different steel models are used;

3. after yield differences are observable when different concrete models are used, however, these differences were smaller compared to the differences seen between the two steel models, and;

4. peak overstrength factors (normalized moment values), for very high curvature demands, are below 1.4.

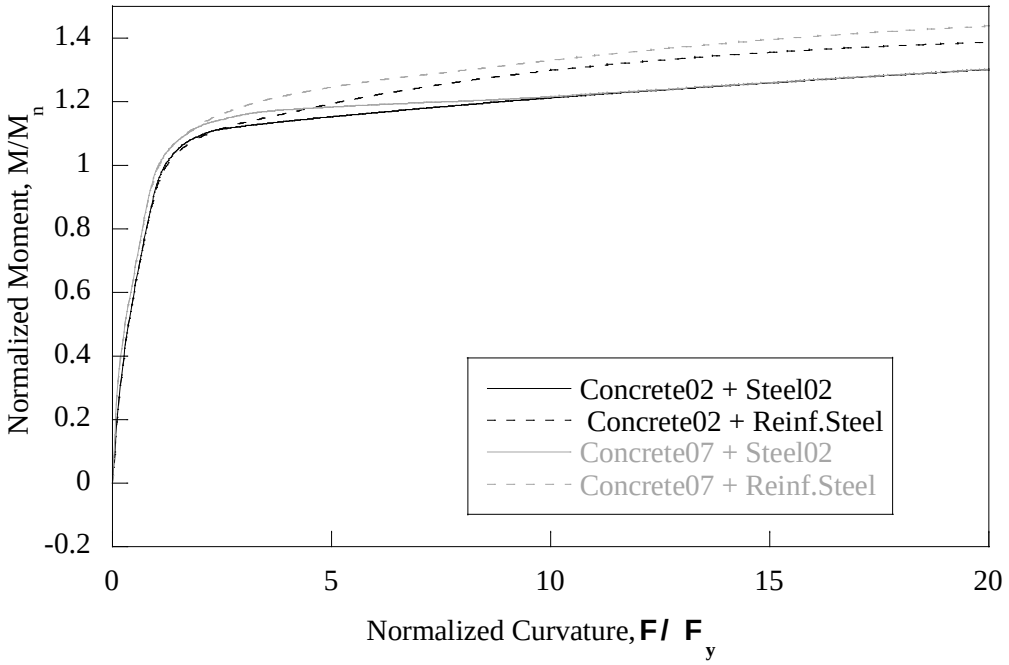

Figure 8.7: Moment-curvature response of Column C3/C5

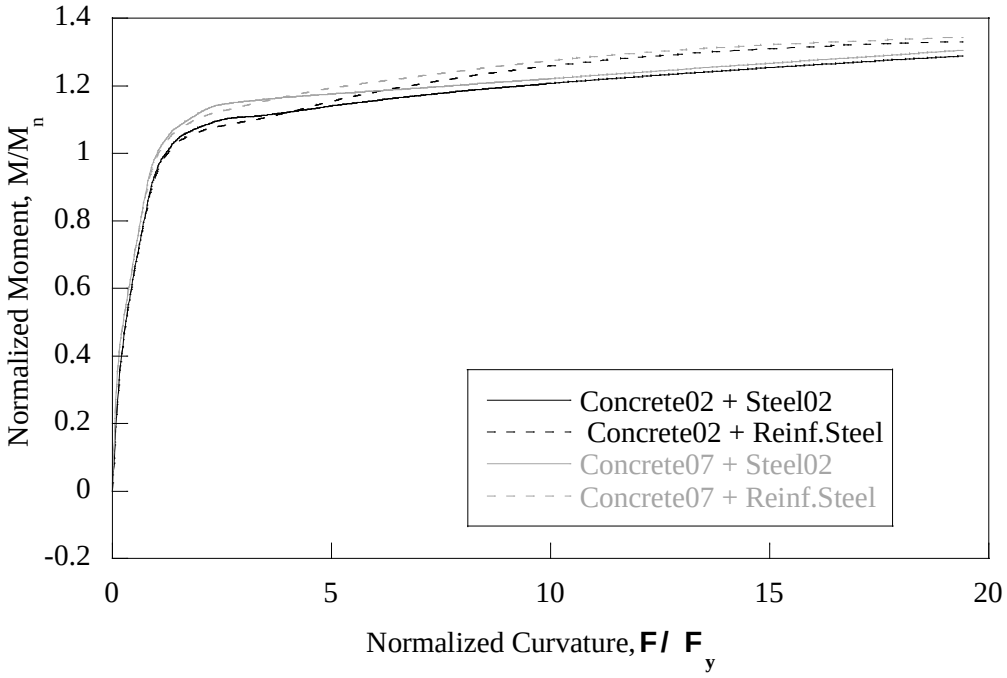

Figure 8.8: Moment-curvature response of Column C4/C6

Figure 8.9 shows the responses for columns C3/C5 and C4/C6 using the *Concrete07* concrete material model and the *ReinforcingSteel* steel material model. Note that the nominal moment capacities between the two columns were not as similar for columns C1 and C2. From these figures it can be seen that columns C3/C5 reinforced with Grade 60 have a larger overstrength factor compared to columns C4/C6 reinforced with Grade 80, which is a confirmation of what was observed in the experimental testing.

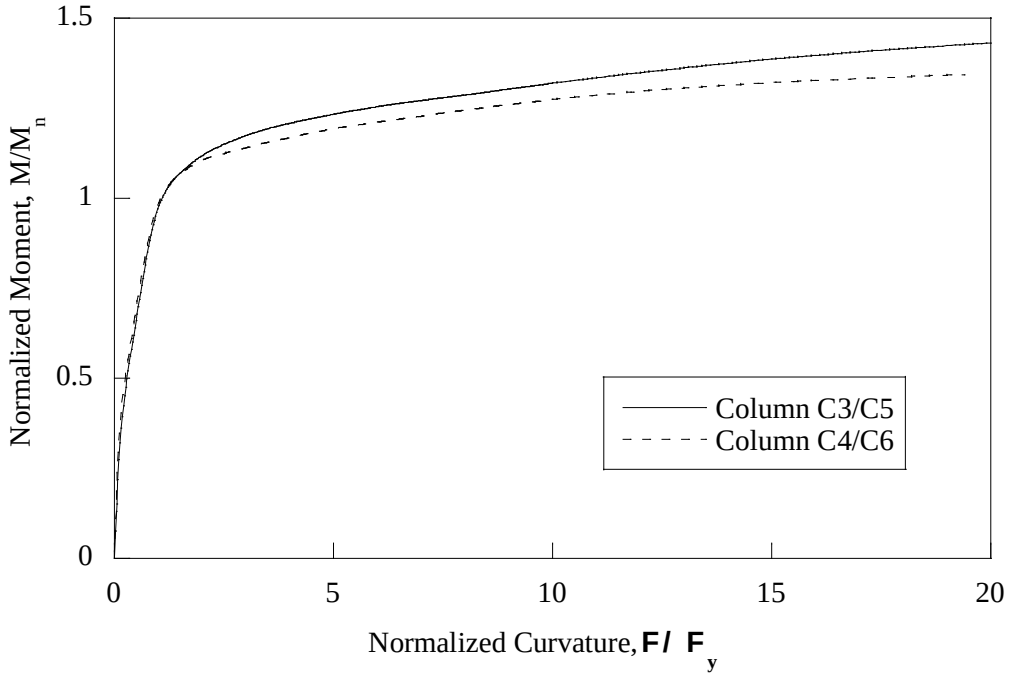

Figure 8.9: Moment-curvature response of columns C3/C5 and C4/C6 using *Concrete07* and *ReinforcingSteel*

8.3 MODELING OF COLUMN LATERAL FORCE-DEFLECTION RESPONSE

In this section the *Concrete07* was used for the concrete material model and *ReinforcingSteel* was used for the steel material model. For comparison of the test results with the numerical results several important sources of deformation need to be accurately modeled. There are various sources of deformation that may influence the response, which include:

1. footing shear deformations;
2. foundation movements, such as foundation rotation and translation;
3. column flexural deformation;
4. column shear deformations, and;
5. column-foundation fixed end rotation (due to strain penetration of column bars anchored in footing).

Footing shear deformations and movements were measured during the experiment and were observed to be negligible and are thus not considered in the modeling.

The column flexural deformations are modeled through the use of a single force-based fiber-section beam column element *(Spacone et al. 1996)*, in which 5 fiber-sections (Gauss-Lobatto integrations points) are defined along the nonlinear finite element. The number of integration points used allow for the modeling of a numerical plastic hinge length that is similar to the expected plastic hinge length *(Coleman and Spacone 2001)*. The fiber-section distributed plasticity element assumes that sections remain plane under deformation. The fiber-section model employed accounts for axial-flexure interaction, but does not account for shear deformations at the section level. Instead, the shear deformations are coupled only at the element level *(OpenSees 2012)*. In the columns analyzed herein, the shear deformations are expected to be small, and the reduced elastic shear stiffness (50 percent of the gross-section stiffness) is assumed to be constant during the analysis.

The column-fixed end rotation, due to strain penetration of the bars anchored in the footing, was noticeable in the experimental data. This is modeled as a concentrated hinge in the interface between the column and the foundation, with the stiffness of the springs given by:

$$k_{\theta,fe} = \frac{M_{po}}{\theta_{sp,y}} \tag{8.2}$$

where $\theta_{sp,y}$ is the estimated rigid body rotation of the column due to strain penetration at yielding, if yielding was observed at the base of the column. This equations thus assumes that the reinforcing bars are fully developed.

To compute $\theta_{sp,y}$ for defining the zero-length stiffness given in Eq. (8.2), the deformation mechanism shown in Figure 8.10 is proposed. As shown in the figure, the strains are assumed to extend over a length of 12 d_b to 15 d_b into the footing. This assumes good vibration and bonding conditions. Thus, based on the mechanism shown in Figure 8.10, the fixed-end rotation at the base is given by:

$$\theta_{sp,s} = 12 d_b \varepsilon_s \frac{0.50}{0.90D - c} \text{ to } 15 d_b \varepsilon_s \frac{0.50}{0.90D - c} \tag{8.3}$$

For columns with low axial load, such as the ones tested in this testing program, it can be assumed that $c \le 0.20D$. Thus, conservatively assuming $c = 0.20D$, the strain penetration rotation at yield is given by:

$$\theta_{sp,y} = 8.5 d_b \frac{\varepsilon_y}{D} \text{ to } 10.7 d_b \frac{\varepsilon_y}{D} \tag{8.4}$$

Table 8.2 provides the yield strain values and the range of strain penetration rotation at yield for each reinforcement bar size and grade. Note that in this model only bar slip is accounted for. Steel and concrete deformations in compression are neglected. To model the strain penetration effects the minimum strain penetration rotation at yield was used.

Table 8.2: Range of strain penetration rotations at yield for all test columns

Column	Bar size and grade	e_y	$\theta_{sp,y,min}$	$\theta_{sp,y,max}$
C1	#5 (#10M), Grade 60	0.0026	0.00058	0.00072
C2	#5 (#10M), Grade 80	0.0031	0.00069	0.00086
C3/C5	#6 (#19M), Grade 60	0.0023	0.00061	0.0007
C4/C6	#6 (#19M), Grade 80	0.0028	0.00074	0.00094

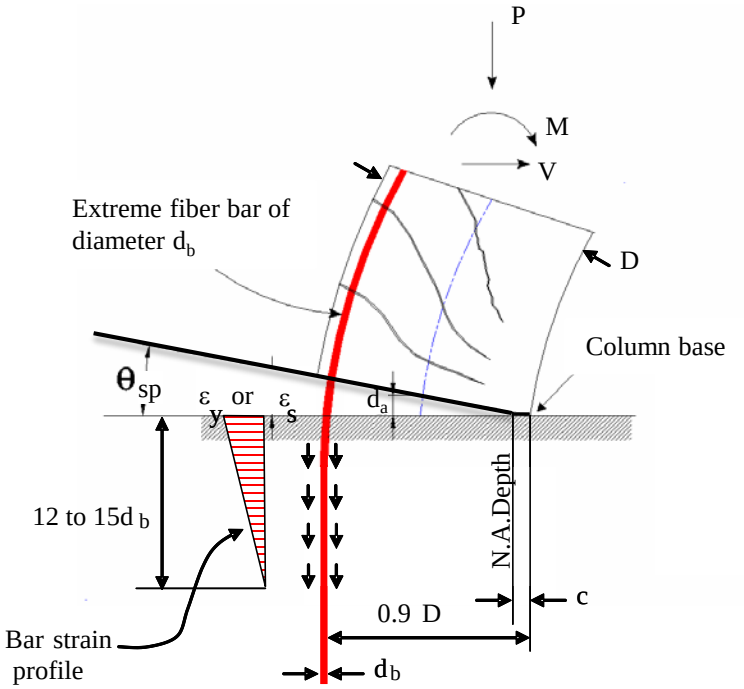

Figure 8.10: Deformation mechanism for strain penetration

The material properties inputted into OpenSees were from the material testing results in Chapter 3. The axial load was set to an initial value of 90 kips (400 kN) and held constant. Note that from the experimental data shown in Chapters 5 and 6 the axial load varied as a function of the tip displacement. This may cause the model to under predict the moment capacity compared to the experimental results.

Figure 8.11 shows the pushover analysis results for the model developed for column C1 as well as the experimental results. It can be seen from this figure that the model that accounts for the strain penetration matches the experimental results very well for column C1. This suggests that the model that accounts for strain penetration should be used. Further investigation of nonlinear static cyclic analyses are warranted for further validation of the model used, including comparison of measured and predicted hysteretic response as well as local section and fiber responses.

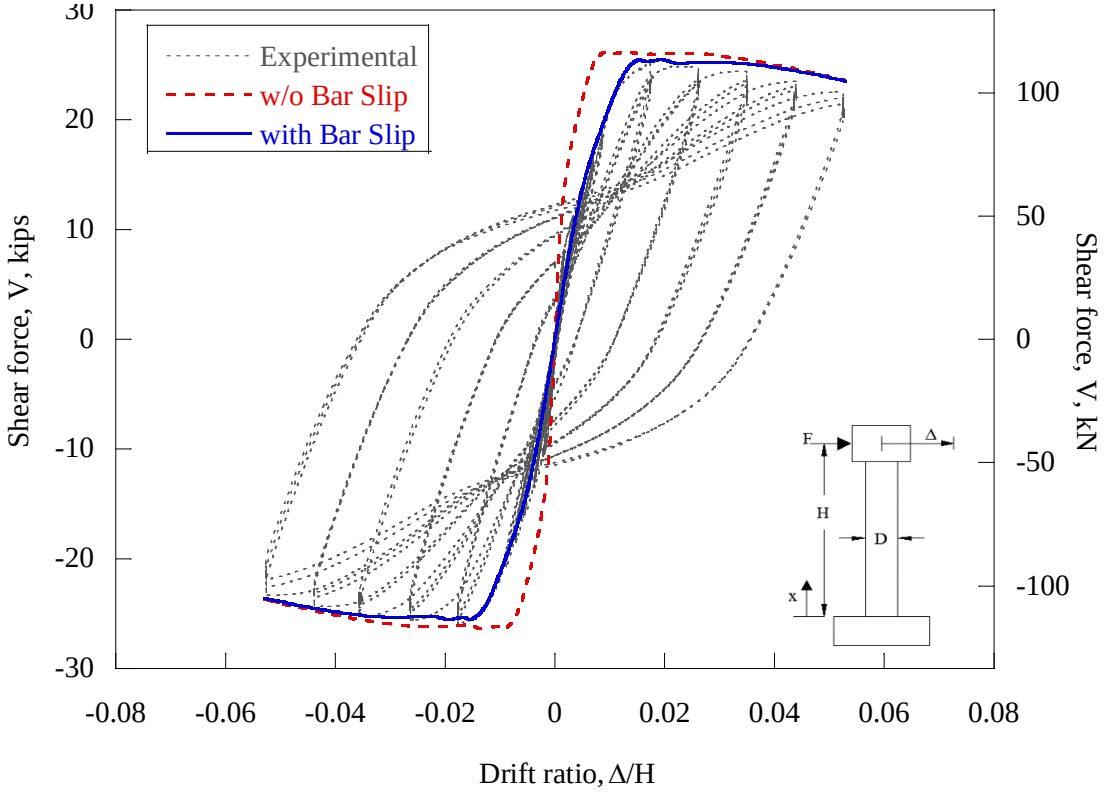

Figure 8.11: Column C1: Testing and pushover analysis results with and without consideration of strain penetration (bar slip)

Figure 8.12 shows the pushover analysis results for the model developed for column C2. The testing results are shown for comparison. It can be seen that the match for the model that accounts for the strain penetration is very good up to drift ratios of 1.7 percent. At larger drift ratio this model under predicts the maximum shear force of each initial curve for each displacement cycle. However, it predicts the diminished shear force of the second and third cycles of each displacement cycle very well. Further investigation of the strain penetration model used, axial load application, and nonlinear static cyclic analyses are warranted for further validation of the model used, including comparison of measured and predicted hysteretic response as well as local section and fiber responses. However, it can already be said that for column C2, the longitudinal reinforcement in the footing did not achieve yielding, and so the current model over predicted the effect of strain penetration. This can be confirmed by the initial stiffness which is under predicted in the modal for column C2 (Figure 8.12).

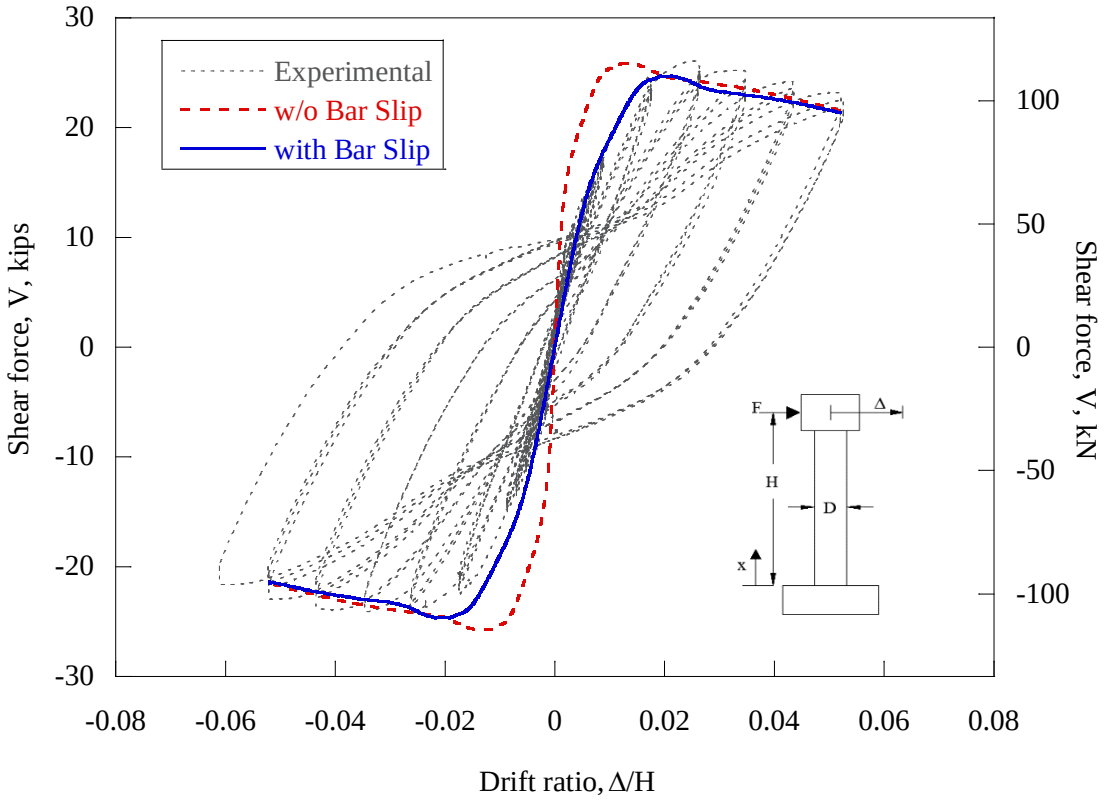

Figure 8.12: Column C2: Testing and pushover analysis results with and without consideration of strain penetration (bar slip)

Figure 8.13 shows the pushover analysis results for the models developed for column C3. The testing results are shown for comparison. It can be seen that the match for the model that accounts for the strain penetration is good for negative drift ratios but under predicts the shear capacity of positive drift ratios. This indicates that the columns shear capacity was different in the north and south directions which may be due to slight variations in the rebar locations and column geometry between the nominal locations and the as built locations. Further investigation of the strain penetration model used, axial load application and nonlinear static cyclic analyses are warranted for further validation of the model used, including comparison of measured and predicted hysteretic response as well as local section and fiber responses.

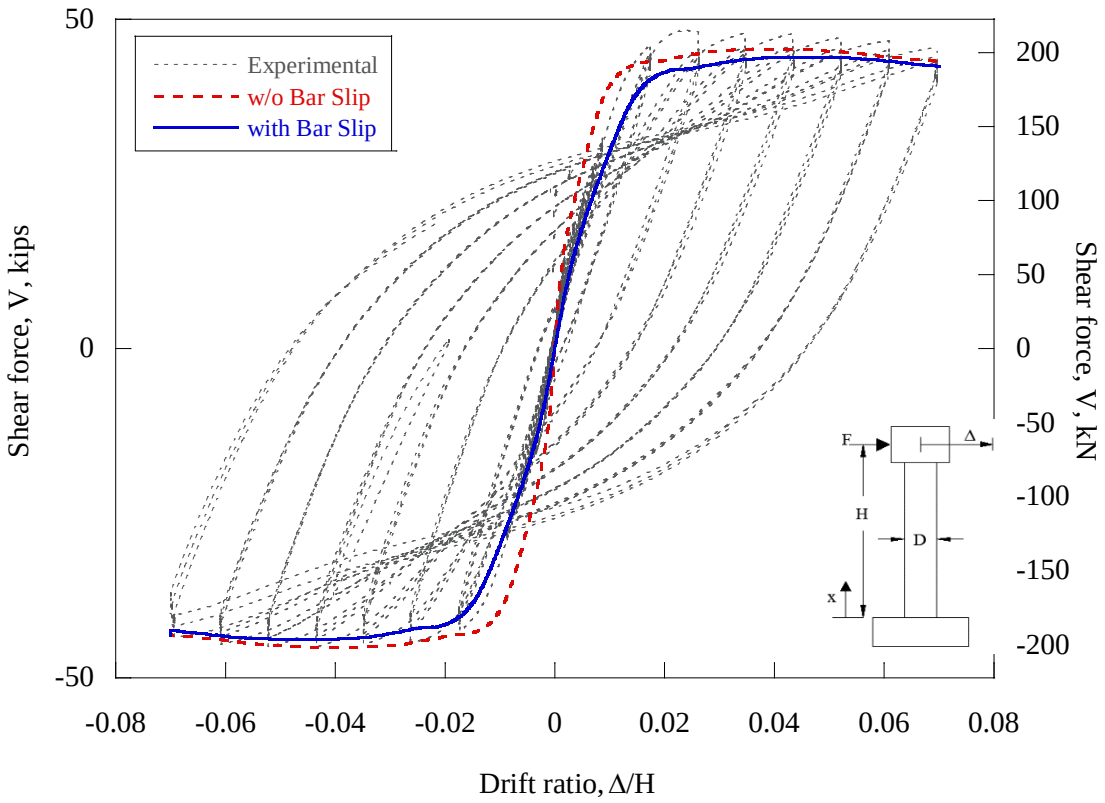

Figure 8.13: Column C3: Testing and pushover analysis results with and without consideration of strain penetration (bar slip)

Figure 8.14 shows the pushover analysis results for the models developed and the experimental results for column C3. It can be seen from this figure that the model that accounts for the strain penetration matches the experimental results well for small drift ratios but under predicts the shear force for larger drift ratios. Further investigation of the strain penetration model and nonlinear static cyclic analyses are warranted for further validation of the model used, including comparison of measured and predicted hysteretic response as well as local section and fiber responses.

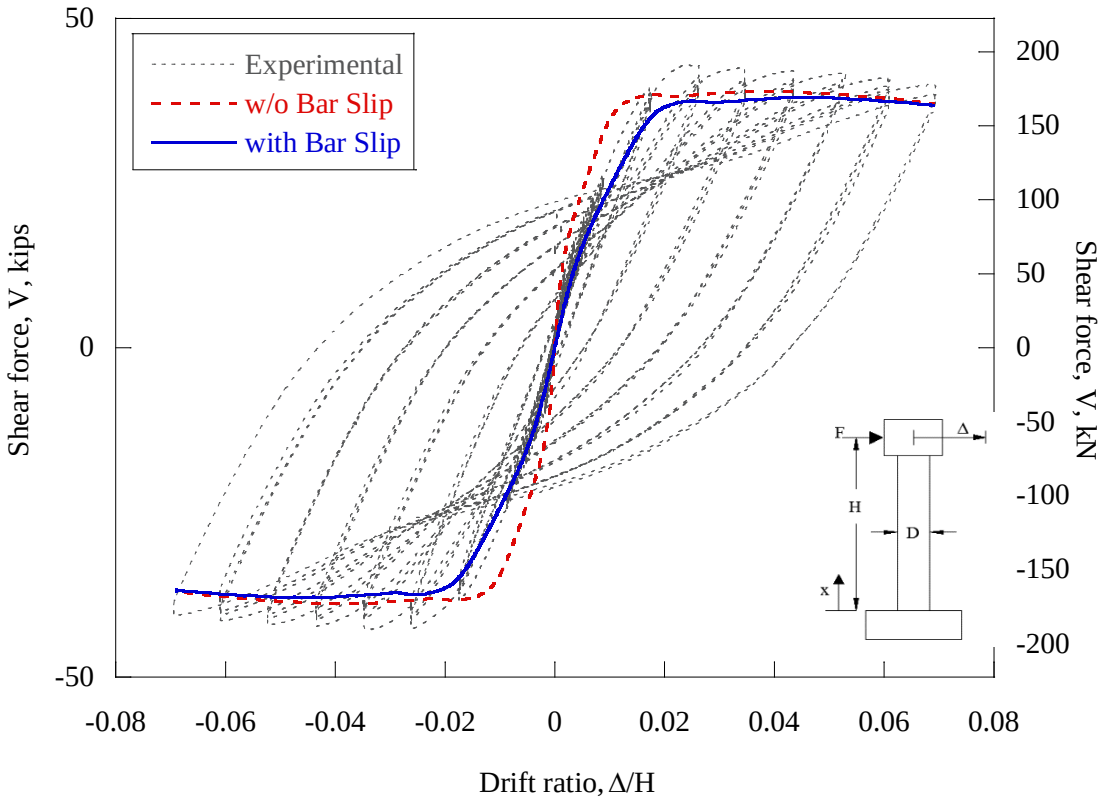

Figure 8.14: Column C4: Testing and pushover analysis results with and without consideration of strain penetration (bar slip)

Figure 8.15 shows the pushover analysis results for the models developed and experimental results for column C5. It can be seen that the match for the model that accounts for the strain penetration is good, except it slightly under predicts the shear force for drift ratios between 1.7 percent and 2.0 percent. The model that does not account for strain penetration better predicts the maximum shear forces for drift ratios greater than 1.7 percent, but does not match the experimental results well for drift ratios smaller than 1.7 percent.

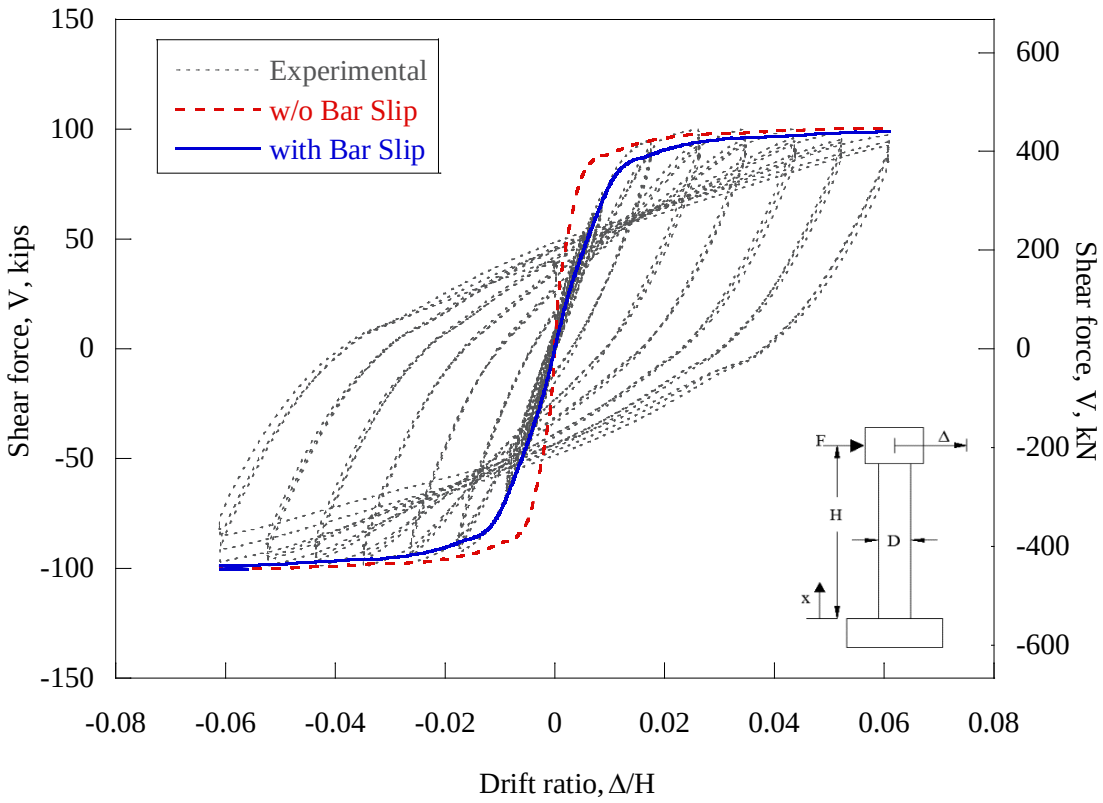

Figure 8.15: Column C5: Testing and pushover analysis results with and without consideration of strain penetration (bar slip)

Figure 8.16 shows the pushover analysis results for the models developed and experimental results for column C6. It can be seen from this figure that the model that accounts for the strain penetration matches the experimental results well for small drift ratios but under predicts the shear force for larger drift ratios. Both models do accurately predict the shear force at the maximum drift ratio. Further investigation of the strain penetration model, axial load application and nonlinear static cyclic analyses are warranted for further validation of the model, including comparison of measured and predicted hysteretic response as well as local section and fiber responses.

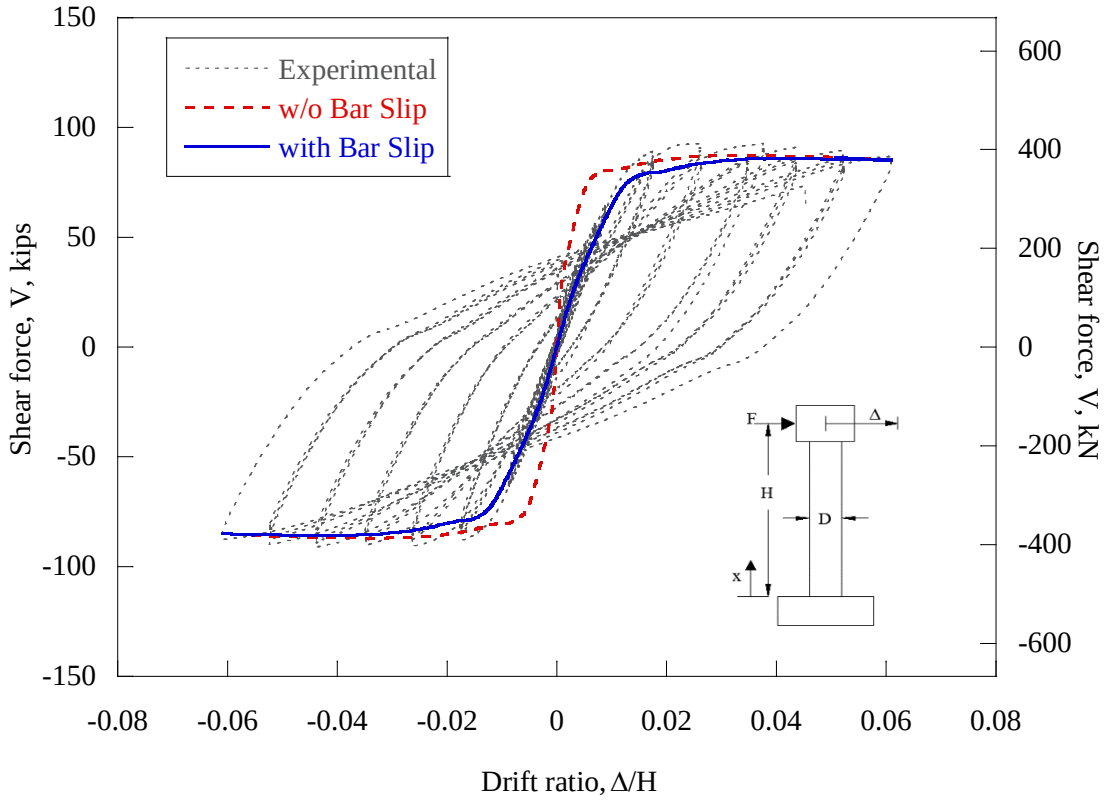

Figure 8.16: Column C6: Testing and pushover analysis results with and without consideration of strain penetration (bar slip)

8.4 SUMMARY

In this chapter two concrete material models and two steel material models were compared. The cross-sectional moment-curvature responses were modeled using the four material model combinations for each column. It is recommended that the *Concrete07* model be used for the concrete material model and *ReinforcingSteel* model be used for the steel material model in OpenSees. The overstrength factor determined from the analysis was larger than the overstrength factor computed from the experimental data for all of the test columns. However, the same trends were seen between the different columns for both the overstrength factor from the moment-curvature analysis and from the experimental data. The drift ratio versus shear force response accounting for strain penetration and neglecting strain penetration was modeled using OpenSees to conduct a pushover analysis for all experimental columns. It was determined that OpenSees can sufficiently predict the drift ratio versus shear force envelope for the columns tested. However the model was seen to under predict the maximum shear force for some drift ratios. Further investigation of the strain

penetration model and nonlinear static cyclic analyses are warranted for further validation of the model used, including comparison of measured and predicted hysteretic response as well as local section and fiber responses.

9.0 SUMMARY AND CONCLUSIONS

9.1 SUMMARY

Grade 80 reinforcement could reduce reinforcement quantities, could reduce reinforcing bar congestion, and could improve the constructability and economy of RC structures. However, limited research has been performed to validate the use of Grade 80 reinforcement. Results from a limited number of research projects indicate that Grade 80 reinforcement should be considered for use in all member types. This research assessed the performance of three pairs columns, each pair consisting of one column constructed with Grade 60 reinforcement and the other constructed with Grade 80 reinforcement. A total of six columns were tested.

Results indicate that the columns constructed with Grade 80 reinforcement achieved similar resistance and displacement ductility values when compared with the reference columns constructed with Grade 60 reinforcement. However the columns containing Grade 60 reinforcement typically exhibited larger curvature ductility values. The columns constructed with Grade 60 reinforcement showed larger hysteretic energy dissipation than the columns constructed with Grade 80 reinforcement. However, comparing the longitudinal reinforcement ratio of columns reinforced with Grade 60 or Grade 80 reinforcement showed that the energy dissipation is primarily a function of the amount of reinforcement rather than a function of the reinforcement grade. Columns constructed with Grade 80 reinforcement had computed overstrength factors slightly lower than the computer overstrength factors used for the columns constructed with Grade 60 reinforcement. Furthermore, the observed modes of failure for columns constructed with Grade 60 or Grade 80 reinforcement were similar. The main mode of failure was reinforcing bar fracture due to longitudinal reinforcing bar buckling after spalling of concrete cover in the plastic hinge region. The effects of the longitudinal reinforcement ratio and moment-shear span ratio were similar between the columns constructed with Grade 60 reinforcement and the columns constructed with Grade 80 reinforcement.

Modeling the test columns shear force versus drift ratio envelopes was sufficiently accomplished using OpenSees. The model does however under predict the maximum shear force for some drift ratios. Further refinement of the model is needed to more precisely predict the shear force. OpenSees may be a valuable option to study other parameters within the range of the parameters studied in this paper affecting the column performance.

9.2 FUTURE TESTING

The results in this study present a promising step towards implementation of Grade 80 reinforcement in the design and construction of reinforced concrete bridge columns, within the bounds of the variables used in the testing program. Other parameters outside of the range studied in this paper should be evaluated such as larger longitudinal reinforcement ratios, larger axial loads, and higher concrete strengths. Additionally to remove the effect of the longitudinal reinforcement spacing, future testing of columns containing bundled longitudinal reinforcing bars is warranted. It should be noted that the design procedure for the use of Grade 80 reinforcement in other areas of a bridge are not clear and additional research is needed. A PacTrans 2/ODOT research project has been funded to investigate the mechanical properties of Grade 80 reinforcement and to assess the shear capacity of members constructed with Grade 80 reinforcement. These results should provide additional information such that the codes can specifically address the use of Grade 80 reinforcement in RC members in seismic regions.

Further investigation of the strain penetration model and nonlinear static cyclic analyses used in OpenSees are warranted for further validation of the model used, including comparison of measured and predicted hysteretic response as well as local section and fiber responses.

10.0 REFERENCES

AASHTO. *AASHTO Guide Specifications for LRFD Seismic Bridge Design*. 2nd ed. American Association of State Highway and Transportation Officials, Washington, D.C., 2011.

AASHTO. *AASHTO LRFD BRIDGE DESIGN SPECIFICATIONS, Customary U.S. Units.* American Association of State Highway and Transportation Officials, Washington, D.C., 2012.

ACI Committee 318. Building Code Requirements for Structural Concrete and Commentary. Vol. 318–11. *American Concrete Institute*, Vol. #318-11, 2011.

American Society for Testing and Materials. (ASTM). *ASTM A706.* American Society for Testing and Materials. 2012.

Bauschinger, J. Variations in the Elastic Limit of Iron and Steel. *The Journal of the Iron and Steel Institute,* Vol. 12, No. 1, 1887, pp. 442–44.

Bentz, E.C. Sectional Analysis of Reinforced Concrete. Ph.D. Thesis, Department of Civil Engineering, University of Toronto. 2000.

CALTRANS. *Caltrans Seismic Design Criteria*. Version 1.6. California Department of Transportation. 2012.

Chang, G., and J. Mander. Seismic Energy Based Fatigue Damage Analysis of Bridge Columns: Part I - Evaluation of Seismic Capacity. *NCEER Technical Report 94-0006*. 1994.

Coleman, J., and E. Spacone. Localization Issues in Force-Based Frame Elements. *Journal of Structural Engineering*, Vol. 127, No. 11, 2001, pp. 1257–1265. doi:10.1061/(ASCE)0733-9445(2001)127:11(1257).

Collins, M.P., and D. Mitchell. *Prestressed Concrete Structures*. Prentice-Hall College Div. 1991.

Dodd, L. L. and J. I. Restrepo-Posada. Model for Predicting Cyclic Behaviour of Reinforcing Steel. *ASCE Journal of Structural Engineering*, Vol. 121, No. 3, 1995, pp. 433-445.

Filippou, F., and V. Bertero. *Effects of Bond Deterioration on Hysteretic Behavior of Reinforced Concrete Joints*. EERC 83-19. Earthquake Engineering Research Center. University of California, Berkeley. 1983.

http://www.ce.berkeley.edu/~filippou/Research/Publications/Reports/EERC-83-19.pdf. Accessed January 2014.

Gustafson, D.P. 2010. Raising the Grade. *Concrete International*, Vol. 32, No. 04, 2010, pp. 59–62.

Karthik, M., and J. Mander. Stress-Block Parameters for Unconfined and Confined Concrete Based on a Unified Stress-Strain Model. *Journal of Structural Engineering*, Vol. 137, No. 2, 2011, pp. 270–273. doi:10.1061/(ASCE)ST.1943-541X.0000294.

Kunnath, S., Y. Heo, and J. Mohle. Nonlinear Uniaxial Material Model for Reinforcing Steel Bars. *Journal of Structural Engineering*, Vol. 135, No. 4, 2009, pp. 335–343. doi:10.1061/(ASCE)0733-9445(2009)135:4(335).

Mander, J. B., M.J.N. Priestley, and R. Park. Theoretical Stress-Strain Model for Confined Concrete. *Journal of Structural Engineering*, Vol. 114, No. 8, 1988, pp. 1804–1826. doi:10.1061/(ASCE)0733-9445(1988)114:8(1804).

Mander, J., F. Panthaki, and A. Kasalanati. Low-Cycle Fatigue Behavior of Reinforcing Steel. *Journal of Materials in Civil Engineering, Vol.* 6, No. 4, 1994a, pp. 453–468. doi:10.1061/(ASCE)0899-1561(1994)6:4(453).

Mander, J., F. Panthaki, and A. Kasalanati. Low-Cycle Fatigue Behavior of Reinforcing Steel. *Journal of Materials in Civil Engineering*, Vol. 6, No. 4, 1994b, pp. 453–468. doi:10.1061/(ASCE)0899-1561(1994)6:4(453).

Nissen, E.. Mill Issues Related to Making High-Strength Reinforcement. Power Point presented at the ACI Hot Topic Session: High-Strength Reinforcing Bars - Balancing Design Requirements with Achievable Material Properties, Phoenix, Arizona. 2013. http://hub.concrete.org/Convention/Fall-Convention/PresentationDetail.asp?EventId=ZHOT. Accessed January 2014.

ODOT. 2012. *ODOT Bridge Design and Drafting Manual*. rev. August 2012. Oregon Department of Transportation. 2012.

OpenSees. *Open Systems for Earthquake Engineering Simulation.* (Version 2.4.0). University of California, Berkeley, California: Pacific Earthquake Engineering Research Center. 2012. http://opensees.berkeley.edu. Accessed January 2014.

Paulson, C. Brief Historical Overview of Yield Strength in ACI 318. Power Point presented at the ACI Hot Topic Session: High-Strength Reinforcing Bars - Balancing Design Requirements with Achievable Material Properties, Phoenix, Arizona. 2012. http://hub.concrete.org/Convention/Fall-Convention/PresentationDetail.asp?EventId=ZHOT. Accessed January 2014.

Priestley, M.J.N. “Myths and Fallacies in Earthquake Engineering, Revisited. The 9th Mallet Milne Lecture,” IUSS Press, Pavia, 2003, p. 121.

Priestley, M.J.N., and G. Benzoni. 1996. Seismic Performance of Circular Columns with Low Longitudinal Reinforcement Ratios. *ACI Structural Journal,* Vol. 93, No. 4, 1996, pp. 474–485.

Rautenberg, J.M., S. Pujol, and A. Lepage. Cyclic Response of Concrete Columns Reinforced with High-Strength Steel. 9th US National and 10th Canadian Conference on Earthquake Engineering 2010, Including Papers from the 4th International Tsunami Symposium 3. 2010. http://nees.org/resources/679/download/2010EQConf-000996.PDF. Accessed January 2014.

Rice, P., and D.Gustafson. Grade 80 Reinforcing Bars and ACI 318-71. *Journal Proceedings,* Vol. 73, No. 4, 1976, pp. 199–206.

Rodriguez, M., J. Botero, and J. Villa. Cyclic Stress-Strain Behavior of Reinforcing Steel Including Effect of Buckling. *Journal of Structural Engineering,* Vol. 125, No. 6, 1999, pp. 605–612. doi:10.1061/(ASCE)0733-9445(1999)125:6(605).

Scott, B., R. Park, and M.J.N. Priestley. Stress-Strain Behavior of Concrete Confined by Overlapping Hoops at Low and High Strain Rates. *ACI Journal,* Vol. 79, No. 1, 1982, pp. 13–27.

Selzer, J. Reinforcing Bar Metallurgy - 101. Power Point presented at the ACI Hot Topic Session: High-Strength Reinforcing Bars - Balancing Design Requirements with Achievable Material Properties, Phoenix, Arizona. 2013. http://hub.concrete.org/Convention/Fall-Convention/PresentationDetail.asp?EventId=ZHOT. Accessed January 2014.

Spacone, E., V. Ciampi, and F.C. Filippou. Mixed Formulation of Nonlinear Beam Finite Element. *Computers & Structures,* Vol. 58, No. 1, 1996, pp. 71–83. doi:10.1016/0045-7949(95)00103-N.

Texler, D. *DT Column* (version 2.1). dtware. 2001. http://www.dtware.com. Accessed January 2014.

The Regents of the University of California. *OpenSees*. University of California. 1999.

Vecchio, F.J., and M.P. Collins. 1986. The Modified Compression Field Theory for Reinforced Concrete Elements Subjected to Shear. *ACI Journal,* Vol. 83, No. 2, 1986, pp. 219–231.

WSDOT. *WSDOT Bridge Design Manual (LRFD)*. M 23-50.12. Washington State Department of Transportation. 2012.

Yassin, M. Nonlinear Analysis of Prestressed Concrete Structures under Monotonic and Cyclic Loads. Ph.D. Thesis, Berkeley: University of California at Berkeley. 1994.

Yeh, I-Cheng. Generalization of Strength versus Water–cementitious Ratio Relationship to Age. *Cement and Concrete Research*, Vol. 36, No. 10, 2006, pp. 1865–1873. doi:10.1016/j.cemconres.2006.05.013.

APPENDIX A: RESPONSE 2000 INPUT AND OUTPUT

Geometric Properties

	Gross Conc.	Trans (n=8.22)
Area (in^2)	447.2	483.0
Inertia (in^4)	15915.2	17727.9
y_t (in)	12.0	12.0
y_b (in)	12.0	12.0
S_t (in^3)	1326.3	1477.3
S_b (in^3)	1326.3	1477.3

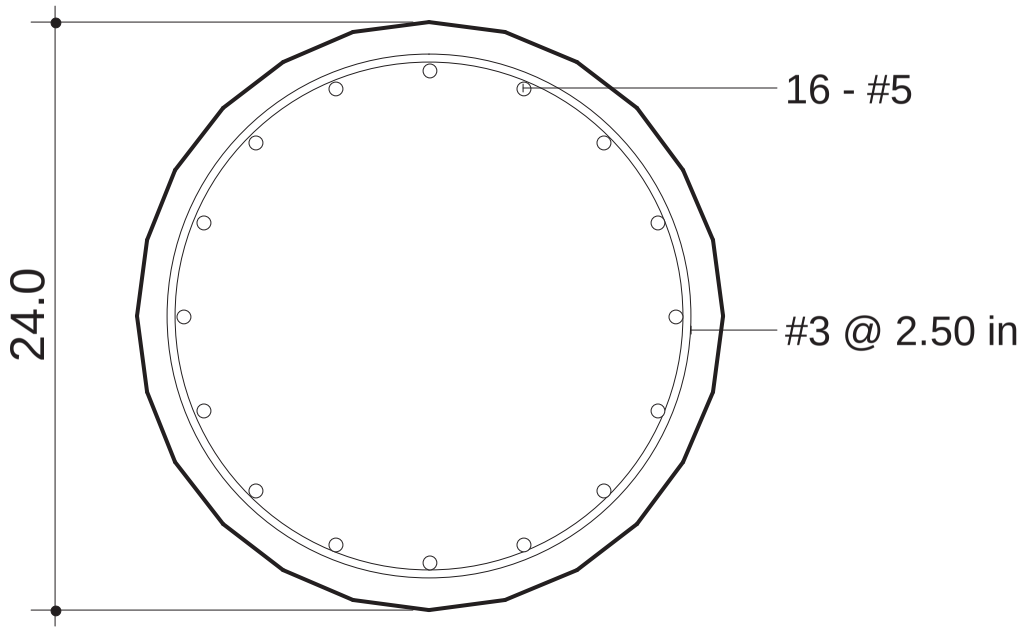

Crack Spacing

2 x dist + 0.1 d_b /ρ

Loading (N,M,V + dN,dM,dV)

-90.0 , -0.0 , 0.0 + 0.0 , 1.0 , 0.0

Concrete

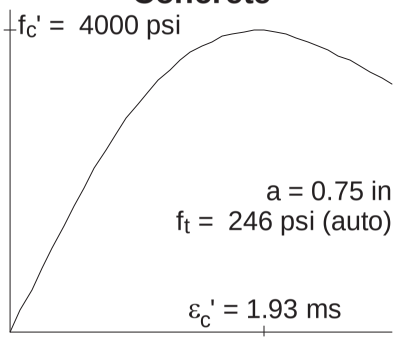

Rebar

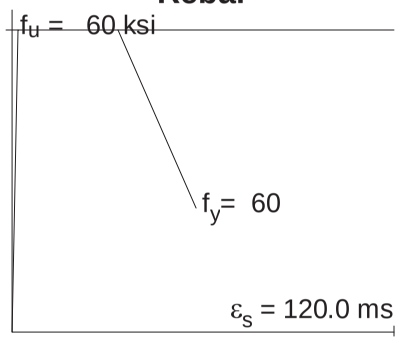

All dimensions in inches
Clear cover to transverse reinforcement = 1.25 in

C1

TBL **2012/10/4**

Response-2000 v 1.0.5

C1

TBL 2013/12/13 - 4:18 pm

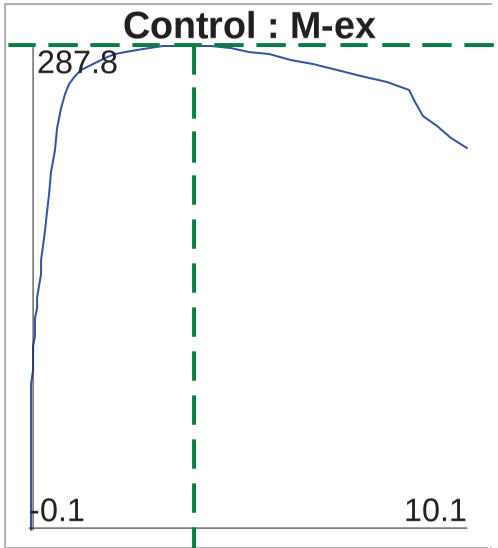

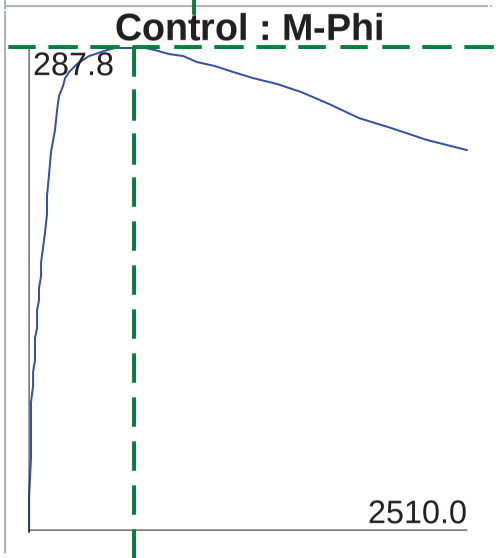

ε_{x0} = 3.76 ms

ϕ = 600.87 rad/10^6 in

γ_{xy}(avg) = 0.00 ms

Axial Load = -90.0 kips

Moment:= 287.8 ft-kips

Shear = 0.0 kips

Cross Section

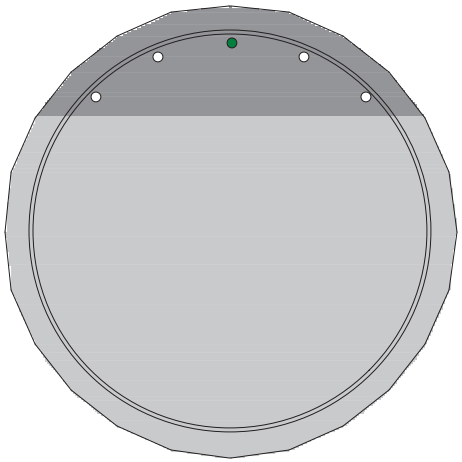

Longitudinal Strain

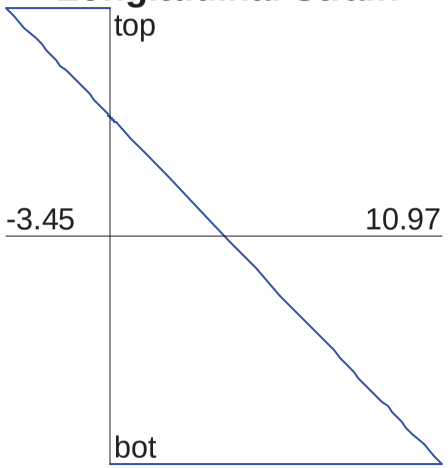

Shrinkage & Thermal Strain

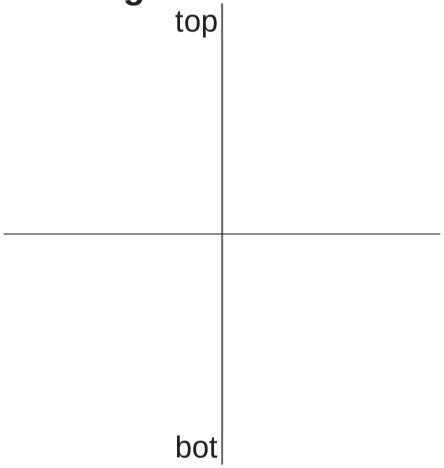

Crack Diagram

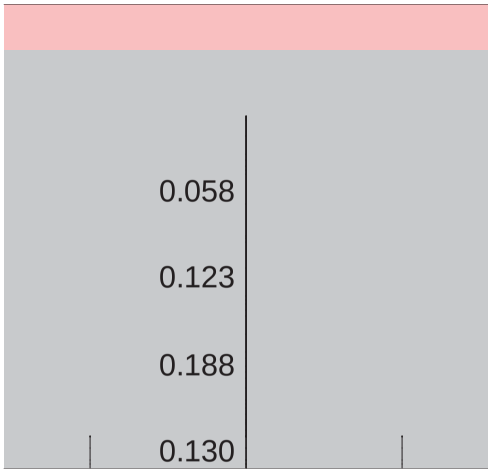

Long. Reinforcement Stress

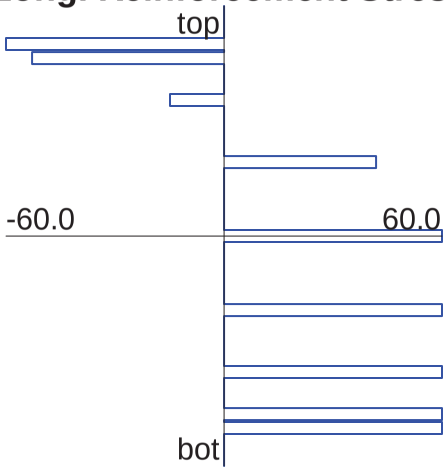

Long. Reinf Stress at Crack

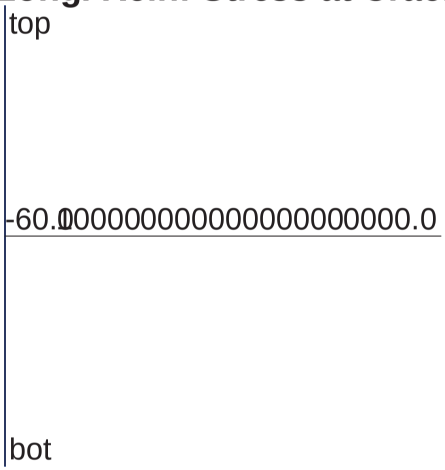

Longitudinal Concrete Stress

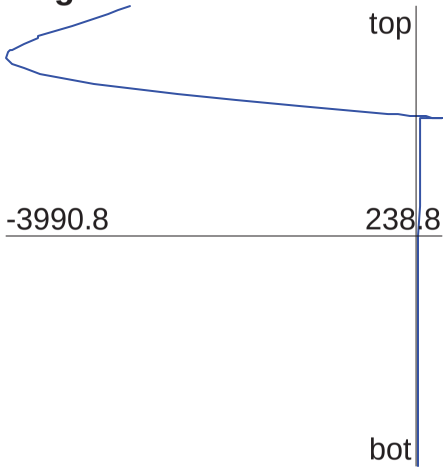

Internal Forces

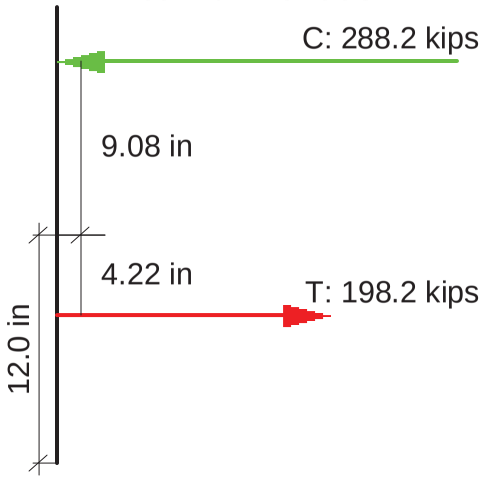

N+M

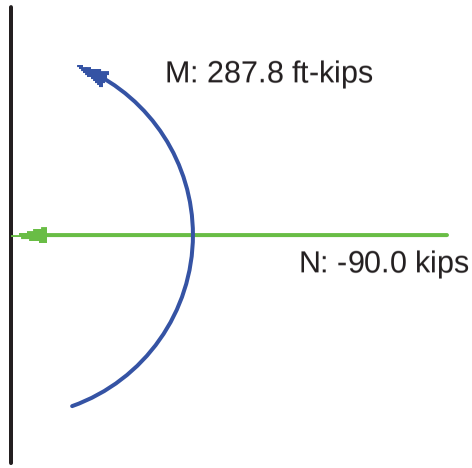

Geometric Properties

	Gross Conc.	Trans (n=8.22)
Area (in^2)	447.2	474.1
Inertia (in^4)	15915.2	17257.9
y_t (in)	12.0	12.0
y_b (in)	12.0	12.0
S_t (in^3)	1326.3	1438.2
S_b (in^3)	1326.3	1438.2

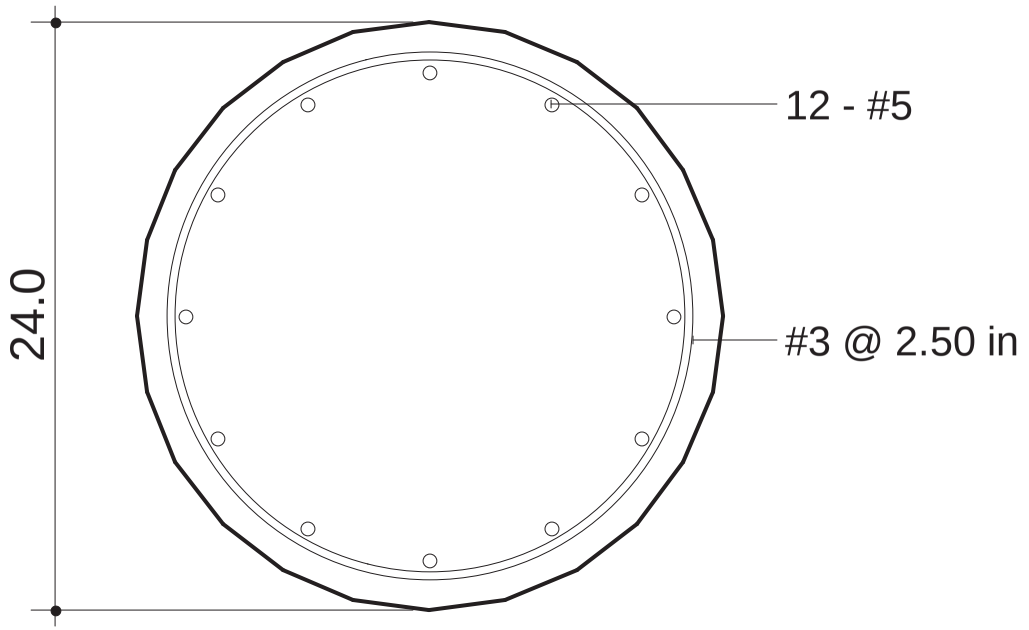

Crack Spacing

2 x dist + 0.1 d_b /ρ

Loading (N,M,V + dN,dM,dV)

-90.0 , -0.0 , 0.0 + 0.0 , 1.0 , 0.0

Concrete

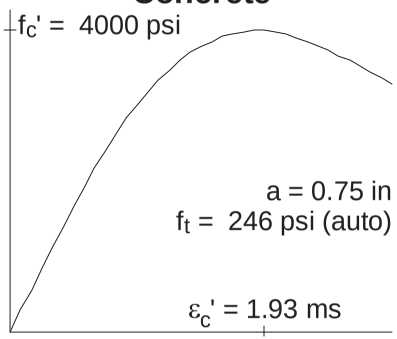

Rebar

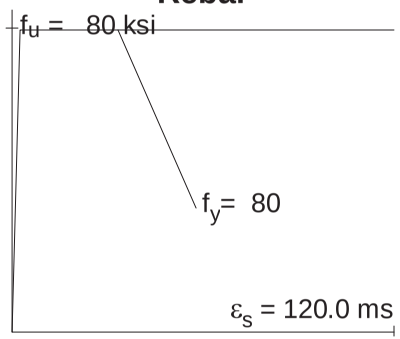

All dimensions in inches
Clear cover to transverse reinforcement = 1.21 in

C2

TBL **2012/10/4**

Response-2000 v 1.0.5

C2

TBL 2013/12/13 - 4:36 pm

Control : M-ex

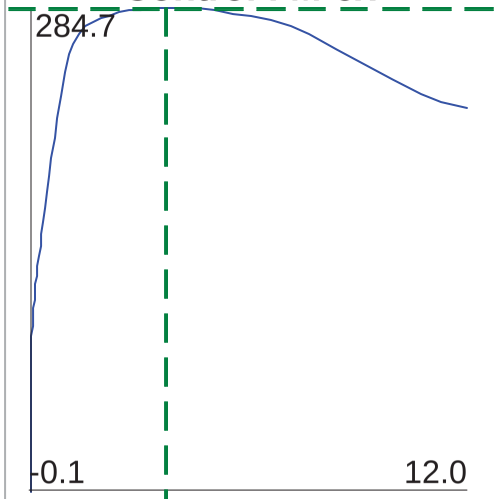

Control : M-Phi

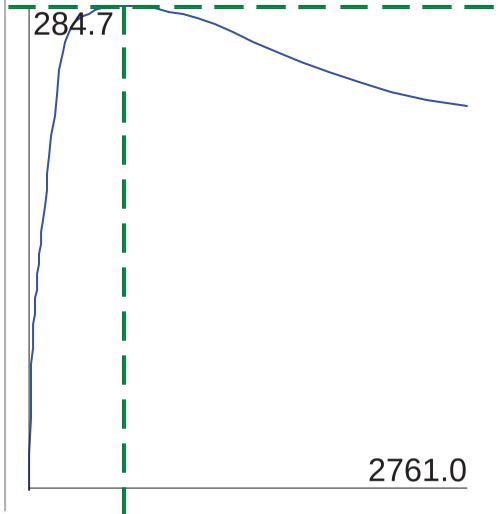

ε_{x0} = 3.70 ms

ϕ = 600.87 rad/10^6 in

γ_{xy}(avg) = 0.00 ms

Axial Load = -90.0 kips

Moment:= 284.7 ft-kips

Shear = 0.0 kips

Cross Section

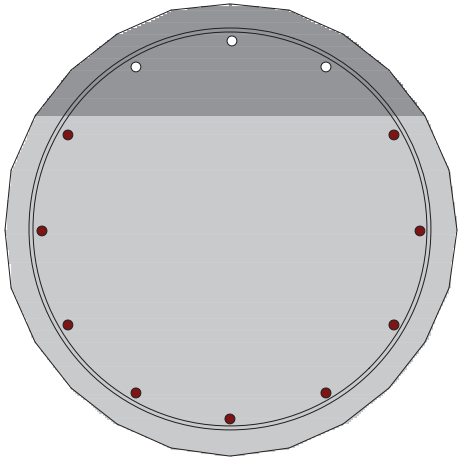

Longitudinal Strain

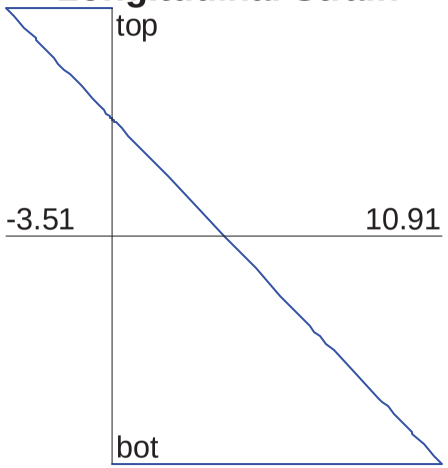

Shrinkage & Thermal Strain

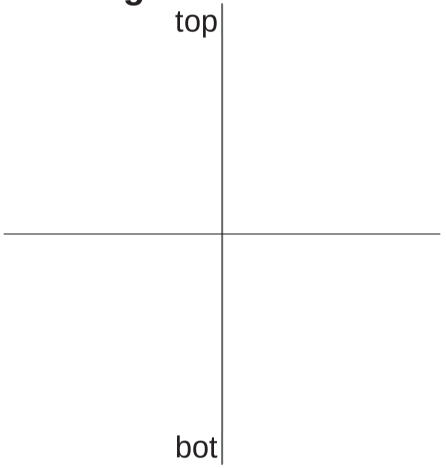

Crack Diagram

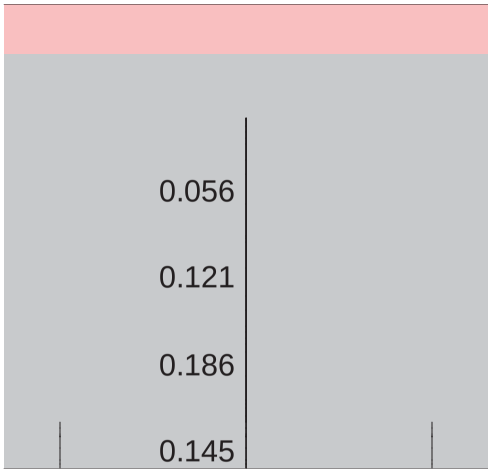

Long. Reinforcement Stress

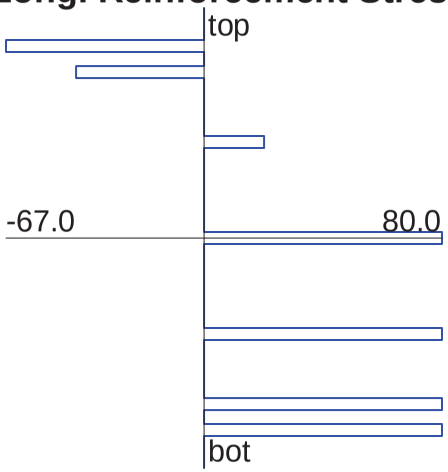

Long. Reinf Stress at Crack

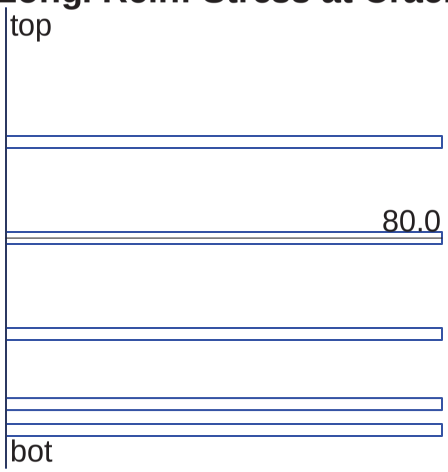

Longitudinal Concrete Stress

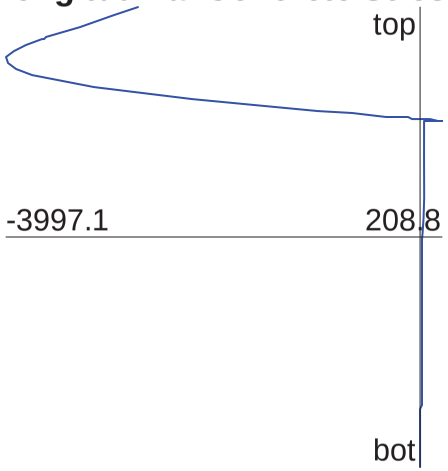

Internal Forces

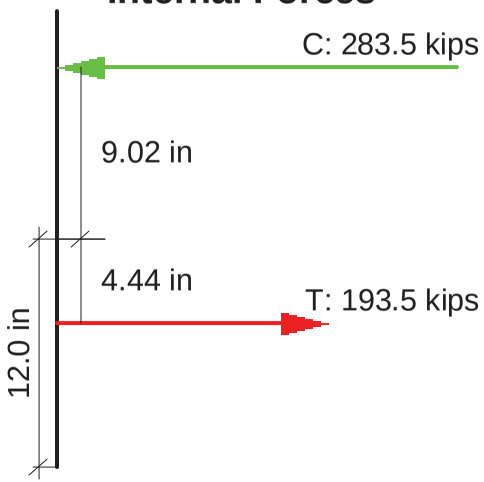

N+M

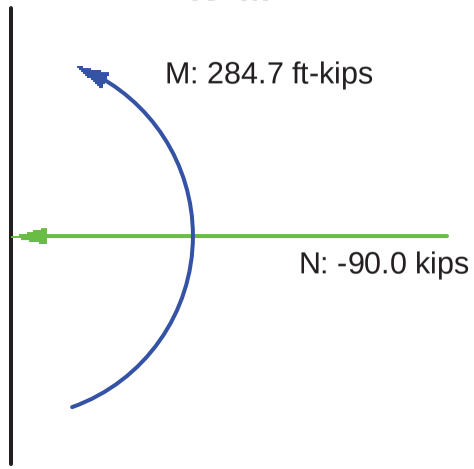

Geometric Properties

	Gross Conc.	Trans (n=8.22)
Area (in^2)	447.2	517.1
Inertia (in^4)	15915.2	19409.1
y_t (in)	12.0	12.0
y_b (in)	12.0	12.0
S_t (in^3)	1326.3	1617.4
S_b (in^3)	1326.3	1617.4

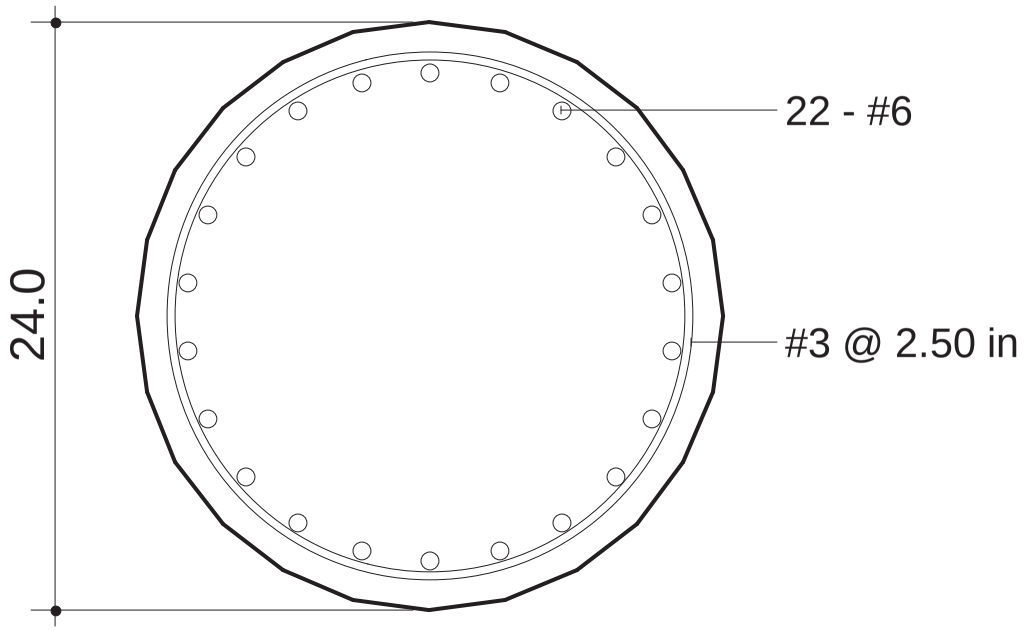

Crack Spacing

2 x dist + 0.1 d_b /ρ

Loading (N,M,V + dN,dM,dV)

-90.0 , -0.0 , 0.0 + 0.0 , 1.0 , 0.0

Concrete

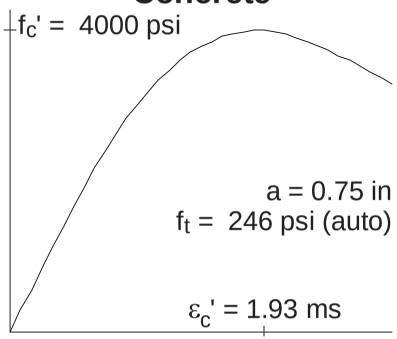

Rebar

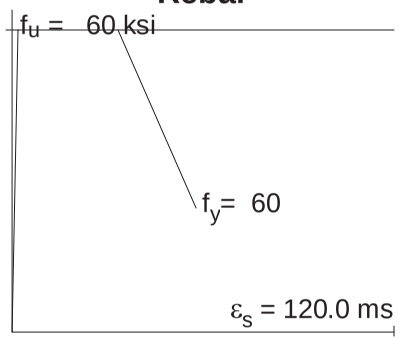

All dimensions in inches
Clear cover to transverse reinforcement = 1.21 in

C3 and C5

TBL **2012/10/4**

Response-2000 v 1.0.5

C3 and C5

TBL 2013/12/13 - 4:36 pm

Control : M-ex

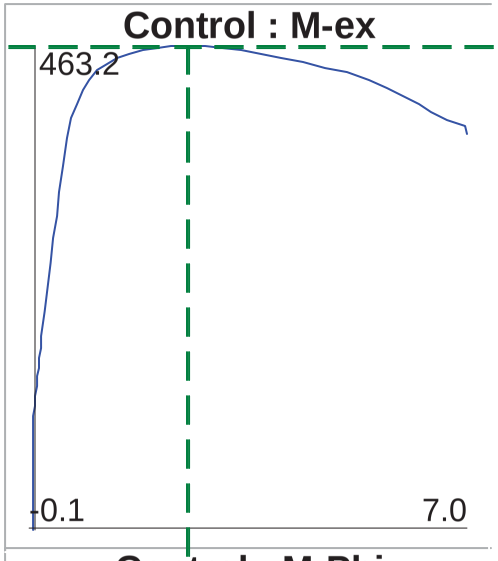

Control : M-Phi

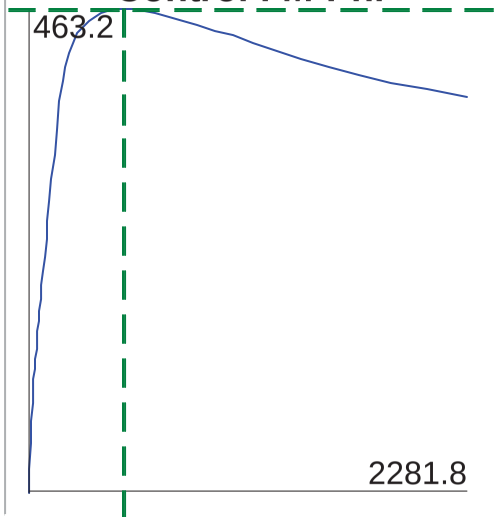

ε_{x0} = 2.46 ms

ϕ = 496.59 rad/10^6 in

γ_{xy}(avg) = 0.00 ms

Axial Load = -89.8 kips

Moment:= 463.2 ft-kips

Shear = 0.0 kips

Cross Section

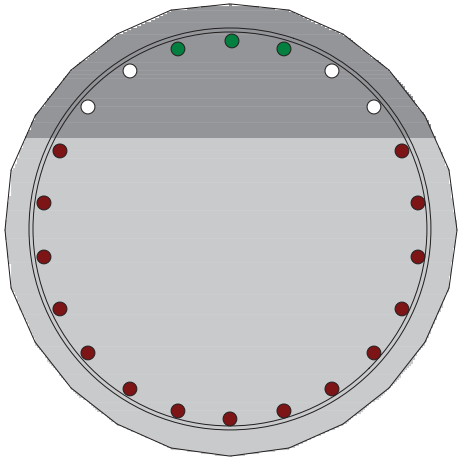

Longitudinal Strain

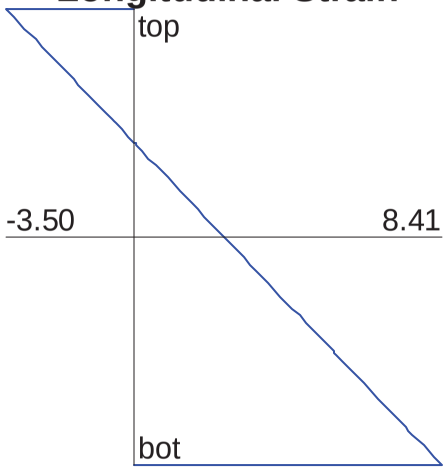

Shrinkage & Thermal Strain

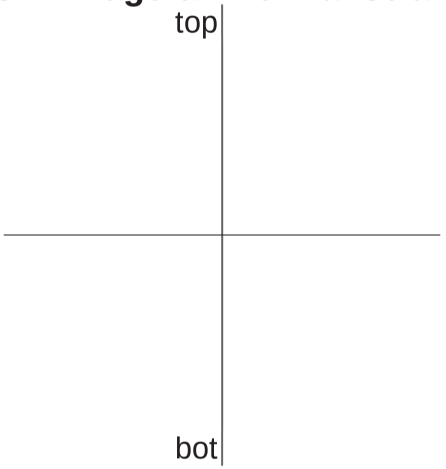

Crack Diagram

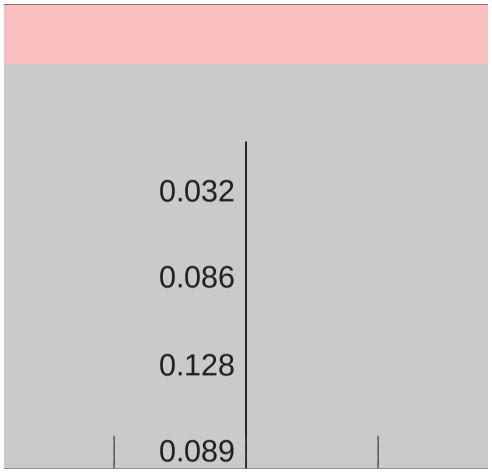

Long. Reinforcement Stress

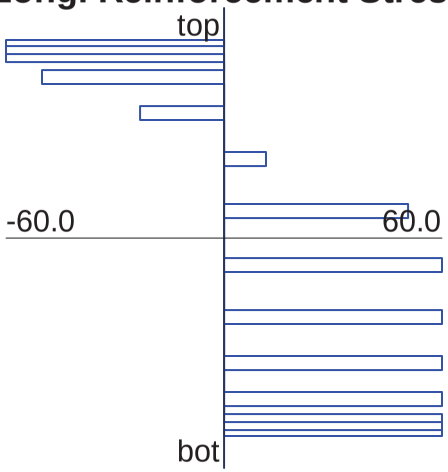

Long. Reinf Stress at Crack

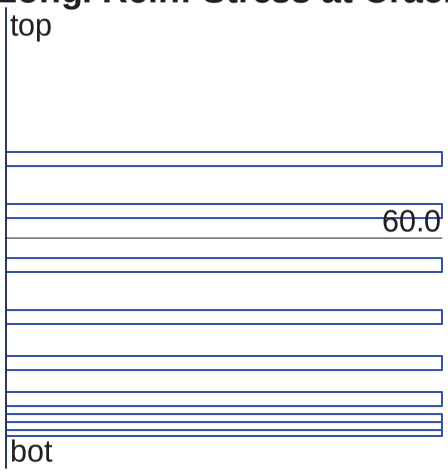

Longitudinal Concrete Stress

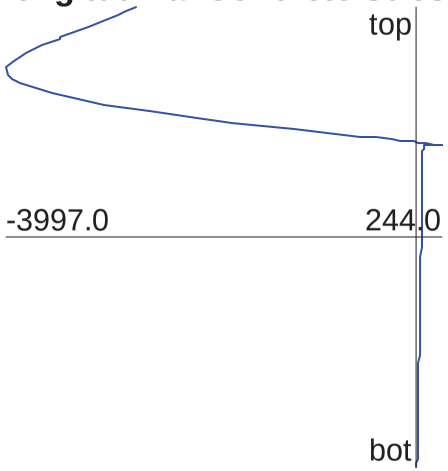

Internal Forces

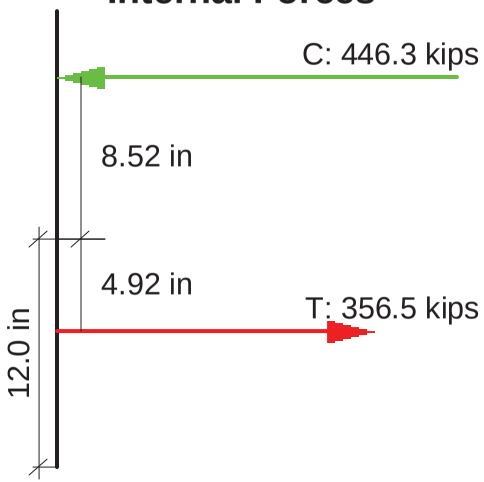

N+M

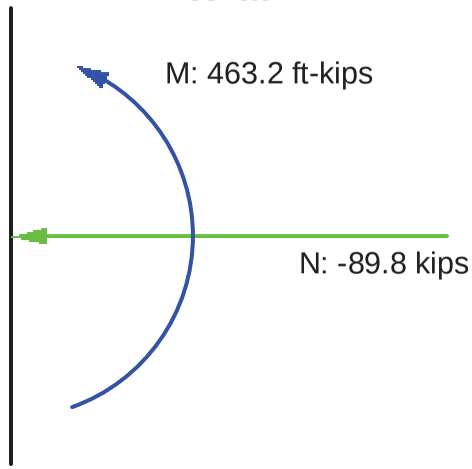

Geometric Properties

	Gross Conc.	Trans (n=8.22)
Area (in^2)	447.2	498.0
Inertia (in^4)	15915.2	18456.2
y_t (in)	12.0	12.0
y_b (in)	12.0	12.0
S_t (in^3)	1326.3	1538.0
S_b (in^3)	1326.3	1538.0

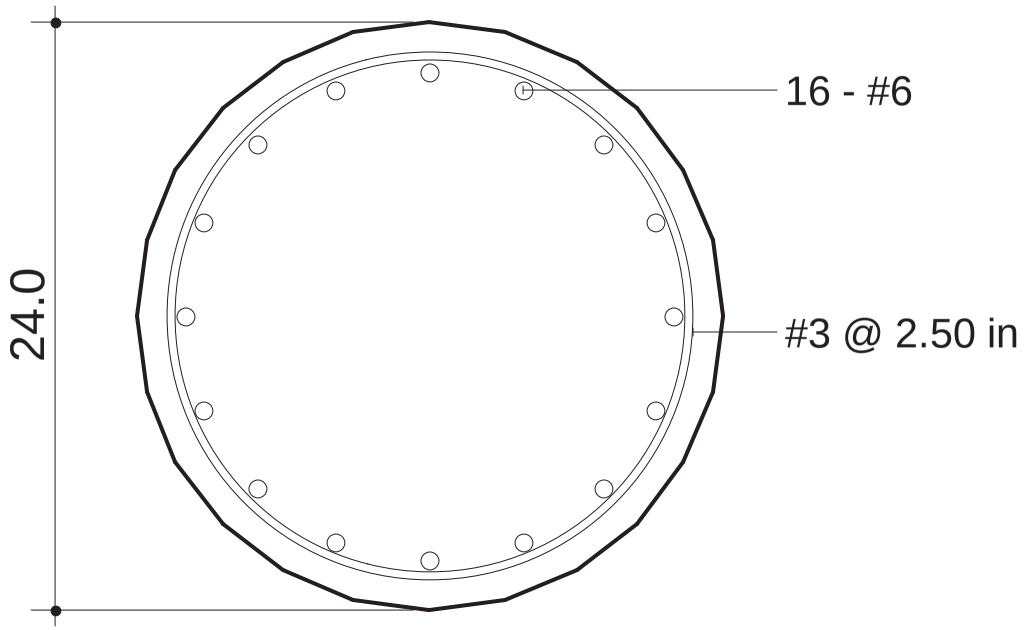

Crack Spacing

2 x dist + 0.1 d_b /ρ

Loading (N,M,V + dN,dM,dV)

-90.0 , -0.0 , 0.0 + 0.0 , 1.0 , 0.0

Concrete

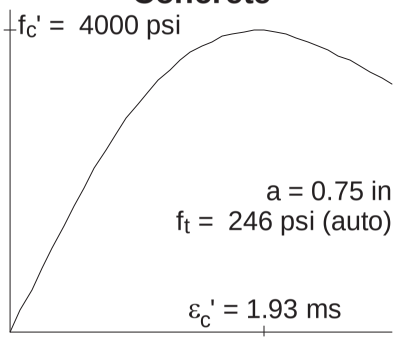

Rebar

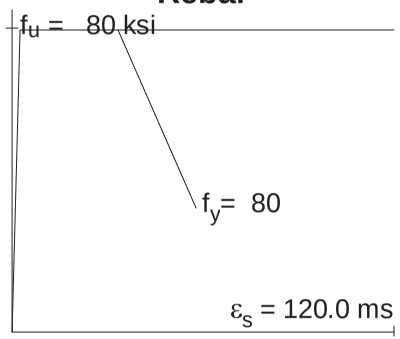

All dimensions in inches
Clear cover to transverse reinforcement = 1.21 in

C4 and C6

TBL **2012/10/4**

Response-2000 v 1.0.5

C4 and C6

TBL 2013/12/13 - 4:37 pm

Control : M-ex

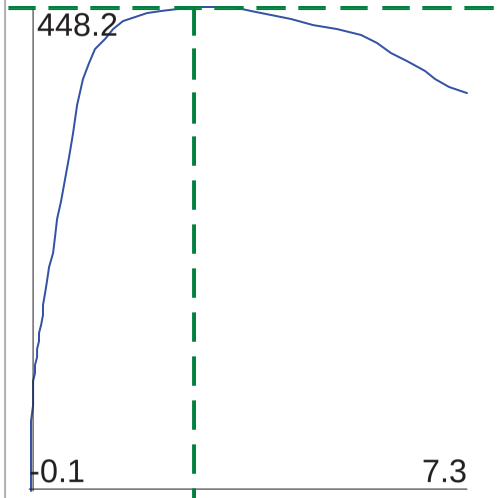

Control : M-Phi

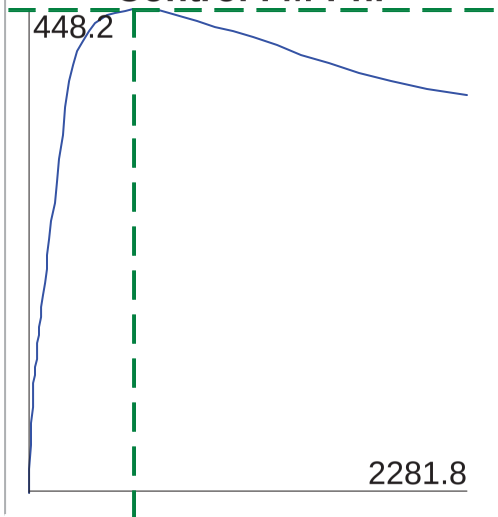

ε_{x0} = 2.69 ms

ϕ = 546.25 rad/10^6 in

γ_{xy}(avg) = 0.00 ms

Axial Load = -90.0 kips

Moment:= 448.2 ft-kips

Shear = 0.0 kips

Cross Section

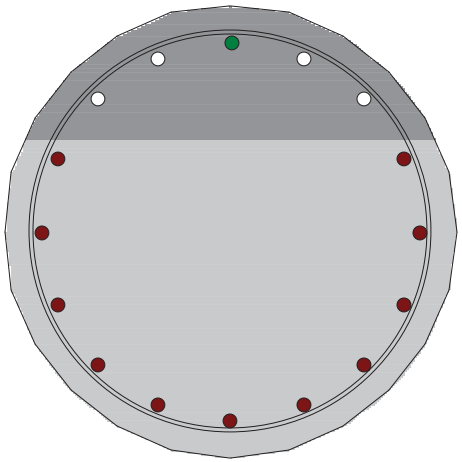

Longitudinal Strain

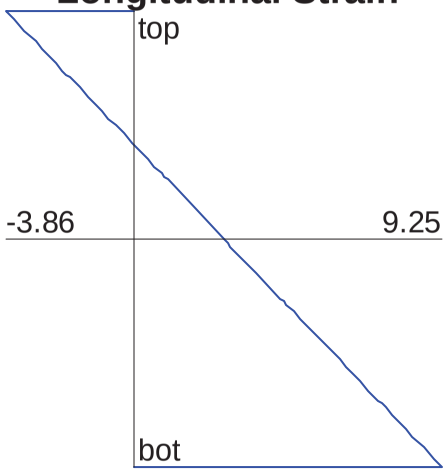

Shrinkage & Thermal Strain

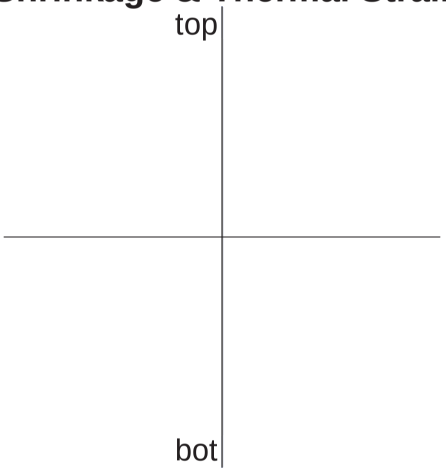

Crack Diagram

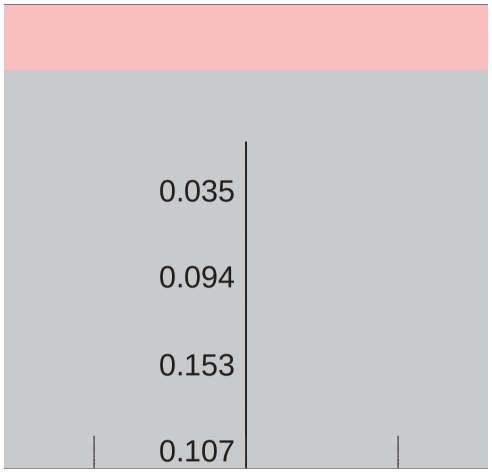

Long. Reinforcement Stress

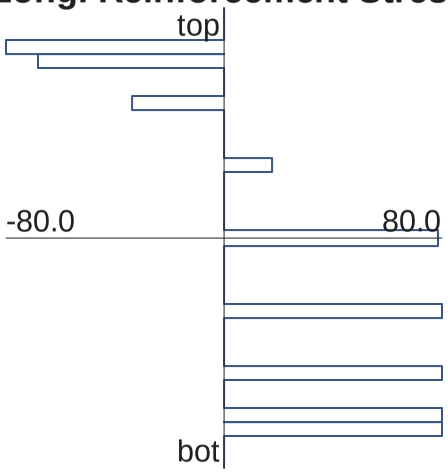

Long. Reinf Stress at Crack

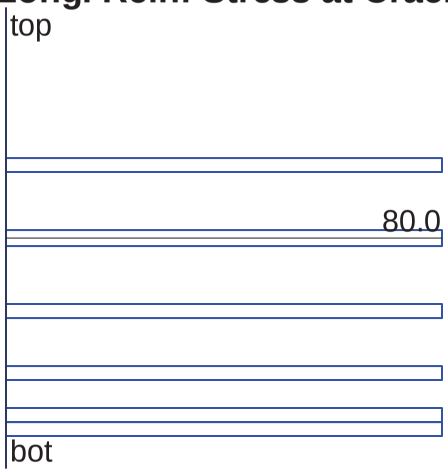

Longitudinal Concrete Stress

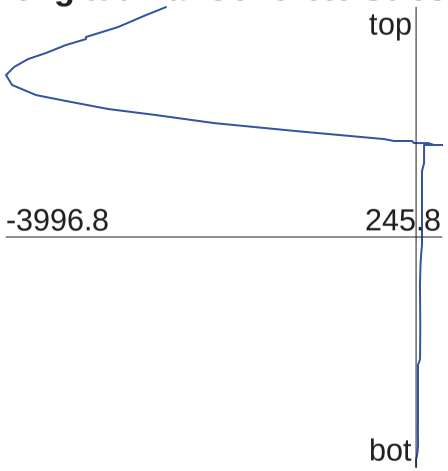

Internal Forces

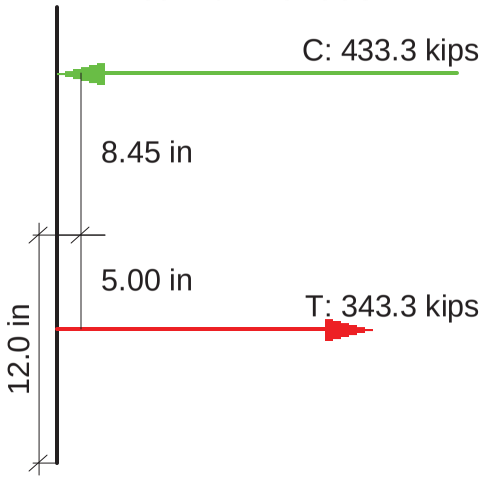

N+M

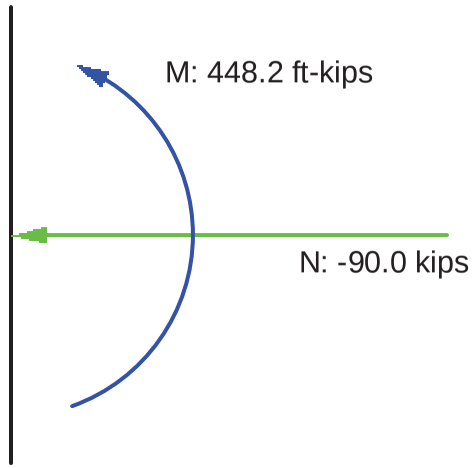

APPENDIX B: TRANSVERSE REINFORCEMENT DESIGN

C1 Spiral Design:

This Mathcad script is for column C1, however the equations and design process are identical for all experimental test columns.

Need to check value according to instructions highlighted.

Input Values.

Step 1.) Adjust input values according to the column properties and loading conditions

Material Properties:

Maximum size aggregate. $MSA := 0.75in$

Diameter of longitudinal reinforcing steel. $D_{bl} := 0.625in$

Nominal concrete compressive strength. $f'_c := 4000psi$

Diameter of transverse reinforcing steel. $D_{bt} := 0.375in$

Yield stress of transverse reinforcement. $f_{yt} := 60ksi$

Cross-sectional area of transverse steel. $A_{st} := 0.11in^2$

Moment over strength factor. $\lambda := 1.4$

Column Properties:

Diameter of column. $D_c := 24in$

Column test height. $h_c := 12ft$

Column clear cover. $c_c := 1.25in$

Effective web width. $b_v := 24in$

Number of spirals within column. $n := 1$

Loading Conditions:

Strength reduction factor defined by AASHTO LRFD BDS Sec. 5.5.4.2.1. $\phi := 0.75$

Prestressing force resisting shear. $V_p := 0kip$

Expected moment capacity. $M_e := 402.9kip \cdot ft$

Applied axial load on column. $P := 90kip$

Global displacement ductility demand ratio. $\mu_D := 6$

Step 2.) Determine the shear force demand according to AASHTO LRFD Bridge Design Specifications 6th Ed. Sec. 5.8.2.9

$D_r := D_c - 2\cdot\left[c_c + D_{bt} + \left(\frac{D_{bl}}{2}\right)\right] = 20.13\cdot in$ Diameter of the core, taken from center-to-center of the longitudinal reinforcement.

$d_e := \left(\frac{D_c}{2}\right) + \left(\frac{D_r}{\pi}\right) = 18.41\cdot in$ Defined by AASHTO 2012 C5.8.2.9-2.

$d_v := 0.9\cdot d_e = 16.57\cdot in$ Effective shear depth.

$V_e := \frac{M_e}{h_c} = 33.6\cdot kip$ Expected peak shear force.

$V_n := \frac{V_e}{\lambda} = 24\cdot kip$ Nominal shear force.

$V_u := \phi\cdot V_n = 18\cdot kip$ Factored shear force.

$v_u := \frac{\left|V_u - \phi\cdot V_p\right|}{\phi\cdot b_v\cdot d_v} = 0.06\cdot ksi$ Shear stress on the concrete section.

$A_g := \left(\frac{\pi}{4}\right)\cdot D_c^{\,2} = 452.39\cdot in^2$ Gross cross-sectional area of column.

$V_{uA} := v_u\cdot A_g = 27.3\cdot kip$ Factored shear force defined by AASHTO.

Step 3.) Determine the maximum and minimum spiral spacing/pitch according to the applicable AASHTO code requirements

Note that according to AASHTO 2012 Sec. 5.10.6.2, spiral reinforcement shall consist of one or more evenly spaced continuous spirals of either deformed or plain bar or wire with a minimum diameter of 0.375 in. Therefore the limits for maximum and minimum spiral reinforcing spacing/pitch for the plastic hinge zone with be applied to the entire length of the column.

$Check\_diameter\_of\_deformed\_bar := \max\left(D_{bt}, 0.375in\right) = 0.375\cdot in$

If the above value is less than 0.375 in, then select a larger bar size for the spiral reinforcement.

A.) Maximum and minimum spiral spacing/pitch according to AASHTO LRFD Bridge Design Specifications 6th Ed Sec. 5.10.6.2

Minimum clear spacing is equal to the lesser of one inch or 1.33 multiplied by the maximum size aggregate.

$c_{smin} := \max(1.0in, 1.33 \cdot MSA) = 1 \cdot in$ Minimum clear spacing of spiral for part A.

$s_{minA} := c_{smin} + D_{bt} = 1.38 \cdot in$ Minimum spiral spacing/pitch for part A.

$s_{maxA} := \min(6.0in, 6.0 \cdot D_{bl}) = 3.75 \cdot in$ Maximum spiral spacing/pitch for part A.

B.) Determine the maximum spiral spacing/pitch according to AASHTO LRFD Bridge Design Specifications 6th Ed Sec. 5.8.2.7

$v_u = 0.06 \cdot ksi$ $0.125 \cdot f'_c = 0.5 \cdot ksi$

$s_{maxB1} := \min(0.8d_v, 24in) = 13.25 \cdot in$ If $v_u < 0.125*f'_c$

$s_{maxB2} := \min(0.4d_v, 12in) = 6.63 \cdot in$ If $v_u >= 0.125*f'_c$

If $v_u < 0.125*f'_c$ set $s_{maxB} = s_{maxB1}$ if not set equal to s_{maxB2}

$s_{maxB} := s_{maxB1} = 13.25 \cdot in$

C.) Determine the maximum spacing/pitch according to AASHTO LRFD Bridge Design Specifications 6th Ed Sec. 5.7.4.6

$D_{cc} := D_c - 2 \cdot c_c = 21.5 \cdot in$ Diameter of core, measure out-to-out of spiral.

$A_c := \frac{\pi \cdot D_{cc}^2}{4} = 363.05 \cdot in^2$ Area of core measured to the outside diameter of the spiral.

$min\_C\_\rho_t := 0.45\left[\left(\frac{A_g}{A_c}\right) - 1\right]\left(\frac{f'_c}{f_{yt}}\right) = 0.007$ Eq. 5.7.4.6-1 for general conditions.

$s_{maxC} := 4 \cdot \frac{A_{st}}{D_{cc} \cdot min\_C\_\rho_t} = 2.77 \cdot in$

D.) Determine the maximum spacing/pitch according to AASHTO LRFD Bridge Design Specifications 6th Ed Sec. 5.10.11.4.1d

$$min\_D\_\rho_t := 0.12\left(\frac{f'_c}{f_{yt}}\right) = 0.008$$

Eq. 5.10.11.4.1d-1 for confinement of plastic hinge zones for seismic zones 3 and 4.

$$s_{maxD} := 4\cdot\frac{A_{st}}{D_{cc}\cdot min\_D\_\rho_t} = 2.56\cdot in$$

E.) Determine the maximum spacing/pitch according to AASHTO LRFD Bridge Design Specifications 6th Ed Sec. 5.8.2.5

$$A_v := n\cdot\left(\frac{\pi}{2}\right)\cdot A_{st} = 0.17\cdot in^2$$

Area of shear reinforcement perpendicular to flexural tension reinforcing.

$$s_{maxE} := \frac{\left(f_{yt}\cdot A_v\right)}{\left(0.0316\cdot\sqrt{psi\cdot f'_c}\cdot b_v\right)} = 216.14\cdot in$$

F.) Determine the maximum spacing/pitch according to AASHTO LRFD Bridge Design Specifications 6th Ed Sec. 5.10.11.4.3

$$s_{maxF} := \min\left(4in, \frac{D_c}{4}\right) = 4\cdot in$$

G.) Determine the maximum spacing/pitch according to AASHTO ASHTO Guide Specifications for LRFD Seismic Bridge Design 2nd Ed. Sec. 8.6.5

$$min\_G\_\rho_t := .005$$

Eq. 8.6.5-3

$$s_{maxG} := 4\cdot\frac{A_{st}}{D_{cc}\cdot min\_G\_\rho_t} = 4.09\cdot in$$

H.) Determine the maximum spacing/pitch according to AASHTO ASHTO Guide Specifications for LRFD Seismic Bridge Design 2nd Ed. Sec. 8.8.9

$$s_{maxH} := \min\left(6\cdot D_{bl}, 6in, \frac{D_c}{5}\right) = 3.75\cdot in$$

I.) Determine the controlling maximum and minimum spiral spacing/pitch from steps A. through H

$s_{min} := s_{minA} = 1.38 \cdot in$

$s_{max} := \min\left(s_{maxA}, s_{maxB}, s_{maxC}, s_{maxD}, s_{maxE}, s_{maxF}, s_{maxG}, s_{maxH}\right) = 2.56 \cdot in$

Step 4.) Calculate V_c according to AASHTO Guide Specifications for LRFD Seismic Bridge Design 2nd Ed. Sec. 8.6.2

guess_s := 2.5in Use the maximum spacing and adjust until the final spacing and this guess are the same value.

$D' := D_c - 2 \cdot c_c - D_{bt} = 21.12 \cdot in$ Cross-section dimension of the confined concrete core measure between the centerline of the spiral.

$guess\_\rho_{st} := 4 \cdot \frac{A_{st}}{guess\_s \cdot D'} = 0.008$ Eq. 8.6.2-6

$A_e := 0.8 \cdot A_g = 361.91 \cdot in^2$ Eq. 8.6.2-2

$f_s := guess\_\rho_{st} \cdot f_{yt} = 0.5 \cdot ksi$ Eq. 8.6.2-6

$\mu_D = 6$ Determined in Sec. 4.9 as the maximum value for a multiple-column bent.

$\alpha' := \left(\frac{f_s}{0.15ksi}\right) + 3.67 - \mu_D = 1$ Eq. 8.6.2-5

$v_c := \min\left[.11 \cdot \sqrt{ksi \cdot f'_c}, 0.047 \cdot \alpha' \cdot \sqrt{ksi \cdot f'_c}, 0.032 \sqrt{ksi \cdot f'_c} \cdot \alpha' \cdot \left[1 + \left(\frac{P \cdot in^2}{2 \cdot A_g \cdot kip}\right)\right]\right] = 71\,psi$

$V_c := \frac{\left(v_c \cdot A_e\right)}{2} = 12.8 \cdot kip$ Eq. 8.6.2-1

The above equation is divided by 2 according to AASHTO LRFD Bridge Design Specifications 6th Ed Sec. 5.10.11.4.1c, since the compression force is equal to 0.05 $f'_c A_g$ which is half the limit.

Step 5.) Calculate the maximum allowed V_s according to AASHTO Guide Specifications for LRFD Seismic Bridge Design 2nd Ed. Sec. 8.6.4

$max\_V_s := 0.25 \cdot A_e \cdot \sqrt{ksi \cdot f'_c} = 181 \cdot kip$ Eq. 8.6.4-1

Step 6.) Calculate V_s according to AASHTO Guide Specifications for LRFD Seismic Bridge Design 2nd Ed. Sec. 8.6.1 and check against the maximum shear reinforcement calculated in step 5.)

$V_s := \left(\frac{V_{uA}}{0.9}\right) - V_c = 17.6 \cdot kip$ Rearranging Eq. 8.6.1-1 and Eq. 8.6.1-2 to solve for V_s

$Check\_V_s := V_s - max\_V_s = -163.4 \cdot kip$ If this value is greater than zero try a smaller spacing/pitch for the initial guess.

Step 7.) Calculate the required spacing/pitch according to AASHTO Guide Specifications for LRFD Seismic Bridge Design 2nd Ed. Sec. 8.6.3

$s_{req} := \frac{\left[\left(\frac{\pi}{2}\right) \cdot n \cdot A_{st} \cdot f_{yt} \cdot D'\right]}{V_s} = 12.48 \cdot in$ Rearranged Eq. 8.6.3-1 to solve for s.

Step 8.) Determine the final spacing/pitch to be used over the entire height of the column and the corresponding transverse reinforcement ratio.

$s_{min} = 1.38 \cdot in$ $s_{max} = 2.56 \cdot in$ $s_{req} = 12.48 \cdot in$ $pitch := 2.50in$

The final spacing/pitch will be set at 2.50 inches to produce a constructible design.

$\rho_t := \frac{\left(4 \cdot A_{st}\right)}{\left(pitch \cdot D_{cc}\right)} = 0.008$ Ratio of spiral reinforcement to total volume of concrete core, measured ou-to-out of spirals.

C2 Spiral Design:

This Mathcad script is for column C2, however the equations and design process are identical for all experimental test columns.

Need to check value according to instructions highlighted.

Input Values.

Step 1.) Adjust input values according to the column properties and loading conditions

Material Properties:

Maximum size aggregate. $MSA := 0.75in$

Diameter of longitudinal reinforcing steel. $D_{bl} := 0.625in$

Nominal concrete compressive strength. $f'_c := 4000psi$

Diameter of transverse reinforcing steel. $D_{bt} := 0.375in$

Yield stress of transverse reinforcement. $f_{yt} := 80ksi$

Cross-sectional area of transverse steel. $A_{st} := 0.11in^2$

Moment over strength factor. $\lambda := 1.4$

Column Properties:

Diameter of column. $D_c := 24in$

Column test height. $h_c := 12ft$

Column clear cover. $c_c := 1.25in$

Effective web width. $b_v := 24in$

Number of spirals within column. $n := 1$

Loading Conditions:

Strength reduction factor defined by AASHTO LRFD BDS Sec. 5.5.4.2.1. $\phi := 0.75$

Prestressing force resisting shear. $V_p := 0kip$

Expected moment capacity. $M_e := 398.6kip \cdot ft$

Applied axial load on column. $P := 90kip$

Global displacement ductility demand ratio. $\mu_D := 6$

Step 2.) Determine the shear force demand according to AASHTO LRFD Bridge Design Specifications 6th Ed. Sec. 5.8.2.9

$D_r := D_c - 2\cdot\left[c_c + D_{bt} + \left(\frac{D_{bl}}{2}\right)\right] = 20.13\cdot in$ — Diameter of the core, taken from center-to-center of the longitudinal reinforcement.

$d_e := \left(\frac{D_c}{2}\right) + \left(\frac{D_r}{\pi}\right) = 18.41\cdot in$ — Defined by AASHTO 2012 C5.8.2.9-2.

$d_v := 0.9\cdot d_e = 16.57\cdot in$ — Effective shear depth.

$V_e := \frac{M_e}{h_c} = 33.2\cdot kip$ — Expected peak shear force.

$V_n := \frac{V_e}{\lambda} = 23.7\cdot kip$ — Nominal shear force.

$V_u := \phi\cdot V_n = 17.8\cdot kip$ — Factored shear force.

$v_u := \frac{\left|V_u - \phi\cdot V_p\right|}{\phi\cdot b_v\cdot d_v} = 0.06\cdot ksi$ — Shear stress on the concrete section.

$A_g := \left(\frac{\pi}{4}\right)\cdot {D_c}^2 = 452.39\cdot in^2$ — Gross cross-sectional area of column.

$V_{uA} := v_u\cdot A_g = 27\cdot kip$ — Factored shear force defined by AASHTO.

Step 3.) Determine the maximum and minimum spiral spacing/pitch according to the applicable AASHTO code requirements

Note that according to AASHTO 2012 Sec. 5.10.6.2, spiral reinforcement shall consist of one or more evenly spaced continuous spirals of either deformed or plain bar or wire with a minimum diameter of 0.375 in. Therefore the limits for maximum and minimum spiral reinforcing spacing/pitch for the plastic hinge zone with be applied to the entire length of the column.

$Check\_diameter\_of\_deformed\_bar := \max\left(D_{bt}, 0.375in\right) = 0.375\cdot in$

If the above value is less than 0.375 in, then select a larger bar size for the spiral reinforcement.

A.) Maximum and minimum spiral spacing/pitch according to AASHTO LRFD Bridge Design Specifications 6th Ed Sec. 5.10.6.2

Minimum clear spacing is equal to the lesser of one inch or 1.33 multiplied by the maximum size aggregate.

$c_{smin} := \max(1.0in, 1.33 \cdot MSA) = 1 \cdot in$ Minimum clear spacing of spiral for part A.

$s_{minA} := c_{smin} + D_{bt} = 1.38 \cdot in$ Minimum spiral spacing/pitch for part A.

$s_{maxA} := \min(6.0in, 6.0 \cdot D_{bl}) = 3.75 \cdot in$ Maximum spiral spacing/pitch for part A.

B.) Determine the maximum spiral spacing/pitch according to AASHTO LRFD Bridge Design Specifications 6th Ed Sec. 5.8.2.7

$v_u = 0.06 \cdot ksi$ $0.125 \cdot f'_c = 0.5 \cdot ksi$

$s_{maxB1} := \min(0.8d_v, 24in) = 13.25 \cdot in$ If $v_u < 0.125 * f'_c$

$s_{maxB2} := \min(0.4d_v, 12in) = 6.63 \cdot in$ If $v_u >= 0.125 * f'_c$

If $v_u < 0.125 * f'_c$ set $s_{maxB} = s_{maxB1}$ if not set equal to s_{maxB2}

$s_{maxB} := s_{maxB1} = 13.25 \cdot in$

C.) Determine the maximum spacing/pitch according to AASHTO LRFD Bridge Design Specifications 6th Ed Sec. 5.7.4.6

$D_{cc} := D_c - 2 \cdot c_c = 21.5 \cdot in$ Diameter of core, measure out-to-out of spiral.

$A_c := \frac{\pi \cdot D_{cc}^2}{4} = 363.05 \cdot in^2$ Area of core measured to the outside diameter of the spiral.

$min\_C\_\rho_t := 0.45\left[\left(\frac{A_g}{A_c}\right) - 1\right]\left(\frac{f'_c}{f_{yt}}\right) = 0.006$ Eq. 5.7.4.6-1 for general conditions.

$s_{maxC} := 4 \cdot \frac{A_{st}}{D_{cc} \cdot min\_C\_\rho_t} = 3.7 \cdot in$

D.) Determine the maximum spacing/pitch according to AASHTO LRFD Bridge Design Specifications 6th Ed Sec. 5.10.11.4.1d

$$min\_D\_\rho_t := 0.12\left(\frac{f'_c}{f_{yt}}\right) = 0.006$$

Eq. 5.10.11.4.1d-1 for confinement of plastic hinge zones for seismic zones 3 and 4.

$$s_{maxD} := 4\cdot\frac{A_{st}}{D_{cc}\cdot min\_D\_\rho_t} = 3.41\cdot in$$

E.) Determine the maximum spacing/pitch according to AASHTO LRFD Bridge Design Specifications 6th Ed Sec. 5.8.2.5

$$A_v := n\cdot\left(\frac{\pi}{2}\right)\cdot A_{st} = 0.17\cdot in^2$$

Area of shear reinforcement perpendicular to flexural tension reinforcing.

$$s_{maxE} := \frac{\left(f_{yt}\cdot A_v\right)}{\left(0.0316\cdot\sqrt{psi\cdot f'_c}\cdot b_v\right)} = 288.187\cdot in$$

F.) Determine the maximum spacing/pitch according to AASHTO LRFD Bridge Design Specifications 6th Ed Sec. 5.10.11.4.3

$$s_{maxF} := \min\left(4in, \frac{D_c}{4}\right) = 4\cdot in$$

G.) Determine the maximum spacing/pitch according to AASHTO ASHTO Guide Specifications for LRFD Seismic Bridge Design 2nd Ed. Sec. 8.6.5

$$min\_G\_\rho_t := .005$$

Eq. 8.6.5-3

$$s_{maxG} := 4\cdot\frac{A_{st}}{D_{cc}\cdot min\_G\_\rho_t} = 4.09\cdot in$$

H.) Determine the maximum spacing/pitch according to AASHTO ASHTO Guide Specifications for LRFD Seismic Bridge Design 2nd Ed. Sec. 8.8.9

$$s_{maxH} := \min\left(6\cdot D_{bl}, 6in, \frac{D_c}{5}\right) = 3.75\cdot in$$

I.) Determine the controlling maximum and minimum spiral spacing/pitch from steps A. through H

$s_{min} := s_{minA} = 1.38 \cdot in$

$s_{max} := \min\left(s_{maxA}, s_{maxB}, s_{maxC}, s_{maxD}, s_{maxE}, s_{maxF}, s_{maxG}, s_{maxH}\right) = 3.41 \cdot in$

Step 4.) Calculate V_c according to AASHTO Guide Specifications for LRFD Seismic Bridge Design 2nd Ed. Sec. 8.6.2

guess_s := 2.5in Use the maximum spacing and adjust until the final spacing and this guess are the same value.

$D' := D_c - 2 \cdot c_c - D_{bt} = 21.12 \cdot in$ Cross-section dimension of the confined concrete core measure between the centerline of the spiral.

$guess\_\rho_{st} := 4 \cdot \frac{A_{st}}{guess\_s \cdot D'} = 0.008$ Eq. 8.6.2-6

$A_e := 0.8 \cdot A_g = 361.91 \cdot in^2$ Eq. 8.6.2-2

$f_s := guess\_\rho_{st} \cdot f_{yt} = 0.667 \cdot ksi$ Eq. 8.6.2-6

$\mu_D = 6$ Determined in Sec. 4.9 as the maximum value for a multiple-column bent.

$\alpha' := \left(\frac{f_s}{0.15ksi}\right) + 3.67 - \mu_D = 2.1$ Eq. 8.6.2-5

$v_c := \min\left[.11 \cdot \sqrt{ksi \cdot f'_c}, 0.047 \cdot \alpha' \cdot \sqrt{ksi \cdot f'_c}, 0.032 \sqrt{ksi \cdot f'_c} \cdot \alpha' \cdot \left[1 + \left(\frac{P \cdot in^2}{2 \cdot A_g \cdot kip}\right)\right]\right] = 149\,psi$

$V_c := \frac{\left(v_c \cdot A_e\right)}{2} = 26.9 \cdot kip$ Eq. 8.6.2-1

The above equation is divided by 2 according to AASHTO LRFD Bridge Design Specifications 6th Ed Sec. 5.10.11.4.1c, since the compression force is equal to 0.05 $f'_c A_g$ which is half the limit.

Step 5.) Calculate the maximum allowed V_s according to AASHTO Guide Specifications for LRFD Seismic Bridge Design 2nd Ed. Sec. 8.6.4

$max\_V_s := 0.25 \cdot A_e \cdot \sqrt{ksi \cdot f'_c} = 181 \cdot kip$ Eq. 8.6.4-1

Step 6.) Calculate V_s according to AASHTO Guide Specifications for LRFD Seismic Bridge Design 2nd Ed. Sec. 8.6.1 and check against the maximum shear reinforcement calculated in step 5.)

$V_s := \left(\frac{V_{uA}}{0.9}\right) - V_c = 3.1 \cdot kip$ Rearranging Eq. 8.6.1-1 and Eq. 8.6.1-2 to solve for V_s

$Check\_V_s := V_s - max\_V_s = -177.9 \cdot kip$ If this value is greater than zero try a smaller spacing/pitch for the initial guess.

Step 7.) Calculate the required spacing/pitch according to AASHTO Guide Specifications for LRFD Seismic Bridge Design 2nd Ed. Sec. 8.6.3

$s_{req} := \frac{\left[\left(\frac{\pi}{2}\right) \cdot n \cdot A_{st} \cdot f_{yt} \cdot D'\right]}{V_s} = 94.58 \cdot in$ Rearranged Eq. 8.6.3-1 to solve for s.

Step 8.) Determine the final spacing/pitch to be used over the entire height of the column and the corresponding transverse reinforcement ratio.

$s_{min} = 1.38 \cdot in$ $s_{max} = 3.41 \cdot in$ $s_{req} = 94.58 \cdot in$ $pitch := 2.50in$

The final spacing/pitch will be set at 2.50 inches to produce a constructible design.

$\rho_t := \frac{\left(4 \cdot A_{st}\right)}{\left(pitch \cdot D_{cc}\right)} = 0.008$ Ratio of spiral reinforcement to total volume of concrete core, measured ou-to-out of spirals.

C3 Spiral Design:

This Mathcad script is for column C3, however the equations and design process are identical for all experimental test columns.

Need to check value according to instructions highlighted.

Input Values.

Step 1.) Adjust input values according to the column properties and loading conditions

Material Properties:

Maximum size aggregate. $MSA := 0.75in$

Diameter of longitudinal reinforcing steel. $D_{bl} := 0.625in$

Nominal concrete compressive strength. $f'_c := 4000psi$

Diameter of transverse reinforcing steel. $D_{bt} := 0.375in$

Yield stress of transverse reinforcement. $f_{yt} := 80ksi$

Cross-sectional area of transverse steel. $A_{st} := 0.11in^2$

Moment over strength factor. $\lambda := 1.4$

Column Properties:

Diameter of column. $D_c := 24in$

Column test height. $h_c := 12ft$

Column clear cover. $c_c := 1.25in$

Effective web width. $b_v := 24in$

Number of spirals within column. $n := 1$

Loading Conditions:

Strength reduction factor defined by AASHTO LRFD BDS Sec. 5.5.4.2.1. $\phi := 0.75$

Prestressing force resisting shear. $V_p := 0kip$

Expected moment capacity. $M_e := 398.6kip \cdot ft$

Applied axial load on column. $P := 90kip$

Global displacement ductility demand ratio. $\mu_D := 6$

Step 2.) Determine the shear force demand according to AASHTO LRFD Bridge Design Specifications 6th Ed. Sec. 5.8.2.9

$D_r := D_c - 2\cdot\left[c_c + D_{bt} + \left(\frac{D_{bl}}{2}\right)\right] = 20.13\cdot in$ Diameter of the core, taken from center-to-center of the longitudinal reinforcement.

$d_e := \left(\frac{D_c}{2}\right) + \left(\frac{D_r}{\pi}\right) = 18.41\cdot in$ Defined by AASHTO 2012 C5.8.2.9-2.

$d_v := 0.9\cdot d_e = 16.57\cdot in$ Effective shear depth.

$V_e := \frac{M_e}{h_c} = 33.2\cdot kip$ Expected peak shear force.

$V_n := \frac{V_e}{\lambda} = 23.7\cdot kip$ Nominal shear force.

$V_u := \phi\cdot V_n = 17.8\cdot kip$ Factored shear force.

$v_u := \frac{\left|V_u - \phi\cdot V_p\right|}{\phi\cdot b_v\cdot d_v} = 0.06\cdot ksi$ Shear stress on the concrete section.

$A_g := \left(\frac{\pi}{4}\right)\cdot D_c^{\,2} = 452.39\cdot in^2$ Gross cross-sectional area of column.

$V_{uA} := v_u\cdot A_g = 27\cdot kip$ Factored shear force defined by AASHTO.

Step 3.) Determine the maximum and minimum spiral spacing/pitch according to the applicable AASHTO code requirements

Note that according to AASHTO 2012 Sec. 5.10.6.2, spiral reinforcement shall consist of one or more evenly spaced continuous spirals of either deformed or plain bar or wire with a minimum diameter of 0.375 in. Therefore the limits for maximum and minimum spiral reinforcing spacing/pitch for the plastic hinge zone with be applied to the entire length of the column.

$Check\_diameter\_of\_deformed\_bar := \max\left(D_{bt}, 0.375in\right) = 0.375\cdot in$

If the above value is less than 0.375 in, then select a larger bar size for the spiral reinforcement.

A.) Maximum and minimum spiral spacing/pitch according to AASHTO LRFD Bridge Design Specifications 6th Ed Sec. 5.10.6.2

Minimum clear spacing is equal to the lesser of one inch or 1.33 multiplied by the maximum size aggregate.

$c_{smin} := \max(1.0in, 1.33 \cdot MSA) = 1 \cdot in$ Minimum clear spacing of spiral for part A.

$s_{minA} := c_{smin} + D_{bt} = 1.38 \cdot in$ Minimum spiral spacing/pitch for part A.

$s_{maxA} := \min(6.0in, 6.0 \cdot D_{bl}) = 3.75 \cdot in$ Maximum spiral spacing/pitch for part A.

B.) Determine the maximum spiral spacing/pitch according to AASHTO LRFD Bridge Design Specifications 6th Ed Sec. 5.8.2.7

$v_u = 0.06 \cdot ksi$ $0.125 \cdot f'_c = 0.5 \cdot ksi$

$s_{maxB1} := \min(0.8d_v, 24in) = 13.25 \cdot in$ If $v_u < 0.125 * f'_c$

$s_{maxB2} := \min(0.4d_v, 12in) = 6.63 \cdot in$ If $v_u >= 0.125 * f'_c$

If $v_u < 0.125 * f'_c$ set $s_{maxB} = s_{maxB1}$ if not set equal to s_{maxB2}

$s_{maxB} := s_{maxB1} = 13.25 \cdot in$

C.) Determine the maximum spacing/pitch according to AASHTO LRFD Bridge Design Specifications 6th Ed Sec. 5.7.4.6

$D_{cc} := D_c - 2 \cdot c_c = 21.5 \cdot in$ Diameter of core, measure out-to-out of spiral.

$A_c := \frac{\pi \cdot D_{cc}^2}{4} = 363.05 \cdot in^2$ Area of core measured to the outside diameter of the spiral.

$min\_C\_\rho_t := 0.45\left[\left(\frac{A_g}{A_c}\right) - 1\right]\left(\frac{f'_c}{f_{yt}}\right) = 0.006$ Eq. 5.7.4.6-1 for general conditions.

$s_{maxC} := 4 \cdot \frac{A_{st}}{D_{cc} \cdot min\_C\_\rho_t} = 3.7 \cdot in$

D.) Determine the maximum spacing/pitch according to AASHTO LRFD Bridge Design Specifications 6th Ed Sec. 5.10.11.4.1d

$$min\_D\_\rho_t := 0.12\left(\frac{f'_c}{f_{yt}}\right) = 0.006$$

Eq. 5.10.11.4.1d-1 for confinement of plastic hinge zones for seismic zones 3 and 4.

$$s_{maxD} := 4\cdot\frac{A_{st}}{D_{cc}\cdot min\_D\_\rho_t} = 3.41\cdot in$$

E.) Determine the maximum spacing/pitch according to AASHTO LRFD Bridge Design Specifications 6th Ed Sec. 5.8.2.5

$$A_v := n\cdot\left(\frac{\pi}{2}\right)\cdot A_{st} = 0.17\cdot in^2$$

Area of shear reinforcement perpendicular to flexural tension reinforcing.

$$s_{maxE} := \frac{\left(f_{yt}\cdot A_v\right)}{\left(0.0316\cdot\sqrt{psi\cdot f'_c}\cdot b_v\right)} = 288.187\cdot in$$

F.) Determine the maximum spacing/pitch according to AASHTO LRFD Bridge Design Specifications 6th Ed Sec. 5.10.11.4.3

$$s_{maxF} := \min\left(4in, \frac{D_c}{4}\right) = 4\cdot in$$

G.) Determine the maximum spacing/pitch according to AASHTO ASHTO Guide Specifications for LRFD Seismic Bridge Design 2nd Ed. Sec. 8.6.5

$$min\_G\_\rho_t := .005$$

Eq. 8.6.5-3

$$s_{maxG} := 4\cdot\frac{A_{st}}{D_{cc}\cdot min\_G\_\rho_t} = 4.09\cdot in$$

H.) Determine the maximum spacing/pitch according to AASHTO ASHTO Guide Specifications for LRFD Seismic Bridge Design 2nd Ed. Sec. 8.8.9

$$s_{maxH} := \min\left(6\cdot D_{bl}, 6in, \frac{D_c}{5}\right) = 3.75\cdot in$$

I.) Determine the controlling maximum and minimum spiral spacing/pitch from steps A. through H

$s_{min} := s_{minA} = 1.38 \cdot in$

$s_{max} := \min(s_{maxA}, s_{maxB}, s_{maxC}, s_{maxD}, s_{maxE}, s_{maxF}, s_{maxG}, s_{maxH}) = 3.41 \cdot in$

Step 4.) Calculate V_c according to AASHTO Guide Specifications for LRFD Seismic Bridge Design 2nd Ed. Sec. 8.6.2

guess_s := 2.5in Use the maximum spacing and adjust until the final spacing and this guess are the same value.

$D' := D_c - 2 \cdot c_c - D_{bt} = 21.12 \cdot in$ Cross-section dimension of the confined concrete core measure between the centerline of the spiral.

$guess\_\rho_{st} := 4 \cdot \frac{A_{st}}{guess\_s \cdot D'} = 0.008$ Eq. 8.6.2-6

$A_e := 0.8 \cdot A_g = 361.91 \cdot in^2$ Eq. 8.6.2-2

$f_s := guess\_\rho_{st} \cdot f_{yt} = 0.667 \cdot ksi$ Eq. 8.6.2-6

$\mu_D = 6$ Determined in Sec. 4.9 as the maximum value for a multiple-column bent.

$\alpha' := \left(\frac{f_s}{0.15ksi}\right) + 3.67 - \mu_D = 2.1$ Eq. 8.6.2-5

$v_c := \min\left[.11 \cdot \sqrt{ksi \cdot f'_c}, 0.047 \cdot \alpha' \cdot \sqrt{ksi \cdot f'_c}, 0.032 \sqrt{ksi \cdot f'_c} \cdot \alpha' \cdot \left[1 + \left(\frac{P \cdot in^2}{2 \cdot A_g \cdot kip}\right)\right]\right] = 149\,psi$

$V_c := \frac{(v_c \cdot A_e)}{2} = 26.9 \cdot kip$ Eq. 8.6.2-1

The above equation is divided by 2 according to AASHTO LRFD Bridge Design Specifications 6th Ed Sec. 5.10.11.4.1c, since the compression force is equal to 0.05 f'_c A_g which is half the limit.

Step 5.) Calculate the maximum allowed V_s according to AASHTO Guide Specifications for LRFD Seismic Bridge Design 2nd Ed. Sec. 8.6.4

$max\_V_s := 0.25 \cdot A_e \cdot \sqrt{ksi \cdot f'_c} = 181 \cdot kip$ Eq. 8.6.4-1

Step 6.) Calculate V_s according to AASHTO Guide Specifications for LRFD Seismic Bridge Design 2nd Ed. Sec. 8.6.1 and check against the maximum shear reinforcement calculated in step 5.)

$V_s := \left(\frac{V_{uA}}{0.9}\right) - V_c = 3.1 \cdot kip$ Rearranging Eq. 8.6.1-1 and Eq. 8.6.1-2 to solve for V_s

$Check\_V_s := V_s - max\_V_s = -177.9 \cdot kip$ If this value is greater than zero try a smaller spacing/pitch for the initial guess.

Step 7.) Calculate the required spacing/pitch according to AASHTO Guide Specifications for LRFD Seismic Bridge Design 2nd Ed. Sec. 8.6.3

$s_{req} := \frac{\left[\left(\frac{\pi}{2}\right) \cdot n \cdot A_{st} \cdot f_{yt} \cdot D'\right]}{V_s} = 94.58 \cdot in$ Rearranged Eq. 8.6.3-1 to solve for s.

Step 8.) Determine the final spacing/pitch to be used over the entire height of the column and the corresponding transverse reinforcement ratio.

$s_{min} = 1.38 \cdot in$ $s_{max} = 3.41 \cdot in$ $s_{req} = 94.58 \cdot in$ $pitch := 2.50in$

The final spacing/pitch will be set at 2.50 inches to produce a constructible design.

$\rho_t := \frac{(4 \cdot A_{st})}{(pitch \cdot D_{cc})} = 0.008$ Ratio of spiral reinforcement to total volume of concrete core, measured ou-to-out of spirals.

C4 Spiral Design:

This Mathcad script is for column C4, however the equations and design process are identical for all experimental test columns.

Need to check value according to instructions highlighted.

Input Values.

Step 1.) Adjust input values according to the column properties and loading conditions

Material Properties:

Maximum size aggregate. $MSA := 0.75in$

Diameter of longitudinal reinforcing steel. $D_{bl} := 0.75in$

Nominal concrete compressive strength. $f'_c := 4000psi$

Diameter of transverse reinforcing steel. $D_{bt} := 0.375in$

Yield stress of transverse reinforcement. $f_{yt} := 80ksi$

Cross-sectional area of transverse steel. $A_{st} := 0.11in^2$

Moment over strength factor. $\lambda := 1.4$

Column Properties:

Diameter of column. $D_c := 24in$

Column test height. $h_c := 12ft$

Column clear cover. $c_c := 1.25in$

Effective web width. $b_v := 24in$

Number of spirals within column. $n := 1$

Loading Conditions:

Strength reduction factor defined by AASHTO LRFD BDS Sec. 5.5.4.2.1. $\phi := 0.75$

Prestressing force resisting shear. $V_p := 0kip$

Expected moment capacity. $M_e := 627.5kip \cdot ft$

Applied axial load on column. $P := 90kip$

Global displacement ductility demand ratio. $\mu_D := 6$

Step 2.) Determine the shear force demand according to AASHTO LRFD Bridge Design Specifications 6th Ed. Sec. 5.8.2.9

$D_r := D_c - 2\cdot\left[c_c + D_{bt} + \left(\frac{D_{bl}}{2}\right)\right] = 20\cdot in$ — Diameter of the core, taken from center-to-center of the longitudinal reinforcement.

$d_e := \left(\frac{D_c}{2}\right) + \left(\frac{D_r}{\pi}\right) = 18.37\cdot in$ — Defined by AASHTO 2012 C5.8.2.9-2.

$d_v := 0.9\cdot d_e = 16.53\cdot in$ — Effective shear depth.

$V_e := \frac{M_e}{h_c} = 52.3\cdot kip$ — Expected peak shear force.

$V_n := \frac{V_e}{\lambda} = 37.4\cdot kip$ — Nominal shear force.

$V_u := \phi\cdot V_n = 28\cdot kip$ — Factored shear force.

$v_u := \frac{\left|V_u - \phi\cdot V_p\right|}{\phi\cdot b_v\cdot d_v} = 0.094\cdot ksi$ — Shear stress on the concrete section.

$A_g := \left(\frac{\pi}{4}\right)\cdot D_c^{\,2} = 452.39\cdot in^2$ — Gross cross-sectional area of column.

$V_{uA} := v_u\cdot A_g = 42.6\cdot kip$ — Factored shear force defined by AASHTO.

Step 3.) Determine the maximum and minimum spiral spacing/pitch according to the applicable AASHTO code requirements

Note that according to AASHTO 2012 Sec. 5.10.6.2, spiral reinforcement shall consist of one or more evenly spaced continuous spirals of either deformed or plain bar or wire with a minimum diameter of 0.375 in. Therefore the limits for maximum and minimum spiral reinforcing spacing/pitch for the plastic hinge zone with be applied to the entire length of the column.

$Check\_diameter\_of\_deformed\_bar := \max\left(D_{bt}, 0.375in\right) = 0.375\cdot in$

If the above value is less than 0.375 in, then select a larger bar size for the spiral reinforcement.

A.) Maximum and minimum spiral spacing/pitch according to AASHTO LRFD Bridge Design Specifications 6th Ed Sec. 5.10.6.2

Minimum clear spacing is equal to the lesser of one inch or 1.33 multiplied by the maximum size aggregate.

$c_{smin} := \max(1.0in, 1.33 \cdot MSA) = 1 \cdot in$ Minimum clear spacing of spiral for part A.

$s_{minA} := c_{smin} + D_{bt} = 1.38 \cdot in$ Minimum spiral spacing/pitch for part A.

$s_{maxA} := \min(6.0in, 6.0 \cdot D_{bl}) = 4.5 \cdot in$ Maximum spiral spacing/pitch for part A.

B.) Determine the maximum spiral spacing/pitch according to AASHTO LRFD Bridge Design Specifications 6th Ed Sec. 5.8.2.7

$v_u = 0.094 \cdot ksi$ $0.125 \cdot f'_c = 0.5 \cdot ksi$

$s_{maxB1} := \min(0.8d_v, 24in) = 13.22 \cdot in$ If $v_u < 0.125*f'_c$

$s_{maxB2} := \min(0.4d_v, 12in) = 6.61 \cdot in$ If $v_u >= 0.125*f'_c$

If $v_u < 0.125*f'_c$ set $s_{maxB} = s_{maxB1}$ if not set equal to s_{maxB2}

$s_{maxB} := s_{maxB1} = 13.22 \cdot in$

C.) Determine the maximum spacing/pitch according to AASHTO LRFD Bridge Design Specifications 6th Ed Sec. 5.7.4.6

$D_{cc} := D_c - 2 \cdot c_c = 21.5 \cdot in$ Diameter of core, measure out-to-out of spiral.

$A_c := \frac{\pi \cdot D_{cc}^2}{4} = 363.05 \cdot in^2$ Area of core measured to the outside diameter of the spiral.

$min\_C\_\rho_t := 0.45\left[\left(\frac{A_g}{A_c}\right) - 1\right]\left(\frac{f'_c}{f_{yt}}\right) = 0.006$ Eq. 5.7.4.6-1 for general conditions.

$s_{maxC} := 4 \cdot \frac{A_{st}}{D_{cc} \cdot min\_C\_\rho_t} = 3.7 \cdot in$

D.) Determine the maximum spacing/pitch according to AASHTO LRFD Bridge Design Specifications 6th Ed Sec. 5.10.11.4.1d

$$min\_D\_\rho_t := 0.12\left(\frac{f'_c}{f_{yt}}\right) = 0.006$$

Eq. 5.10.11.4.1d-1 for confinement of plastic hinge zones for seismic zones 3 and 4.

$$s_{maxD} := 4\cdot\frac{A_{st}}{D_{cc}\cdot min\_D\_\rho_t} = 3.41\cdot in$$

E.) Determine the maximum spacing/pitch according to AASHTO LRFD Bridge Design Specifications 6th Ed Sec. 5.8.2.5

$$A_v := n\cdot\left(\frac{\pi}{2}\right)\cdot A_{st} = 0.17\cdot in^2$$

Area of shear reinforcement perpendicular to flexural tension reinforcing.

$$s_{maxE} := \frac{\left(f_{yt}\cdot A_v\right)}{\left(0.0316\cdot\sqrt{psi\cdot f'_c}\cdot b_v\right)} = 288.187\cdot in$$

F.) Determine the maximum spacing/pitch according to AASHTO LRFD Bridge Design Specifications 6th Ed Sec. 5.10.11.4.3

$$s_{maxF} := \min\left(4in, \frac{D_c}{4}\right) = 4\cdot in$$

G.) Determine the maximum spacing/pitch according to AASHTO ASHTO Guide Specifications for LRFD Seismic Bridge Design 2nd Ed. Sec. 8.6.5

$$min\_G\_\rho_t := .005$$

Eq. 8.6.5-3

$$s_{maxG} := 4\cdot\frac{A_{st}}{D_{cc}\cdot min\_G\_\rho_t} = 4.09\cdot in$$

H.) Determine the maximum spacing/pitch according to AASHTO ASHTO Guide Specifications for LRFD Seismic Bridge Design 2nd Ed. Sec. 8.8.9

$$s_{maxH} := \min\left(6\cdot D_{bl}, 6in, \frac{D_c}{5}\right) = 4.5\cdot in$$

I.) Determine the controlling maximum and minimum spiral spacing/pitch from steps A. through H

$s_{min} := s_{minA} = 1.38 \cdot in$

$s_{max} := \min(s_{maxA}, s_{maxB}, s_{maxC}, s_{maxD}, s_{maxE}, s_{maxF}, s_{maxG}, s_{maxH}) = 3.41 \cdot in$

Step 4.) Calculate V_c according to AASHTO Guide Specifications for LRFD Seismic Bridge Design 2nd Ed. Sec. 8.6.2

guess_s := 2.5in Use the maximum spacing and adjust until the final spacing and this guess are the same value.

$D' := D_c - 2 \cdot c_c - D_{bt} = 21.12 \cdot in$ Cross-section dimension of the confined concrete core measure between the centerline of the spiral.

$guess\_\rho_{st} := 4 \cdot \frac{A_{st}}{guess\_s \cdot D'} = 0.008$ Eq. 8.6.2-6

$A_e := 0.8 \cdot A_g = 361.91 \cdot in^2$ Eq. 8.6.2-2

$f_s := guess\_\rho_{st} \cdot f_{yt} = 0.667 \cdot ksi$ Eq. 8.6.2-6

$\mu_D = 6$ Determined in Sec. 4.9 as the maximum value for a multiple-column bent.

$\alpha' := \left(\frac{f_s}{0.15ksi}\right) + 3.67 - \mu_D = 2.1$ Eq. 8.6.2-5

$v_c := \min\left[.11 \cdot \sqrt{ksi \cdot f'_c}, 0.047 \cdot \alpha' \cdot \sqrt{ksi \cdot f'_c}, 0.032 \sqrt{ksi \cdot f'_c} \cdot \alpha' \cdot \left[1 + \left(\frac{P \cdot in^2}{2 \cdot A_g \cdot kip}\right)\right]\right] = 149\,psi$

$V_c := \frac{(v_c \cdot A_e)}{2} = 26.9 \cdot kip$ Eq. 8.6.2-1

The above equation is divided by 2 according to AASHTO LRFD Bridge Design Specifications 6th Ed Sec. 5.10.11.4.1c, since the compression force is equal to 0.05 f'_c A_g which is half the limit.

Step 5.) Calculate the maximum allowed V_s according to AASHTO Guide Specifications for LRFD Seismic Bridge Design 2nd Ed. Sec. 8.6.4

$max\_V_s := 0.25 \cdot A_e \cdot \sqrt{ksi \cdot f'_c} = 181 \cdot kip$ Eq. 8.6.4-1

Step 6.) Calculate V_s according to AASHTO Guide Specifications for LRFD Seismic Bridge Design 2nd Ed. Sec. 8.6.1 and check against the maximum shear reinforcement calculated in step 5.)

$V_s := \left(\frac{V_{uA}}{0.9}\right) - V_c = 20.4 \cdot kip$ Rearranging Eq. 8.6.1-1 and Eq. 8.6.1-2 to solve for V_s

$Check\_V_s := V_s - max\_V_s = -160.5 \cdot kip$ If this value is greater than zero try a smaller spacing/pitch for the initial guess.

Step 7.) Calculate the required spacing/pitch according to AASHTO Guide Specifications for LRFD Seismic Bridge Design 2nd Ed. Sec. 8.6.3

$s_{req} := \frac{\left[\left(\frac{\pi}{2}\right) \cdot n \cdot A_{st} \cdot f_{yt} \cdot D'\right]}{V_s} = 14.3 \cdot in$ Rearranged Eq. 8.6.3-1 to solve for s.

Step 8.) Determine the final spacing/pitch to be used over the entire height of the column and the corresponding transverse reinforcement ratio.

$s_{min} = 1.38 \cdot in$ $s_{max} = 3.41 \cdot in$ $s_{req} = 14.3 \cdot in$ $pitch := 2.50in$

The final spacing/pitch will be set at 2.50 inches to produce a constructible design.

$\rho_t := \frac{\left(4 \cdot A_{st}\right)}{\left(pitch \cdot D_{cc}\right)} = 0.008$ Ratio of spiral reinforcement to total volume of concrete core, measured ou-to-out of spirals.

C5 Spiral Design:

This Mathcad script is for column C5, however the equations and design process are identical for all experimental test columns.

Need to check value according to instructions highlighted.

Input Values.

Step 1.) Adjust input values according to the column properties and loading conditions

Material Properties:

Maximum size aggregate. $MSA := 0.75in$

Diameter of longitudinal reinforcing steel. $D_{bl} := 0.75in$

Nominal concrete compressive strength. $f'_c := 4000psi$

Diameter of transverse reinforcing steel. $D_{bt} := 0.375in$

Yield stress of transverse reinforcement. $f_{yt} := 60ksi$

Cross-sectional area of transverse steel. $A_{st} := 0.11in^2$

Moment over strength factor. $\lambda := 1.4$

Column Properties:

Diameter of column. $D_c := 24in$

Column test height. $h_c := 6ft$

Column clear cover. $c_c := 1.25in$

Effective web width. $b_v := 24in$

Number of spirals within column. $n := 1$

Loading Conditions:

Strength reduction factor defined by AASHTO LRFD BDS Sec. 5.5.4.2.1. $\phi := 0.75$

Prestressing force resisting shear. $V_p := 0kip$

Expected moment capacity. $M_e := 648.5kip \cdot ft$

Applied axial load on column. $P := 90kip$

Global displacement ductility demand ratio. $\mu_D := 6$

Step 2.) Determine the shear force demand according to AASHTO LRFD Bridge Design Specifications 6th Ed. Sec. 5.8.2.9

$D_r := D_c - 2\cdot\left[c_c + D_{bt} + \left(\frac{D_{bl}}{2}\right)\right] = 20\cdot in$ — Diameter of the core, taken from center-to-center of the longitudinal reinforcement.

$d_e := \left(\frac{D_c}{2}\right) + \left(\frac{D_r}{\pi}\right) = 18.37\cdot in$ — Defined by AASHTO 2012 C5.8.2.9-2.

$d_v := 0.9\cdot d_e = 16.53\cdot in$ — Effective shear depth.

$V_e := \frac{M_e}{h_c} = 108.1\cdot kip$ — Expected peak shear force.

$V_n := \frac{V_e}{\lambda} = 77.2\cdot kip$ — Nominal shear force.

$V_u := \phi\cdot V_n = 57.9\cdot kip$ — Factored shear force.

$v_u := \frac{\left|V_u - \phi\cdot V_p\right|}{\phi\cdot b_v\cdot d_v} = 0.195\cdot ksi$ — Shear stress on the concrete section.

$A_g := \left(\frac{\pi}{4}\right)\cdot D_c^{\,2} = 452.39\cdot in^2$ — Gross cross-sectional area of column.

$V_{uA} := v_u\cdot A_g = 88\cdot kip$ — Factored shear force defined by AASHTO.

Step 3.) Determine the maximum and minimum spiral spacing/pitch according to the applicable AASHTO code requirements

Note that according to AASHTO 2012 Sec. 5.10.6.2, spiral reinforcement shall consist of one or more evenly spaced continuous spirals of either deformed or plain bar or wire with a minimum diameter of 0.375 in. Therefore the limits for maximum and minimum spiral reinforcing spacing/pitch for the plastic hinge zone with be applied to the entire length of the column.

$Check\_diameter\_of\_deformed\_bar := \max\left(D_{bt}, 0.375in\right) = 0.375\cdot in$

If the above value is less than 0.375 in, then select a larger bar size for the spiral reinforcement.

A.) Maximum and minimum spiral spacing/pitch according to AASHTO LRFD Bridge Design Specifications 6th Ed Sec. 5.10.6.2

Minimum clear spacing is equal to the lesser of one inch or 1.33 multiplied by the maximum size aggregate.

$c_{smin} := \max(1.0in, 1.33 \cdot MSA) = 1 \cdot in$ Minimum clear spacing of spiral for part A.

$s_{minA} := c_{smin} + D_{bt} = 1.38 \cdot in$ Minimum spiral spacing/pitch for part A.

$s_{maxA} := \min(6.0in, 6.0 \cdot D_{bl}) = 4.5 \cdot in$ Maximum spiral spacing/pitch for part A.

B.) Determine the maximum spiral spacing/pitch according to AASHTO LRFD Bridge Design Specifications 6th Ed Sec. 5.8.2.7

$v_u = 0.195 \cdot ksi$ $0.125 \cdot f'_c = 0.5 \cdot ksi$

$s_{maxB1} := \min(0.8d_v, 24in) = 13.22 \cdot in$ If $v_u < 0.125*f'_c$

$s_{maxB2} := \min(0.4d_v, 12in) = 6.61 \cdot in$ If $v_u >= 0.125*f'_c$

If $v_u < 0.125*f'_c$ set $s_{maxB} = s_{maxB1}$ if not set equal to s_{maxB2}

$s_{maxB} := s_{maxB1} = 13.22 \cdot in$

C.) Determine the maximum spacing/pitch according to AASHTO LRFD Bridge Design Specifications 6th Ed Sec. 5.7.4.6

$D_{cc} := D_c - 2 \cdot c_c = 21.5 \cdot in$ Diameter of core, measure out-to-out of spiral.

$A_c := \frac{\pi \cdot D_{cc}^2}{4} = 363.05 \cdot in^2$ Area of core measured to the outside diameter of the spiral.

$min\_C\_\rho_t := 0.45\left[\left(\frac{A_g}{A_c}\right) - 1\right]\left(\frac{f'_c}{f_{yt}}\right) = 0.007$ Eq. 5.7.4.6-1 for general conditions.

$s_{maxC} := 4 \cdot \frac{A_{st}}{D_{cc} \cdot min\_C\_\rho_t} = 2.77 \cdot in$

D.) Determine the maximum spacing/pitch according to AASHTO LRFD Bridge Design Specifications 6th Ed Sec. 5.10.11.4.1d

$$min\_D\_\rho_t := 0.12\left(\frac{f'_c}{f_{yt}}\right) = 0.008$$

Eq. 5.10.11.4.1d-1 for confinement of plastic hinge zones for seismic zones 3 and 4.

$$s_{maxD} := 4\cdot\frac{A_{st}}{D_{cc}\cdot min\_D\_\rho_t} = 2.56\cdot in$$

E.) Determine the maximum spacing/pitch according to AASHTO LRFD Bridge Design Specifications 6th Ed Sec. 5.8.2.5

$$A_v := n\cdot\left(\frac{\pi}{2}\right)\cdot A_{st} = 0.17\cdot in^2$$

Area of shear reinforcement perpendicular to flexural tension reinforcing.

$$s_{maxE} := \frac{\left(f_{yt}\cdot A_v\right)}{\left(0.0316\cdot\sqrt{psi\cdot f'_c}\cdot b_v\right)} = 216.14\cdot in$$

F.) Determine the maximum spacing/pitch according to AASHTO LRFD Bridge Design Specifications 6th Ed Sec. 5.10.11.4.3

$$s_{maxF} := \min\left(4in, \frac{D_c}{4}\right) = 4\cdot in$$

G.) Determine the maximum spacing/pitch according to AASHTO ASHTO Guide Specifications for LRFD Seismic Bridge Design 2nd Ed. Sec. 8.6.5

$$min\_G\_\rho_t := .005$$

Eq. 8.6.5-3

$$s_{maxG} := 4\cdot\frac{A_{st}}{D_{cc}\cdot min\_G\_\rho_t} = 4.09\cdot in$$

H.) Determine the maximum spacing/pitch according to AASHTO ASHTO Guide Specifications for LRFD Seismic Bridge Design 2nd Ed. Sec. 8.8.9

$$s_{maxH} := \min\left(6\cdot D_{bl}, 6in, \frac{D_c}{5}\right) = 4.5\cdot in$$

I.) Determine the controlling maximum and minimum spiral spacing/pitch from steps A. through H

$s_{min} := s_{minA} = 1.38 \cdot in$

$s_{max} := \min(s_{maxA}, s_{maxB}, s_{maxC}, s_{maxD}, s_{maxE}, s_{maxF}, s_{maxG}, s_{maxH}) = 2.56 \cdot in$

Step 4.) Calculate V_c according to AASHTO Guide Specifications for LRFD Seismic Bridge Design 2nd Ed. Sec. 8.6.2

guess_s := 2.5in Use the maximum spacing and adjust until the final spacing and this guess are the same value.

$D' := D_c - 2 \cdot c_c - D_{bt} = 21.12 \cdot in$ Cross-section dimension of the confined concrete core measure between the centerline of the spiral.

$guess\_\rho_{st} := 4 \cdot \frac{A_{st}}{guess\_s \cdot D'} = 0.008$ Eq. 8.6.2-6

$A_e := 0.8 \cdot A_g = 361.91 \cdot in^2$ Eq. 8.6.2-2

$f_s := guess\_\rho_{st} \cdot f_{yt} = 0.5 \cdot ksi$ Eq. 8.6.2-6

$\mu_D = 6$ Determined in Sec. 4.9 as the maximum value for a multiple-column bent.

$\alpha' := \left(\frac{f_s}{0.15ksi}\right) + 3.67 - \mu_D = 1$ Eq. 8.6.2-5

$v_c := \min\left[.11 \cdot \sqrt{ksi \cdot f'_c}, 0.047 \cdot \alpha' \cdot \sqrt{ksi \cdot f'_c}, 0.032 \sqrt{ksi \cdot f'_c} \cdot \alpha' \cdot \left[1 + \left(\frac{P \cdot in^2}{2 \cdot A_g \cdot kip}\right)\right]\right] = 71\,psi$

$V_c := \frac{(v_c \cdot A_e)}{2} = 12.8 \cdot kip$ Eq. 8.6.2-1

The above equation is divided by 2 according to AASHTO LRFD Bridge Design Specifications 6th Ed Sec. 5.10.11.4.1c, since the compression force is equal to 0.05 $f'_c A_g$ which is half the limit.

Step 5.) Calculate the maximum allowed V_s according to AASHTO Guide Specifications for LRFD Seismic Bridge Design 2nd Ed. Sec. 8.6.4

$max\_V_s := 0.25 \cdot A_e \cdot \sqrt{ksi \cdot f'_c} = 181 \cdot kip$ Eq. 8.6.4-1

Step 6.) Calculate V_s according to AASHTO Guide Specifications for LRFD Seismic Bridge Design 2nd Ed. Sec. 8.6.1 and check against the maximum shear reinforcement calculated in step 5.)

$V_s := \left(\frac{V_{uA}}{0.9}\right) - V_c = 85.1 \cdot kip$ Rearranging Eq. 8.6.1-1 and Eq. 8.6.1-2 to solve for V_s

$Check\_V_s := V_s - max\_V_s = -95.9 \cdot kip$ If this value is greater than zero try a smaller spacing/pitch for the initial guess.

Step 7.) Calculate the required spacing/pitch according to AASHTO Guide Specifications for LRFD Seismic Bridge Design 2nd Ed. Sec. 8.6.3

$s_{req} := \frac{\left[\left(\frac{\pi}{2}\right) \cdot n \cdot A_{st} \cdot f_{yt} \cdot D'\right]}{V_s} = 2.57 \cdot in$ Rearranged Eq. 8.6.3-1 to solve for s.

Step 8.) Determine the final spacing/pitch to be used over the entire height of the column and the corresponding transverse reinforcement ratio.

$s_{min} = 1.38 \cdot in$ $s_{max} = 2.56 \cdot in$ $s_{req} = 2.57 \cdot in$ $pitch := 2.50in$

The final spacing/pitch will be set at 2.50 inches to produce a constructible design.

$\rho_t := \frac{(4 \cdot A_{st})}{(pitch \cdot D_{cc})} = 0.008$ Ratio of spiral reinforcement to total volume of concrete core, measured ou-to-out of spirals.

C6 Spiral Design:

This Mathcad script is for column C6, however the equations and design process are identical for all experimental test columns.

Need to check value according to instructions highlighted.

Input Values.

Step 1.) Adjust input values according to the column properties and loading conditions

Material Properties:

Maximum size aggregate. $MSA := 0.75in$

Diameter of longitudinal reinforcing steel. $D_{bl} := 0.75in$

Nominal concrete compressive strength. $f'_c := 4000psi$

Diameter of transverse reinforcing steel. $D_{bt} := 0.375in$

Yield stress of transverse reinforcement. $f_{yt} := 80ksi$

Cross-sectional area of transverse steel. $A_{st} := 0.11in^2$

Moment over strength factor. $\lambda := 1.4$

Column Properties:

Diameter of column. $D_c := 24in$

Column test height. $h_c := 6ft$

Column clear cover. $c_c := 1.25in$

Effective web width. $b_v := 24in$

Number of spirals within column. $n := 1$

Loading Conditions:

Strength reduction factor defined by AASHTO LRFD BDS Sec. 5.5.4.2.1. $\phi := 0.75$

Prestressing force resisting shear. $V_p := 0kip$

Expected moment capacity. $M_e := 627.5kip \cdot ft$

Applied axial load on column. $P := 90kip$

Global displacement ductility demand ratio. $\mu_D := 6$

Step 2.) Determine the shear force demand according to AASHTO LRFD Bridge Design Specifications 6th Ed. Sec. 5.8.2.9

$D_r := D_c - 2\cdot\left[c_c + D_{bt} + \left(\frac{D_{bl}}{2}\right)\right] = 20\cdot in$ — Diameter of the core, taken from center-to-center of the longitudinal reinforcement.

$d_e := \left(\frac{D_c}{2}\right) + \left(\frac{D_r}{\pi}\right) = 18.37\cdot in$ — Defined by AASHTO 2012 C5.8.2.9-2.

$d_v := 0.9\cdot d_e = 16.53\cdot in$ — Effective shear depth.

$V_e := \frac{M_e}{h_c} = 104.6\cdot kip$ — Expected peak shear force.

$V_n := \frac{V_e}{\lambda} = 74.7\cdot kip$ — Nominal shear force.

$V_u := \phi\cdot V_n = 56\cdot kip$ — Factored shear force.

$v_u := \frac{\left|V_u - \phi\cdot V_p\right|}{\phi\cdot b_v\cdot d_v} = 0.188\cdot ksi$ — Shear stress on the concrete section.

$A_g := \left(\frac{\pi}{4}\right)\cdot {D_c}^2 = 452.39\cdot in^2$ — Gross cross-sectional area of column.

$V_{uA} := v_u\cdot A_g = 85.2\cdot kip$ — Factored shear force defined by AASHTO.

Step 3.) Determine the maximum and minimum spiral spacing/pitch according to the applicable AASHTO code requirements

Note that according to AASHTO 2012 Sec. 5.10.6.2, spiral reinforcement shall consist of one or more evenly spaced continuous spirals of either deformed or plain bar or wire with a minimum diameter of 0.375 in. Therefore the limits for maximum and minimum spiral reinforcing spacing/pitch for the plastic hinge zone with be applied to the entire length of the column.

$Check\_diameter\_of\_deformed\_bar := \max\left(D_{bt}, 0.375in\right) = 0.375\cdot in$

If the above value is less than 0.375 in, then select a larger bar size for the spiral reinforcement.

A.) Maximum and minimum spiral spacing/pitch according to AASHTO LRFD Bridge Design Specifications 6th Ed Sec. 5.10.6.2

Minimum clear spacing is equal to the lesser of one inch or 1.33 multiplied by the maximum size aggregate.

$c_{smin} := \max(1.0in, 1.33 \cdot MSA) = 1 \cdot in$ Minimum clear spacing of spiral for part A.

$s_{minA} := c_{smin} + D_{bt} = 1.38 \cdot in$ Minimum spiral spacing/pitch for part A.

$s_{maxA} := \min(6.0in, 6.0 \cdot D_{bl}) = 4.5 \cdot in$ Maximum spiral spacing/pitch for part A.

B.) Determine the maximum spiral spacing/pitch according to AASHTO LRFD Bridge Design Specifications 6th Ed Sec. 5.8.2.7

$v_u = 0.188 \cdot ksi$ $0.125 \cdot f'_c = 0.5 \cdot ksi$

$s_{maxB1} := \min(0.8d_v, 24in) = 13.22 \cdot in$ If $v_u < 0.125*f'_c$

$s_{maxB2} := \min(0.4d_v, 12in) = 6.61 \cdot in$ If $v_u >= 0.125*f'_c$

If $v_u < 0.125*f'_c$ set $s_{maxB} = s_{maxB1}$ if not set equal to s_{maxB2}

$s_{maxB} := s_{maxB1} = 13.22 \cdot in$

C.) Determine the maximum spacing/pitch according to AASHTO LRFD Bridge Design Specifications 6th Ed Sec. 5.7.4.6

$D_{cc} := D_c - 2 \cdot c_c = 21.5 \cdot in$ Diameter of core, measure out-to-out of spiral.

$A_c := \frac{\pi \cdot D_{cc}^2}{4} = 363.05 \cdot in^2$ Area of core measured to the outside diameter of the spiral.

$min\_C\_\rho_t := 0.45\left[\left(\frac{A_g}{A_c}\right) - 1\right]\left(\frac{f'_c}{f_{yt}}\right) = 0.006$ Eq. 5.7.4.6-1 for general conditions.

$s_{maxC} := 4 \cdot \frac{A_{st}}{D_{cc} \cdot min\_C\_\rho_t} = 3.7 \cdot in$

D.) Determine the maximum spacing/pitch according to AASHTO LRFD Bridge Design Specifications 6th Ed Sec. 5.10.11.4.1d

$$min\_D\_\rho_t := 0.12\left(\frac{f'_c}{f_{yt}}\right) = 0.006$$

Eq. 5.10.11.4.1d-1 for confinement of plastic hinge zones for seismic zones 3 and 4.

$$s_{maxD} := 4\cdot\frac{A_{st}}{D_{cc}\cdot min\_D\_\rho_t} = 3.41\cdot in$$

E.) Determine the maximum spacing/pitch according to AASHTO LRFD Bridge Design Specifications 6th Ed Sec. 5.8.2.5

$$A_v := n\cdot\left(\frac{\pi}{2}\right)\cdot A_{st} = 0.17\cdot in^2$$

Area of shear reinforcement perpendicular to flexural tension reinforcing.

$$s_{maxE} := \frac{\left(f_{yt}\cdot A_v\right)}{\left(0.0316\cdot\sqrt{psi\cdot f'_c}\cdot b_v\right)} = 288.187\cdot in$$

F.) Determine the maximum spacing/pitch according to AASHTO LRFD Bridge Design Specifications 6th Ed Sec. 5.10.11.4.3

$$s_{maxF} := \min\left(4in, \frac{D_c}{4}\right) = 4\cdot in$$

G.) Determine the maximum spacing/pitch according to AASHTO ASHTO Guide Specifications for LRFD Seismic Bridge Design 2nd Ed. Sec. 8.6.5

$$min\_G\_\rho_t := .005$$

Eq. 8.6.5-3

$$s_{maxG} := 4\cdot\frac{A_{st}}{D_{cc}\cdot min\_G\_\rho_t} = 4.09\cdot in$$

H.) Determine the maximum spacing/pitch according to AASHTO ASHTO Guide Specifications for LRFD Seismic Bridge Design 2nd Ed. Sec. 8.8.9

$$s_{maxH} := \min\left(6\cdot D_{bl}, 6in, \frac{D_c}{5}\right) = 4.5\cdot in$$

I.) Determine the controlling maximum and minimum spiral spacing/pitch from steps A. through H

$s_{min} := s_{minA} = 1.38 \cdot in$

$s_{max} := \min(s_{maxA}, s_{maxB}, s_{maxC}, s_{maxD}, s_{maxE}, s_{maxF}, s_{maxG}, s_{maxH}) = 3.41 \cdot in$

Step 4.) Calculate V_c according to AASHTO Guide Specifications for LRFD Seismic Bridge Design 2nd Ed. Sec. 8.6.2

guess_s := 2.5in Use the maximum spacing and adjust until the final spacing and this guess are the same value.

$D' := D_c - 2 \cdot c_c - D_{bt} = 21.12 \cdot in$ Cross-section dimension of the confined concrete core measure between the centerline of the spiral.

$guess\_\rho_{st} := 4 \cdot \frac{A_{st}}{guess\_s \cdot D'} = 0.008$ Eq. 8.6.2-6

$A_e := 0.8 \cdot A_g = 361.91 \cdot in^2$ Eq. 8.6.2-2

$f_s := guess\_\rho_{st} \cdot f_{yt} = 0.667 \cdot ksi$ Eq. 8.6.2-6

$\mu_D = 6$ Determined in Sec. 4.9 as the maximum value for a multiple-column bent.

$\alpha' := \left(\frac{f_s}{0.15ksi}\right) + 3.67 - \mu_D = 2.1$ Eq. 8.6.2-5

$v_c := \min\left[.11 \cdot \sqrt{ksi \cdot f'_c}, 0.047 \cdot \alpha' \cdot \sqrt{ksi \cdot f'_c}, 0.032 \sqrt{ksi \cdot f'_c} \cdot \alpha' \cdot \left[1 + \left(\frac{P \cdot in^2}{2 \cdot A_g \cdot kip}\right)\right]\right] = 149\,psi$

$V_c := \frac{(v_c \cdot A_e)}{2} = 26.9 \cdot kip$ Eq. 8.6.2-1

The above equation is divided by 2 according to AASHTO LRFD Bridge Design Specifications 6th Ed Sec. 5.10.11.4.1c, since the compression force is equal to 0.05 $f'_c A_g$ which is half the limit.

Step 5.) Calculate the maximum allowed V_s according to AASHTO Guide Specifications for LRFD Seismic Bridge Design 2nd Ed. Sec. 8.6.4

$max\_V_s := 0.25 \cdot A_e \cdot \sqrt{ksi \cdot f'_c} = 181 \cdot kip$ Eq. 8.6.4-1

Step 6.) Calculate V_s according to AASHTO Guide Specifications for LRFD Seismic Bridge Design 2nd Ed. Sec. 8.6.1 and check against the maximum shear reinforcement calculated in step 5.)

$V_s := \left(\frac{V_{uA}}{0.9}\right) - V_c = 67.7 \cdot kip$ Rearranging Eq. 8.6.1-1 and Eq. 8.6.1-2 to solve for V_s

$Check\_V_s := V_s - max\_V_s = -113.2 \cdot kip$ If this value is greater than zero try a smaller spacing/pitch for the initial guess.

Step 7.) Calculate the required spacing/pitch according to AASHTO Guide Specifications for LRFD Seismic Bridge Design 2nd Ed. Sec. 8.6.3

$s_{req} := \frac{\left[\left(\frac{\pi}{2}\right) \cdot n \cdot A_{st} \cdot f_{yt} \cdot D'\right]}{V_s} = 4.31 \cdot in$ Rearranged Eq. 8.6.3-1 to solve for s.

Step 8.) Determine the final spacing/pitch to be used over the entire height of the column and the corresponding transverse reinforcement ratio.

$s_{min} = 1.38 \cdot in$ $s_{max} = 3.41 \cdot in$ $s_{req} = 4.31 \cdot in$ $pitch := 2.50in$

The final spacing/pitch will be set at 2.50 inches to produce a constructible design.

$\rho_t := \frac{\left(4 \cdot A_{st}\right)}{\left(pitch \cdot D_{cc}\right)} = 0.008$ Ratio of spiral reinforcement to total volume of concrete core, measured ou-to-out of spirals.